DECOMMISSIONING CONSIDERATIONS FOR MOLTEN SALT TYPE REACTORS

By:

Tzu Yen Yvonne Lin

A thesis submitted to the

School of Graduate and Postdoctoral Studies in partial

fulfillment of the requirements for the degree of

Master of Applied Science in Nuclear Engineering

The Faculty of Engineering and Applied Science

University of Ontario Institute of Technology (Ontario Tech University)

Oshawa, Ontario, Canada

May 2023

Thesis Examination Information

Submitted by Tzu Yen Yvonne Lin

Master of Applied Science in **Nuclear Engineering**

Thesis title: DECOMMISSIONING CONSIDERATIONS FOR MOLTEN SALT TYPE REACTORS

An oral defense of this thesis took place on March 20th, 2023, in front of the following examining committee:

Examining Committee:

Chair of Examining Committee	Dr. Lixuan Lu
Research Supervisor	Dr. Glenn Harvel
Examining Committee Member	Dr. Jennifer McKellar
Thesis Examiner	Dr. Matthew Kaye

The above committee determined that the thesis is acceptable in form and content and that a satisfactory knowledge of the field covered by the thesis was demonstrated by the candidate during an oral examination. A signed copy of the Certificate of Approval is available from the School of Graduate and Postdoctoral Studies.

Abstract

Molten salt type small modular reactors are presently being developed as an option for providing electricity and alternative energy forms. The current proposed designs do not document how decommissioning will be addressed. The decontamination activities necessary for these reactor technologies upon their shut-down are not available in the open literature. The intent of the experiments performed in this work is to investigate the decommissioning considerations that are associated with molten salt reactors as well as identify some of the concerns that will need to be addressed. Two separate experimental systems were used: one for the synthesis of FLiNaK salt and the other for the remelting and drainage of residue FLiNaK from a Hastelloy-C276 segment. The results of these experiments have demonstrated that FLiNaK salt, given contact with atmospheric moisture, tends to change in condition over time and migrate from one location to another as a result of hygroscopy and deliquescence. Consequently, the technical challenges that may arise during molten salt reactor decommissioning as a result of this phenomenon are also discussed and explored. Similarly, the application of heating and pressure reduction to assist in collecting the salt for removal processes was also examined to better determine suitable decontamination and end-of-life options for molten salt reactors. The results of this experiment demonstrated that it would be difficult to completely drain solidified molten salts in a reactor system by reheating the structure only once; residual salt is likely to be present, and the use of flush salt would increase the volume of waste.

Keywords: Molten Salt Reactors, FLiNaK, Nuclear Decommissioning, Salt Migration, Salt Preparation, Nuclear Decontamination

Declaration of Authorship

I, Tzu Yen Yvonne Lin, declare that this thesis titled, "Decommissioning Considerations for Molten Salt Type Reactors" and the work presented in it are my own. I confirm that:

- I hereby declare that this thesis consists of original work of which I have authored. This is a true copy of the thesis, including any required final revisions, as accepted by my examiners.

- I authorize the University of Ontario Institute of Technology to lend this thesis to other institutions or individuals for the purpose of scholarly research. I further authorize the University of Ontario Institute of Technology to reproduce this thesis by photocopying or by other means, in total or in part, at the request of other institutions or individuals for the purpose of scholarly research. I understand that my thesis will be made electronically available to the public.

Signed:

_____

Date:

_____

Statement of Contributions

Dedicated to my dearest girl, Astrid Chang …

"All that we see or seem is but a dream within a dream."

- Edgar Allen Poe

"Why do I always get the crazies ?"

- Anonymous

Acknowledgements

The following individuals and groups are acknowledged:

Table of Contents

List of Figures

List of Tables

Chapter 1

Introduction

Nuclear power reactors have been a reliable source of commercial scale base-load electricity since the 1950s. Averaging between twenty to forty years of power generation, Gen III power reactors are now approaching the end of their operating lifetime. Numerous generating stations around the world have also ended their operations prior to the scheduled shut-down date as a result of increased alarm and concern of the public as well as regulatory bodies in response to the 2011 Fukushima Daiichi Nuclear Disaster.

As these large-scale power reactors retire and begin decommissioning, they leave behind a significant energy gap. Undoubtedly, demand for electricity around the world is expected to increase in the coming years; thus, there is now an opportunity for new energy sources and technologies to be deployed. A potential solution is to replace Gen III power reactors with Gen IV Small Modular Reactor (SMR) technologies. Defined as any nuclear reactor with an electrical output under 300 MWe and thermal output under 1000 MWth, these modular reactors offer the potential to fulfil flexible power generating needs for a wider range of users and applications. Deployable either as a single or multi-module plant, SMRs offer the possibility of combining nuclear energy with alternative energy sources [1].

Amongst the wide range of SMRs, the molten salt type reactor (MSR) has been proposed as one of the options for commercial power generation. These reactor designs usually select eutectic mixtures such as $LiF\text{-}BeF_2$ or FLiNaK as fuel and cooling salts to reduce their melting temperature [2]. Unlike water, the use of molten salt allows the reactors to operate at or near atmospheric pressure and at higher temperatures. Such features mean that MSRs do not require large, costly pressure vessels used in many water-based technologies and are capable of greater efficiency and/or provide process-heat opportunities [3][4]. Two vendors in Canada, Terrestrial Energy and MoltEx, are keenly interested in developing such types of reactors [5][6].

Initially developed in the 1960's, the Molten Salt Reactor Experiment (MSRE) by the Oak Ridge National Laboratory (ORNL) demonstrated that the use and operation of a molten salt

fueled reactor concept was possible and viable. Despite only being online for an equivalent of 1.5 years of full-power operation, the MSRE proved a series of predictions that renewed interest in this technology some fifty years later: that the fuel salt was immune to radiation damage, the graphite core was not attacked by the hot salt, and corrosion of Hastelloy-N was minimal [7]. Despite such discoveries, the selection of materials, be it for the structure, fuel, or coolant, remains one of the major sources of uncertainty for this technology. The MSRE experiments also indicated that significant information is required prior to the establishment of commercial scale nuclear power plants. Much of this missing information was related to the specifics in decommissioning, decontamination, and storage of the salt-facing reactor components, fuel salt, and cooling salt [8].

Similarly, vendors currently developing MSR technologies in Canada advertise features such as higher efficiencies, usable heat, closed fuel cycles, *etc.* but neglect to mention any decommissioning plans and end-of-life processes in detail if at all. However, according to CNSC regulations, it is necessary and a requirement for any reactor technology to have a decommissioning plan as part of its design, planning, and licensing process [9]. In other words, the deployment and realization of commercial molten salt reactors is largely contingent on the development of a safe and thorough decommissioning plan.

1.1 Problem Statement

Significant considerations and resources have been dedicated to the research and development, design, operation, materials, fuel cycles, and plant layout/facilities of MSRs, but insufficient information is available on the decommissioning, dismantlement, and disposal activities of MSR component and salt once the reactors shut down. Current regulations require during the design phase that decommissioning be considered. The intent is to select materials, prepare structures, facilities, and services necessary for the safe and successful decommissioning of the plant. To do that would require some knowledge of what would be expected during decommissioning of a molten salt reactor.

The decommissioning of MSRs encompasses a wide variety of activities. These include the removal of fuel and cooling salt from the reactor system and their eventual long-term storage or reprocessing. Limited operational experience regarding the end-of-life of such a novel

reactor technology also means that the extent of potential complications and hazards of decommisoning a MSR has yet to be fully explored. In the case of potential future deployments, the use of enriched Uranium in molten salt fuel, especially in Canada, would require more stringent regulatory controls during the construction, operation, and decommissioning of the reactor. End-of-life operations would be expected to become more complex, expensive, and require careful planning to ensure the safety of workers and the environment alike. Given the wide range of proposed metals for salt-facing components and various feasible eutectic fuel and coolant salts that can be used, it is necessary to devise a process that models the behaviour of the salt and their drainage process in a controlled system.

This work will attempt to simulate the molten salt removal process at the end of reactor operations during decontamination processes as well as observe salt behaviour under extended storage.

1.2 Objectives

This work will explore some of the issues that may be found related to decommissioning of a molten salt reactor. The main objective is to identify phenomena that may occur during the draining or dismantling of a molten salt loop. To achieve this objective, the following sub-objectives will be pursued:

1. Produce controlled and experimental samples of FLiNaK salt to ensure control of the inputs to the experiments;
2. Assess FLiNaK Salt behaviour under different environmental conditions and their implications for decommissioning;
3. Simulate the drainage of salt from a representative component by re-melting and removing the FLiNaK salt inside a tube segment of the laboratory's Molten Salt Loop (MSL).

1.3 Thesis Structure

This thesis provides the findings related to the above objectives. Chapter 2 provides a literature review related to known salts, molten salt reactor design, ageing phenomena, and

Chapter 1. Introduction

information related to decommissioning of molten salt reactors. Chapter 3 provides the methodology for the experiments to manufacture salt samples, to monitor their behaviour under different environmental conditions, and to test dismantling of a molten salt test section. Chapter 4 describes the quantitative and qualitative observations made in the experiments while Chapter 5 discusses the implications of the results in terms of the decommissioning activities of MSRs. Chapter 6 will provide a summary of the conclusions obtained from this work and finally Chapter 7 discusses potential future work.

Chapter 2

Literature Review

2.1 Introduction

This chapter intends to illustrate the implications and considerations that must be made when a molten salt reactor technology reaches its end of life, specifically, in terms of nuclear decommissioning. To break this task into more manageable chunks, this section will outline the current understanding of the behaviour and properties of molten salt with regards to its eventual removal from the reactor system, long-term storage, and disposal.

It is crucial to have a high-level comprehension of the workings of a molten salt reactor as well as the significance of the design choices made in their historical context. This overview of the history behind the development of the first molten salt reactor technology will primarily focus on the decommissioning challenges and activities of the Molten Salt Reactor Experiment (MSRE) that were observed. From its military origins to a potential civilian power source, the MSRE and its findings are still the main source of inspiration for GEN IV SMR vendors hoping to commercialize the molten salt reactor today.

A summary of current proposed GEN IV molten salt reactor models offer insight into the evolution of this technology as global energy demand shifts along with relevant decommissioning and dismantlement strategies currently used in industry. Finally, an investigation of the fluid properties (thermophysical and physicochemical) of the salt compounds and material selection issues regarding reactor structure must be included for better overall understanding.

2.2 The Molten Salt Reactor

Molten salt reactors are a class of nuclear fission reactor in which the primary coolant, or the fuel itself, is a molten salt mixture. Originally developed in the 1960s by the Oak Ridge

National Laboratory, details of the history of the reactor will be discussed in a later section, the components of an MSR are largely similar to that of commercial water-cooled reactor technologies. MSRs can be burner or breeder reactors whose reactor physics have been optimized for operation within the fast and thermal energy ranges. The thermal designs usually use a graphite moderator to slow-down neutrons and control temperature. The MSR is also capable of using various fuels (low-enriched uranium, thorium, and even depleted uranium) as well as coolants; they can adopt a loop, modular, or integral configuration [3]. MSRs can be categorized into two main sub-classes. The first, more basic concept, uses fuel in the form of a eutectic molten salt mixture with fissile materials dissolved in it while the reactor core consists of unclad graphite moderators that have been arranged to allow the flow of salt at high temperatures and low pressure.

In the second subclass, molten salt is used as the coolant to a solid, coated particle fueled core also at low pressure. The core of this solid fuel variant is very similar to that of High-Temperature Reactors (HTRs); thus, this subclass is often referred to as the Fluoride salt-cooled High-temperature Reactor (FHR) [10][11]. Currently, reactor designs of the second subclass are varyingly called "molten salt reactor system" in the Generation IV proposals, which includes concepts such as molten salt converter reactors (MSCR) and advanced high-temperature reactors (AHTRs) [12].

In the much more common liquid fuelled MSR designs, the nuclear fuel is dissolved in the molten fluoride salt coolant as fissile (UF_4, PuF_3) and/or fertile (ThF_4) elements depending on the intended reactor application, either as a breeder or actinides burner. In the core of the reactor, fission takes place within the fuel salt, which then flows into an intermediary heat exchanger where secondary liquid-salt coolants remove the heat [10]. Numerous design variants of MSRs are being proposed. Figure 2.1 (a) and (b) illustrate the reactor schematic of two MSR models by Canadian companies MoltEx and Terrestrial Energy.
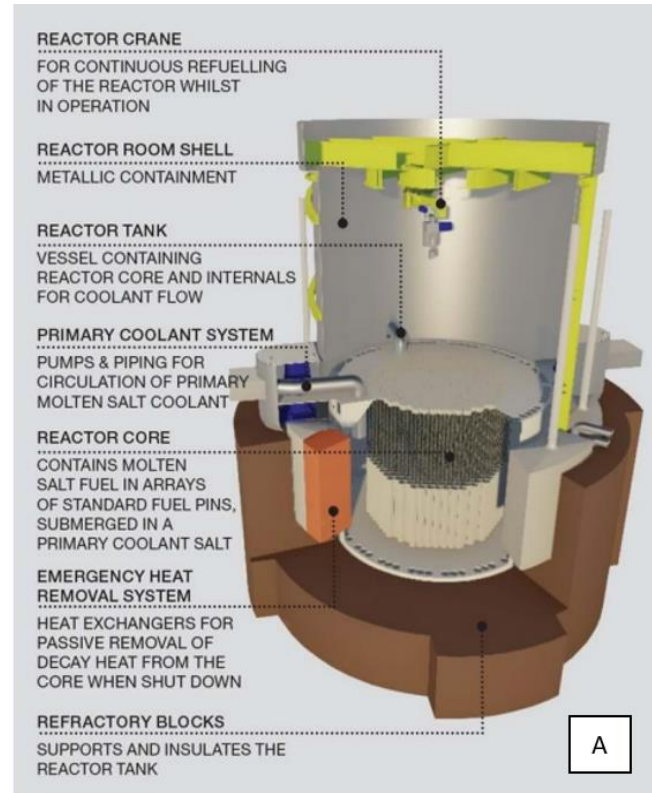
Figure 2.1: Schematic of the Stable Salt Reactor proposed by MoltEX [5].
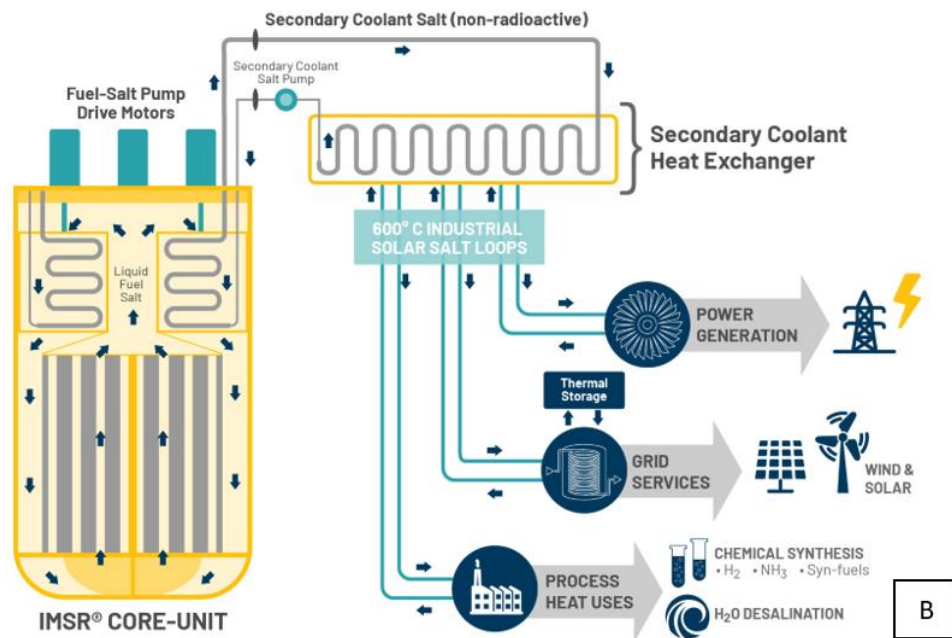
Figure 2.2: Schematic of the IMSR-400 by Terrestrial Energy [6].

MSRs can further be subdivided into three main categories in terms of how the molten salt is utilized in the system:

1) Molten Salt Fuelled- Circulating;
2) Molten Salt Fuelled- Static;
3) Molten Salt Coolant Only.

A summary of proposed MSR designs can be found in Table 2.1.

Table 2.1: Summary of Molten Salt Reactor Designs Currently being Proposed [5-6] [13-18].

Name of Reactor	Sub-category	Design Organization	Coolant	Moderator	Output Capacity	Design Status	Stakeholder Country
Integral Molten Salt Reactor-400 (IMSR-400)	Burner-type Molten salt fuelled circulating	Terrestrial Energy	Fluoride Salts	Graphite	400 MWth 194 MWe	Under Design	USA Canada
Liquid Fluoride Thorium Reactor (LFTR)	Breeder-type Molten salt fuelled circulating	Flibe Energy	Fluoride Salts	Graphite	600 MWth 250MWe	Conceptual Design	USA
Mark 1 Pebble-Bed Fluoride-Salt-Cooled High-Temperature Reactor (Mk1 PB-FHR)	Solid Fuel Molten salt coolant only	University of California, Berkeley	Fluoride Salts	Graphite	236 MWth 100 MWe	Pre-conceptual Design	USA
Molten Salt Fast Reactors (MSFR)	Breeder-type Molten salt fuelled circulating	CNRS France (The French National Center for Scientific Research)	Molten salt (unspecified)	No moderator	3,000 MWth 1,500 MWe	Conceptual Design	France

Stable Salt Reactor-Waste Burner (SSR-W)	Molten Salt Fuelled-Static	MoltEX	Chloride-based coolant salt	Graphite	300-450 MWth Unspecified Electrical Output	Vendor Design Review Phase	United Kingdom Canada
Molten Salt Reactor FUJI (MSR-FUJI)	Breeder-type LFTR Molten salt fuelled circulating	International Thorium Molten-Salt Forum	Fluoride Salts	Graphite	450 MWth 200 MWe	Conceptual Design	Japan
Molten Salt Thermal Waste burner (MSTW)	Burner-type Molten salt fuelled circulating	Seaborg Technologies	Molten salt (unspecified)	Graphite	270 MWth 115 MWe	Conceptual Design	Denmark
Small Fluoride Salt-cooled High Temperature Reactor (SmAHTR)	Solid Fuel (Plate TRISO) Molten salt coolant only	Oak Ridge National Laboratory	FLiBe	Carbon	125 MWth N/A Electrical Output	Under Design	USA
ThorCon- TMSR500	Molten salt fuelled circulating	ThorCon US, Inc.	Molten Salts	Graphite	557 MWth 250 MWe	Detailed Design	USA
Dual-fluid Molten Salt Reactor (DFR)	Breeder-type Molten salt fuelled circulating	Dual Fluid Energy Inc.	Molten Salt (Primary) Lead (Secondary)	Unspecified	~600 MWth ~300 MWe	Conceptual Design	Germany Canada

There are several unique characteristics of the MSR that suggest a potentially safer, less wasteful, and efficient form of nuclear power generation compared to current water-based reactor technologies.

Firstly, MSRs operate at much higher temperatures, usually between 700-750 °C, compared to conventional Light Water Reactors (LWRs) that operate at around 300 °C. The molten salts are attractive coolant candidates because of their high boiling point - typically around 1400 °C - and volumetric heat capacities [19]. This allows the reactor to provide greater electricity-generation efficiency; several Gen IV MSR vendors promote the possibility for energy storage, cogeneration of medical isotopes and hydrogen, as well as various usable-heat applications [6][10].

MSRs also operate at or close to atmospheric pressure and are not cooled by water, eliminating the possibility of catastrophic steam explosions thus not requiring large, expensive reactor pressure vessels [3]. Other advantages of the MSR include its potential to be refueled while operating; it is capable of online-nuclear reprocessing like the CANDU design. MSRs can also implement a closed fuel cycle, where spent fuel is reprocessed and/or partly reused, which offers reassurance in terms of non-proliferation [20].

Despite its numerous benefits, there are still technological gaps and design challenges that must be addressed prior to the deployment of commercial MSRs. Issues regarding power cycle implementation, fuel inventory, storage, fuel/coolant selection, as well as end-of-life operations are as applicable in proposed Gen IV designs as they were to the original MSRE [21].

The requirements for all power reactors have changed in terms of safety, sustainability, and nuclear security since the Fukushima Daiichi Nuclear Disaster. These changes mean that MSRs developed for the current market will have significantly different features than those required 40 years ago and present new opportunities for optimization and innovation.

2.3   The Aircraft Reactor Experiment

The concept of a molten salt reactor took its earliest form in the 1950s Aircraft Reactor Experiment (ARE). Initially studied by the US Air Force in 1946, the ARE was an experimental nuclear reactor designed to investigate the feasibility of using fluid-fuel in high-temperature, high-power-density reactors for the propulsion of supersonic aircrafts [22]. This project saw the design, construction, operation, and decommissioning of the very first reactor to circulate molten salt fuel, from which the resulting experimental data and experience laid the foundation for and enabled the broader development of molten salt reactors as well as liquid metal cooled reactors [22-24].

The ARE used a fuel composed of NaF, ZrF_4, and UF_4 in 53.09-40.73-6.18 mol percentages, respectively. The designed fuel temperature was supposed to be 820 °C with a 180 °C temperature rise across the core. However, the peak temperature reached 860 °C in steady operation and 882 °C in transient states [25]. The reactor itself was comprised of a BeO cylinder connected to bent tubes that directed the flow of the fuel through its core in both directions and surrounded by an Inconel shell [26]. Figure 2.3 below presents a schematic of the design of the reactor [22]. The material selection was based upon the results of a series of Natural-convection corrosion test loops set up prior to the construction of the system, which can be on the next page in Figure 2.4 [22][25][26].
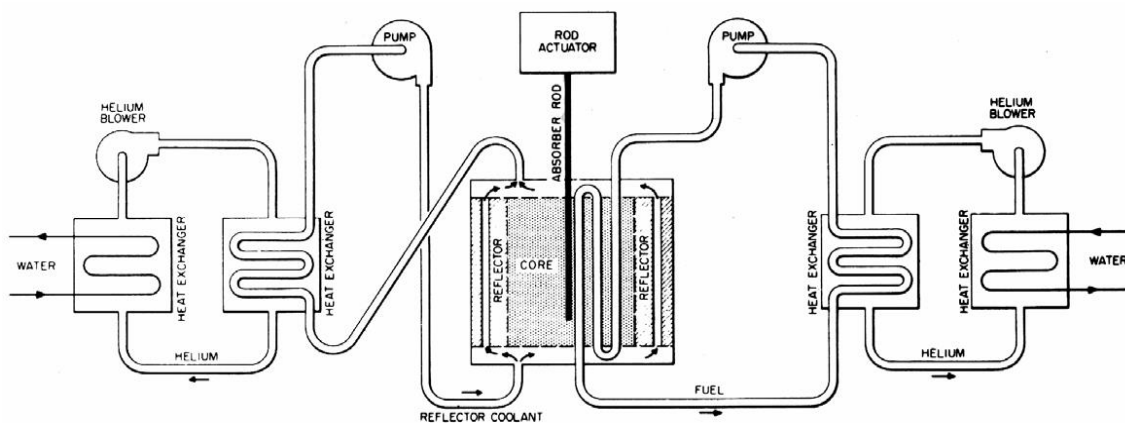
Figure 2.3: Schematic of the Circulating-Fuel Aircraft Reactor System [22].
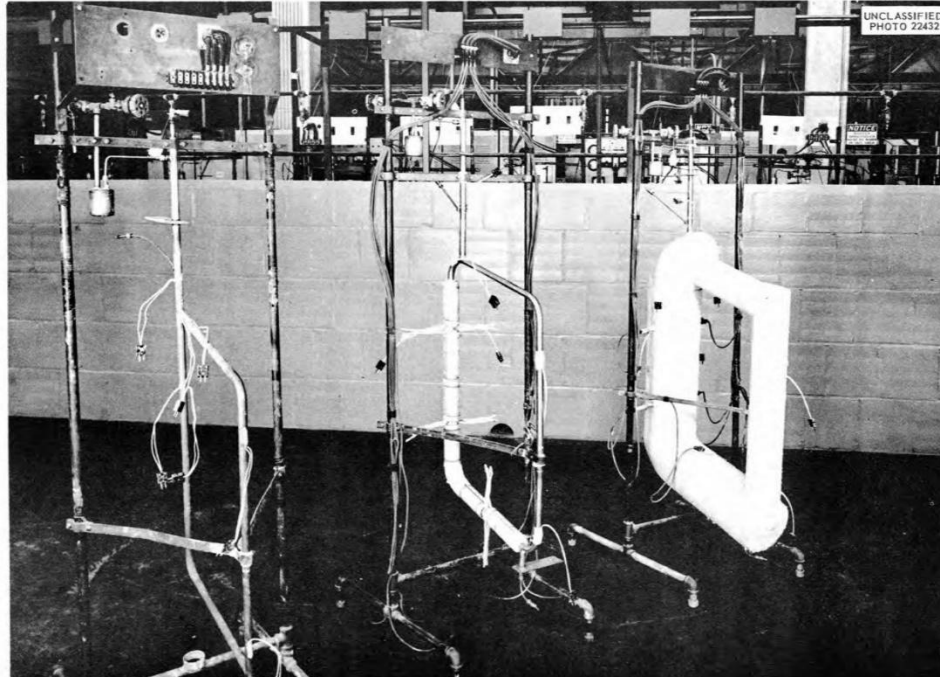
Figure 2.4: Natural-convection Loops Constructed for Corrosion Testing [23].

About 170 litres of the NaF-ZrF$_4$-UF$_4$ fuel flowed through the ARE per minute under a core pressure of around 275.8 kPa. At the same time, sodium was pumped through the reactor at a much higher rate of 570 litres per minute with 344.7 kPa of pressure [25][27]. Heat from the fuel salt was subsequently transferred to a helium loop that in turn heated water. The ARE only had one neutron source, a polonium-beryllium source of 15 curies (5.55^10^{11} Bq), one regulating rod, and three helium-cooled boron carbide shim rods [22][28].

The ARE operated at its maximum sustained power of 2.5 MW between the dates of November 8th to the 12th in 1954 and generated a total of 96 MW-hours of energy [24][28]. At 4:19 pm on November the 8th, during its ascent to full power, the reactor was abruptly shut down due to high airborne radioactivity measurements detected in the basement of the facility. It was discovered that the gas fittings to the main fuel pump were leaking fission-product gases and vapours into the basement through defective seals in some of the electrical junction panel [29]. Similar leaks would eventually be observed in the waste salt tanks of the Molten Salt Reactor Experiment during its storage, also the result of failed mechanical components. The safety detectors would shut down the ARE a few more times during the subsequent attempted restarts, they were eventually withdrawn further away from the reactor as to not be triggered

so easily, By the end of the day, the ARE had started back up and reached full power [24][28][29]. Operation of the ARE was demonstrated to United States Air Force and Aircraft Nuclear Propulsion personnel who gathered at the ORNL for a quarterly information meeting. Load following features were demonstrated by turning the blowers of the reactor on and off. Having obtained all operational objectives, the decision to cease operation was made and the experiment was terminated [24][28][30].

2.3.1 Decommissioning of the ARE

The decommissioning work of the ARE began immediately after its termination. On the 13th of November, the fuel salt was transferred to the fuel dump tank. However, it was noted that between the period of reactor shutdown and fuel dumping, all operating personnel had to wear gas masks because of the high levels of airborne radioactivity in the facility. This was caused by a leak in the off-gas system, the exact location of which was never identified or located [29][30]. A fluoride flush salt was then heated to 38 °C (100 °F) above the system operating temperature and pumped through the fuel channels. The operators observed the thermocouples throughout the ARE to ensure flush salt flowed through all channels.

Two flat lead shields, each 1.83 m by 1.22 m and 0.05 m thick, were used in the heat exchanger cell to protect any decommissioning personnel from radiation from the fuel systems [27][30]. Firstly, the water lines were cut; this was followed by the cutting of sodium lines which were immediately sealed with multiple layers of masking tape. It was noted in the post-operation report of the ARE that upon the removal of the sodium pump and heat exchanger, the radiation field in the room had increased to 6 mSv/hr and that these components were shielding the area from the fuel system radiation [24][30].

By February 1955, the fuel system was being dismantled. The reactor itself was cut from the system using grinders then put into storage and later buried. Photographs of the ARE reactor core dismantling process are featured in Figures 2.5 and 2.6. The fuel salt in the dump tanks remained in storage as it awaited the development of fused-salt fluoride-volatility reprocessing techniques. Approximately 60 samples were taken from the decommissioned ARE equipment and material for analysis; metallographic, activation, visual, stereophotographic, and leak tests were performed [30].

Figure 2.5: Dismantling of the ARE Reactor Core through Cutting [30].

Figure 2.6: Top of the Reactor with the Pressure Shell and Some Fuel Tubes Removed [30].

2.4   The Molten Salt Reactor Experiment

Stemming from the Aircraft Reactor Experiment and its initial goal of producing an aircraft propulsion reactor, the Molten-Salt Reactor Experiment was an experimental molten salt reactor built by the Oak Ridge National Laboratory in the 1960s. Its construction was complete by 1964; the reactor achieved criticality in 1965 and was operated until 1969. The MSRE was a liquid fluoride thorium test reactor with a thermal output of 7.4 MWth which had demonstrated the feasibility of an epithermal thorium breeder reactor [31]. The reactor primarily used two fuels: first Uranium-235 then Uranium-233. At the end of the U-233 fuel campaign, which was the second campaign in the overall series, PuF_3 was used as fuel to demonstrate flexible reactor operations [31][32]. At the design power level of 10 MW, the reactor ran between the temperatures of 635 °C and 700 °C, which is well above the melting temperature of FLiBe, the molten salt selected as both fuel and coolant, at 459 °C [33]. Molten salts will be described in further detail in Section 2.5. Figure 2.7 below illustrates the plant layout of the MSRE facility.

1. Reactor Vessel   2. Heat Exchanger   3. Fuel Pump
4. Freeze Flange   5. Thermal Shield   6. Coolant Pump
7. Radiator   8. Coolant Drain Tank
9. Fans   10. Fuel Drain Tanks
11. Flush Tank   12. Containment Vessel
13. Freeze Valve
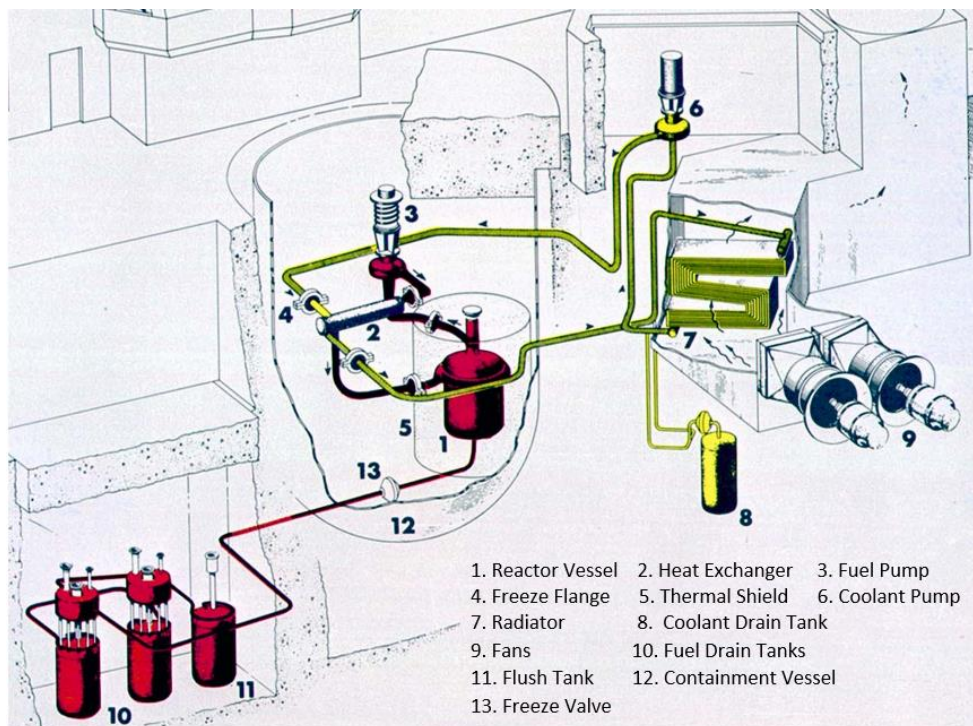
Figure 2.7: MSRE Plant Diagram with Key Reactor Components [34].

The plant diagram presented in Figure 2.7 illustrates the salt facing components within the MSRE by highlighting them in red and yellow, which are the primary loop with fuel salt and the secondary loop with coolant salt, respectively. By identifying the physical operating range of the molten salts within a reactor system, one can begin to identify the potential areas that would eventually need to undergo nuclear decontamination and decommissioning. Figure 2.8 presents a cross-sectional view of the MSRE facility. In the case of the MSRE, based upon Figures 2.7 and 2.8, would include all the named components and their immediate cells.
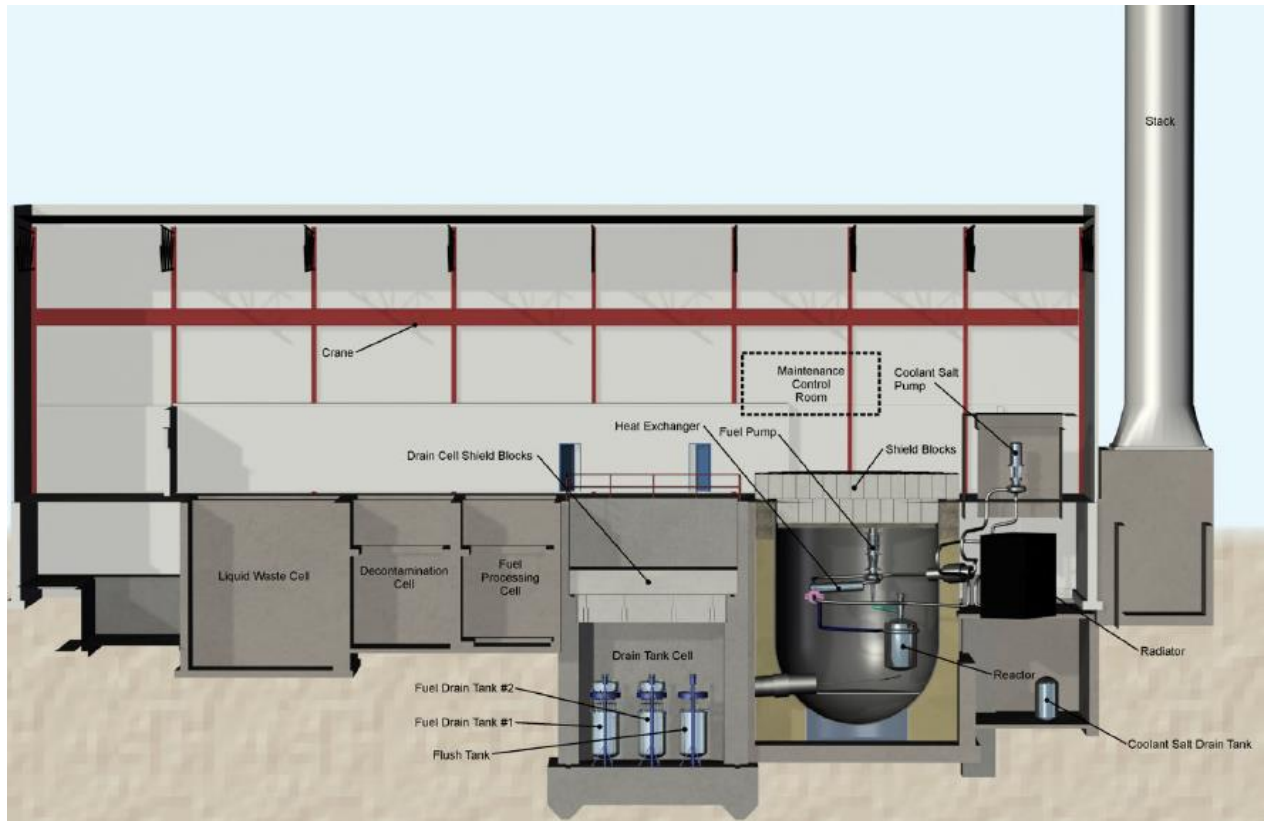
Figure 2.8: Cross-Section View of the MSRE Facility [35].

The initial cost estimate for the MSRE was $4.18 million USD in 1960, but by the time the project reached its detailed design phase the cost estimate had doubled; this was mainly the result of having to develop a custom corrosion-resistant structural alloy: Hastelloy-N. The site itself is considered a Category II nuclear facility [31][35][36]. This implies that future MSRs would also likely fall under this category, which, according to the licensing requirements of the CNSC, must include a proposed plan for the decommissioning.

2.4.1   Reactor Description and Operation

The MSRE had a pyrolytic graphite core that also served as the moderator. Prior tests conducted during the ARE demonstrated that salt does not permeate graphite given certain desired pore structures, which were on the order of a micrometer. Though it is uncertain whether the two materials interacted with one another in some other form. Images of the reactor vessel and core of the MSRE can be seen in Figure 2.8 below. All the salt-facing components of the MSRE including piping, reactor vessel, core vat, and structural components were made from Hastelloy-N.

A low chromium, nickel-molybdenum alloy, Hastelloy-N was the most corrosion resistant and compatible with the fluoride salts FLiBe and FLiNaK [37].
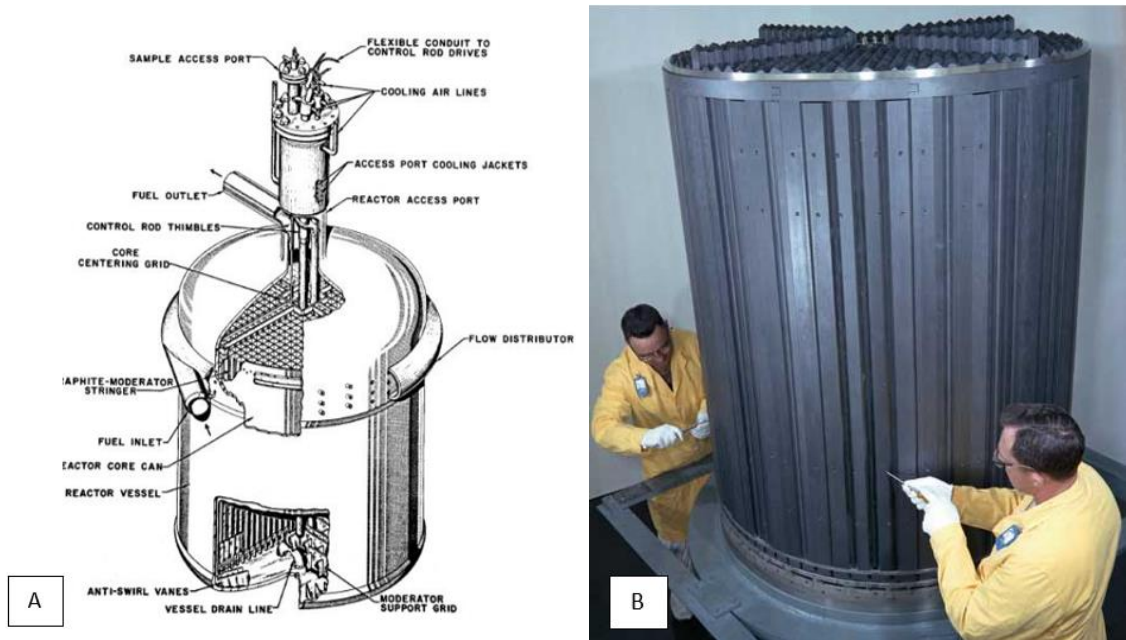
Figure 2.9: MSRE Reactor Components (a): Reactor Vessel (b): Pyrolytic Graphite Core [34].

The MSRE used liquid LiF-BeF$_2$-ZrF$_4$-UF$_4$ as fuel and FLiBe as secondary coolant. The fuel salt circulated through channels of graphite which provided geometry and moderation necessary to sustain a nuclear chain reaction in the reactor vessel [31]. The heat is then transferred from the fuel salt to the secondary coolant salt in the primary heat exchanger. The coolant salt is passed from the primary heat exchanger to an air-cooled radiator, a coolant salt pump, and then returned to the primary heat exchanger [4][33][38].

The reactor was originally fueled with approximately 218 kg of uranium (30% U-235 and 70% U-238), then later refuelled with another 37 kg or so of uranium, this time consisting of 80% U-233 and 20% U-235, making the MSRE the first nuclear reactor to operate with U-233 [31][36][38].

2.4.2 Experimental Findings of the MSRE

The results produced from the MSRE, and the conclusions drawn from them reshaped the nuclear industry in many ways and continue to be a source of inspiration for present-day vendors. The primary, and perhaps most important, conclusion from the MSRE was that a molten salt fueled reactor concept was feasible and viable. Its maintenance was accomplished safely and without excessive delay; no radiation detectors were set-off during these operations, and they were completed within the allotted timeline as discussed in the MSRE quarterly reports [7][39]. The addition of uranium and plutonium batches to the salt took place in a matter of days; the recovery of uranium by fluorination was also successful. The MSRE confirmed expectations and predictions [7][40]. The experiment demonstrated that the fuel salt was immune to radiation damage and did not corrode the graphite core. Similarly, the corrosion of Hastelloy-N was also negligible [36][38]. Prior calculations on the neutronics, such critical loading, reactivity coefficients, dynamics, and long-term reactivity changes, were confirmed by the experiments. It was also noticed that by limiting oxygen in the salt, the tendency of fission products to be dispersed from contaminated equipment during maintenance would decrease [8][31].

The experiments also provided information regarding the excessive production and unexpected transport of tritium in a molten-salt reactor. It was recognized prior to the operation of the reactor that the MSRE would produce significant amounts of tritium, which is a ternary fission product of Uranium that occurred at a rate of about one atom per 10^4 fissions. The tritium atoms were predominantly produced (around 80%) through thermal neutron absorptions in Lithium-6, an isotope found in the fuel of the reactor (FLiBe) [41].

$$\mathrm{^6_3Li} + \mathrm{^1_0n} = \mathrm{^4_2He} + \mathrm{^3_1H} \tag{2.1}$$

Similarly, fast neutrons can also be absorbed by Lithium-7 to produce tritium, but this reaction is far less probable [41].

$$\ce{^7_3Li} + \ce{^1_0}n = \ce{^4_2He} + \ce{^3_1H} + \ce{^1_0}n \tag{2.2}$$
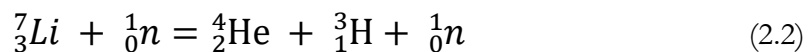
During the design and initial operation of the MSRE, it was expected that most, if not all, of the tritium produced would exit the system through the stack. However, as the experiment progressed, tritium was detected in liquid waste and the metallic structures of the reactor, all of which were promptly treated with newly instated health precautions [41][42]. Figure 2.10 illustrates the production and transport pathways of tritium in the MSRE.
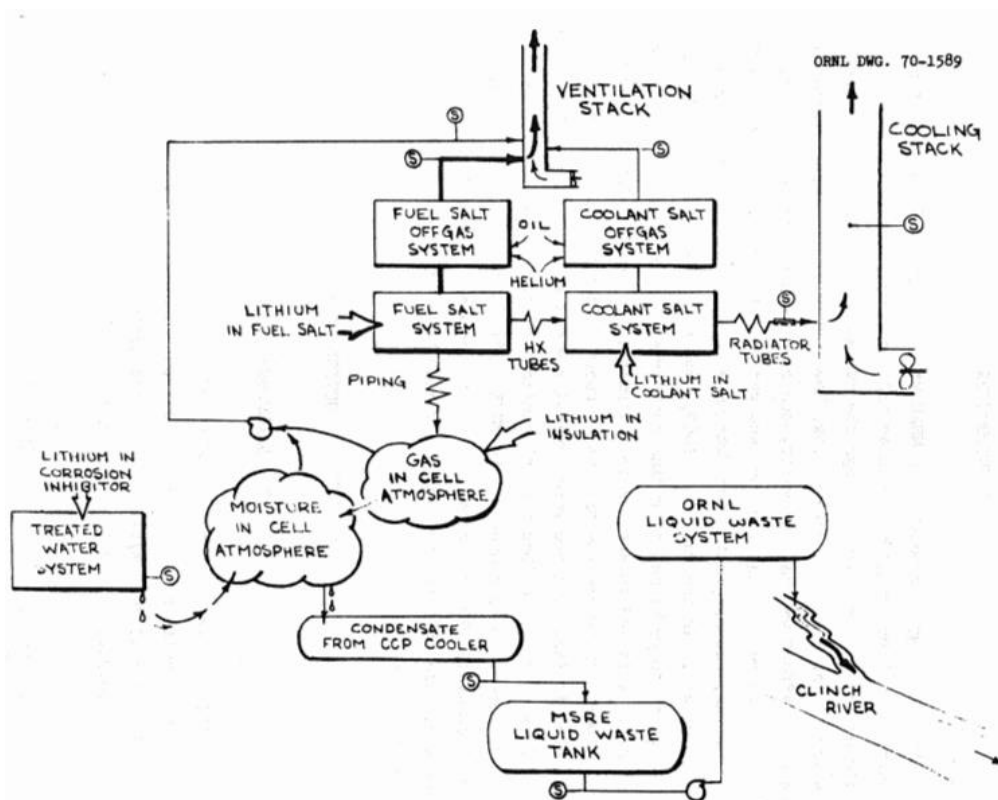
Figure 2.10: Tritium Production and Transport in the MSRE [41].

Since tritium is a beta emitter, it is not dangerous externally as it is unable to penetrate clothing or the skin. However, it becomes a health hazard if inhaled or ingested. Thus, this production and presence of tritium in molten salt reactor technologies will also have to be addressed during decommissioning [42].

A surprising and unanticipated finding was the discovery of intergranular cracking in all the salt-facing metal surfaces as a result of tellurium (a fission product produced in the fuel) embrittlement. The crack growth observed was so rapid that it would be problematic for the originally planned thirty-year operating life of thorium breeder reactors and MSRs. In the

short-term, the cracking can be reduced by adding small quantities of niobium to the Hastelloy-N; a long-term solution would still require further studies [43]. Recent experimental results presented by Liu *et. al.* demonstrated that when compared to Inconel-600 and Hastelloy-X, Hastelloy-C-276 exhibits the best corrosion resistance in molten FLiNaK salts at 750 °C [44]. Figure 2.11 below are the cross-sectional SEM images of Inconel-600 and Hastelloy-X, Hastelloy-C-276 that have been corroded by FLiNaK at 750 °C for 320 hours.
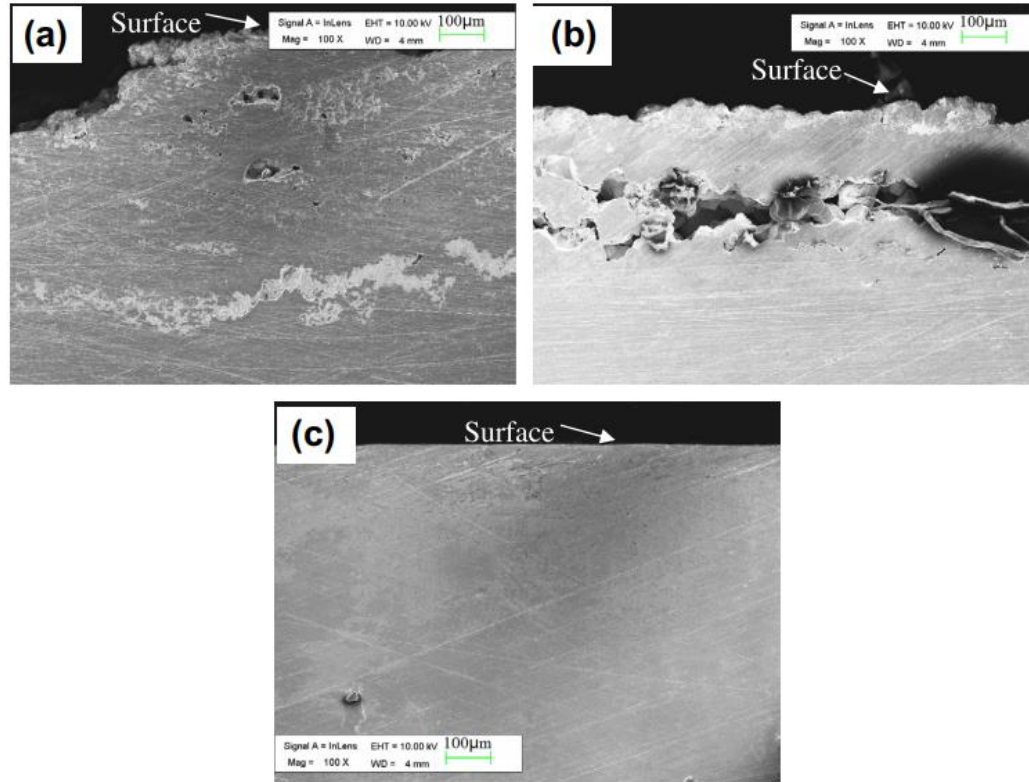
Figure 2.11: SEM images of the cross-sectional samples after being corroded in FLiNaK salts at 750 °C for 320 hours: (a) Inconel 600, (b) Hastelloy X and (c) Hastelloy C-276 [44].

Overall, the results and experience from the MSRE imply that the decommissioning of such a facility would be administratively complex and technically challenging in addition to being expensive. The presence of tritium can pose additional health risks to the workers as well as the environment. Extensive decontamination would also be required for all salt-facing components, which may or may not be repurposed while the radioactive fuel and flush salts remain in storage for indefinite periods of time. All of which are processes more extensively discussed in the following section which details the decommissioning activities performed at the MSRE facility thus far.

2.4.3   Shut-down and Decommissioning

The MSRE was shut down in December of 1969; its decommissioning planning began almost immediately and continues until present day due to a series of technical challenges. The decommissioning project was originally predicted to cost upwards of 30 million USD, but by 1988, it was suggested that the true costs would be at least triple the initial estimates [45].

The primary concerns revolve around the treatment and disposal of more than five tonnes of solid fuel salt that contained over 30 kg of fissionable Uranium-233; fission products, as well as higher actinides were also problematic [44]. This is further complicated by the chemistry of the mixture; radiolysis reactions in the solid waste salt releases elemental fluorine gas and as a countermeasure, the salt was reheated annually to $\sim$ 150 °C (302 °F) until 1989. [44-46]. Various supporting and investigative studies were conducted, including:

a)   a broad scope analysis of possible options for storage/disposal of the salts;

b)   calculation of nuclide decay in future years;

c)   technical evaluation of the containment facility and hot cell penetrations;

d)   review and update of surveillance and maintenance procedures;

e)   measurements of facility groundwater radioactivity and sump pump operation;

f)   laboratory studies of the radiolysis reaction; and

g)   laboratory studies on determining the suitable "getter" for elemental fluorine [45].

Geological and hydrologic factors of the surrounding area were also considered to analyze the potential implications of the entombment of the fuel with concrete. The results of this evaluation demonstrated that the fuel salt cannot simply be left in its form and location permanently; however, extended storage is feasible for 20 to 30 years- and at the time, projected for even longer. The studies recognized that for the "Safe Storage" or deferred dismantling strategy of decommissioning, some facility modifications to the MSRE site were necessary [43][44].

The 1988 ORNL report *Decommissioning of the MSRE* recommended that for a permanent basis of disposal, the fuel and flush salt mixture should be remelted and repackaged into smaller containers for ease of handling. Fluorine getters should also be added to eliminate the need for periodic reheating. These procedures alluded to a solution to final disposal yet recognized

that none of them were available at the time of the publication of the document [8]. These methods included the disposal of MSRE salts and components in a high-level waste repository, in the Waste Isolation Pilot Plant, via intermediate depth disposal, or blending the salt in with a fluoride-based high-level liquid waste from reprocessing at other Department of Energy (DOE) sites [45-47].

The lack of conclusive decommissioning actions taken for the MSRE became a bottleneck and an obstacle for new, Gen IV MSR vendors as they worked towards licensing their designs. The enthusiasm dedicated towards the technical design and operation of the MSR system is not shared towards its inevitable decommissioning; vendors often neglect to include any concrete plans for the end-of-life activities of their products. This inability to provide a solid, thorough decommissioning plan to the Canadian regulatory body, the CNSC, in many ways further inhibits the chances at commercial application.

2.4.3.1 Increased Pressure to Take Decommissioning Actions

There is a need to take more permanent decommissioning actions with regards to the MSRE facility in recent years. Even though surveillance and maintenance (S&M) activities have been providing adequate extended storage of the MSRE and its components, the DOE, ORNL, and other stakeholders agree that a lasting decommissioning outcome must be achieved [35][45].

This is both to avoid interfering with ongoing ORNL research operations as well as preventing any accidental releases into the environment through mediums such as groundwater or air. However, the costs of S&M activities are expensive; the salts required annual reheating until 1988 while physical barriers including concrete cell walls and the stainless-steel liners must be constantly inspected for structural integrity to ensure the proper storage of the waste-salt tanks [35][45][46]. Table 2.2 below is a summary of all the major decommissioning and dismantlement (D&D) activities performed up until October 2021.

Table 2.2: Major D&D Activities Performed "to Date" [35].

Time Frame	Notable Activities
1971-1989	Routine maintenance and "salt annealing" (to prevent F_2 accumulation in drain tank cell)
1994	Positive confirmation of "uranium migration" • Failed off-gas valve resulted in notable uranium deposits in off-gas charcoal bed
1995-2000	Uranium denaturing and removal, install Reactive Gas Removal System
2001-2008	Restoring salt chemistry, defueling, attempt salt transfer
2008-present	Reactive gas management operations, surveillance and maintenance

2.4.3.2 Challenges in Decommissioning

The three major challenges regarding the D&D activities of the MSRE are that:

1) the MSRE is an aging facility with equally old equipment (50 years +);

2) the presence of radiological and other chemical hazards makes for a challenging work environment. Workers would require significant personal protective equipment (PPE), special tools, as well as portable maintenance shields (PMS); and

3) the manner in which waste salts will ultimately be disposed of has yet to be determined [35].

Concerns over Potential breaches in the drain tanks worsened after the MSRE Remediation Project discussed in further detail in the following section. Considered to be highest risk at the facility, a rupture in these salt-containing tanks risks the release of radiological hazards in addition to F_2 and HF, which are difficult to isolate. There is a constant need to assess the integrity and the extent of corrosion on heat exchanger thimbles and the walls of the waste salt tanks. Piping and tubing containing residual salt, however, are infrequently monitored. The site also primarily relies on the original ventilation system of the MSRE for "safety significant functions" [35, 45-47]. Figure 2.12 below is a diagram of the MSRE fuel salt drain tank.
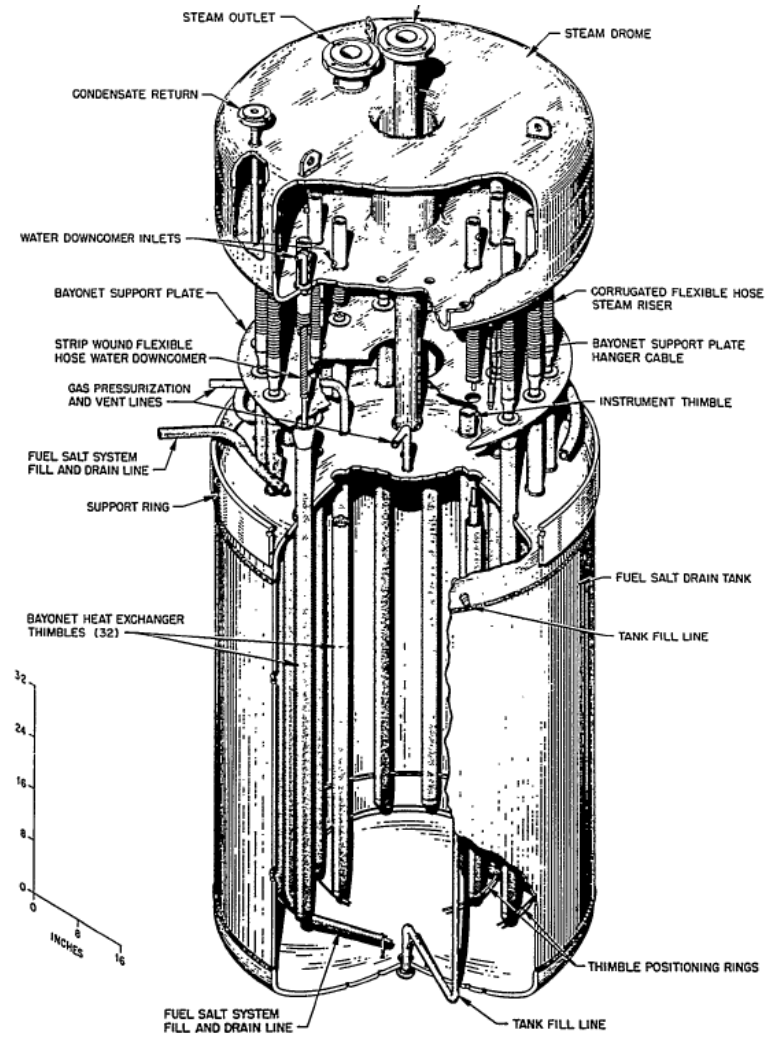
Figure 2.12: MSRE Fuel-Salt Drain Tank [45].

The working conditions of D&D activities at the MSRE are also intensely difficult; portable maintenance shields (PMS) are necessary to ensure adequate ventilation flow rate -as seen in Figure 2.13- whenever workers access the drain tank pit while wearing extensive PPE to mitigate hazardous fluorine gas and radiological contamination.

Figure 2.13: Workers Operating the Portable Maintenance Shield [35].

Figure 2.14 illustrates the position of the PMS in relation to the salt tanks.

1. Portable Maintenance Shield
2. Fuel Drain Tank #1
3. Fuel Drain Tank #2
4. Fuel Flush Tank
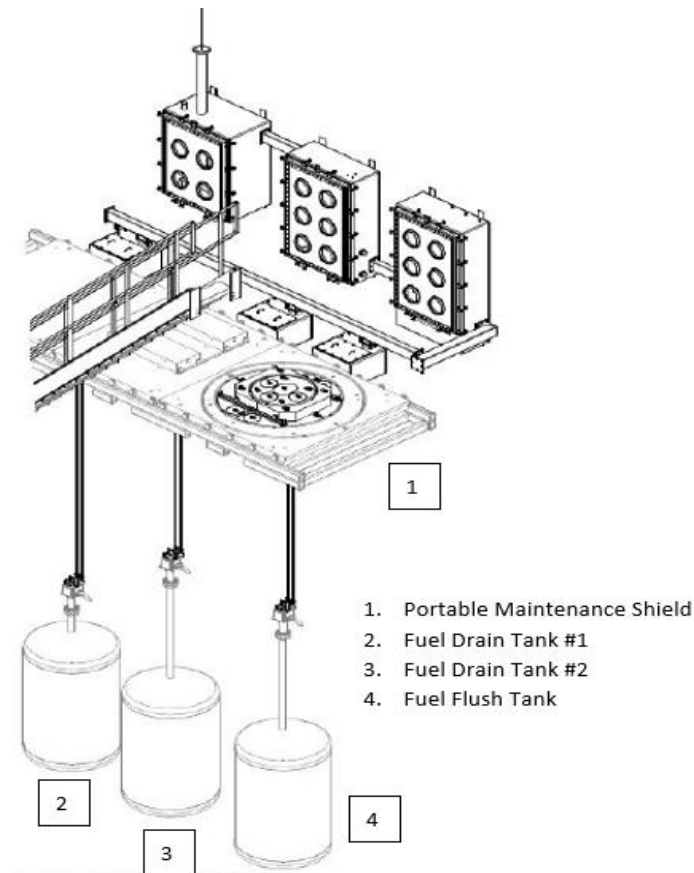
Figure 2.14: Location of the PMS in relation to the Fuel Drain and Flush Tanks [35].

The work area surrounding the salt storage tanks is highly radioactive mainly due to Cesium-137, other fission products, and Uranium-232 progeny (Tl-208). Exposure rates from Fuel Drain Tank (FDT) #1 and #2 exceed 1000 Roentgen and require the use of remote tools on top of significant shielding [35][46]. Table 2.3 summarizes the radioactivity of waste-salts in the fuel drain and flush tanks (FFT):

Table 2.3: Radioactivity and Volume of Waste-salt in Fuel Drain and Flush Tanks [35].

Location	Volume of Salt	Radioactivity (Ci)	Radioactivity from CS-137 (Ci)
Fuel Drain Tank #1	0.99 m^3	6800	3000
Fuel Drain Tank #2	0.88 m^3	5700	2500
Fuel Flush Tank	1.93 m^3	200	2500

The final challenge lies in the inevitable generation and disposal of waste from any D&D projecting of the MSRE. This includes:

- the fuel, coolant, and flush salts;
- any salt-contaminated components;
- the uranium laden charcoal collection canister;
- residual uranium in the charcoal beds;
- Asbestos;
- Lead; and
- Any PCB-contaminated equipment.

Since the decision for final disposal has yet to be made, propositions for sending the waste products to the Waste Isolation Pilot Plant (WIPP) have been made. However, the salts will need to meet the fissile material content limit and require passive fluorine management. Preliminary analysis done by United Cleanup Oak Ridge for ORNL in 2021 suggests that the salts do meet the legal limit as identified in Table 2.4.

Table 2.4: Preliminary Analysis of MSRE Salt in Meeting WIPP Waste Acceptance Criteria [35].

Regulation	RH Waste Limit	FDT #1 Salt	FDT #2 Salt	FFT Salt
LWA Sec 7(a)(2)	Specific Activity <23 Ci/L	9.43 Ci/L	9.57 Ci/L	0.167Ci/L
LWA Sec 2(18)	TRU Activity Density >100 nCi/g	13696 nCi/g	13711 nCi/g	275 nCi/g

2.4.3.3 The MSRE Remediation Project

In the years following the shut down and transition into indefinite storage of the MSRE, indications of the migration of radioactive materials in the piping connected to the drain tank cell and the off-gas system were noted [48]. Specifically, increased radiation levels were detected in a service area next to the drain tank cell. Alpha activity was observed during maintenance activities on the off-gas system while subsequent Gamma scans indicated the presence of Thallium-208, a decay product of Uranium-233. Consequently, the annual reheating, referred to as "annealing" by the ORNL, of the salt was halted in December 1989 partly because this procedure was speculated to have aided the migration of the radioactive materials [47-50].

In March 1994, positive confirmation of uranium migration was made by the ORNL when a sample withdrawn from the off-gas system serving the drain tanks was found to be unexpectedly containing UF_6. Furthermore, it was discovered that a faulty valve had led to the leak of about 3.9 kg of the UF_6 which deposited onto the auxiliary charcoal bed while another 1 kg or so migrated to four other charcoal beds via the off-gas system [33-35][45-49]. Following this revelation, the extensive MSRE Remediation Project was initiated to assess, control, remove and recover the Uranium-233, convert the recovered uranium to uranium oxide (U_3O_8) for long term storage, and to decommission the reactor as much as possible [8][35][45-48]. Figure 2.15 outlines the key components of the uranium recovery process.
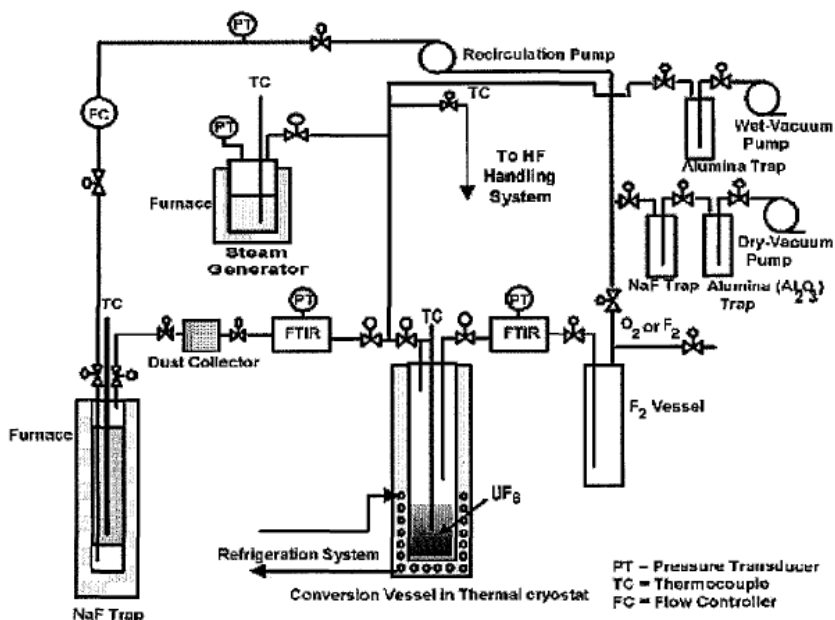
Figure 2.15: Diagram of Major Components of the Uranium Recovery and Conversion Process [48].

From 1995-2000, the primary tasks of remediation project consisted of the:

- removal and denaturing of Uranium-233 in the charcoal beds;

- recovery of Uranium from the piping system;

- removal of Uranium from the fuel salt;

- conversion to Uranium-233 to uranium oxide; and

- installation of the Reactive Gas Removal System.

Fuel recovery tasks were completed by the mid-2000s; the reactor was de-fuelled and salt chemistry was restored through hydrofluorination processes. Currently, the MSRE facility continues to require reactive gas management in addition to scheduled surveillance and maintenance operations [35][45-47]. The overall costs of this clean-up project were estimated at about 130 million USD [51].

2.4.3.4 Current Status of the MSRE

The residual fuel salt remains stored in the two fuel drain tanks (each 2.27 m^3) as of today, each having less than 2.5 kg of Uranium-233. Flush salts (FLiBe) which contain less than 2% of uranium and fission products are stored in the fuel flush tank. Volatile fission products are

treated via an off-gas system and not retained in fuel [35][50]. A series of planned, upcoming facility upgrades include additional sump pump systems, an electrical distribution system, fire detection and suppression measures, process monitoring systems, as well as improved roof and drainage. The ORNL also intends to replace the Reactive Gas Removal System with a Continuous Purge System while incorporating more automation into their surveillance and maintenance operations to lower radiological risks to facility workers [35][51].

2.5   Molten Salts

In terms of chemistry, a salt is a chemical compound composed of ionically bonded positively charged cations and negatively charged anions, resulting in a compound with no net charge. Likewise, a molten salt is a salt that is solid at standard temperature and pressure (STP = 0 °C and 1 atm) but enters the liquid phase when heated to and beyond its melting temperature. Molten salts are unlike ionic liquids, which are salts that are liquid at, or close to, room temperature [52]. These molten salts are highly corrosive in their hot, liquid state and pose one of the main design challenges of the MSR. The structural alloys of the reactor must be highly resistant to corrosion and REDOX reactions and must be carefully managed to mitigate any safety risks (such as ruptures and spills) [31].

The first salts developed were the molten fluoride salts used by the ORNL since fluorine only has one stable isotope, Fluorine-19 (100% abundance), compared to lithium or chloride-based salts [53]. Familiar to both aluminium and uranium industries, all the enriched uranium used in reactors today have been converted to and from a fluoride form during the enrichment process [31][36][52]. As Gen IV MSR designs were developed, the types of molten salts being proposed for use as fuel, coolant, or flushing agents have diversified as well.

The following sections will discuss the properties of the various fuel, coolant, and flush salts historically used as well as those currently being developed and proposed.

2.5.1   Fuel Salt

As mentioned before, MSRs can use either liquid or solid fuel depending on its design. However, there are substantial and fundamental differences between the two fuel options. Their thermal, chemical, and physical behaviours must be sufficiently understood during the

fuel qualifying process to ensure adequate modelling under normal and accident conditions [54].

Since a liquid fuel salt serves both as the nuclear fuel and primary source of heat transfer, it must meet the requirements for both purposes. Eutectic mixtures of molten salts are usually selected for their lower melting point, usually around 450 °C, while boiling temperatures are in the range of 1400 °C [19]. It could be argued that the boiling of molten fuel salt within a reactor could potentially have catastrophic effects on the system, but since most MSRs are designed to operate at temperatures around 600-800 °C, there is still a significant safety margin that makes the event extremely unlikely [10]. Liquid fuel also offers the advantage of bypassing critical heat flux considerations and risks associated with the melting of fuel elements in severe accident conditions. Similarly, modelling challenges regarding multi-phase flow found in Light Water Reactors also do not hold for liquid fuel salts. Although there is less flexibility in the margins of properties such as reactivity in solid fuels, they can still be adjusted for safety using chemistry controls. Overall, liquid fuels are more favourable and are selected for most MSR designs. Some of the key features of both types of fuels are illustrated below in Figure 2.16.
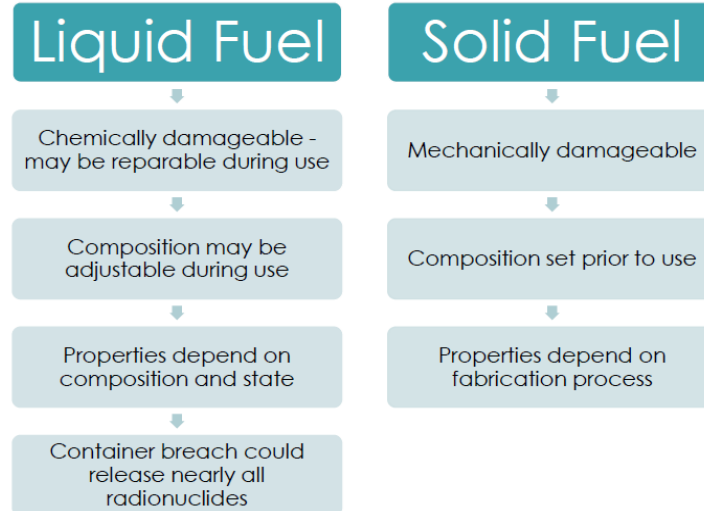
Figure 2.16: Key Differences between Solid and Liquid Fuel Salt Mixtures [54].

In terms of decommissioning, one may expect solid fuel to be more compact. Fewer components would be in direct contact with the fuel which would lower the amount of high-level radioactive waste and limit the contaminated areas. On the other hand, the use of liquid fuel would result in the contamination of all salt facing components. The reactor structure

would have to be decontaminated before it is either released from regulatory control, recycled, or disposed of. However, the liquid fuel salts do not have a mechanically determined lifetime, unlike solid fuel, and is likely to be more consistent in property and behaviour [54].

Halide characteristics of fuel salt mixtures such as high boiling points at low pressure and natural circulation heat transfer properties are applicable to all MSRs [52][54]. Elements such as fluorine, chlorine, and lithium are typically considered for use in molten salt compounds [56].

Some fuel salt compositions of current proposed MSR designs remain proprietary. Limited information is available with regards to their specific properties. However, they remain invariably fluoride-based and a combination of LiF, BeF_2, ThF_4, and UF_4 are the most common mixtures used for MSRs [56].

A study conducted by the ORNL which investigated the physical properties of seven molten salt mixtures (four fuel salt, two coolants, one flush salt), provided experimental and estimated values on properties such as viscosity, phase transition behaviour, electrical conductivity, density, heat of fusion, vapour pressure, and compressibility. However, the following properties have a more direct impact on the selection of molten salt mixtures in terms of decommissioning [57]:

- Expansivity; and
- Solubility of the gases He, Kr, Xe, BF_3.

The four fuel salt mixture samples, each containing some quantities of LiF, BeF_2, ThF_4, and UF_4 were selected based on the decision of the ORNL to combine fissile and fertile material within the same loop [16]. It is worth noting that due to the age of the document and the significant margins of error the authors provide, that these numbers are an estimate and should not be relied upon. A much more recent ORNL report detailing fuel salt qualification technologies highlighted the importance of other relevant parameters in molten salt fuel such as wettability, retention of radionuclides, storage stability, and interactions with various metals [57].

Table 2.5: Mixture Composition of the Four Fuel Salts [57].

Salt Mixture	Composition (mole %)			
	LiF	BeF$_2$	ThF$_4$	UF$_4$
F1	73	16	10.7	0.3
F2	72	21	6.7	0.3
F3	68	20	11.7	0.3
F4	63	25	11.7	0.3

Salts F1 and F3 were thought to be appropriate fuel for a prismatic configuration of the graphite moderator since the lesser concentrations of BeF$_2$ and ThF$_4$ might prove more favourable with rare-earth fission product removal while salt F2, with low thorium, would be ideal for a reactor where good breeding performance is not a prime consideration. Alternately, the high beryllium concentration of salt F4 would improve breeder performance through the greater opportunity to increase neutrons by the (n, 2n) reactions [36][52][55-58].

The mixture that was eventually selected as the fuel salt of the MSRE and primary coolant was LiF-BeF$_2$-ZrF$_4$-UF$_4$ (mole ratio: 65-29-5-1), whose base-mixture, FLiBe, was also the secondary coolant and flush salt for the system. FLiBe will be discussed in more detail in a later section.

2.5.1.1 Secondary Coolant Salts

The secondary coolant salt removes heat from the primary coolant, *i.e.*, fuel salts in an MSR. Like fuel salts, these mixtures are largely fluoride-based because it gives them a stable nature. Fluoride salts are also excellent media for heat transfer due to their high thermal conductivities and heat capacities. The secondary coolants, unlike the fuel salts, are non-fissile [57].

2.5.1.2 Flush Salts

Flush salts are fluoride-based molten salt mixtures used to flush out any remaining radioactive salt deposits within the primary and secondary cooling loops whenever salt-facing reactor components are drained, either for maintenance or at the end of service life of the MSR. Flush salts usually do not contain sufficient radionuclides to self-heat when stored long-term but consist of various fission products and are radioactive, though to a lesser extent compared to the fuel salt. The flush salts and their containers would remain under regulatory control until

a solution becomes available for their decommissioning, repurposing, or disposal; they would likely require maintenance and surveillance throughout storage [58].

2.5.2 FLiBe

FLiBe is a molten salt composed of a mixture of lithium fluoride (LiF) and beryllium fluoride (BeF_2). The mixture ratio of this stoichiometric compound is 2:1 (64-34 mole %), forming Li_2BeF_4 [55]. Both a nuclear reactor coolant and a solvent for fissile and fertile materials, FLiBe served both purposes in the 1960s MSRE in addition to being used as the flush salt [34][51].

2.5.2.1 Physical, Chemical, and Thermal Properties

FLiBe has a relatively low melting point of 459 °C, a boiling point of 1430 °C, and a density of 1.94 g/cm^3. It also has a volumetric heat capacity that is slightly higher but similar to that of water (4180kJ/m^3K) at 4540 kJ/m^3K making FLiBe more suitable for typical reactor conditions [59]. In addition, molten FLiBe can be used as a coolant at high temperatures without reaching high vapour pressure; unlike sodium and potassium metals, which are also candidates for high-temperature coolants. FLiBe does not react violently with air or water.

The eutectic mixture of FLiBe contains slightly more than 50% of BeF_2 and has a melting point of 360 °C [57]. Although a lower melting point may appear desirable at first, the eutectic mixture of FLiBe never had any practical applications because the addition of BeF_2 caused an overwhelming increase in the viscosity of the mixture. BeF_2 on it own behaves as a glass and is only fluid in salt mixtures with enough molar percent of Lewis base. Lewis bases are atomic or molecular species with highly localized highest occupied molecular orbitals such as the alkali fluorides. These compounds will donate fluoride ions to the beryllium, breaking the glassy bonds which increase viscosity [60].

In its solid state, FLiBe appears transparent to white, with visible crystalline grains, but upon melting, it turns into a completely clear liquid as seen in Figure 2.17. This optimal transparency makes FLiBe a desirable coolant salt because it allows for easy visual inspection of any contaminants or impurities dissolved in the salt in a laboratory setting. However, soluble fluorides such as UF_4 and NiF_2, can dramatically change the salt's color in both solid and liquid

state. This made spectrophotometry a viable analysis tool, and it was employed extensively during the MSRE operations [61-64].
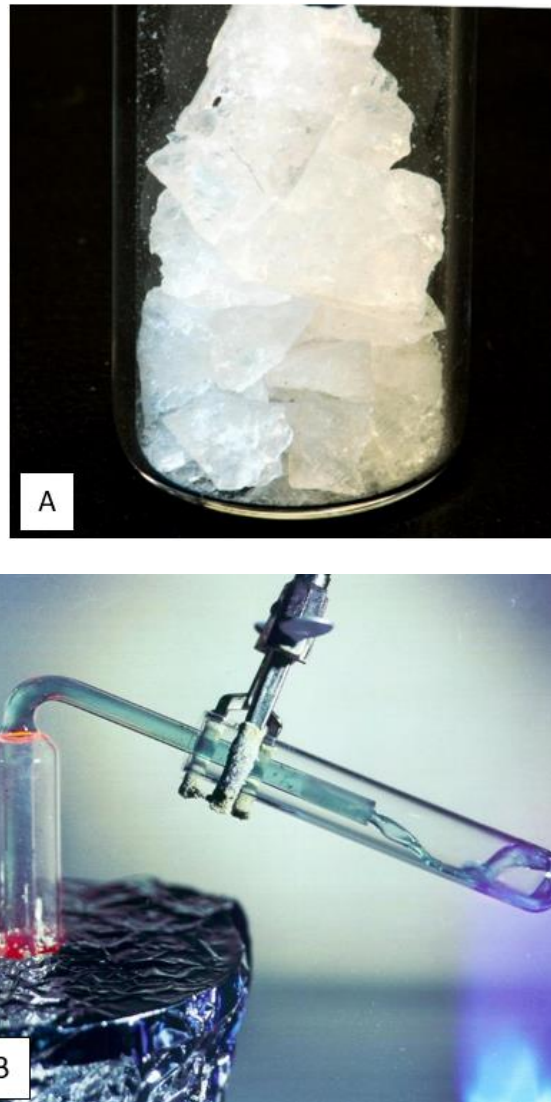
Figure 2.17 (a): FLiBe in Solid State (b): Molten FLiBe: The Blue-green Tint is from Dissolved Uranium Tetrafluoride [64].

2.5.2.2 Nuclear Properties

FLiBe is an effective neutron moderator because of the low atomic weight and large scattering cross-section of lithium, beryllium and less prominently, fluorine. The atomic structure and nuclear properties of these elements enable them to efficiently thermalize fast neutrons through elastic collisions. Since Lithium-6 (approximately 7.5 % of natural lithium) tends

to absorb neutrons thus producing alpha particles and tritium, nearly-pure Lithium-7 (99.993%) is used instead for the MSRE. Figure 2.18 illustrates the fuel salt-FLiBe with Uranium 233 tetrafluoride- of the MSRE in both solid and liquid state. In its solid form, the fuel salt takes the appearance of irregular, opaque, turquoise crystals which, when molten, becomes a transparent, light blue-green fluid. Lithium-7 in the compound gave the FLiBe mixture a small neutron absorption cross-section and assisted in breeding purposes. When Lithium-7 does absorb a neutron, it instantaneously decays via successive beta and then alpha decay into a beta particle and two alpha particles [62]. Beryllium will occasionally disintegrate into two alpha particles and two neutrons when hit by a fast neutron. Fluorine has a non-negligible cross section for (α,n) reactions, which needs to be taken into account when calculating neutronics [66][67].
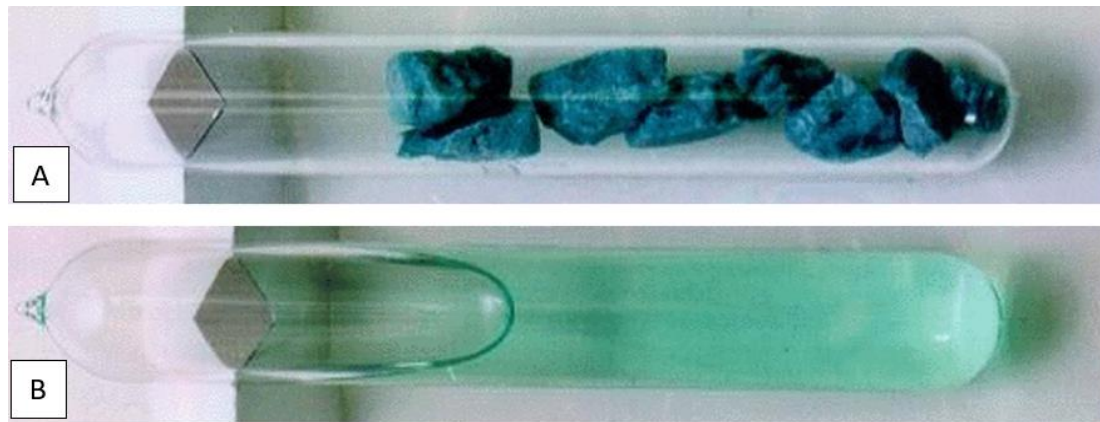
Figure 2.18 Samples of FLiBe with Uranium-233 Tetrafluoride [67]
(a): Top - Solidified Crystals (b): Bottom - Molten Liquid.

2.5.3 FLiNaK

FLiNaK is a ternary eutectic alkaline metal fluoride salt mixture of LiF-NaF-KF (46.5-11.5-42 mol%). It was heavily researched by the ORNL in the late 1950s as a potential coolant candidate for the MSRE because of its low melting point, high heat capacity, and chemical stability at high temperatures [68][69]. In the end, FLiBe was selected for use in the MSRE instead of FLiNaK because of its more desirable neutron cross-section. However, Gen IV reactor vendors are now contemplating the use of FLiNaK in future molten salt SMR designs [6][21].

FLiNaK is the salt mixture used in all experiments that will be discussed in this work. In addition to being a potentially promising fuel and coolant salt for Gen IV MSRs [6][10], this mixture was selected mainly because it is a non-proprietary salt that can be synthesized and prepared with readily available compounds. Similarly, publicly-accessible literature resources can also provide a baseline with regards to the behaviour of FLiNaK throughout the experiments conducted in later chapters.

2.5.3.1 Physical, Chemical, and Thermal Properties

A "sister salt" of FLiBe, FLiNaK has a melting point of 454 °C and a boiling point of 1570 °C [19]. It is worthy to note that the widely-accepted melting temperature of 454 °C is based on phase-rule type cooling curves; thus, some sources recommend that 462 °C, determined using heat of fusion, be used instead for conservative operation [70][71]. The density of FLiNaK has also been investigated extensively by numerous sources, dating from the 1960s until present day. It was determined that within the temperature range of 940 to 1170 K, the density of FLiNaK is best represented by the following four correlations presented in Table 2.6 and plotted in Figure 2.19, though a density of 2.02 g/cm^3 has been suggested for use in general reactor calculations [19].

Table 2.6: Density Correlations of FLiNaK between 940 to 1170 K [19][72-76]

Density Correlation (kg/m^3)	Uncertainty (%)
2579.30 - 0.624 x T [K]	2
2603.00 - 0.669 x T [K]	3
2655.64 - 0.680 x T [K]	2 - 4
2729.29 - 0.730 x T [K]	5
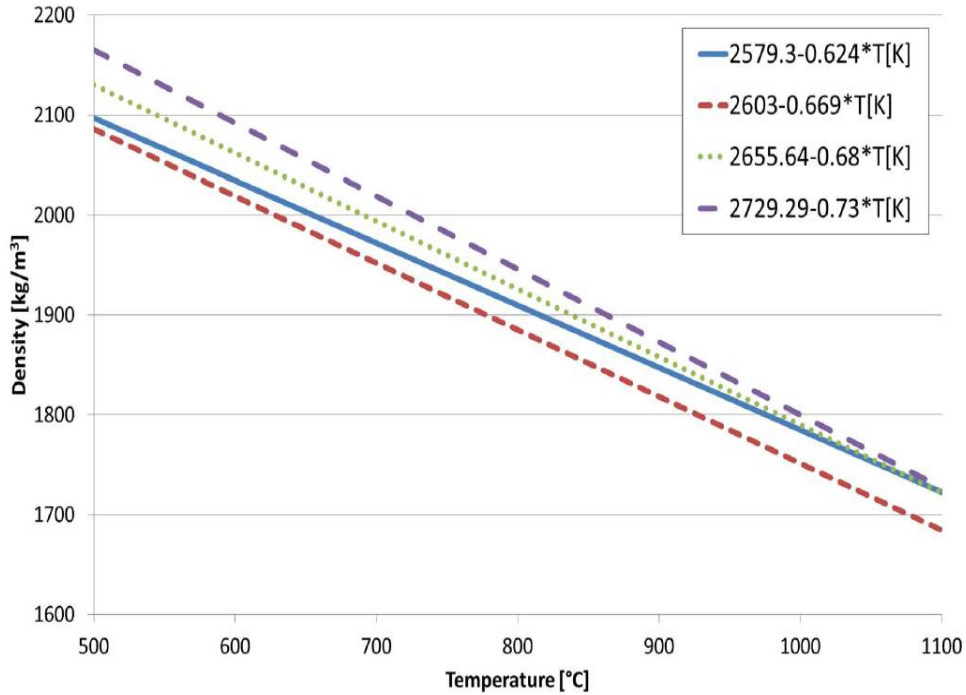
Figure 2.19: FLiNaK Density vs. Temperature [19].

FLiNaK has a thermal conductivity of 0.92 W/m-K and a volumetric heat capacity of 3807.4 kJ/m^{3}K [58]. This implies that the salt is also suitable for typical MSR operating conditions [57]. Furthermore, molten FLiNaK has a low vapour pressure of about 0.7 mm Hg compared to that of FLiBe, which is about 1.2 mm Hg at a temperature of 900 °C [58]. Vapor pressure is a concern because in these high-temperature salt systems, a purged cover gas is necessary. The transport of large amounts of salt vapour into the cover gas system can cause contamination problems. The vapour pressure of a salt mixture is very sensitive to its composition, certain compounds such as ZrF_4 and BeF_4 would increase the risk of salt vapour leaks which can lead to system instability [60][77].

Early ORNL studies of FLiNaK also confirmed that the mixture is capable of dissolving "useful quantities" of fissile and fertile material while remaining stable under intense radiation [76][77]. The fluid transport properties of FLiNaK were also on-par with FLiBe, though it was noted by S. Cantor et. al. that molten FLiNaK was significantly less viscous (2.9 vs. 5.6 centipoise) [57].

Since Molten salts exhibit normal fluid behaviour and are Newtonian fluids, their densities would also exhibit the typical exponential decrease in viscosity, μ, with the reciprocal temperature [60]. Consequently, correlations are often used to calculate the viscosity of FLiNaK at specific temperatures [19]. Figure 2.20 presents a plot of common correlations used for viscosity calculations between the temperatures of 770 to 1270 K.
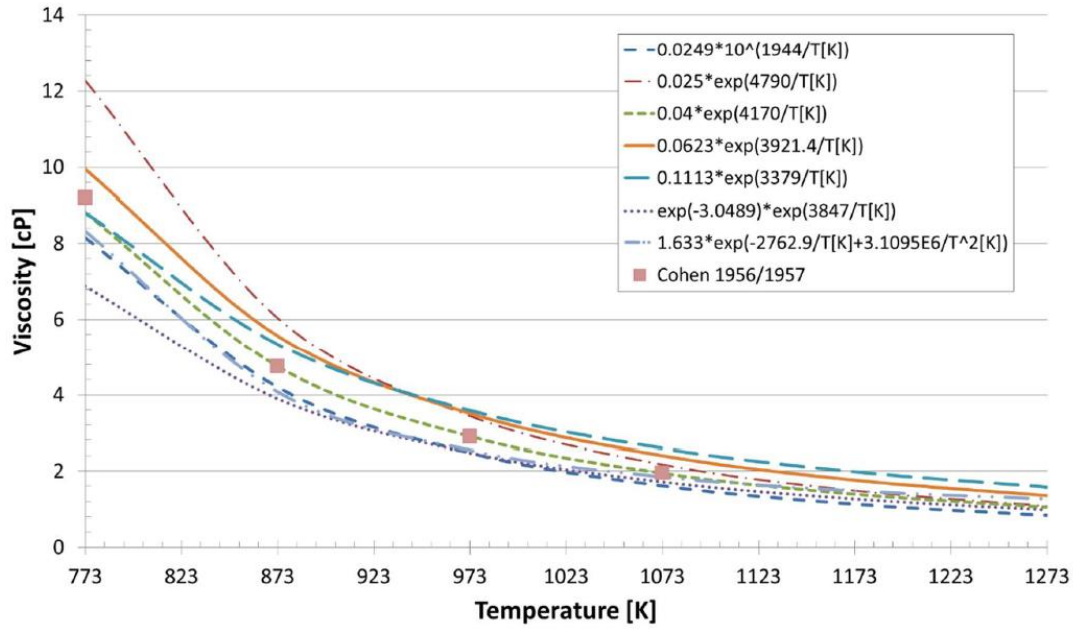
Figure 2.20: FLiNaK Viscosity vs. Temperature [19].

Visually, FLiNaK appears white and is opaque in its solid form. Taking the shape of its synthesis container, the resulting FLiNaK ingot has smooth exterior surfaces with slight granularity along its edges [8][66]. Once melted, it becomes a colourless, transparent liquid. Similar to FLiBe, this optical transparency of FLiNaK also allowed for the visual inspection for contaminants or impurities dissolved in the molten salt when in a laboratory setting and was considered to be an advantage. It is expected that the inclusion of soluble fluorides would also change the colour of the salt in both its solid and liquid state, making spectrophotometry analysis viable as well [10]. Figure 2.21 shows a photograph of commercially sold FLiNaK ingots by Copenhagen Atomics Inc. while Figure 2.22 presents images of a FLiNaK sample synthesized in this work in both solid and liquid states.
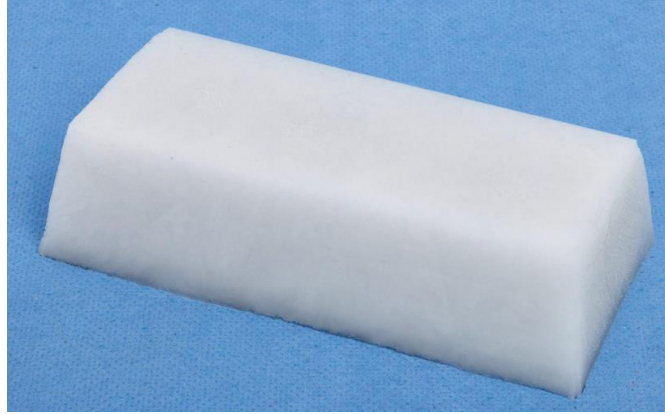
Figure 2.21: Loop Grade FLiNaK Ingot as Sold by Copenhagen Atomics Inc. [79].
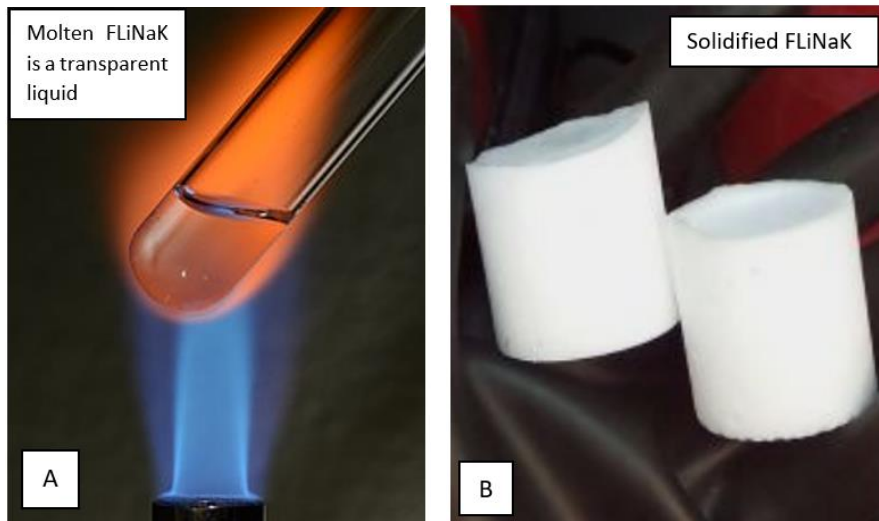
Figure 2.22 (a): Liquid Molten FLiNaK (b): Solid FLiNaK [79].

Even though the exact chemical structure of FLiNaK has not been determined and is not entirely well understood [80], it is generally recognized that FLiNaK is the main alternative to FLiBe due to its similar physico-chemical and thermal properties as well as low toxicity.

2.5.3.2 Nuclear Properties

The nuclear properties of FLiNaK are less favourable than those of FLiBe, which ultimately led to the latter salt being selected for use in the MSRE despite their very similar physiochemical and thermal properties. The ORNL has conducted numerous assessments of the neutronics properties of potential coolant-salts, including FLiNaK, and examined their

effects given standard operating conditions of an AHTR. The long- and short-term effects of neutron activation on the salts were also investigated [60].

Two main nuclear properties, the parasitic-neutron-capture rate and moderation ratio, are especially crucial in determining the suitability of a candidate salt for use in thermal-spectrum Advanced High-Temperature Reactors (AHTR)[60]. This is because such cores are usually composed of the following three main components: the fuel, the moderator, and the coolant. The moderator material is almost always graphite because it has a very small probability of capturing neutrons and is exceedingly efficient in reducing their energy for subsequent fission reactions. Since any neutrons that are captured and fail to generate a fission reaction are considered parasitic to the critical chain reaction in the core, it is then evident that the major source of parasitic neutron capture would be the liquid-salt coolant [60][66].

Consequently, the parasitic-neutron-capture rate is directly related to the efficiency of fuel utilization in MSRs. In the case of FLiNaK, the total neutron capture (per unit volume) relative to graphite is 90 while the same property for FLiBe is 8. Similarly, if the coolant can also moderate neutrons, this benefit can offset the parasitic capture. However, the moderating ratio of FLiNaK is 2, while that of FLiBe is 60 [60][72].

Table 2.7 compares the neutronic efficiency of FLiNaK to other candidate salts and materials. As seen in the table, the BeF_2 salts (FLiBe) have the best neutronics properties with large moderating ratios and small parasitic capture rates, while the alkali fluorides (FLiNaK) have the worst [60].

Similarly of concern are the effects of short-and long-term activation of candidate coolant salts and their associated hazards regarding maintenance and decommissioning. Short-term activation, defined in the case of this study to be within ten days, observes the activation of coolant materials as a result of the parasitic neutron captures in the salt [60]. Since the alpha and beta radiation will not penetrate the coolant pipes, the activation products of significant interest are thus the high-energy gamma emitters [72]. Figures 2.23 and 2.24 show the activation levels of the coolant salts studied and their constituent components, respectively, at three different time intervals after the irradiation stops - either because the coolant left the core or because the reactor was shut down [60].

Table 2.7: Neutronic Efficiencies of Various Materials and Coolant Salts [61].

Material	Total Neutron Capture (per unit volume) Relative to Graphite	Moderating Ratio (avg. over 0.1–10 eV)
Heavy water	0.2	11449
Light water	75	246
Graphite	1	863
Sodium	47	2
UCO	285	2
UO2	3583	0.1
LiF-BeF$_2$	8	60
LiF-BeF$_2$-ZrF$_4$	8	54
NaF-BeF$_2$	28	15
LiF-BeF$_2$-NaF	20	22
LiF-KF	97	2
LiF-RbF	19	9
LiF-NaF-KF	90	2
LiF-NaF-RbF	20	8

Like in sodium-cooled reactors, salts with a sodium component such as FLiNaK have a significant concentration of Sodium-24 (t1/2 = 15 h) when irradiated. As a result, refueling or any maintenance operations will be impeded because the exposure levels will still be dangerous after a few days of decay [60]. Furthermore, another component of FLiNaK, Potassium, is naturally radioactive due to Potassium-40. However, with activation, a substantial amount of Potassium-42 (t1/2 = 12 h) is produced along with several other isotopes, which then leads to very large activation levels for several days after irradiation ceases [60][66]. The effects of these two constituents combined suggest that the immediate investigation of FLiNaK coolant should irregularities be observed during reactor operation would not be possible and that it would be hazardous for workers to examine the system for at least ten or more days, during which the situation may have aggravated.
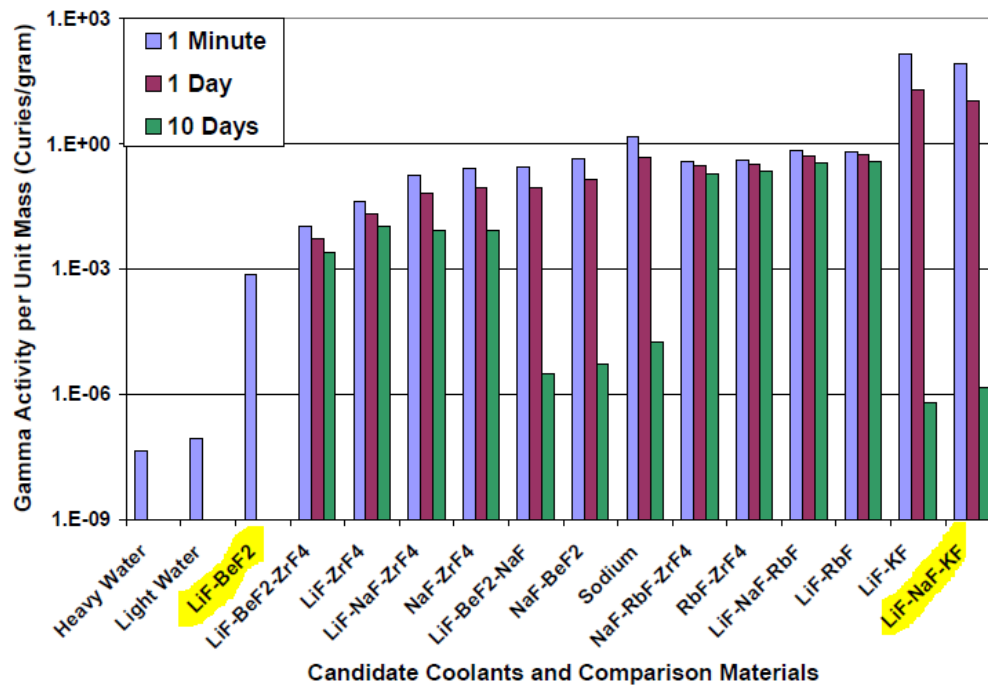
Figure 2.23: Activity levels for Candidate Coolant Salt Compared to Other Materials [60].
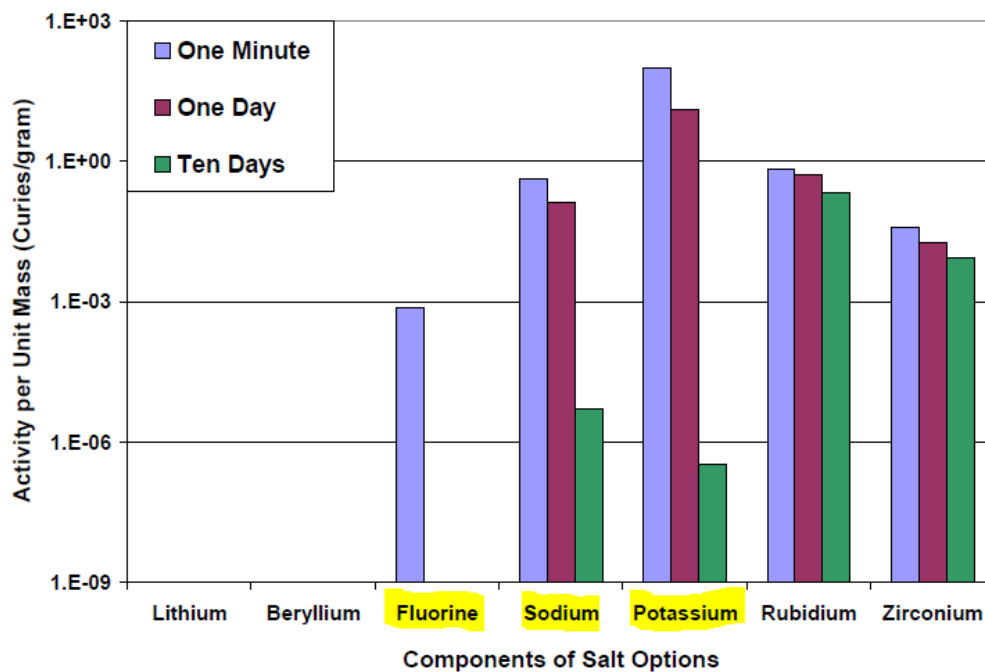
Figure 2.24: Activity Levels for Constituents in Various Coolant Salt Options [60].

2.6 Nuclear Decommissioning

Nuclear decommissioning is the process of retiring and removing a nuclear facility from its site through technical and administrative actions. This process includes several stages that easily span over decades: starting with the cessation of licensed activities, then the removal of fuel, de-watering, or in the case of MSRs, de-salting of systems, decontamination of components, dismantling of systems, and removal of material from the site. The goal of these activities being the release of the nuclear facility from regulatory control, with or without restrictions on its future use and the disposal of radioactive material in a manner that is safe to the environment and that is approved of by the public [81].

The International Atomic Energy Agency (IAEA) has defined three options for decommissioning, namely:

1) Immediate Dismantling (DECON);
2) Deferred Dismantling (Safe Enclosure/ SAFSTOR); and
3) Entombment.

These options and their definitions have been widely adopted by the IAEA member states and are applicable to all nuclear facilities [81-83]. Figure 2.25 below illustrates the three options during nuclear facility phase-out and decommissioning.
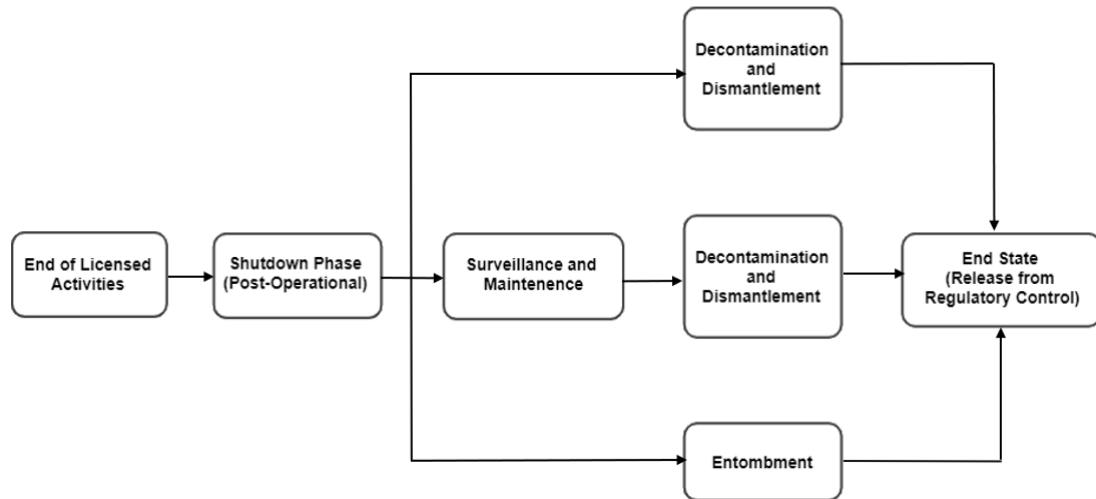
Figure 2.25: Decommissioning Options of Nuclear Facilities at End-of-Life [82].

Nuclear decommissioning is also an expensive undertaking; project estimates at completion can reach billions of dollars and in the case of many European decommissioning reactors, the costs continue to increase throughout operations causing the programmes to run over their initial budgets [84]. It can be challenging to optimize the scope and costs of decommissioning activities despite the fact that most of these retiring facilities use well-understood, water-based reactor technologies and have been in use for many years. There is uncertainty in terms of contamination type and level, the potential for contaminants to spread, and the generation of secondary wastes [85][86].

Although immediate dismantling is often the most popular and preferred option for the decommissioning of a nuclear facility, the specific path forward regarding the end-of-life operations of a reactor can often be uncertain, especially for novel technologies such as the molten salt reactor. In such cases, deferred dismantling, or long-term safe storage, is usually the strategy implemented.

Deferred dismantling is where the dismantlement of a nuclear facility is delayed; this can range from a few years to over 50 years, after which decommissioning process will take place and the facility can be released from regulatory control. As mentioned before, this is the option chosen for the MSRE due to the lack of fuel salt processing or disposal options. The safety of the MSRE facility is then ensured through the continuous performing of surveillance and maintenance activities which has been taking place since the 1960s until present. This method usually involves some initial decontamination or dismantling; the used fuel is typically removed from the reactor vessel along with any other radioactive liquids so that the facility is in stable condition.

The option of entombment was also briefly contemplated by the ORNL. This would involve encasing contaminated parts of the facility in a structurally long-lasting material until the radioactivity decays to a level that permits release of the facility from regulatory control [35]. However, this strategy was ultimately not selected because it would be extremely difficult to keep the ground water from penetrating the facility and subsequently leaking out. It was also too challenging to permanently isolate contamination from the environment [82][83].

Based upon the current status of the technology, an MSR is likely to have some amount of salt remaining within its system for long periods of time after its shutdown. Through exploring

the decommissioning considerations of an MSR, some technical clarity can be outlined for the selection of its appropriate end-of-life strategies, which would in turn be critical in the pursuit of commercializing molten salt reactor technology.

2.6.1 Decontamination

In nuclear decommissioning programmes, some form of decontamination is always necessary in reducing the level of radioactivity in system components, waste, or in the environment [87]. Defined as "the removal of contamination from surfaces of facilities or equipment by washing, heating, chemical or electrochemical action, mechanical cleaning, or other techniques" [88], the key objectives of decontamination are:

- to reduce radiation exposure for public health and safety;
- to salvage facility equipment and materials;
- to reduce the volume of equipment and materials that require storage and disposal in licensed disposal facilities;
- to restore the site and facility, or any parts thereof, to unconditional release status;
- to remove loose radioactive contaminants and fix any remaining contamination in place for protective storage or permanent disposal work activities; and
- to minimise long-term monitoring and surveillance requirements [88].

For an MSR, it would be expected that the floor, walls, as well as any internal and external structural surfaces of the reactor facility would be cleaned of loose contamination - especially if there had been a spill of salt. However, the question as to how to decontaminate the salt-facing, radioactive piping systems, tanks, and components has not been addressed. An overview of current decontamination techniques (which may apply to MSR systems as well as water-based reactor facilities) is presented in the following section.

The same techniques that were developed for supporting maintenance work in nuclear installations have been adopted for the decommissioning of nuclear installations and components with relative success [88][89]. Figure 2.26 is a logic map that guides the selection of appropriate decontamination techniques given the circumstance.
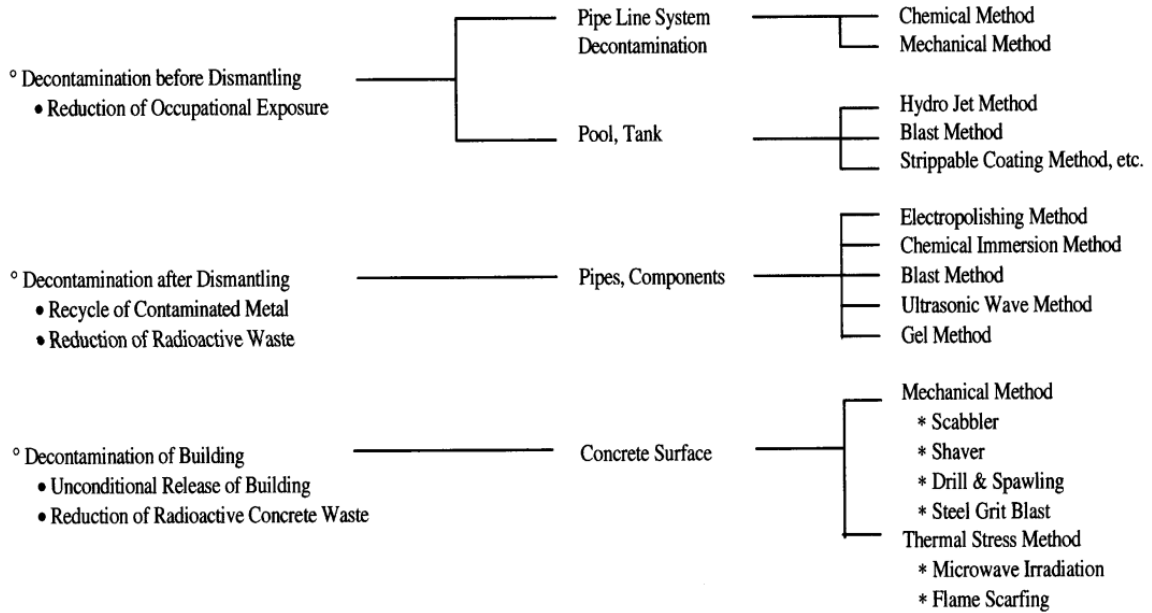
Figure 2.26: Decontamination Techniques for Decommissioning [88].

2.6.1.1 Overview of Decontamination Techniques

Presently, decontamination processes for the purpose of nuclear decommissioning are carried out in several different stages, all of which aim to reach unconditional-release criteria. Nevertheless, certain requirements, such as safety, efficiency, cost-effectiveness, waste minimization, and the feasibility of industrialization should be considered when selecting a specific technique for decontamination [87][90].

Table 2.8 below categorizes the applicability of decontamination techniques based on the type of system being worked on (open vs. closed) and the material of the components and/ or equipment (metals vs. concrete).

Experience from the MSRE demonstrated that long-term storage without decisive plans for decontamination can be costly as the facility and its equipment ages. Maintenance and surveillance operations become increasingly challenging due to the radiological hazards still present in the undisposed salts; extra precaution has been dedicated to the prevention of breaches in the salt drain tanks [86]. Since a permanent waste disposal solution has yet to be determined for the salts, the MSRE facility is still unable to decontaminate large portions of its original reactor system [35][45].

Table 2.8: Overview of Decontamination Processes for Decommissioning [88].

METAL DECONTAMINATION	Closed systems	Open systems	METAL DECONTAMINATION	Closed systems	Open systems
Chemical processes			**Physical processes**		
• Oxidation processes			• Ultrasonic cleaning		×
− ODP/SODP	×		• High pressure water		×
− Cerium/Sulphuric acid		×	• CO_2 ice blasting		×
− Cerium/Nitric acid		×	• Ice water		×
• Oxidation-reduction processes			• Freon substitutes		×
− APCE/NPOX	×	×	• Abrasives wet	×	×
− TURCO	×	×	• Abrasives dry		×
− CORD	×	×	• Grinding/Planing		×
− CANDEREM, CANDECON		×			
− CONAP		×	**Combined mechanical/Chemical processes**		
− AP/NP + LOMI for PWR	×		• Pastes + HP cleaning		×
− EMMA	×		• Foams/Gels/HP cleaning		×
• LOMI for BWR	×		• Vacuum cleaning (Dry/Wet)		×
• Phosphoric-acid-based processes		×			
• Foams	×				
• Various reagents				**Surface decont.**	**Concr. demol.**
− HNO_3		×	**CONCRETE DECONTAMINATION**		
− HNO_3 + HF	×	×	• Kelly process	×	
− HNO_3/NaF	×	×	• Scabbling	×	
− HCl	×	×	• Sand blasting	×	
− DECOHA		×	• Wet abrasives	×	
			• Milling	×	
Electrochemical processes			• Explosives		×
• Phosphoric acid		×	• Microwaves	×	
• Nitric acid		×	• Drill/Spalling		×
• Nitric acid - Electrodeplating		×	• Drill/Lime expansion		×
• Sodium sulphate - ELDECON Proc.		×	• Jackhammer		×
• Oxalic acid		×			
• Citric acid		×	× : decontamination technique applied for open or closed systems.		
• Sulphuric acid		×			
• Other electrolytes		×			

2.6.2   Nuclear Dismantlement

The dismantlement process is the physical removal and deconstruction of a nuclear site using mechanical, thermal, and/or electrical methods in a safe, controlled, and planned manner. It is one of the many steps in the nuclear decommissioning process and can continue until the site is released from regulatory control. In some cases, no dismantling is required; it all depends on the desired end-state [90][91].

Oftentimes, the equipment, components, and the facility structure itself are composites of multiple material types, such as metals, cement, and liquids. Thus, depending on the dismantling techniques, which are discussed in the next section, the characteristics of the waste can differ and must be stored and/or disposed of appropriately.

The original MSRE facility has not been dismantled due to the various reasons mentioned in previous sections. However, risks of radioactive leaks continue to increase as the facility ages, especially after the positive confirmation of "uranium migration" in 1994 where a failed off-gas valve led to uranium deposits in the off-gas charcoal bed. This further complicates the site's eventual dismantling as the building structures have been contaminated by radionuclides [35][91].

2.6.2.1 Overview of Dismantlement Techniques

There is a wide array of dismantlement technologies available; the three main categories being mechanical, thermal, and electrical dismantlement techniques. Table 2.9 below summarizes these methods and their suitable applications.

Some processes have advantages over others depending on their dismantlement rates, costs, and the volume of secondary waste produced. It is expected that secondary wastes would be generated in the form of sludges, dusts, and even contaminated water, which is one of the major sources of D&D costs [91]. As discussed in *Development of a Selection Tool for Choosing Decontamination Technology for Canadian Applications* by Khurmi *et. al.*, such techniques and processes exist and have been proven effective on light water reactors [92]. Yet, for MSRs, scarcely any methodologies, let alone a complete set, have been demonstrated.

Table 2.9: Overview of Dismantlement Technologies for Decommissioning [90]

Metal Cutting Technologies
Mechanical Processes
• Nibblers
• Shears
• Saws (Circular, Reciprocating, Band)
• Pipe Cutter (High-speed Clamshell, Plunging)
• Abrasive Wheels
• Circular Cutter
• Diamond Wire
• Pipe Crimper
• Controlled Explosives
• Guillotine Saws
Electrical Processes
• Arc Saw
• Metal Disintegration Machining (MDM)
• Electrical Discharge Machining (EDM)
• Electric Arc Gouging
Thermal Processes
• Plasma Arc (Electrical/Gas) Torch
• Oxy-fuel Torch
• Metal Powder Injection Cutting (Iron Powder Torch)
• Thermite Reaction Lance
Other Technologies
• Abrasive Water Jet (AWJ) Cutting
• Laser Cutting

Concrete Cutting Technologies
Mechanical Processes
• Nibblers
• Shears
• Saws (Circular, Reciprocating, Band)
• Pipe Cutter (High-speed Clamshell, Plunging)
• Abrasive Wheels
• Circular Cutter
• Diamond Wire
• Pipe Crimper
• Controlled Explosives
• Guillotine Saws
Thermal Processes
• Plasma Arc (Electrical/Gas) Torch
• Oxy-fuel Torch
• Metal Powder Injection Cutting (Iron Powder Torch)
• Thermite Reaction Lance
Other Technologies
• Abrasive Water Jet (AWJ) Cutting
• Laser Cutting

2.7   Potential Decommissioning Environments

Since the purpose of this work is to investigate the decommissioning considerations of an MSR, it is therefore important to identify and discuss the potential plant environments and conditions of such facilities at its end-of-life. This can include premature reactor shutdowns due to accident scenarios or planned retirement of aged reactors. This section highlights some of the possible environments or risks that decommissioning workers may eventually face when working with MSRs and sets the general scope for the context in which the experiments in the following chapters are conducted.

One may expect, should nothing go awry during the operation and initial shut down of the MSRs, to find the reactor vessel and any salt-facing components and piping to be drained of molten salt. Similarly, the fuel, coolant, and flush salts should have cooled and be stored in

their respective tanks, awaiting final disposition or long-term storage. However, for components that are unsuitable for high-level, deep-depository disposal and if maximum equipment/material salvage is the intention, then more scenarios should be examined, such as:

- Residual salt bridges stuck within the reactor piping system;
- Potential uranium and fluorine migration through the off-gas system;
- Corrosion of fuel drain and flush tanks;
- Potential need for waste-salt reheating and the associated operations and risks; and
- Fully vs. partially filled drain tanks.

Moreover, accidents can happen- as they have in the past. Spills, ruptures, and other forms of failure-including meltdowns-can catastrophically complicate the decommissioning process since anything in contact with the waste salt would become highly radioactive and contaminated. Literature sources such as Briggs *et. al.* and Toth *et. al.* emphasize the importance of salt purity for the proper operation of an MSR, which would no longer be the case in accident conditions. It would thus be worthwhile to investigate the following contingencies for remediation clean-up activities:

- Spills of fuel and/or flush salt during operation vs. post shut down;
- Leaks, breaches, or ruptures in the waste salt storage tanks;
- Leaks in the off-gassing of elemental fluorine because of radiolysis in the waste-salt;
- Unexpected uranium deposits-on surfaces or in components; and
- Component (valves, fitting, pipes) failures.

Other environmental factors, such as pressure, temperature, and humidity can also vary depending on the location of the MSR plant. Their impact on the behaviour of the molten salts, and by extension the decommissioning operations of the facility, is another equally important aspect studied in this work.

2.8   Molten Salt Reactor Technology Decommissioning

Based on the experience of current decommissioning programs, it would be beneficial technically, economically, and regulatory-wise for new, Gen IV reactor technology vendors to

devise a detailed outline of the decommissioning plan of their designs. In the case of the MSR, very few sources discuss the decommissioning and decontamination aspects besides the ORNL's publications regarding the problematic aftermath post-shutdown of the MSRE. There is little to no information available regarding the necessary considerations for an MSR facility to reach required clearance levels according to Canadian regulation.

It is unclear whether the existing decommissioning and decontamination techniques are suitable for MSR applications, and it is doubtful that they are adequately complete for the salt-based systems. If, when, and how various components are decontaminated during the dismantlement process can be a complicated operation. Most treatment processes, such as electrochemical washes, acid baths, ultrasonic cleaning, and mechanical removal, have been developed for large-scale light water reactors. Hence, this work seeks to investigate and provide a preliminary understanding of the decommissioning concerns of MSR technologies. Figure 2.27 below visualizes the potential end-of-life conditions of an MSR as well as some possible areas of concern for decontamination.

Reactor Core

Some amount of radioactive salt may remain within the reactor system even after the salt drainage.

Turbine

Freeze Plug

Heat Exchanger

Cracks and ruptures in the piping system can lead to molten salt leaking into its environment.

Fuel Drain Tanks

Fuel drain tanks may require maintenance and monitoring programs.
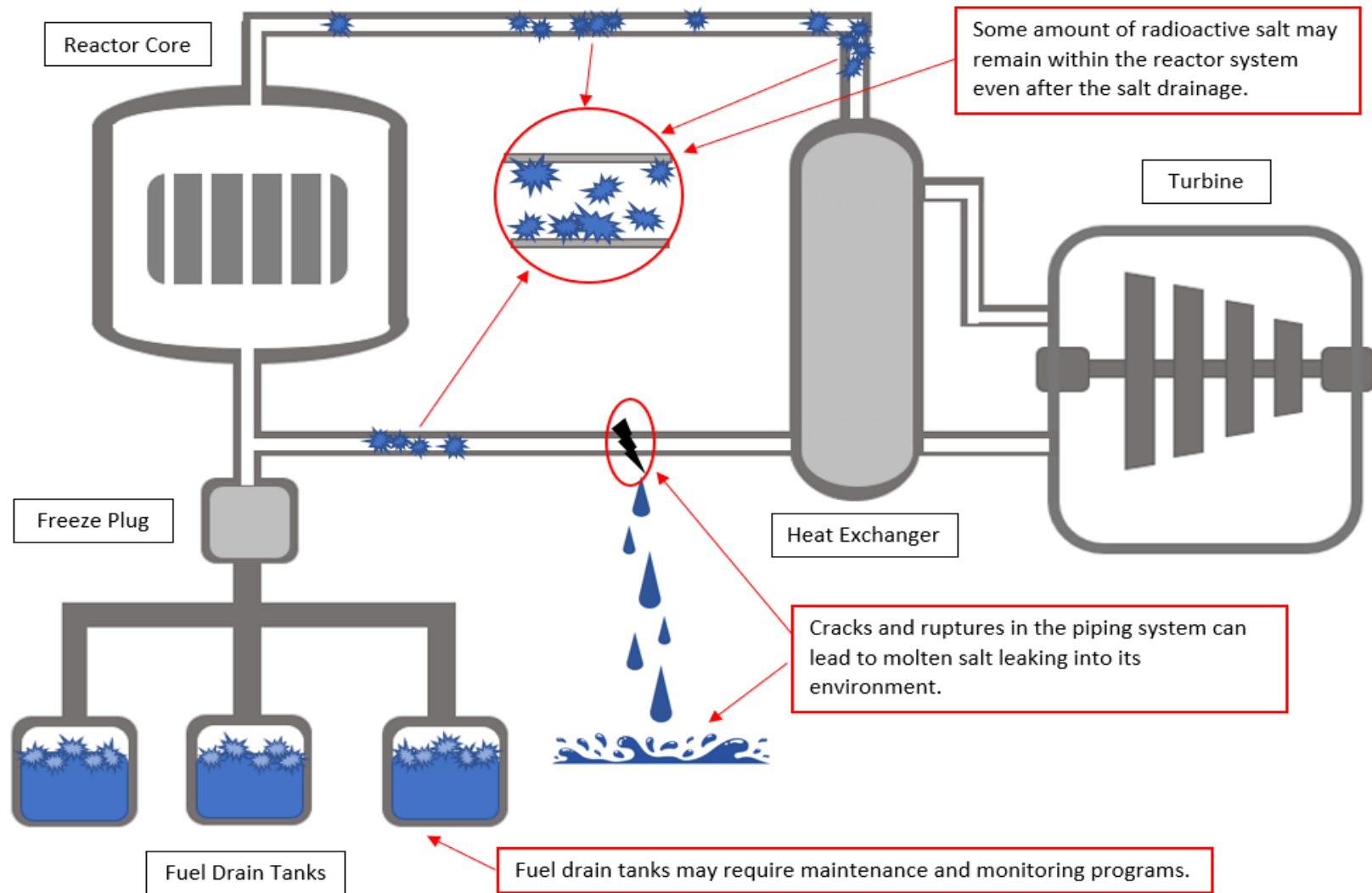
Figure 2.27: Visualization of Potential Challenges in Molten Salt Reactor Decommissioning

2.9   Theoretical Framework

This section provides a foundational review of the existing theories and methodologies that support and contextualize the research conducted in this work. Any preceding experiments and/or research performed by the Nuclear Design Laboratory (NDL) on the topic of molten salts, which subsequently motivated and informed this thesis project, are also discussed.

Section 2.9.1 discusses the theory of FLiNaK salt behaviour with water and Section 2.9.2 describes the theory for using ultrasonic non-destructive evaluation methods for salt diagnostics.

2.9.1 Antecedent FLiNaK Experimentation

In 2018, prior to the commencement of this work, a coin-sized sample of FLiNaK was synthesized by a group of undergraduate Capstone students using a VULCAN D-1750 furnace. This sample was not produced by the author of this thesis project. The sample was synthesized in a ceramic crucible with a graphite base as seen in Figure 2.28. Upon re-solidification and cooling-down, the sample was removed from its synthesis vessel and subsequently placed into storage in a lidded plastic petri-dish.

Figure 2.29 is a photograph of the initial conditions of this sample. This sample was a solid white disc similar in appearance to samples produced by other researchers discussed earlier in this chapter (see Section 2.5.2, Figures 2.21 and 2.22).

The top slide of the salt, as seen in Figure 2.28, had a porous look as the gases that had been trapped in the ground salt ingredients escaped leaving minor pits. The sides and bottom of the salt as shown in Figure 2.9. The sides are smooth from contact with the ceramic tube. The bottom has a layer of carbon dust that was present to prevent sticking to the bottom of the graphite plate. The salt puck had a hard ceramic-like structure.

Figure 2.28: Synthesized FLiNaK in Ceramic and Graphite Container.

Figure 2.29: Initial Conditions of Furnace Synthesized FLiNaK Sample.

2.9.1.1 Observations and Limitations

The FLiNaK sample was manufactured in January in a basement lab that had very low moisture in the air. The sample was placed in a plastic petri dish, with cover and then enclosed in a Ziploc sealed bag to prevent contamination and was left on the lab bench for observation. After being in storage for approximately six months, physical changes such as salt crystal migration, disintegration, and water retention were first observed. The diameter would decrease and the height would increase with filaments forming near the top. This occurred for several months. Then during the summer, when the lab had relatively normal humidity levels,

the sample then appeared slightly damp or wet. The sample began to disintegrate faster forming salt granules and smaller crystals which then separated and latched onto the surfaces of its storage vessel away from the main salt. This process is documented in Figure 2.30 below. Finally, the FLiNaK puck fragmented and was immersed in a solution hypothesized to be atmospheric moisture absorbed by the salt. Figure 2.31 is a photo of the sample two years after its preparation.
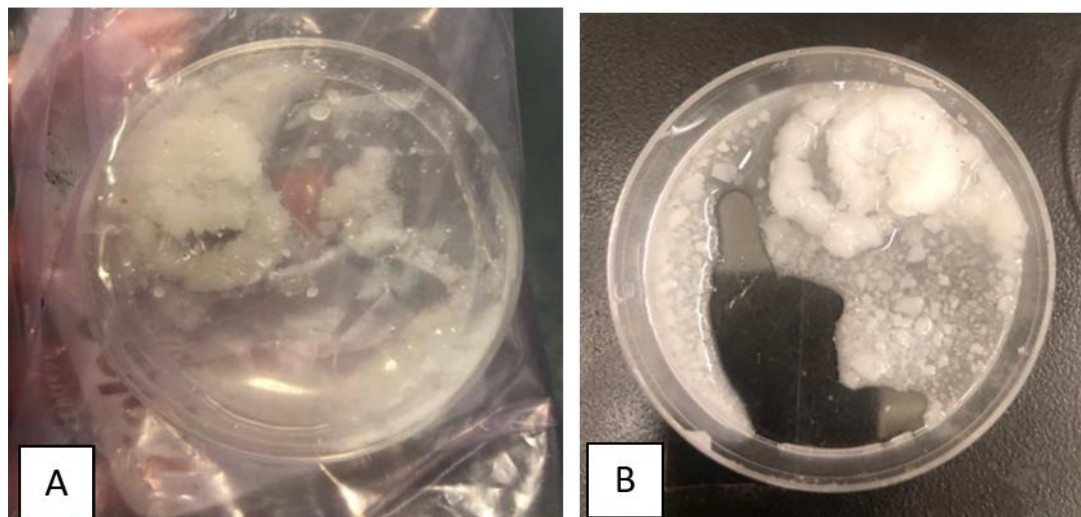
Figure 2.30: Physical changes observed in FLiNaK Salt (a): Photo Taken August 2021 (b): Photo Taken October 2021.

Figure 2.31: The conductivity of the aqueous solution formed as a result of FLiNaK deliquescence in % IACS

By that time the sample had absorbed sufficient moisture that the salt fragments became partially or fully submerged in small pools of clear aqueous solution. The conductivity of this solution was measured to verify whether the ions that comprise FLiNaK are indeed dissolved within it. The resulting reading was between 18-19 % International Annealed Copper Standard (IACS); for a sense of scale, pure water is 0% IACS.

The above observations demonstrated the hydroscopic nature of FLiNaK, a property which makes the salt suspectable to contamination by water [93]. Furthermore, deliquescence, a property characterized by the ability of a material to absorb sufficient moisture from its environment to form an aqueous solution, was also evident in this sample [94].

Discussed in literature sources such as Peng *et. al.* and Sohal *et. al.,* both FLiBe and FLiNaK readily absorb atmospheric moisture; freshly prepared FLiNaK can contain as much as 16 wt% moisture according to Kondo *et al.* [93][95]. Hence, Zhang *et. al.*, whose work focuses on the preparation of high-purity FLiNaK, note the importance of chemical purity and stringent water removal processes required to maintain the physiochemical properties of FLiNaK salt ingots [96][97]. The results and descriptions from these sources are validated through and rationalized some of physical changes and phenomena that this furnace-synthesized underwent since it was prepared without any water removal processes.

Although the hygroscopicity of FLiNaK can explain how the salt became damp over time and its deliquescence, it is not able to explain the breakdown of smaller salt crystals around the sample's edges and their migration away from the main salt mass along its storage vessel. This is a phenomenon which had not been previous described in literature and will henceforth be referred to as salt migration in this work. Salt migration, and its implications for the decommissioning of an MSR, is a major topic to be explored in this thesis project.

2.9.2 FLiNaK Salt Migration

The phenomenon of salt migration involves molecular interactions in a series of processes for which the effects are not observable with the naked human eye and span over extended periods of time, which can range from a few weeks to years.

FLiNaK, being hygroscopic, attracts and holds water molecules by absorbing them from the surrounding environment, which is usually and the case for this work, at standard temperature

and pressure. This hygroscopy is the result of cations in the FLiNaK - Lithium, Sodium, and Potassium - being attracted to the slight negative charge of the oxygen atom in water molecules [98]. Given fluctuations in pressure and humidity levels, the water absorbed may evaporate once more, bringing with it FLiNaK particles and granules; the water vapour that condenses along the inner surfaces of the storage container causes the salt to be deposited and recrystallize away from its originally synthesized main crystal. However, it is hypothesized that the force of attraction between FLiNaK cations and the oxygen atoms of water molecules in vapour form is weaker than that of the force required for the same reaction to occur with the oxygen atom in water molecules when in liquid form.

This may explain why once immersed in water, the physical changes in the appearance of the FLiNaK subsided. This relative stability may also have been the result of instant, solid-to-solid hydration of the FLiNaK salt specimen, a process described by Sögütoglu *et. al.* in *Understanding the Hydration Process of Salts: The Impact of a Nucleation Barrier*. The two pathways of salt hydration are illustrated in Figure 2.32 [99].
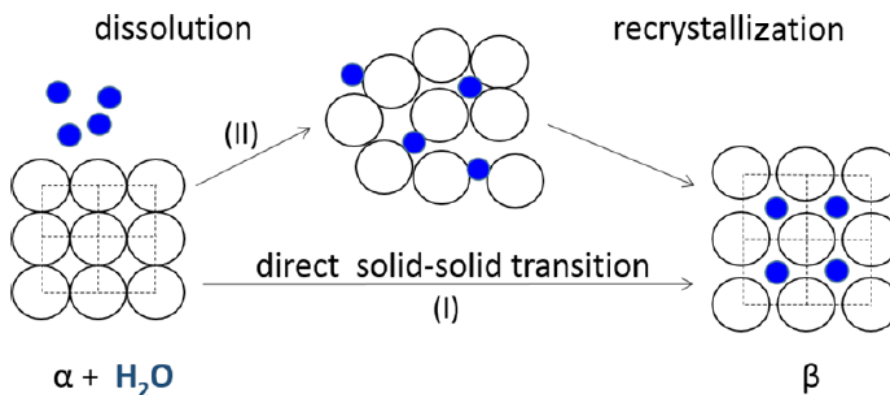
Figure 2.32: The two possible pathways of hydration: (I) a direct solid−solid transition and (II) a solution-mediated transition. α and β represent different crystal structures while water molecules are represented using the blue solid circles [99].

The paper also discusses the manner in which the nucleus of hydrated salt grows, some of which reflected the way in which FLiNaK absorbed and retained water throughout its storage, leading to salt migration. Figure 2.33 below is a schematic of hydrated salt nucleation [99].
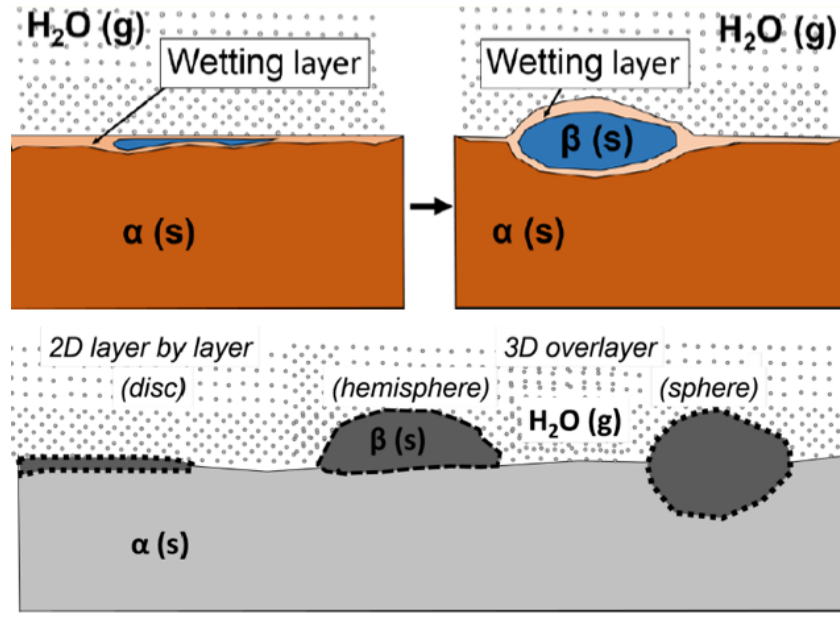
Figure 2.33: Schematic of the side view of nucleus shapes. The hydrated phase, β, nucleates through absorbing gaseous water in the air. For a 2-dimensional nucleus, growth occurs layer by layer, whereas a 3D nucleus grows as an expanding sphere. The dotted line represents the interface between the nucleus and its surrounding [99].

Thus, in the context of nuclear decontamination and decommisoning, it is hypothesized that the removal of water, as well as proper, air-tight storage of FLiNaK salt should be able to mitigate, to a significant extent, its extent of salt migration through limiting moisture absorption.

2.9.3 Ultrasonic Testing for Nuclear Applications

Non-destructive testing (NDT) methods are used in the nuclear industry to evaluate the integrity and properties of reactor material or components without causing damage to the tested object [100]. NDT methods are often used for the quality control, maintenance, safety and reliability, as well as decommisoning of nuclear power systems. While there are hundreds of methods available, one of the most common methods is ultrasonic testing (UT), which uses the propagation of ultrasonic pulse-waves transmitted into materials through a transducer to detect internal flaws or to characterize materials [100].

Similarly, for the decommisoning of an MSR, UT may be an option for identifying residual radioactive molten salt deposits within the reactor system once the fuel and flush salt have

been drained in addition to detecting flaws in the structure. Thus, this work includes experiments that explore the possibility of pin-pointing areas with residual salt within an MSR by using ultrasonic methods in the form of a pulser-receiver and an oscilloscope.

2.9.3.1   Signal Identification

This section focuses on the identification of signals generated by the oscilloscope in correspondence to the object being analyzed. Since UT can be used to characterize the thickness of a test piece, a series of objects with simple geometries can be examined first as a means of validating the equipment configuration.

The basic operating principle of the system is presented below in Figure 2.34. The transducer, in pulse-echo mode, both sends and receives the pulsed sound waves. It is placed on the test subject, through which the high-frequency sound waves pass through, bouncing back each time they encounter an interface or a defect in the material. The results would be in the form of an oscilloscope signal; its amplitude represents the intensity of the reflection while the arrival time of the reflection and distance can be interpreted based on the oscilloscope setting. It is also important to note that the distance is twice that of the thickness of the material because the pulsed waves have to first go through it and then be reflected back.
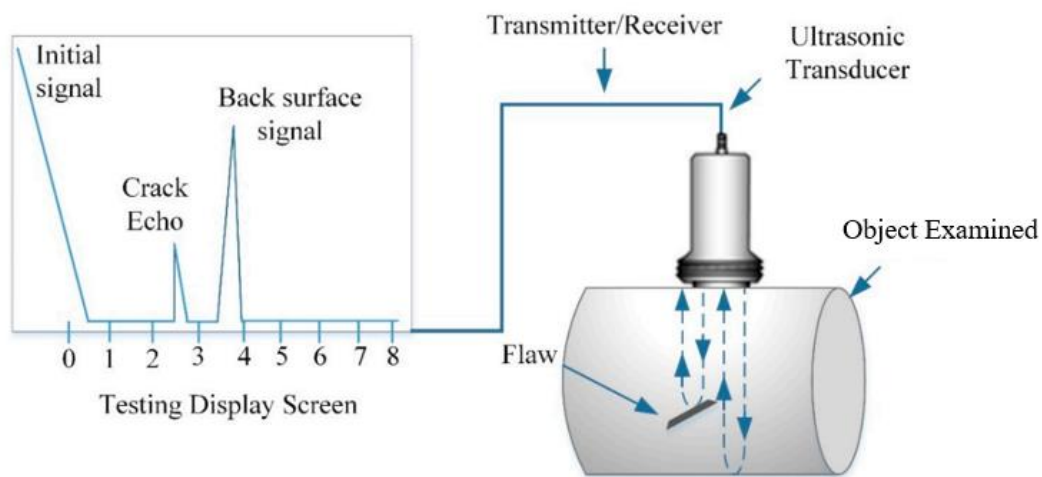
Figure 2.34: Schematic Diagram of the Ultrasonic Testing Set-up with a Depiction of the Corresponding Test Screen Signal [101].

As a preliminary experiment, a solid, rectangular block of steel with a thickness of one inch was examined using the pulser-receiver and oscilloscope; the results of which are featured in Figure 2.35.
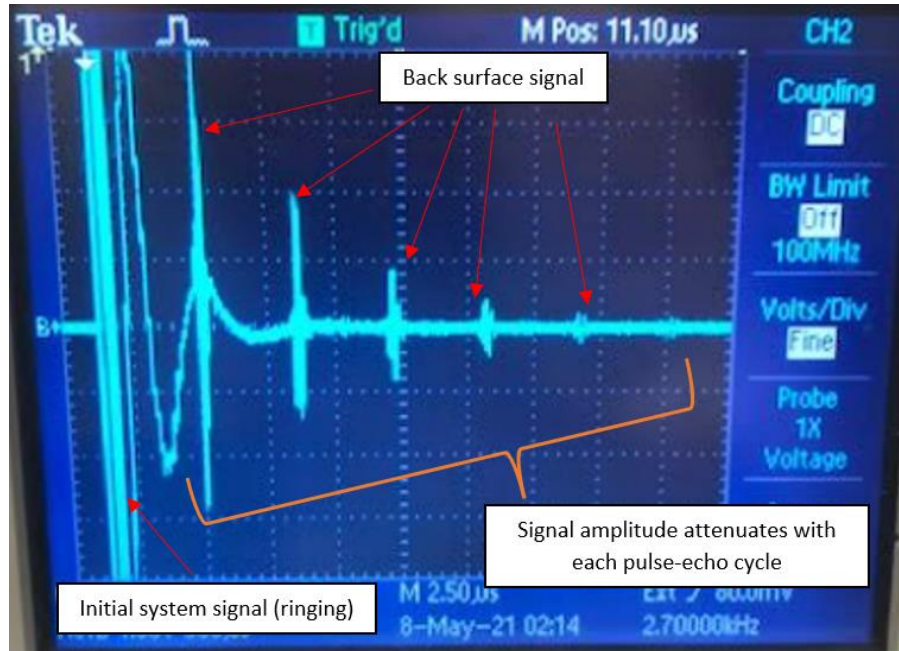
Figure 2.35: Ultrasonic Scan of Steel Block.

The numerous and intense peaks observed at the start of the signal is the initial signal or "initial ring" of the transducer and does not actually correspond with the material being examined. The subsequent peaks are the ones that reflect the interactions between the sound waves and the test object. Small fluctuations, attributed to noise in the system, were observed in between the larger back surface signals.

2.9.3.2   Signal Verification

This section describes the validation process of signals generated by the oscilloscope. To verify the signals, calculations were performed to determine the speed of sound through the object being examined at room temperature, then comparing the results to standard tabulated values for that specific material.

Knowing the composition and thickness of the object being analyzed, the following, simple equation was used:

$$\text{Velocity (m/s)} \times \text{Time (s)} = \text{Distance (m)} \qquad (2.3)$$

Where the velocity is the speed of sound through a specific material and the distance (Δd) is twice the thickness of the examined object since the signal must first travel through it and bounce back the far surface. From the voltage-time plot generated by the oscilloscope, information such as seconds per divisions and the number of divisions between each local maximum can be extracted; multiplying the two values would yield the time it takes for the pulsed signal from the transducer to travel the distance mentioned above:

$$\text{Time (s)} = \frac{Seconds}{Division} \times Number\ of\ Divisions \qquad (2.4)$$

Combining the two equations to solve for the velocity, *i.e.*, speed of sound gives:

$$\text{Velocity (m/s)} = \frac{2\Delta d}{\left(\frac{seconds}{divsions}\right)} \times Number\ of\ Divisions \text{ (m/s)} \qquad (2.5)$$

This method was first used to verify the signals generated from ultrasonic scans of the steel block, once again due to its geometric simplicity and was proven effective. Consequently, it was also used to verify signals from the scans of the flanges and middle tube section of the MSL Tube Segment.

It is important to note that the tabulated speed of sound through common metals are given in both transverse or longitudinal directions and these values can often differ significantly. Thus, to avoid errors when making comparisons to calculated values, visual inspections for the grain direction of the metal were performed before each ultrasonic scan. This involved observing the surface of the metal blocks to see the microstructure with the help of a magnifying glass. Table 2.10 on the next page was used to validate the signals generated using ultrasonic methods in this work.

Table 2.10 Summary of Ultrasonic Signal Verification Calculations [102].

Object Examined	Thickness (m)	Distance (m)	Seconds / Division (µs)	Number of Divisions	Calculated Velocity (m/s)	Tabulated Longitudinal Velocity (m/s)
Solid Stainless-Steel Block	0.0254	0.0508	2.5	3.6	5644.45	5613-5740
Stepped Acrylic Block	0.0508	0.1016	10	2.8	2705.65	2667-2769
Flange of MSL Segment	0.01	0.0204	2.5	1.4	5828	5842
Tube of MSL Segment	0.00325	0.0065	2.5	0.45	5777	5842

Overall, the calculated velocity corresponded to and was within the range of tabulated longitudinal velocities for the various materials examined. The margin of error was likely the result of issues in signal resolution and noise in the Ultrasonic Detection System. However, since there is no tabulated value for the speed of sound through FLiNaK, the recorded oscilloscope data require numerical analysis to try identifying residual FLiNaK once the Hastelloy-C signals were verified.

2.9.3.3   Signal Processing

This section describes the two signal processing techniques applied in this work: Fast Fourier Transform (FFT) and Zero-padding.

One of the most commonly used techniques for signal analysis across all industries, the FFT method transforms signals from the time domain to the frequency domain. In the case of this work, the recorded voltages corresponding to a series of sampling time would then be transformed into an amplitude. In the frequency domain, signal characteristics are described by independent frequency components, whereas in the time domain, a singular waveform would represent the sum of all these characteristics. Hence, by performing FFT analysis, signal characteristics that correspond to specific materials should be able to be investigated

individually and in greater detail compared to inspecting the same information in the time domain.

Another signal processing technique, Zero-padding, is used to ensure that all data sets have the same dimension. Zero-padding makes the size of the input data equal to a power of two by adding zeros at the end of the input signal, was applied to each transformed data set to minimize any distortion of dimensions after applying filters. Since adding zeros in a signal does not add any extra information, the characteristics and response of the signal thus will remain constant and will increase the frequency resolution of the signal in Fourier transform.

Chapter 3

Experimental Materials and Methods

This chapter will provide the methodologies used to achieve the objectives. The general approach to the problem is provided first, followed by the specific experiments to identify certain phenomena. Several experiments were conducted and the experimental methods and associated materials are described.

3.1 Description of Approach

The approach of this work is to emulate the potential physical and environmental conditions of a molten salt reactor at the time of the facility's decommissioning. Through the use of available representative components, characterization studies and experiments can be performed to offer insight regarding the decommissioning activities of an MSR.

Literature described in Chapter 2 suggested that physical conditions of metallic reactor components once the molten salts are drained can be difficult to gauge. It is likely that residual radioactive contamination can render the entire system un-recyclable due to the remaining hazards. The residual salt deposits may be released into the environment during dismantling processes. It can also be challenging to safely conduct remediation work in the case of shut-downs due to accident scenarios (spills, ruptures, *etc.*) without first understanding the behaviour of molten salts under various environmental factors. Overall, there is significant uncertainty in the appropriate decommissioning procedures and processes of molten salt reactors.

It is in the interest of this work to examine the behaviour of molten salt in the scenarios discussed in later sections and assess their implications on decommissioning operations. Publicly available information on the specific design details (fuel salt mixture, plant configuration, reactor system material, *etc.*) of Gen IV MSRs is limited and often proprietary; design concepts also vary depending on the vendor. Consequently, precise, accurate

simulations of an MSR in the decommissioning phase is difficult. A preliminary understanding of the overall decommissioning considerations is achievable.

As discussed in Chapter 2, there is a variety of different salts considered for different loops within a molten salt reactor. To date, the next generation salt has not been finalized. As such, it is not possible to choose one of the proposed salts. Instead, FLiNaK was chosen as a representative salt for the purpose of this work based in part upon the information obtained during the literature review. Furthermore, FLiNaK could be manufactured in our laboratory facilities from already available constituent components since the procurement of lab-grade salt ingots would be difficult to achieve. Either the type of salt is controlled or the manufacturer will only sell in quantities of one tonne or more. While it is true that properties will vary from one salt to the next, from a decommissioning perspective, the results obtained from FLiNaK should be representative. This general approach is given in Figure 3.1.

While some samples of FLiNaK were previously available, they were in very small quantities, unstable, and deviated from their original state. Thus, they were unsuitable for further experimentation. It was noticed in these samples that the salt pucks migrated within their vessels and appeared to be hygroscopic. It was therefore important, for the purpose of this work, to devise a method for synthesizing consistent samples of FLiNaK under controlled parameters, and the samples could be observed and diagnosed (as in the case of the salt bridge stuck within the MSL Tube Segment). Finally, heat experiments could then be conducted to simulate salt drainage in an MSR while noting phenomena that may be relevant to the decommissioning aspects of this technology.

As mentioned, consistent, controlled, and repeatable samples of laboratory FLiNaK salt need to be created. One set of experiments used test tube scale apparatus for the production of salt samples under controlled conditions as discussed in Section 3.3. The exploratory nature of this work meant that there was a need for a method to detect and locate potential salt deposits, and by extension, contamination, in a representative component of a molten salt loop before further D&D activities can take place.
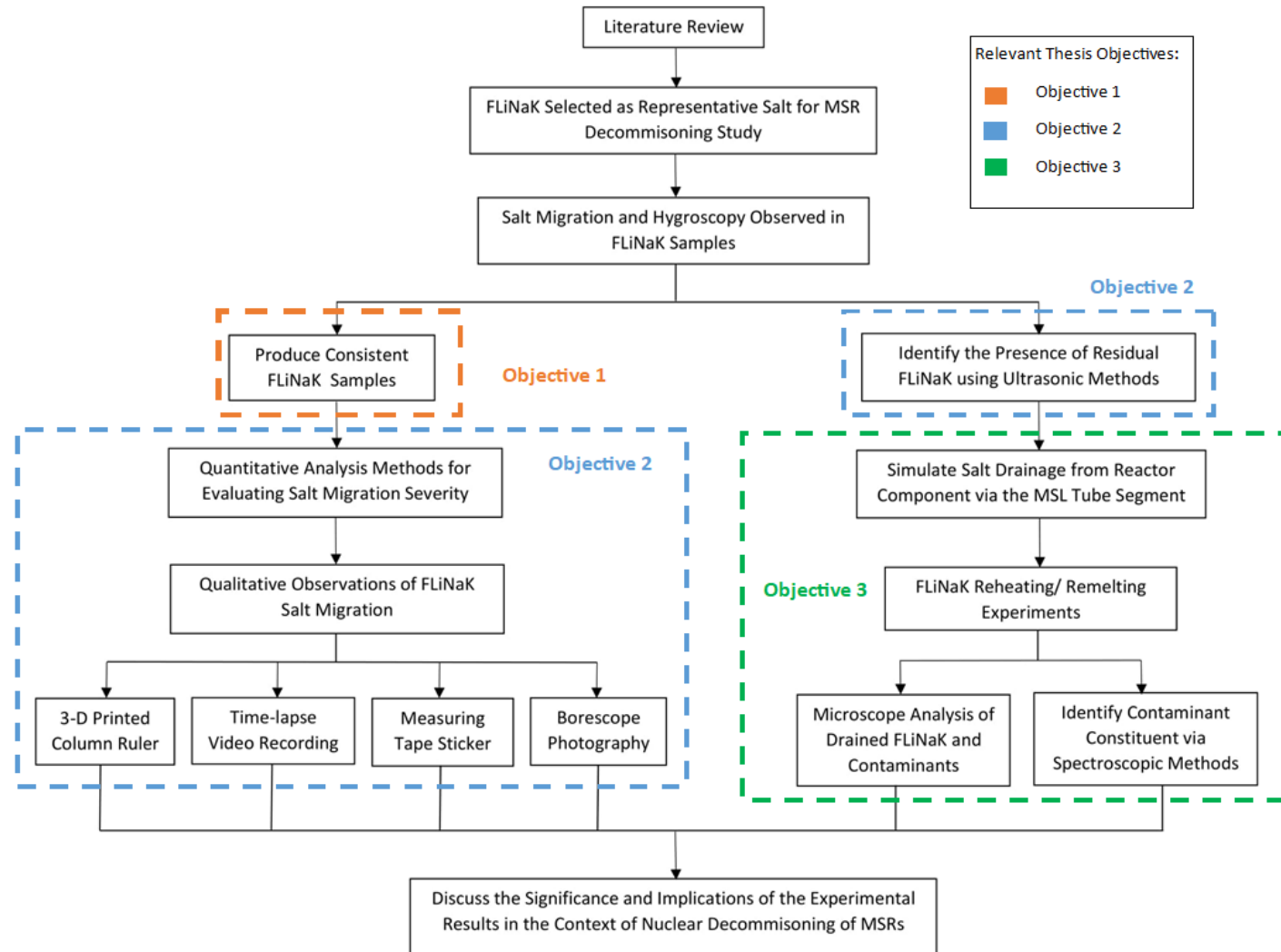
Figure 3.1: Approach of Thesis in Relation to the Three Main Objective

An ultrasonic pulser-receiver system paired with an oscilloscope was effective in confirming the presence of salt stuck in a tube segment; this may offer some preparatory guidelines to decommissioning work. The data recorded were analysed to ensure the signals corresponded to the speed of sound of the material being examined.

After producing the first set of four controlled FLiNaK samples, the salt pucks were sealed in their respective test tubes then stored; this was done to simulate long-term storage conditions. Through a period of six to eight months, salt migration was observed in all samples with varying extensiveness (the amount of salt granules that migrated away from the main crystal). Moisture was hypothesised as the key driver in this reaction; from the literature review, it is inferred that moisture removal was critical to preserving the purity and properties of FLiNaK.

Since it was not possible to add Hydrofluorination processes to salt purification for the purpose of this work, the vacuum pump acts as a substitute. A second set of five FLiNaK samples were made to quantify and observe the correlation between salt migration and moisture content within the test tube. Additional water in different quantities were introduced to the samples to simulate accident conditions in addition to normal operating conditions. The height of the crystal growth was recorded and analysed to identify a relationship; this may help identify the possibility of contaminants spreading within salt-facing components as well as narrow-down the types of technologies that can be used to dismantle and decontaminate the reactor structure.

A Hastelloy-C Test Chamber was used to simulate the drainage of salt and the removal of remaining salt deposits in decommissioning operations using electric heat tapes. An adaptor was designed to measure the temperature and pressure within the system while it was heated and the air within removed using a vacuum pump. The chamber consisted of a tube segment of the molten salt loop (MSL). This segment had been previously subjected to salt melting experiments and as a result had a salt bridge/deposit lodged within the tube. The test chamber acted as a representative component from which molten salt will be drained at the shut-down of an MSR; it offered insight into the challenges of multiple melting, remelting, and draining procedures.

3.2 Furnace Performance Testing

A VULCAN D -1750 manufactured by NeyTech, shown in Figure 3.2, was initially selected for the synthesis of FLiNaK samples for this work based on the procedures used to prepare the FLiNaK sample discussed in Section 2.9.1. A preliminary experiment was conducted based on the "One Hour Plan" outlined in Appendix A to verify and determine the heating rate of the furnace. However, the furnace was ultimately not selected for FLiNaK synthesis in this work because:

- The heating rate was slow compared to other heat sources such as Bunsen burners;
- It is not possible to visually verify whether all the salt had liquefied/melted;
- This method required the use of ceramic crucibles with graphite bases to hold the FLiNaK, which previously yielded a porous sample that was difficult to remove once it solidified;
- A second layer of containment would be needed to prevent leaks; and
- Components would be at temperatures well above 450 °C, which can be dangerous to maneuver.
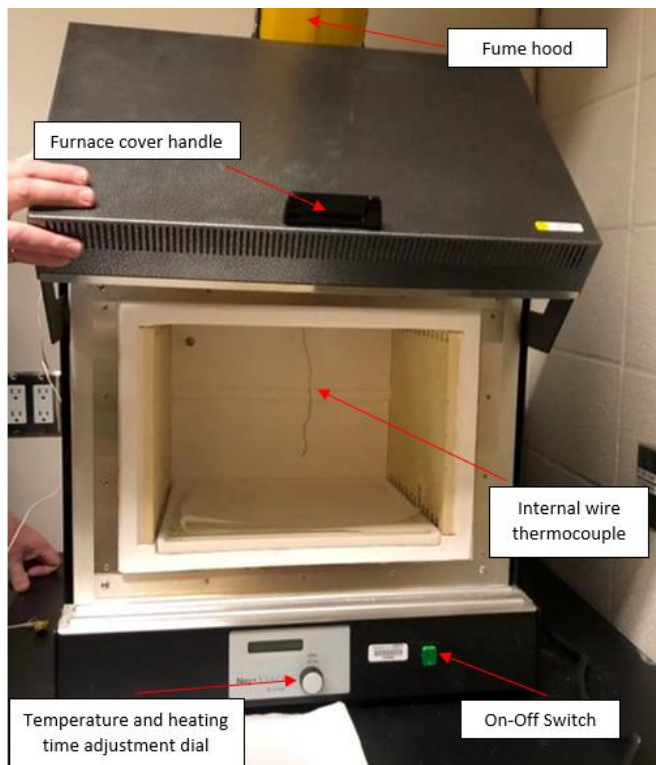
Figure 3.2 Photo of Furnace with Internal Wire Thermocouple.

3.3   Preparing Controlled FLiNaK Salt Samples

The FLiNaK samples produced in this work must be repeatable and consistent because they were the baseline for all subsequent salt behaviour observations and experimentations. Two batches of FLiNaK salts, Cycle-A and Cycle-B, were produced for analysis. Cycle-A consisted of four samples while Cycle-B consisted of five; the test matrices for each cycle are featured in Section 5.8.1. The qualitative and quantitative characterization of these samples were intended to shed light on the hygroscopic properties of FLiNaK and the environmental factors that may affect the salt during nuclear decommissioning.

3.3.1   Vacuum FLiNaK Salt Melting System

The FLiNaK salt samples analyzed in this work were prepared using the Vacuum FLiNaK Salt Melting System; it produced consistent samples of synthesized FLiNaK up to 3.5 g and consisted of a vacuum pump, a Bunsen burner, as well as a test tube held by a screw-operated clamp on a retort stand. The system was used to synthesize pre-mixed FLiNaK powder that consisted of NaF, KF, and LiF in ratios of 46.5-11.5-42 mol % respectively.

Firstly, the FLiNaK powder was weighed; the samples ranged between 1.5 g to 3.5 g. Then, the FLiNaK was placed inside a glass test tube and fastened to a retort stand via the test tube clamp. A two-holed rubber stopper was used to seal the test tube opening. In one hole, a thin metal tube connected to the vacuum pump was inserted while the other hole holds the K-Type thermocouple probe. Finally, the Bunsen burner was ignited and paced underneath the bottom of the test tube to melt the FLiNaK salt.

The system performed two distinct stages of salt melting through adjusting the configuration of sub-components. One configuration was for the removal of moisture in the pre-mixed, powdered FLiNaK, and the other was for the synthesis of the salt sample.

Schematics of the two melting configurations are featured in Figures 3.3 and 3.4. The main difference between each stage is the temperature of the flame from the Bunsen burner, which was controlled through the air hole (see Appendix B) [103]. In addition, the use of a vacuum pump for the later stage also marks a distinction.
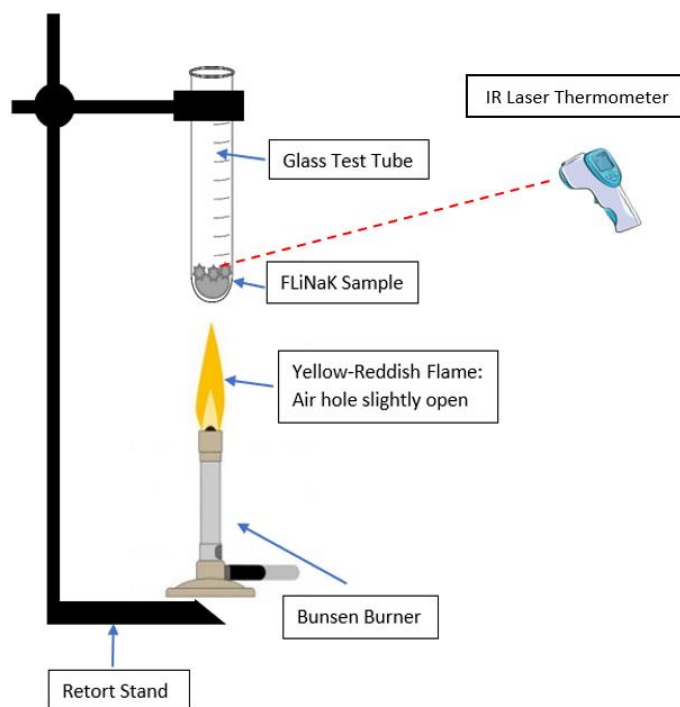
Figure 3.3: Schematic of Vacuum FLiNaK Salt Melting System during Moisture Removal.
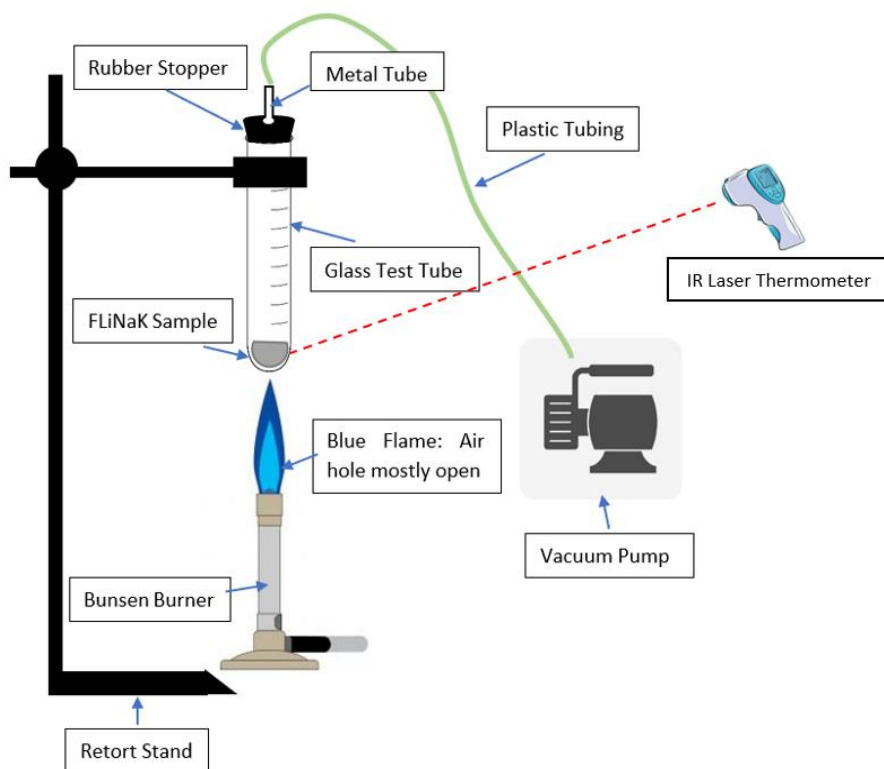
Figure 3.4: Schematic of Vacuum FLiNaK Salt Melting System during Salt Synthesis.

The moisture removal stage used a yellow flame (300-500 °C) to boil off water; firstly, without the use of a vacuum pump. Then, the pump was turned on to remove any water droplets that gathered along the test tube walls. The melting configuration used a hotter blue flame (up to 1200°C) with the vacuum pump on to melt the FLiNaK. A photograph of the assembled vacuumed test tube FLiNaK salt melting system is shown in Figure 3.5.

1. Test Tube with Molten FLiNaK
2. One-hole Rubber Stopper
3. Vacuum Pump Connector
4. Ventilation Tube, Connected to Vacuum Pump
5. Bunsen Burner with Blue Flame
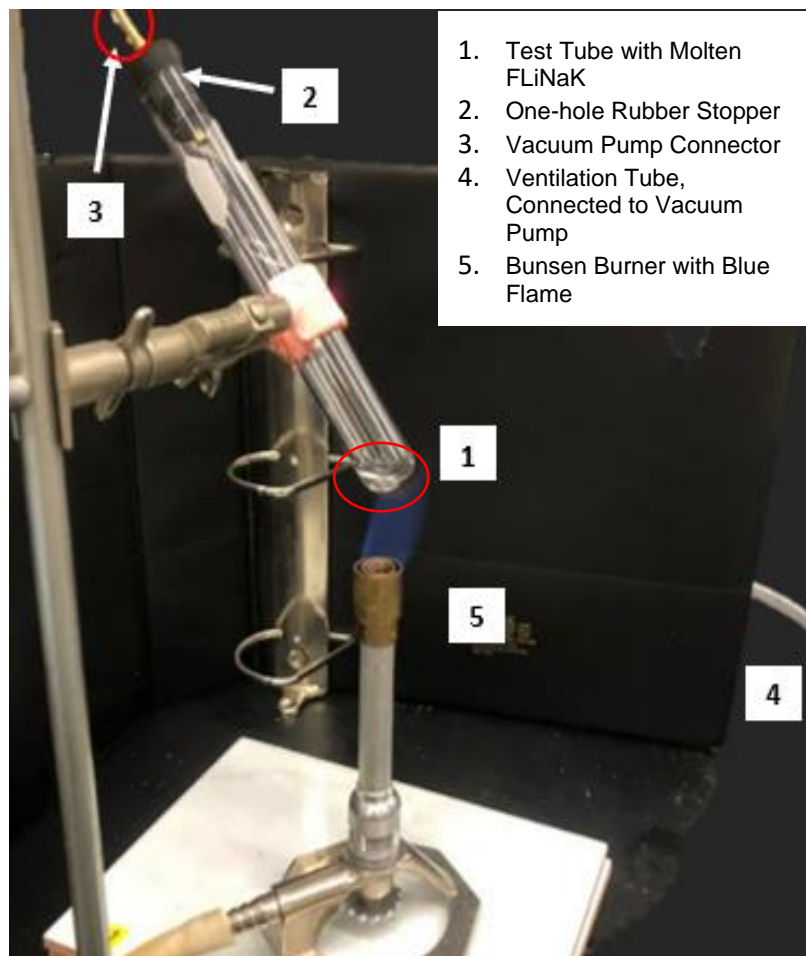
Figure 3.5: Photo of Vacuum FLiNaK Melting System – the Salt is Fully Melted Using the Blue Flame

3.3.1.1   Vacuum Pump

The vacuum pump used in the experiments in this work was the SpeediVac High Vacuum Pump manufactured by Edwards Ltd. By incorporating vacuum pumping into the FLiNaK synthesis process, samples were prepared more consistently and in less time. Since the vacuum pump continuously draws gas molecules from the sealed test tube leaving behind a partial

vacuum, it removes water vapour and any contaminants trapped in the powered FLiNaK mixture and prevents external contaminants from entering the system. The absence of impurities within the test tube allows the heat from the Bunsen burner to transfer to the FLiNaK more effectively, shortening the melting time. The SpeediVac vacuum pump could run continuously for twenty-five minutes, after which the pump must be turned off to allow the system to cool down.

3.3.1.2   Supporting Components and Equipment

The following components and equipment were also used for FLiNaK preparation in this work:

- Analytical balance;
- Weighing paper;
- Retort stand;
- One and two-holed rubber stoppers;
- Thin metal tube;
- Plastic tubing; and
- Test tube rack.

3.3.2   Instruments for Temperature Measurement

Throughout the FLiNaK synthesis process and all other experiments in this work, many components of the vacuum melting system required temperature readings to verify that they remained within safe, operating conditions. Similarly, temperature measurements were taken of FLiNaK salt samples throughout preparation to ensure thorough melting as well as explore and record temperatures that correlate with certain salt phenomena (onset of melting, solidification, *etc.*).

Three types of instruments for temperature measurements were used to achieve the purposes outlined above in this work: an infrared temperature gun thermometer, a thermal infrared camera, and K-type thermocouples. The three instruments were calibrated using ANSI standards included in their operation manuals and used simultaneously as they complement one another in accuracy and rated temperature range.

Infrared Laser Thermometer

A handheld infrared laser thermometer of the model 62 Max by Fluke Corporation was used for various temperature measurement applications in this work. Infrared laser thermometers deduce the temperature of the object being measured by detecting thermal radiation (blackbody radiation) and use a laser to help aim the thermometer. The non-contact approach of the handheld thermometer reduces safety risks associated with the high temperatures required to melt FLiNaK. In addition, the device is easy to use, clean, and decontaminate; it is capable of rapidly measuring temperature and displaying a reading.

Unlike contact thermometers, the infrared laser thermometer had the ability of retaking a temperature quickly. The 62 Max has a temperature range of -30°C to 650°C and accurate to ±1.0°C of a given reading which is sufficient for FLiNaK salt melting. The response time is < 500 ms for 95% of readings, thus the device was often repeatedly used in short time frames for multiple readings [104].

Thermal Infrared Camera

The thermal infrared camera used was the Ti105 Thermal Camera manufactured by Fluke Corporation. The camera, another non-contact temperature sensor, operates by creating a monochrome image using infrared radiation by detecting wavelengths from about 9 μm to about 14 μm [105]. Images generated by the thermal camera were captured for thermographic analysis. The Ti105 has a fixed focus system with an infrared resolution of 320 x 240 (76,800 pixels) and requires a minimum focus distance of 46 cm. Its temperature range spans from 20 °C to 275 °C with an accuracy of 2%, which is roughly ± 2°C. The camera's thermal sensitivity is ≤ 0.045 °C at 30 °C [106].

3.3.2.1   Thermocouples

The main method of conducting temperature measurement in this work was using thermocouples. Thermocouples consist of two dissimilar electrical conducts that are connected to form an electrical junction. To measure temperature at any given point, the

thermal junction makes direct contact at the desired measurement location and develops a temperature-dependent voltage, this voltage is then interpreted to measure temperature [107].

Commercial thermocouples can measure a wide range of temperatures; they are inexpensive, easy-to-use, replaceable, and use standard connectors. Unlike non-contact temperature sensors, thermocouples can be and were inserted into melting chambers containing FLiNaK to provide a more accurate temperature measurement of the interior environment while confirming the state of synthesis of the salt when visual observation was not possible. It was determined that nickel-based, Type-K thermocouples were the most appropriate for high temperature FLiNaK synthesis and melting environments and thus the experiments conducted in this work uses Type-K thermocouples.

Type-K Thermocouple

Type-K thermocouples (chomel-alumel) are the most common general-purpose thermocouples with an approximate sensitivity of 41 µV/°C [108]. They have a wide temperature range, high accuracy, and an abundant variety of standard connecting components available. Type-K thermocouples are inexpensive compared to other thermocouple types with similar temperature ranges and properties (Type-N). Table 3.1 summarizes the properties and costs of Type-K thermocouples.

Table 3.1: Type-K Thermocouple Properties [108][109].

Positive Leg Composition	Negative Leg Composition	Temperature Range (°C)				Unsheathed Cost	Accuracy
90% Nickel	95% Nickel	Continuous		Short-term		$160 CAD / 200 feet for unsheathed wire	±0.75%
	2% Aluminum	Low	High	Low	High		
10% Chromium	2% Manganese	0	+1100	-180	+1370		
	1% Silicon						

These thermocouples operate accurately in oxidizing atmospheres, making them suitable for corrosive molten salt applications, especially if fluorine gas is released. However, preferential oxidation or "green rot", usually caused by hydrogen in the atmosphere, can occur when thermocouple wires are exposed; the chromium in the chromel alloy oxidizes which reduces the emf output causing the thermocouple to read low [108-110].

For this work, Type-K thermocouple probes with 0.187" outer diameters were selected for experiments that required taking temperature measurements in environments containing heated FLiNaK salt [108]. Figure 3.6 below compares a wired and probe Type-K thermocouple.
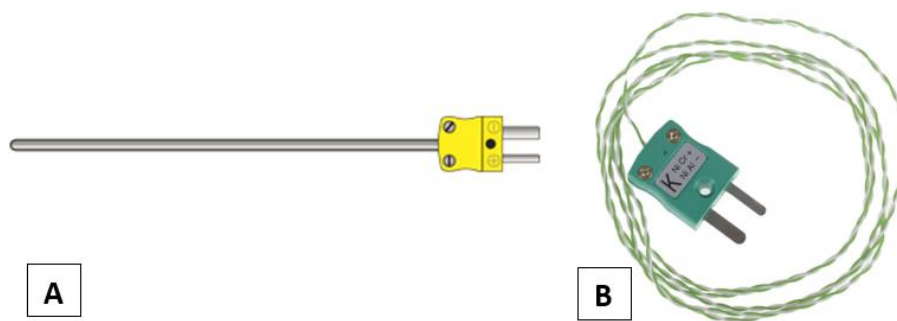
Figure 3.6 (a): Type-K Thermocouple Probe (b): Wired Type-K Thermocouple.

Thermowell

Thermowells 6" in length and 3/16" in inner diameter were used whenever there is a possibility of direct contact between the thermocouple probe and molten FLiNaK. This was done to protect the K-Type thermocouple probes from corrosion as well as avoid contaminating the molten salt with metal oxides.

Dual-Probe Digital Thermometer

The Fluke 52 II dual-input digital thermometer was used to deliver temperature readings from thermocouples, both probe and wire. The thermometer can measure two contact temperature inputs simultaneously and display the calculated temperature difference; it is capable of temperature measurements up to 900°C. Reading results can be displayed in °C, °F or Kelvin (K). The Fluke 52 II was the most suitable thermometer for various FLiNaK melting and

synthesis experiments in this work because it was compatible with standard thermocouples including the K-type. Table 3.2 shows the specification of the Fluke 52 II Dual-Probe Digital Thermometer [111].

Table 3.2: Fluke 52 II Dual-Probe Digital Thermometer Specifications [111].

Temperature Accuracy	Above -100 °C	J, K, T, E-Type: ± [0.05%+ 0.3°C]
	Below -100°C	J, K, E-Type: ± [0.20%+ 0.3°C]
		T-Type: ± [0.50%+ 0.3°C]
Temperature Range	K-Type	-200°C to 1372°C
	J-Type	-210 °C to 1200°C
	T-Type	-250°C to 400°C
	E-Type	-150°C to 1000°C

3.4 Methods of Salt Migration Analysis

Several self-devised methods were used as modes of analysis due to the unavailability of literature information or known methods for observing, recording, and evaluating the migration behaviour of FLiNaK salt in the nuclear decommissioning context. The only precedent being the decommissioning reports on the MSRE that confirmed the migration of radioactive material, primarily uranium, in piping connected to the drain tank cells. However, the role and behaviour of the molten FLiBe waste salts in the process of material migration was not discussed in the associated publicly available reports.

In this work, a series of simple techniques were used to explore and quantify the hygroscopic nature of FLiNaK salt and its subsequent migration within a vessel. Firstly, measuring tape stickers were stuck onto the exterior of the test tube walls to observe and record the physical changes in the sample salts within. Since the movement of FLiNaK can occur over the span of months, the transparency of the test tube allowed salt migration to be noted immediately and photographed. The measuring tape sticker acted at a static reference for photograph comparisons. For opaque components containing FLiNaK, namely the MSL Tube Segment,

a thin, 3-D Printed Column Ruler was designed and used with a borescope for the observing and recording of FLiNaK salt behaviour.

For FLiNaK samples melted in test tubes, an action camera on a tripod was set up to record time-lapse videos. This type of recording allowed movements to progress much faster than in reality and is a passive form of observation, which can facilitate the analysis of any changes within the test tube through video evidence.

3.4.1 Observation and Evaluation Methods for Extent of Salt Migration

There are three methods to observe and evaluate the extent of salt migration of a sample within its container. Primarily, this was done through determining the distance between the site of new salt-crystal growth from the location of the original synthesized salt puck. These methods are similar to one another because they all attempt to describe, in a quantitative manner, the changes in the physical condition of FLiNaK salt under standard temperature and pressure. The measuring tape sticker monitored salt behaviour in a transparent test tube while the column ruler did the same in the MSL Tube Segment where direct visual observation was not possible. The recording of time lapse videos provided a means of capturing the process of salt migration which was not very obvious to the human eye. These methods may offer insight into the potential challenges that can arise from the indefinite storage of molten salts given delayed decommissioning of an MSR.

Measuring Tape Sticker

An economic and simple means of monitoring FLiNaK salt behaviour, measuring tape stickers were applied to synthesized salt samples that were stored in test tubes. In an effort to correlate humidity with the extent of salt migration, this method was devised to evaluate and record, in a more quantitative manner, the visually observed changes in FLiNaK salt appearance overtime. The strips of measuring tape were cut individually, each between 12-15 cm in length; the 0cm mark being aligned with the initial height of the FLiNaK sample near the bottom of the test tube (see Figure 3.7).

Since the FLiNaK samples varied slightly in mass, there was no uniform height baseline; the tape allowed the "0 cm" to be set where appropriate so that there was no discrepancy in the

initial reference point between the samples. The measuring tape sticker was efficient in providing a static reference of starting locations of newly synthesized salt samples from which any subsequent signs of salt migration can be observed and recorded. In addition, the measuring tape sticker was trimmed to only have measurements in centimetres (it originally had both inches and cm) to minimize the surface area that it occupied on the exterior of the test tube so as to not obstruct the view of the FLiNaK salt within.
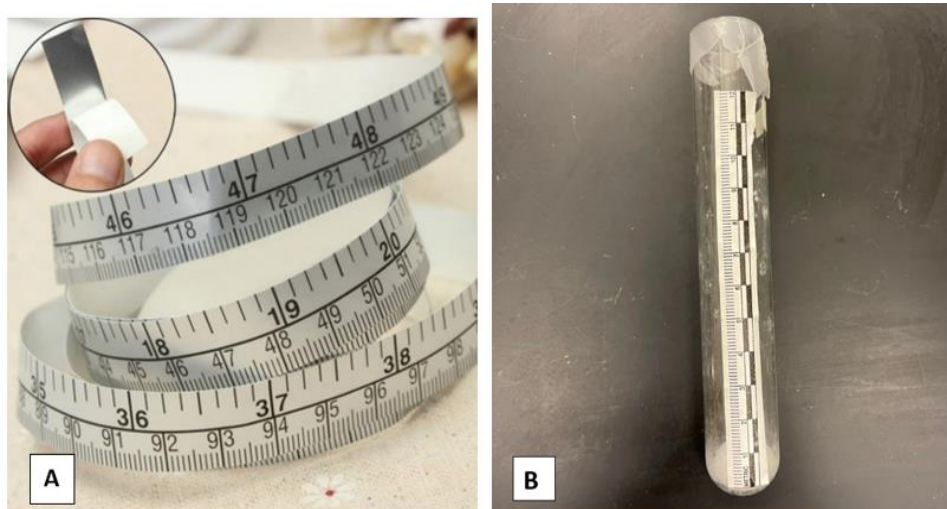
Figure 3.7 (a): Self-adhesive Measuring Tape Sticker (b): "0 cm" Set at the Initial Height of FLiNaK Sample in Test Tube.

Borescope

The YINAMA Dual-Lens Digital Borescope was used alongside the 3-D Printed Column Ruler to observe, record, and analyze the condition of the FLiNaK salt plug and residue within the MSL Tube Segment throughout the series of remelting experiments performed.

This borescope model had a flexible cable that was 5 m in length, adjustable LED light, and both front and side-facing cameras; it was used to take high-definition photos and record videos of the salt over the course of this work. These features combined, allowed for the visual inspection of the narrow, dark, and hard-to-reach interiors of the MSL Tube Segment.

Figure 3.8: YINAMA Dual-Lens Digital Borescope.

3D-Printed Column Ruler

To quantify the extent of salt migration within the MSL Tube Segment throughout the remelting experiments, a 3-D printed column ruler was designed and fabricated. Unlike the test tube, the MSL Tube Segment is opaque and made of Hastelloy-C. The tube section has a narrow opening, 25 cm in length, dark, and difficult to access for measurements using calipers. Thus, the column ruler was designed to be shaped like a straw; the hollow middle comfortably fits the borescope camera to enable measurements and photographs to be taken in well-lit environments and high resolution.

The column ruler was 3-D printed using PLA filament; it was 1.45 cm in outer diameter, 1 cm in inner diameter, and 18 cm in length. It featured 2.5 cm-spaced slots on the side as a means to reference salt particulate migration distances within the MSL Tube Segment.

The 3-D printed column ruler served the same function as the measuring tape sticker, but for a different vessel material. The slot spacing in the column ruler was initially designed for gaps to be in centimetre increments; however, test prints of the design repeatedly collapsed due to the numerous amounts of hollowed-out spaces in close proximity. As a result, slot spaces in inches were adapted.

Figure 3.9: 3D-Printed Column Ruler.

Time-lapse Video Recording

The final method of observation applied in this work was the use of time-lapse photography. The salt migration process takes extensive periods of time, is unpredictable, and often too minute for the human eye to observe. Time-lapse video recording was able to address such issues because the frequency of the frame rate is significantly slower than the one used to view the sequence. When the recorded video was played at normal speed, time appears to move or "lapse" faster. Time-lapse photography is often used to display processes that are very subtle, slow to the human eye, and hard to capture, such as the motion of celestial bodies in the night sky or plant growth. The same idea was applied to the experiments in this work; time-lapse video recording was used for documenting the changes in FLiNaK salt stored in test tubes because it facilitated the direct visual observation of salt crystal growth away from the original salt mass.

A 4K 20 MP Action Camera manufactured by ACTMAN was purchased for this purpose. The action camera was mounted on a tripod using the included accessories and together the setup was then placed in front of a retort stand with a clamp holding a FLiNaK containing test tube. The camera recorded in increments of 36 hours, which was the maximum amount of time possible given the battery life. Cycles of time-lapse video recording were necessary to observe physical changes.

3.5   Ultrasonic Detection System

To simulate the MSR decommissioning process that was studied in this work, non-destructive evaluation (NDE) was conducted using an ultrasonic pulser-receiver system connected to an oscilloscope. This is referred to as the Ultrasonic Detection System; the purpose being to locate any remaining salt bridges and deposits within a salt-facing component.

A Hastelloy-C256 tube segment belonging to a larger Molten Salt Loop (MSL) had previously molten FLiNaK stuck within it and is an ideal component for representing decommissioning operations of MSRs on a very small scale. Detecting, identifying, and locating remnant salts within MSRs using NDE prior to any D&D activities can minimize contamination from spreading or being released into the environment. Figures 3.10 are photographs of the MSL and the salt plug within the contaminated tube segment.
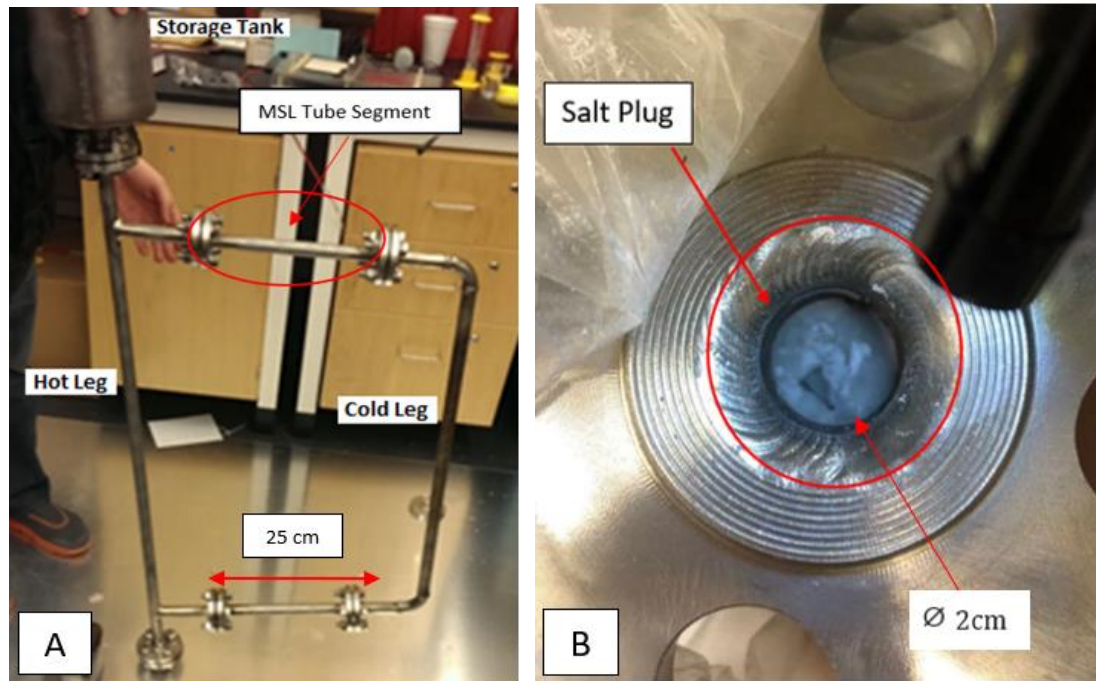
Figure 3.10 (a): Photo of Assembled Molten Salt Loop (b): Photo of Salt Plug in Contaminated MSL Tube Segment.

The pulser-receiver system is a model UT340 manufactured by UTEX Scientific Instruments Inc. Both the pulse width and voltage of the pulser are adjustable so that it can more precisely match the characteristics of a transducer given the application [112]. The pulser-receiver was connected to an oscilloscope to observe ultrasonic waves for salt detection through material

characterization, two models of oscilloscopes, the 2225 50mHz Oscilloscope and the TDS 2012B 2 Channel Digital Oscilloscope produced by Tektronix, were used for this work. The schematic of the oscilloscope connection to the ultrasonic pulser-receiver on pulse-echo mode is featured in Figure 3.11 in the following page.

As seen in Figure 3.11, the ultrasonic transducer was connected to the PULSE/REC connector on the UT 340 while the RF OUT on the instrument was connected to the input on the oscilloscope. The input impedance of the oscilloscope must be set to 50 Ω [112]. The user manual of the UT 340 also notes that the PULSE/REC output should not be directly connected to the oscilloscope as this could destroy the input circuitry of the oscilloscope.
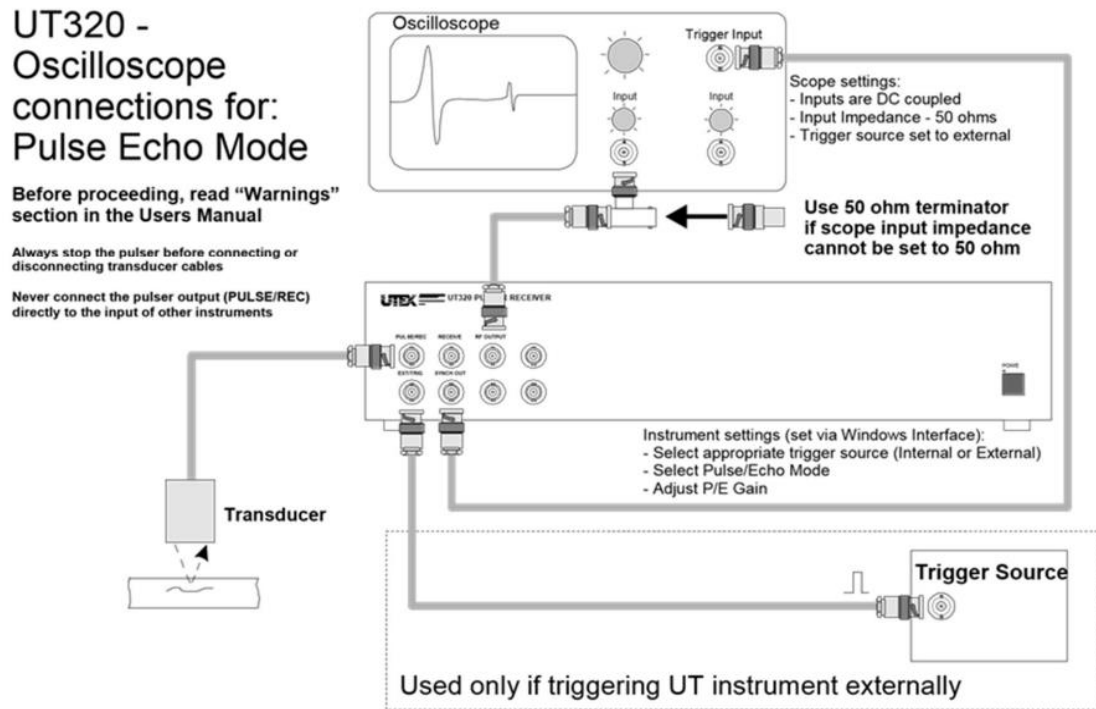
Figure 3.11: Oscilloscope connections for: Pulse Echo Mode from the UT320/340 Operations Manual [112].

3.5.1   UTEX UT340 Pulser-Receiver

The main component of the ultrasonic detection system is the ultrasonic pulser-receiver. The pulser section of the instrument generates short, large amplitude, controlled electric pulses that are converted into short ultrasonic waves when applied to an ultrasonic transducer.

Suitable for small-scale non-destructive testing and evaluation within a laboratory setting, the UEX UT 340 can pulse and amplify centre frequencies from 1 MHz to 150 MHz using ultrasonic transducers [112]. During nuclear decommissioning, ultrasonic testing can be used for flaw detection and thickness gauging. In the case of this work, the additional purpose of salt residue detection is added to the list. The pulser-receiver has two main operating modes: pitch-catch and pulse-echo; the ultrasonic testing in this work was done using pulse-echo mode. The settings of the pulser-receiver are shown in Figure 3.12.
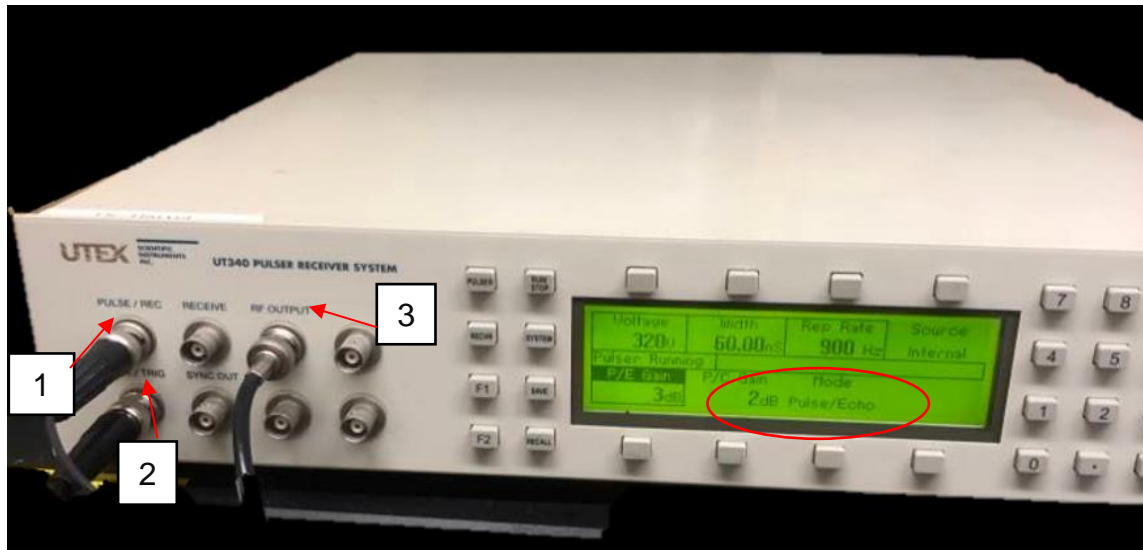
Figure 3.12: Pulser-receiver Setting for Detecting FLiNaK in MSL Tube Segment.

1. The ultrasonic transducer was attached to the PULSE/REC connector on the pulser receiver;
2. The pulser-receiver (EXT/TRIG) was set up to be triggered by the oscilloscope and the receive mode was set to Pulse/Echo (highlighted in red). No digitizer cards were used; and
3. The RF OUT on the instrument was connected to the CH2 input on the oscilloscope.

The pulser-receiver must be appropriately triggered for the oscilloscope to display the correct signal. The instrument was set-up to use the oscilloscope as an external trigger source and the receive mode was set to Pulse/Echo. The RF signal received could be amplified using the gain controls on the instrument and the pulse shape can be fine tuned using the voltage and width

controls. Table 3.3 below summarized the pulser-received setting used in this work as a "starting point" to successfully trigger a signal for the MSL Tube Segment.

Table 3.3: Initial Settings of UT340 Pulser-Receiver System.

Control System Key	Setting	
Instrument Mode Key	Pulser Mode	Pulse-Echo
Display Menu Key	Voltage	320 V
	Pulse-Width	60.00 ns
	Rep-Rate	900 Hz
	Source	Internal
	P/E Gain	3 dB
	P/C Gain	2 dB

The pulse-width, voltage, and rep-rate were often fine-tuned during experimentation depending on the objects examined. Once the system was triggered and the oscilloscope displayed the input signal, then adjusting the settings to focus on the residual salt bridge in the MSL Segment was possible.

3.5.2 Piezoelectric Transducers

This work used piezoelectric transducers along with the pulser-receiver system to transmit (pulse) and receive ultrasonic waves with the help of sonofluids. These transducers use the piezoelectric effect, which is the accumulation of electric charge in certain solids (piezoelectric crystal) in response to applied mechanical stress, to convert the ultrasonic waves into electrical signals for the oscilloscope to display. The transducers house the piezoelectric crystal with damping materials, an acoustic lens, and an electrical cable [113].

3.5.3 Tektronix TDS 2012B 2 Channel Digital Oscilloscope

An oscilloscope was used to graphically display the converted ultrasonic waves in the form of electrical voltages as a two-dimensional plot of one signal as a function of time. The model used was the TDS 2012B 2 Channel Digital Oscilloscope produced by Tektronix, see Figure

3.13. The waveform was positioned at the centre both horizontally and vertically as much as possible to allow for the most complete view of the signal.
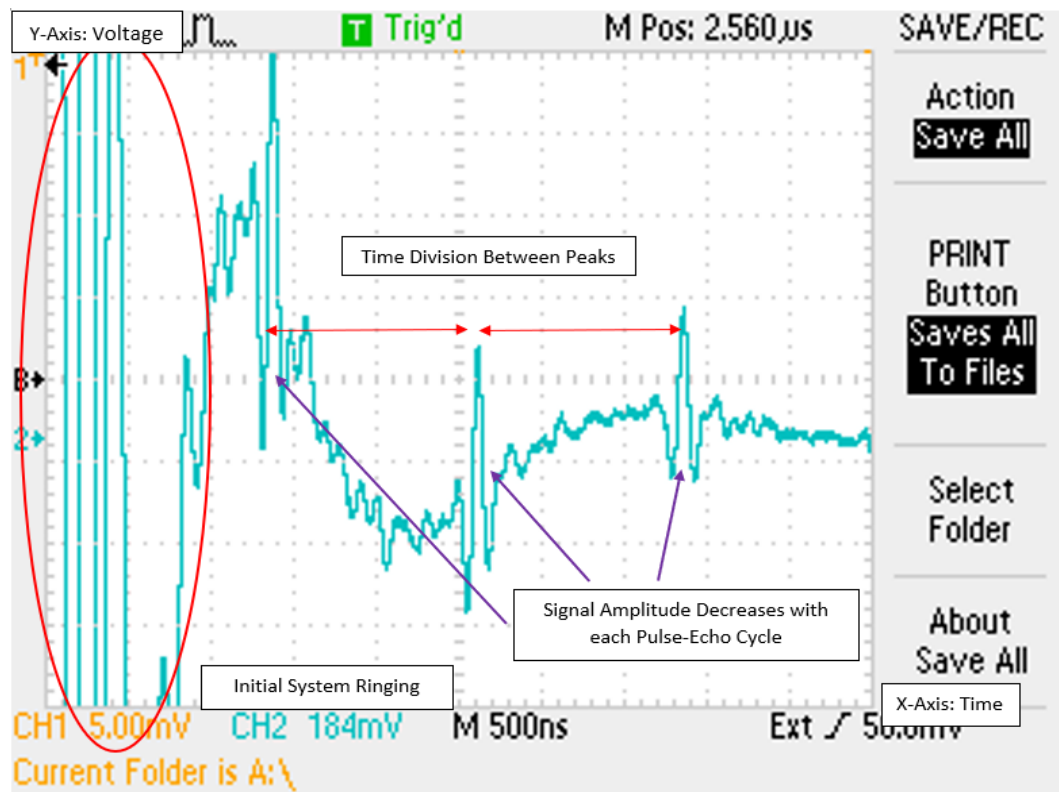
Figure 3.13: Labelled Oscilloscope Waveform of MSL Tube Segment Containing the Salt Bridge.

Like the pulser-receiver, there was a "starting-point" setting for the oscilloscope as well; it is summarized in Table 3.4 on the next page. This setting was experimentally determined to be the most suitable for generating relatively clean signals from the MSL Tube Segment with enough visual detail.

From the displayed waveform, the following information was extracted and documented for analysis: time interval, number of divisions, time per division, frequency, and any visible signal distortion. Signal data were also recorded since irregularities in the wave that are invisible to the human eye can be detected using analysis methods discussed in Chapter 4. They may correspond to larger salt deposits or flaws within the MSL tube structure.

Table 3.4: Initial Setting of the Tektronix TDS 2012B 2 Channel Digital Oscilloscope.

Channel/Controls	Setting	
Trigger Menu	Type	Edge
	Source	External
	Slope	Rising
	Mode	Auto
	Coupling	A/C
Horizontal Sensitivity	Sec/div	2.50 μs
Channel 2	Voltage	150 mV
	BW Limit	100 MHz/Off
	Volts/div	Fine
	Invert	Invert Off

3.6   Molten Salt Loop (MSL) Tube Segment Remelting System

The MSL Segment Remelting System was designed, constructed, and used for the purpose of emulating molten salt removal at the end of operating life of an MSR by remelting and drainage of FLiNaK Salt from a representative Hastelloy-C276 component. A test matrix for the salt drainage experiments is in Section 5.8.1.

The MSL Remelt System consisted of a MSL segment containing residue FLiNaK salt; it was capped at the bottom and connected to the Melting Chamber Monitoring Attachment (MCMA) at the top flange. The MCMA measured the internal pressure and temperature of the tube segment during the FLiNaK remelting process. Heating was achieved by wrapping the MSL Tube Segment in fibreglass heating tapes controlled by an electric heater. The FLiNaK within was melted in a similar fashion to that of the Salt Synthesis System where a vacuum pump was used for the removal of moisture and contaminants. Thus, the MCMA also consisted of a valve that when opened, provided a connection to the vacuum pump, and when

closed, sealed the entire system into a vacuum melting chamber. Figure 3.14 illustrates the MSL Segment Remelting System. This MSL Tube Segment Remelting System facilitated the observation of physical conditions of drained waste salts and end-of-life salt-facing metallic components to offer insights into the decommissioning challenges of MSRs as well as any associated implications for reactor component decontamination.
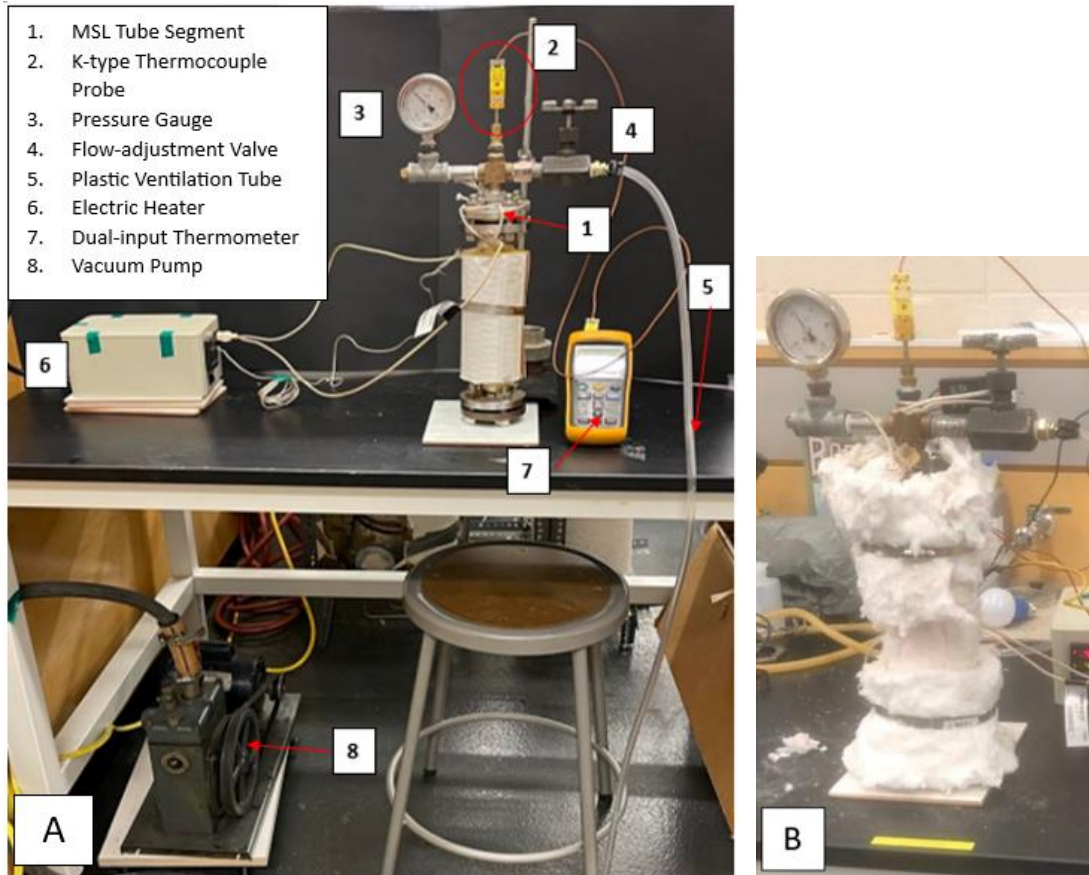
Figure 3.14 (a): Photo of the MSL Segment Remelting System with the Vacuum Pump Attached (b): Loose Wool Insulation used in Sixth Trial of the MSL Tube Segment Salt Remelting Experiment.

3.6.1 Molten Salt Loop Segment

The Hastelloy-C276 MSL tube segment used for this work is a subcomponent of the Molten Salt Loop belonging to the laboratory of the same material. An ASME and TSSA qualified metal fabricator with super-alloy manufacturing experience, GENFABCO was chosen because of their availability of Hastelloy-C that fit the design requirements and dimensions. Selecting a vendor based in Ontario also reduced shipping costs and manufacturing lead time.

The vendor drawing of the Molten Salt Loop, presented in Figure 3.15, describes the   overall dimension of the assembly. The tube segment itself was a welded sub-assembly that consisted of a tube 250 mm in length, 25 mm in width, and 1.75 mm in thickness that was joined at each end to slipped-on flanges (SORF) 85 mm in width and 15 mm in thickness featuring four holes for M20 sized bolts.
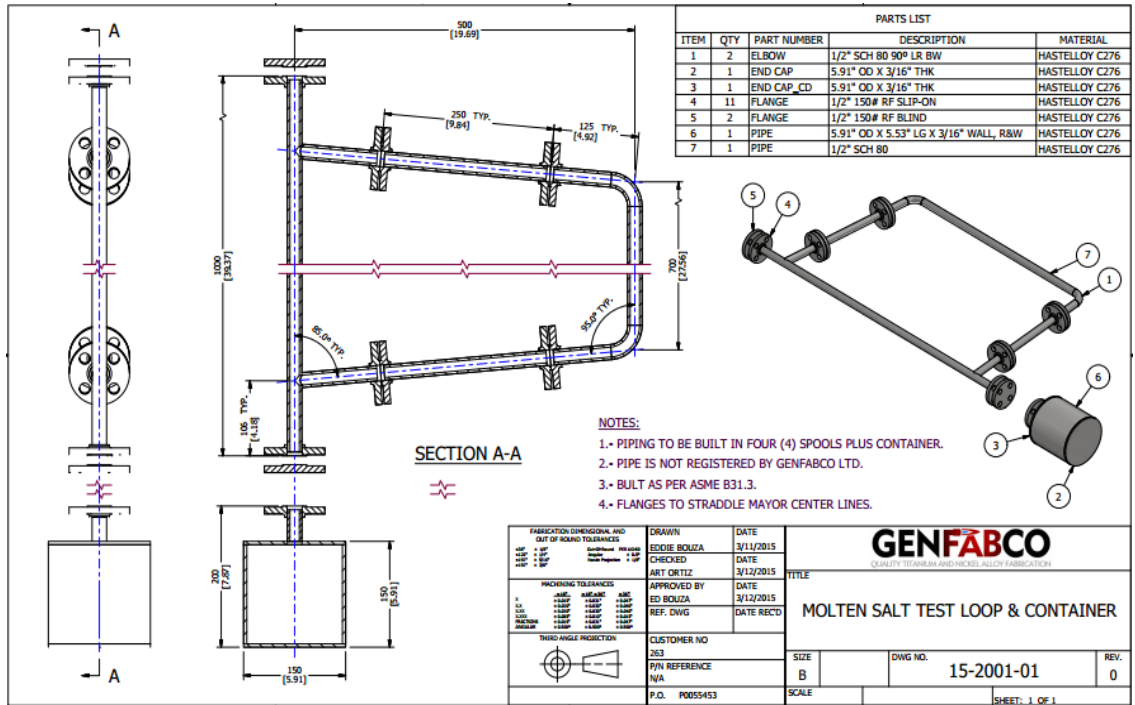
Figure 3.15: Vendor Drawing of Molten Salt Test Loop and Salt Storage Container.

This specific section was selected because it contained a FLiNaK salt plug near one of its flanges and contained smaller crystals of FLiNaK residue throughout its interior from previous salt synthesis experiments conducted prior to the commencement of this work. The scenario represented in this case is deferred decommissioning where the component was mostly drained of salt, but some residual salt remained.
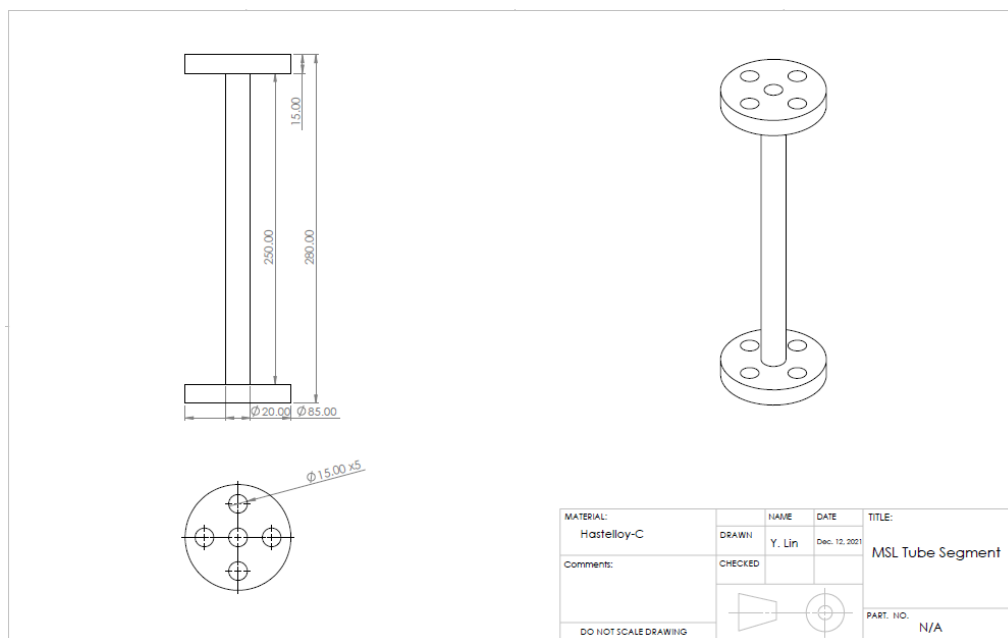
Figure 3.16: Engineering Drawing of MSL Tube Segment.

3.6.1.1 Hastelloy

Based on the design considerations presented in Appendix C, the material selected for the fabrication of the MSL was Hastelloy-C267, which is a subclass of the nickel-based, corrosion-resistant super-alloy Hastelloy from Haynes International, Inc. [114]. Hastelloy contains chemical elements such as chromium and molybdenum whose proportions change depending on the variety; it is resistant to many aggressive chemicals and tolerates high temperatures. These alloys are also ductile, easily fabricated and formed with high weldability [115].

Hastelloy-N

Another variety of this material, Hastelloy-N, was invented at the ORNL and historically used for molten salt applications. The reactor structure, as well as any salt-contacting metal components of the MSRE, were all constructed from Hastelloy-N [116]. The metal proved compatible with fluoride salts including FLiBe and FLiNaK; previous data from the Aircraft Reactor Experiment showed that irradiation did not have a significant effect on the creep rate and strength of Hastelloy-N. However, it was later discovered that the stress-rupture life and fracture strain were severely reduced because of thermal neutron irradiation [117]. Out-of-pile corrosion test programs were conducted for Hastelloy-N and found minimal corrosion

under MSRE conditions. Properties of Hastelloy-N can be found in Appendix D [118]. Seemingly ideal for the construction of the MSL featured in this work, Hastelloy-N was ultimately not selected due to its lack of commercial availability and significant price premium compared to Hastelloy-C276.

3.6.1.2 Hastelloy-C276

As mentioned in the previous section, the Molten Salt Loop is fabricated by GENFABCO in Hastelloy-C276. Hastelloy-C276 is a wrought, nickel-chromium molybdenum alloy that addresses common issues in welding such as porosity, splatter, and cracking through its low carbon and silicon content [114].

Hastelloy-C276 is commonly used in chemical processes and was selected for the construction of the MSL because it is ductile, easy to form, and extremely corrosion resistant in chloride and fluoride solutions at a wide range of temperatures [119]. However, hot working of this alloy must be performed in the temperature range 870-1230 °C followed by a water quench to ensure it maintains maximum corrosion resistance [120]. Tables 3.5, 3.6, and 3.7 below feature the chemical composition, mechanical, and thermal properties of Hastelloy-C276 from several known vendors to provide a range of values.

Table 3.5: Chemical Composition of Hastelloy-C276 [119-124].

Element	Weight %	Atomic %
Nickel	57	60.74
Cobalt	0-2.5	0-2.7
Chromium	16	19
Molybdenum	16	10.5
Iron	5	6
Tungsten	4	1
Manganese	0-1	0-1.14
Vanadium	0-0.35	0-0.43
Silicone	0-0.08	0-0.18
Carbon	0-0.01	0-0.05
Copper	0-0.5	0-0.49

Table 3.6: Mechanical Properties of Hastelloy-C276 [119-124]

Property	Value
Density	8.89 g/cm^3
Poisson's Ratio	0.31
Toughness (Charpy V-notch 10 mm Plate)	472 J
Young's Modulus	205 GPa
Shear Modulus	79 GPa
Yield Strength	355-365 MPa
Ultimate Tensile Strength	785-792 MPa
Elongation at Failure	60 %
Hardness	88 HRB (Rockwell B)

Table 3.7: Thermal Properties of Hastelloy-C276 [119-124]

Property	Value
Thermal Conductivity	10.5 W/(m°K)
Coefficient of Thermal Expansion	11.2 µm/(m°K)
Specific Heat	427 J/kg °K
Melting Range	1323-1371 °C

Corrosion Resistant Properties

Besides its general availability and affordable pricing, Hastelloy-C276 was selected for the experiments in this work because of its exceptional resistance to corrosion at high temperatures. As mentioned in Section 2.4.2 of the Literature Review, Hastelloy-C276 is mostly immune to pitting and stress corrosion cracking in sulfuric, hydrochloric, formic, acetic, and phosphoric acids; it is capable of operating under wet chlorine gas, hypochlorite, or chlorine dioxide environments [122]. Its high molybdenum content also enhanced the corrosion resistance of the alloy in molten fluoride salts.

3.6.2 Fibreglass Heater Tape

Fibreglass heater tapes of the model SST051-040 manufactured by Omega were used to heat the MSL Tube Segment to 475 °C in this work. The heater tapes were rated up to 760 °C (1400 °F), which was well above the desired temperature, 1 inch wide and 4 feet long. The SST051-040 needed 313 Watts of power, had a power density of 13W/in^2, and used a 120 V

voltage supply [125]. The MSL Tube Segment was heated by wrapping the fibreglass heater tapes tightly along the exterior of the segment, both on the middle tubal area and the flanges. Figure 3.17 is a photo of the heater tape setup.
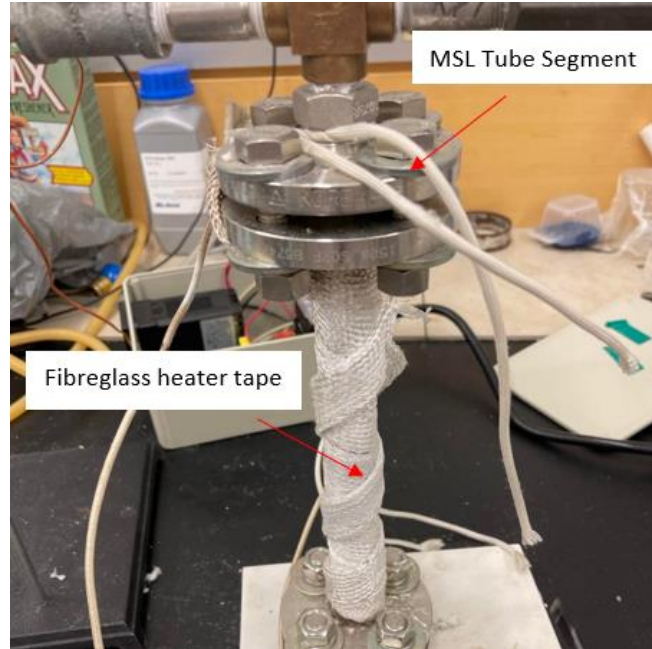
Figure 3.17: Heater Tape Wrapped around the MSL Tube with Flanges Unwrapped.

3.6.2.1   Loose Fibreglass Wool Insulation

Loose fibreglass wool was used to insulate the heat tape wrapped MSL Tube Segment throughout the series of remelting experiments. The fibreglass wool was divided into three sections to cover the tube segment and the two flanges, then, the wool was fastened in place using stainless steel hose clamps. This material is non-combustible and will not decay or absorb moisture. It also did not support the growth of mildew, mold, or fungus which makes it suitable for long-term storage as the experiments of this work spanned over the course of several months [126].
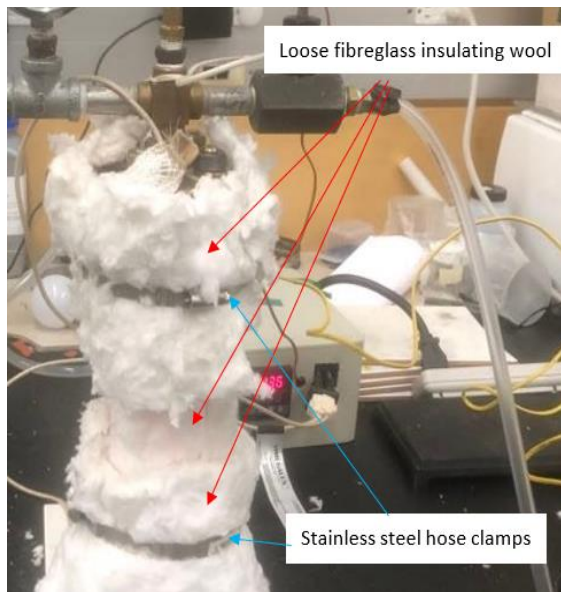
Figure 3.18: Loose Fiberglass Wool Insulation covering the MSL Tube Segment during Heating.

3.6.3   Electric Heater

An electric heater was used to control the temperature of the heater tapes used in the salt melting experiments in this work. The electric heater is turned on and off using a switch. Temperature settings, adjustments, and readings were made via a small display screen featured on the front side of the heater (see Figure 3.19).
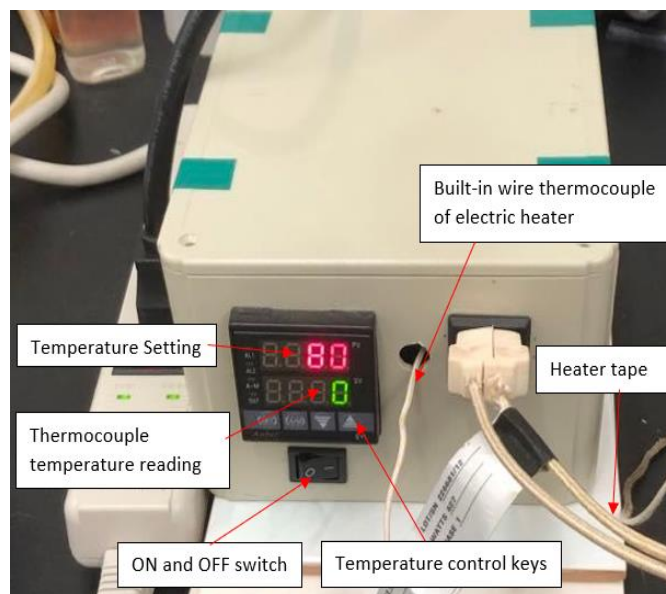
Figure 3.19: Electric Heater Controls with Heater Tape Plugged-in.

3.6.4 Melting Chamber Monitoring Attachment

The Melting Chamber Monitoring Attachment (MCMA) is a subassembly of the Molten Salt Loop (MSL) Tube Segment Remelting System. The MCMA was designed to quantify and, therefore, better describe the interior environment of the MSL Tube Segment during melting experiments. Prior to the construction and use of the MCMA, there were three unsuccessful attempts to melt and drain the FLiNaK from the MSL Tube Segment; this was largely due to the fact that there was no method of accurately measuring the internal temperature and pressure within the melting chamber. A preliminary engineering drawing of the MCMA is illustrated below in Figure 3.20. The full drawing can be found in Appendix E.

The MCMA consisted of a compound pressure gauge, a flow-adjustment valve, and a thermowell; all these components are connected to a cross fitting using various other connection fittings. The bottom connection of the cross fitting is joined to the top connection flange of the MSL using a male-to-male fitting. The flange is then bolted to the MSL Tube Segment using M20 bolts, flat washers, split locks, and M20 Nuts.

Item No.	Item Description
1	½ in. Cross Fitting
2	¼ in. Elbow Fitting
3	Reducing Adaptor
4	Reducing Coupling
5	Pressure Gauge
6	Press-fit Pipe Fitting
7	K-type Thermocouple
8	Set-screw Shaft Collar
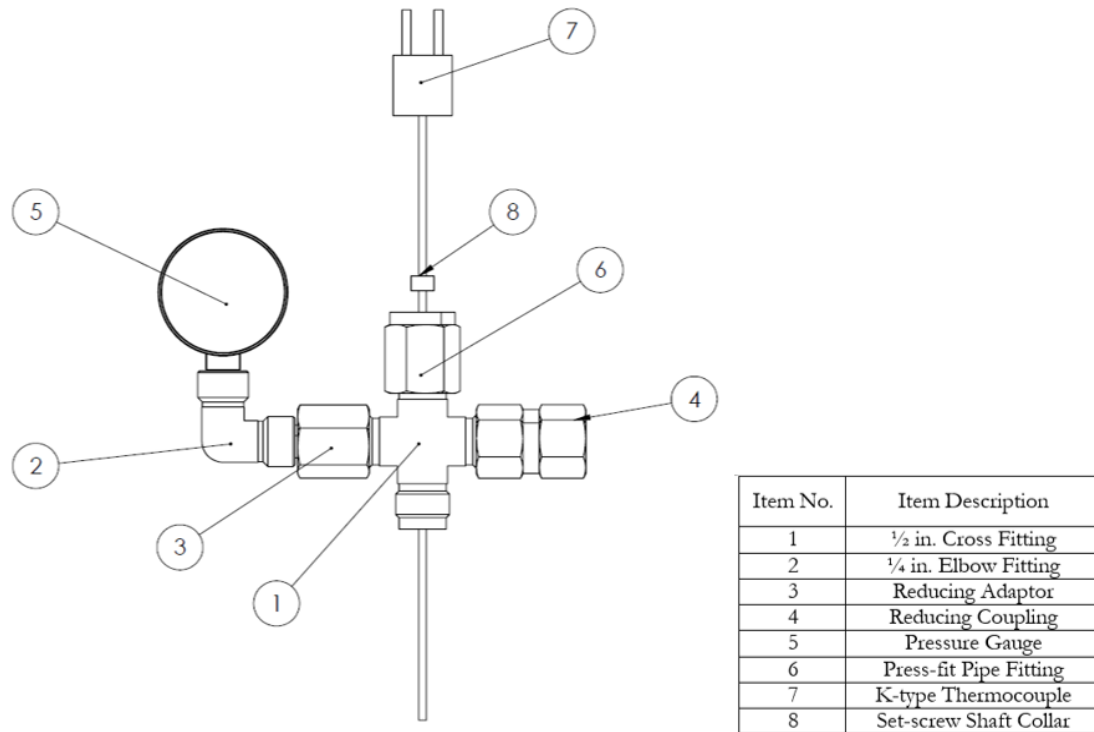
Figure 3.20: Preliminary Engineering Drawing of the MCMA Assembly.

The MCMA consisted of a compound pressure gauge, a flow-adjustment valve, and a thermowell; all these components are connected to a cross fitting using various other connection fittings. The bottom connection of the cross fitting is joined to the top connection flange of the MSL using a male-to-male fitting. The flange is bolted to the MSL Tube Segment using M20 bolts, flat washers, split locks, and M20 Nuts. The valve was connected to the vacuum pump on one side and the right opening cross fitting on the other; it acted as a seal to the MSL Tube Segment Remelting System when closed and facilitated the vacuuming of the system when opened.

The compound gauge, on the left of the cross fitting, provided a reading of the vacuum within the system throughout the experiment in case re-vacuuming is necessary. The thermowell was clamped by a compression fitting that connected to the top opening of the cross connection. All fittings are wrapped in Teflon tape prior to protecting the part. A K-Type thermocouple probe was inserted into the thermowell for temperature measurement.
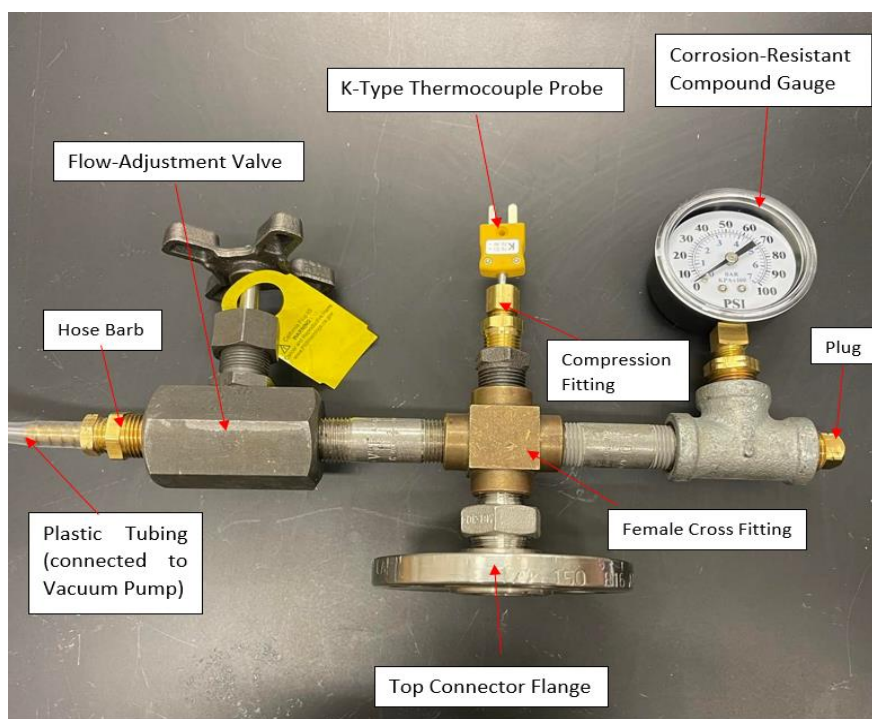
Figure 3.21: Photo of the MCMA.

All instruments were selected based on their ability to operate under high temperatures and corrosion resistance. The assembly itself, though well situated away from the residue salt plug, may be in contact with corrosive fluorine gas released during heating.

The fittings and connections of the final model differed from the initial engineering to prioritize the use of components already available in laboratory hardware storage (cross fitting was female instead of male, *etc.*). Fittings were only purchased to "fill-in-the-gap", which was when fitting of the right sizes were unavailable. Thus, these fittings and connectors were a combination of different materials including brass, copper, and stainless steel.

Considerations were made for the potential of galvanic corrosion, but since the MCMA was not intended to operate in electrolyte solutions and will be disassembled frequently, the phenomenon was not a problem. Similarly, the maximum heating temperature of 475 °C is not high enough for the different coefficient of heat expansion of dissimilar metals used for fittings to become damaged. These two reasons combined invalidated the initial plan to purchase all components in uniform materials.

3.6.4.1 Corrosion-Resistant Gauge

A corrosion-resistant compound gauge, model 38595K12 from McMaster-Carr, was used in this work as part of the MCMA to quantify the pressure within the MSL Tube Segment during remelting experiments. These salt drainage/remelting experiments were conducted under vacuum condition, in high temperature, and a potentially corrosive environment due to released fluorine gas. Consequently, this pressure gauge model was selected because it was capable of measuring both pressure and vacuum, rated for temperatures between -40 °C to 99 °C, and had a stainless steel-304 case coupled with stainless steel-326 connection threads that protect the gauge from corrosive environments [127].

This pressure gauge had a dial diameter of 5 cm; it was small and light enough to fit into the MCMA assembly without interfering with other subcomponents or becoming too heavy for the MSL Tube Segment to support upright during experimentation. In addition, compared to other compound gauges of the same specification, the model 38595K12 was relatively inexpensive, being priced just under $100.

3.6.4.2 High-Pressure Precision Flow-Adjustment Valve

In section 3.3.1.1, it was mentioned that the vacuum pump cannot run safely for more than 30-35 minutes because the internal components overheat. However, salt remelting

experiments often last more than two hours for the MSL Tube Segment to reach the melting temperature set by the electric heater. Thus, a valve was needed to seal the MSL Tube Segment into a vacuum chamber, hold the vacuum for several hours, and provide access by connecting to the vacuum pump when opened. The valve purchased was the high-pressure precision flow-adjustment valve model 4644K48 from McMaster-Carr; it was a needle valve rated for a temperature range of -45.5 °C to 538 °C and uses graphite as its packing material with stainless steel as body material [128]. This valve was ideal for molten-salt application because it was corrosion-resistant and capable of withstanding high temperatures. In the case that the MSL Tube Segment needed to be vacuumed again during heating, fluorine gas released may be withdrawn from the system and contact the valve, hence the selection of corrosion-resistant materials.

Ideally, a ball-valve would have sufficed for this application since only "open" and "closed" modes are required for the MCMA and fine-tuning is not necessary, but ball-valves with comparable specifications were significantly larger and heavier than the 4644K48 and could not possibly fit into the assembly or be incorporated without overturning the entire MSL Tube Melting System. In fact, this valve is the heaviest component of the MCMA, and the attachment had to be carefully balanced during assembly with the top flange of the MSL Tube Segment.

3.7   Procedures

Detailed procedures have been developed with the intention for future researchers to successfully replicate the experimental apparatuses built, experiments performed, as well as operate any equipment or devices that were used in this work. Appendix A lists and includes all of the procedures developed and a brief description of their purpose [129].

3.8   Outline of Tasks and Experiments Performed to Fulfill Thesis Goals

To fulfill the goals of this thesis, the procedures and methods developed in previous sections were implemented. Tables 3.8 and 3.9 outline the procedures and activities conducted to

complete the experiments. The tables also include various tasks and mini experiments that partially fulfilled and offered further insights into the overarching thesis objectives.

Table 3.8: Table of tasks and experiments performed to produce consistently synthesized samples of FLiNaK salt in test tubes using the vacuum melting system and describe the phenomenon of FLiNaK Salt Migration given varied environmental factors

Tasks & Experiments	Relevant Thesis Objective	Relevant Methods, Procedures, and Manuals	Systems Used
Furnace performance testing through heating metallic objects	1	Procedure 1 and Furnace user manual	Furnace, 500g metal nut, smaller chunk of metal
Choosing FLiNaK synthesis vessel	1,2	N/A	Ceramic tube, graphite base, ceramic tube, glass test tube
FLiNaK synthesis testing	1,2	Procedure 4, 5	Bunsen burner, powdered FLiNaK salt, glass test tube
FLiNaK Synthesis testing with vacuum pump	1	Procedure 4, 5	Bunsen burner, powdered FLiNaK salt, glass test tube, and vacuum pump
Incorporation of 2-stage heating and moisture removal	1	Procedure 4, 5	Vacuum FLiNaK Salt Melting System, powdered FLiNaK
Observing salt migration in samples 1-4	1,2	Procedure 9	Vacuum FLiNaK Salt Melting System, measuring tape sticker
Remelting Sample 3	1,2,3	Procedure 4,5	Vacuum FLiNaK Salt Melting System
Relocating Sample 3 to new test tube (Previous one was fluorine corroded)	2,3	N/A	Glass test tube

Monitoring and recording salt migration in sample 3	2	Procedure 9	Measuring tape sticker, retort stand
FLiNaK synthesis of 5 more test tube samples for simulated environmental studies	1,2	Procedure 4,5	Vacuum FLiNaK Salt Melting System
Time-lapse video recording of FLiNaK samples	1,2	Procedure 10 and Camera User Manual	Tripod, time-lapse camera

Table 3.9: Table of tasks and experiments performed to remelt and drain the FLiNaK salt plug and residue from the MSL Tube Segment and to identify the effects of repeated heating on both Hastelloy-C and waste FLiNaK salt

Tasks & Experiments	Relevant Thesis Objective	Relevant Methods, Procedures, and Manuals	Systems Used
Ultrasonic system start-up	2	Ultrasonic pulser-receiver user manual	Ultrasonic detection system, transducers, and stepped acrylic cylinder
Ultrasonic system testing and signal interpretation using different objects	2	Procedure 2, and Ultrasonic pulser-receiver user manual	Ultrasonic detection system, transducers, stepped acrylic cylinder, hollow cylinder (with and without water)
Testing fibreglass heater tape	3	Procedure 3	Heater tape and electric heater
Drain testing of MSL Tube segment using heater tape	2,3	Procedure 3,6	MSL Tube Segment, blind flange, connector flange, heater tape, and electric heater
Drain testing of MSL Tube segment using heater tape with vacuum pump	2,3	Procedure 6	MSL Tube Segment, blind flange, connector flange, heater tape, electric heater, and vacuum pump

Design and construction of MCMA	3	Procedure 7	Molten Salt Loop Tube Segment Remelting System, MCMA
Addition of fibreglass insulation sleeve	2,3	Procedure 6,7	Molten Salt Loop Tube Segment Remelting System, Fibreglass insulation sleeve
Replaced heater tapes (used 1" instead of 1/2") and insulation (loose fibreglass wool instead of sleeve)	3	Procedure 6,7	Molten Salt Loop Tube Segment Remelting System
Collection and storage of drained salt in sealed container	2,3	Procedure 8	FLiNaK salt crystals and a glass jar
Microscope analysis of contaminants within drained FLiNaK	2,3	Procedure 11	Dark flecks of contaminants in FLiNaK salt crystals, microscope, microscope slides
Spectroscopy analysis of contaminants found within drained FLiNaK [43]	2,3	NDL-RCT-PRO-011	Microwave plasma system, Black Comet spectrometer

3.8.1 Experiment and Test Matrices

Tables 3.10 to 3.12 feature test matrices for the experiments performed for FLiNaK synthesis and observation, as well as salt plug drainage from the MSL Tube Segment. Table 3.10 and 3.11 outline the test conditions applied during the preparation of individual FLiNaK samples in Cycles-A and B, respectively. Not all samples were synthesized with the use of the vacuum pump; their storage conditions also vary to emulate distinct potential decommisoning environments. The mass of FLiNaK is the measured mass of the powder prior to melting. Table 3.12 outlines the test matrix for FLiNaK salt drainage experiments.

Table 3.10: Test Matrix for the Synthesis of Cycle-A FLiNaK Samples. Table generated from procedures 4 and 5.

Testing	Sample	Mass of FLiNaK (g)	Synthesis Heat Source	Use of Vacuum Pump	Storage Condition
Initial test sample. Verified that the Bunsen burner was a sufficient heat source for melting FLiNaK.	A-1	1.25	Bunsen Burner	Not used.	Sealed with Parafilm, some time after sample cool-down .
Testing the effects of using vacuum pump for impurity removal during salt synthesis of samples.	A-2	1.50		Used during melting and cool-down.	Immediately sealed with Parafilm upon sample cool-down.
	A-4	2.50			
Testing the effects of using vacuum pump for impurity removal during salt synthesis and cooling-down of sample.	A-3	2.31		Used during melting .	Immediately sealed with Parafilm upon sample cool-down.

For Cycle-B, the synthesis heat source is the same as in Cycle-A (Bunsen burner) and thus not repeated.

Chapter 3. Experimental Materials and Methods

Table 3.11: Test Matrix for the Synthesis of Cycle-B FLiNaK Samples. Table generated from procedures 4, 5, and 9.

Testing	Sample	Mass of FLiNaK (g)	Mass of Water Added (g)	Use of Vacuum Pump	Storage Condition
Testing the effects of adding liquid water to freshly prepared FLiNaK.	B-1	1.497	1.03	Used during melting and cool-down.	Immediately sealed with Parafilm upon sample cool-down.
	B-2	1.502	0.55		
Testing and examining the effects of not using the vacuum pump and not removing moisture from FLiNaK powder during salt synthesis.	B-3	1.498	0.0	Not Used.	Immediately sealed with Parafilm upon sample cool-down.
Controlled sample.	B-4	1.499	0.0	Used during melting and cool-down.	Immediately sealed with Parafilm upon sample cool-down.
Testing the effects of cyclically remelting FLiNaK to prevent salt migration and mitigate hygroscopicity and deliquescence.	B-5	1.501	0.0		Immediately sealed with Parafilm upon sample cool-down. Cyclically remelted every 3 weeks.

Table 3.12: Test Matrix for FLiNaK Salt Plug Drainage Experiments. Table generated from procedures 3, 6, and 7.

Testing	Material Used
Verifying the proper functioning of heater tapes.	Heater tapes, electric heater
Measuring the internal temperature and pressure of the MSL Tube Segment during heating while keeping the system under vacuum conditions.	Design, construction, and incorporation of the MCMA
Testing the effectiveness of fibreglass insulation heat retention for heat sinks (flanges of MSL Tube segment).	Fibreglass sleeve insulation, fibreglass wool insulation

Chapter 3. Experimental Materials and Methods

Having devised the appropriate procedures as well as procured and produced all the necessary apparatus, the experiments outlined in this section were performed throughout a 26-month period. The results of these investigations and any subsequent analysis of the outcomes are presented in the next chapter – Results and Analysis.

Chapter 4

Results and Analysis

4.1 Introduction

This chapter presents the experimental results obtained to achieve the objectives of this work. Firstly, results of detecting the FLiNaK salt plug and residue salt within the MSL Tube Segment using non-invasive surveying methods that may be used for the decommissioning of MSRs are discussed. Then, the results of FLiNaK synthesis, storage, and remelting experiments are presented in reference to the consistently observed phenomenon of FLiNaK salt migration. Finally, the outcomes of the MSL Tube Segment remelting experiments are illustrated, including the condition of the salt plug and residue, the effects of repeated heating on the Hastelloy-C vessel, and the state of the drained salt.

The exploratory and novel nature of these experiments meant that the results are predominantly qualitative observations, then as patterns emerged, methods of analysis were devised and implemented to quantify the previously noted phenomenon.

4.2 Molten Salt Detection through Ultrasonic Methods

This section describes the results of a series of short, investigative experiments involving the use of ultrasonic methods for the detection of residual FLiNaK salt in a Hastelloy component representative of those found in MSR systems. As mentioned in the previous chapter, this segment of the MSL Tube Segment had a salt plug within it near one of the flanges of the tube segment; the section had been placed in storage for about a year at the start of this thesis project. Since one of the main objectives of this project was to emulate molten salt drainage from a component, it was thus sensible to start this process by identifying the presence of FLiNaK and its location within a component.

105

The Ultrasonic Detection System was used; signals generated by the oscilloscope were recorded then verified to ensure they corresponded with the materials being analysed. These signals were subsequently downloaded from the digital oscilloscope in Excel files for signal processing using a Fast Fourier Transform. This method attempted to identify specific signals that could have been the FLiNaK salt plug to establish an NDT screening method for residual molten salts in the reactor system during decommissioning and decontamination activities. It is worth noting that the lack of salt consistency, due to the salt plug being irregular in shape and thickness within the tube segment, made getting a clean signal passing extremely challenging. Hence the need for signal processing.

Upon having effectively triggered, generated, and identified a signal that corresponded to the solid steel block using the Ultrasonic Detection System, the following experiments focused on the examination of the MSL Tube Segment. The transducer was placed along the exterior walls of the tube to examine areas near and at the location of the salt plug. The digital oscilloscope processed the reflected signal into sinusoidal waveforms while the voltage and time data were recorded. Adjustments were made to the vertical and horizontal scale of the oscilloscope display screen to center the signal produced, which visually corresponded with the physical features of the tube as seen in Figure 4.1. The signal was verified to reflect the tube wall of the MSL Tube Segment using the method discussed in Section 2.9.3.
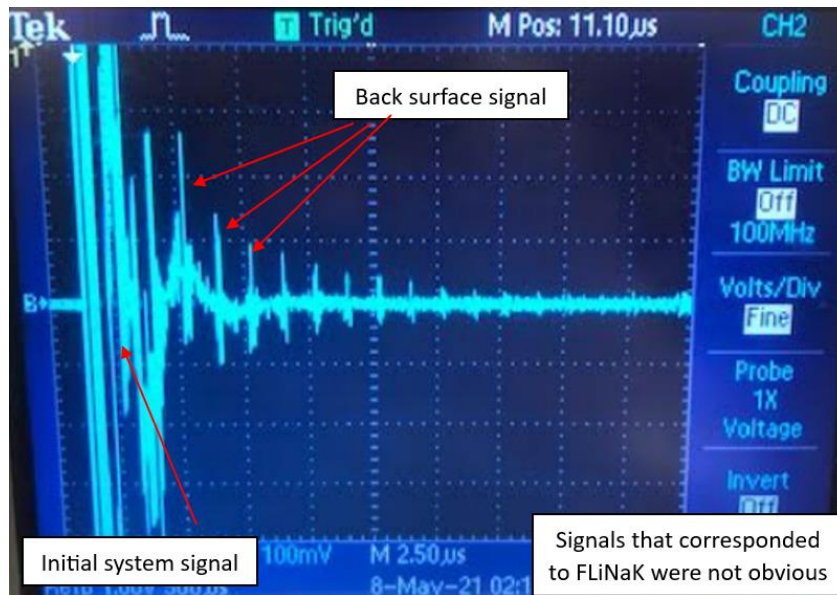
Figure 4.1: Ultrasonic Scan of MSL Tube Segment at the Location of FLiNaK Salt Plug.

4.2.1 Fast Fourier Transform Analysis

Fast Fourier Transform (FFT) analysis was performed using the FFT feature embedded in MATLAB, then verified using the same function in Microsoft Excel. Signals recorded from the oscilloscope of both the salt-filled and empty sections of the MSL Tube Segment were saved in Excel files that contained a column each of time and voltage data. The data were then imported into MATLAB for FFT data processing.

As a reference, filtered time domain signals of the tube section with and without FLiNaK are featured in Figures 4.2.
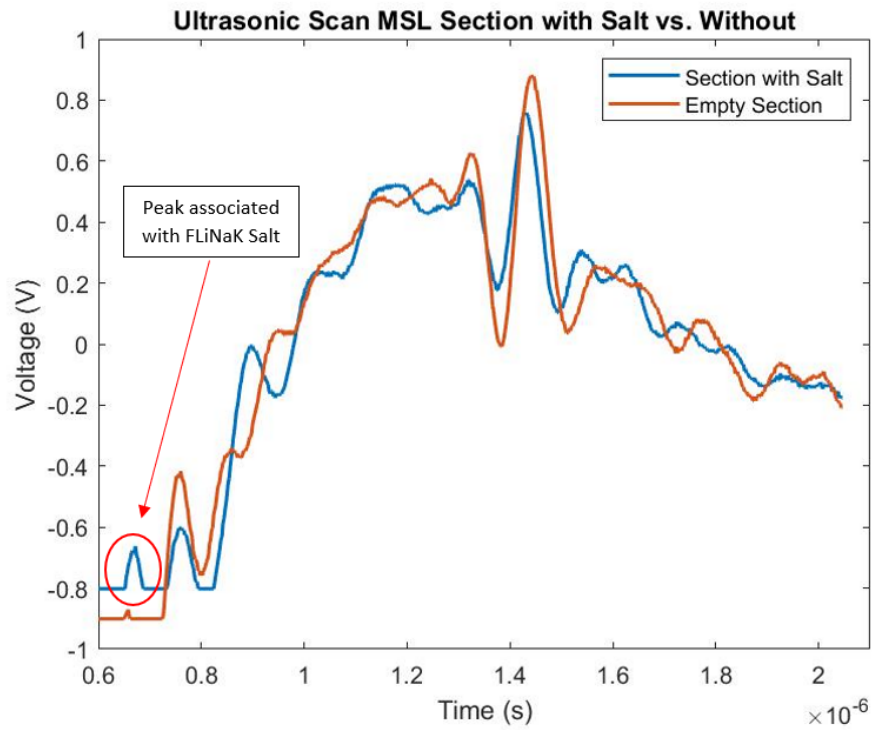
Figure 4.2: Voltage vs. Time Plot of Both MSL Tube Segments.

One of the immediately noticeable differences between the two is that the scan of the section containing the salt plug has two prominent peaks near the 0.8 mark on the time axis while the section without salt only has one; this extra peak could imply the presence of FLiNaK salt within the Hastelloy. Other differences were also observed between the signals, though they are not distinct enough to definitively identify which ones correspond to the salt plug within the MSL Tube Segment. Thus, FFT analysis and zero-padding were applied to the data sets in an attempt to pinpoint signals which represent FLiNaK.

Ideally, a series of discrete signals corresponding to distinct materials would be visible in the frequency domain from which one or more signals that represent the FLiNaK salt plug should be able to be identified. This was achieved by comparing the differences between the FFT of ultrasonic signals of tube sections with and without salt. The results of which are presented in Figures 4.3 and 4.4.

The X-axes (frequency) of the figures are shown in both linear and logarithmic scales; they have been modified to filter out noise and symmetrical signals in order to focus on areas in which signals are most likely to suggest whether there was a presence of FLiNaK salt. To ensure consistency, the same sampling frequency, duration, and number of data points were used to map the oscilloscope signals to the frequency domain.
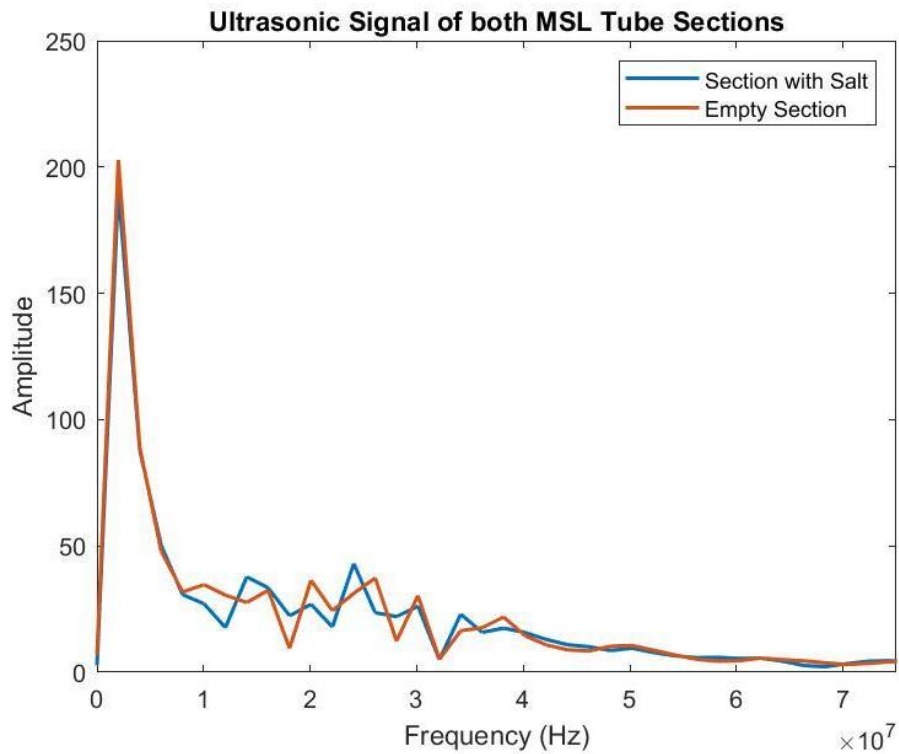
Figure 4.3: Ultrasonic Signal of Both MSL Tube Segments in the Frequency Domain (Linear Scale).
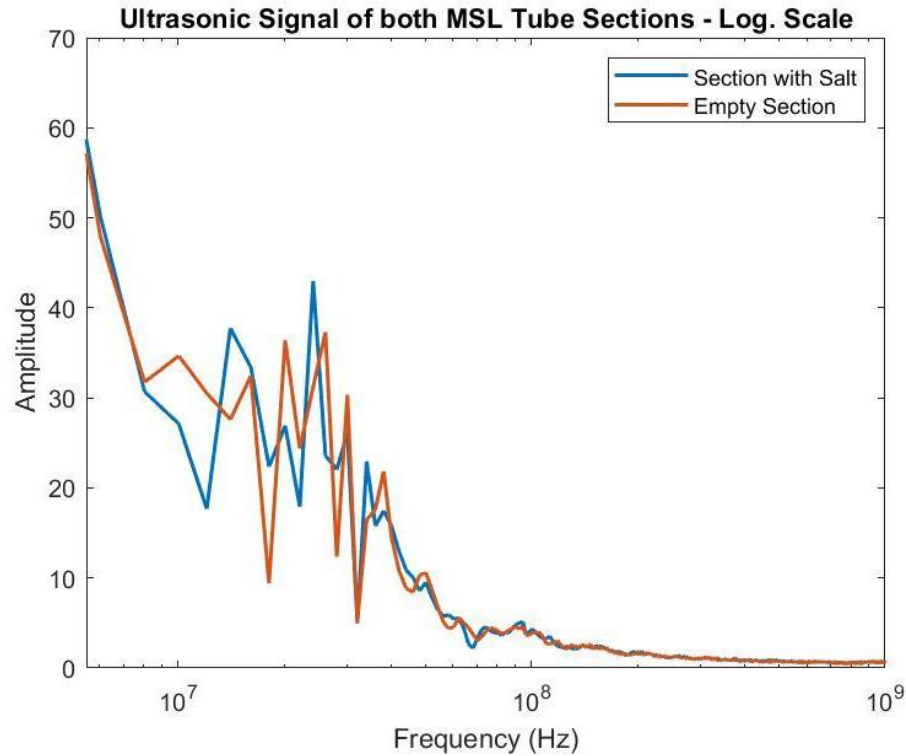
Figure 4.4: Ultrasonic Signal of Both MSL Tube Segments in the Frequency Domain (Logarithmic Scale).

The results of the FFT analysis for both tube sections did not appear significantly different. Overall, more peaks were noted in the 10-30 MHz range for the FFT plots representing the 4.3 and tube segment with residual salt; this was observed in both frequency scales. Figures 4.4 also showed a change in shape and difference in the signals at 5.2E9 Hz, which may be indicative of the presence of the salt plug being registered. However, this could not be verified or confirmed because of low signal resolution (despite the FFT) and the lack of literature values regarding the speed of sound through molten salts, which is a property previously used to verify the material being analyzed, such as stainless steel.

Given the inconclusive results obtained from this series of experiments, it was determined that a more direct, intrusive method of observation would be required to monitor and investigate the behaviour of FLiNaK within the MSL Tube Segment for the purpose of drainage. As mentioned earlier in this section, it was very difficult to get a signal passing through the MSL Tube Segment due to the lack of internal salt consistency. Hence, a digital borescope with front and side cameras was used in all subsequent experiments involving the salt plug.

4.3   FLiNaK Salt Characterization

This section describes the observations made during experiments involving the production of FLiNaK salt samples. The section first detailed qualitative observations made of the samples when they were in test tubes then subsequently explored the effects of various parameters during the synthesis process that affect the extent of salt migration. Then, results from employing quantitative analysis methods described in Chapter 3 are presented in order to correlate environmental factors and cyclic remelting on FLiNaK salt behaviour under long-term storage. The section is finally concluded with an analysis of all the phenomena observed.

It was discussed in Section 2.9.1 that the removal of water and proper, air-tight storage of FLiNaK samples could significantly mitigate their extent of salt migration and moisture absorption. Photos A through C of Figure 4.5 show that the migrated salt particles also appear different depending on the synthesis process and storage condition of that particular sample. Using the vacuum pump during salt preparation allowed FLiNaK samples to remain dry for extended periods of time. On the other hand, samples synthesized without the vacuum pump became damp much more quickly. How well the salt retained its shape was also influenced by contact with atmospheric moisture; some samples remained intact while others appeared powdered like. This will be discussed in further detail in section 4.3.2.
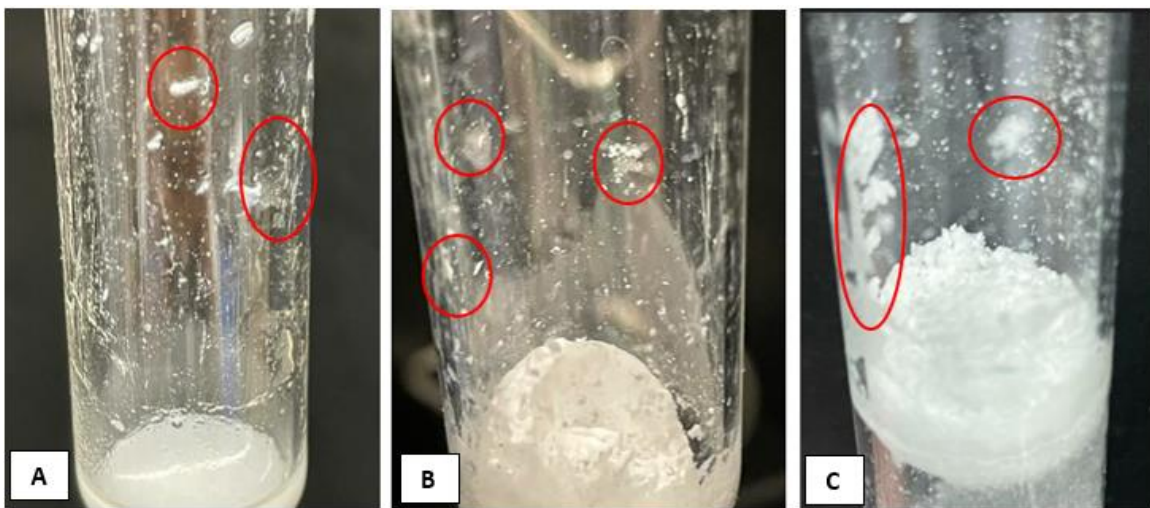
Figure 4.5: Difference in the Appearance of Migrated Salt Crystals (a): The Crystals and Granules are Wet and Surrounded by a Thin Layer of Liquid (b): Dry Crystal Growth Along Test Tube Wall (c): Powdered FLiNaK Migrating Away from Main Salt Mass.

4.3.1 Qualitative Behaviour

The first sample synthesized using the Vacuum FLiNaK Salt Melting System failed to fully melt via heat from the Bunsen burner. This was mostly due to inexperience with adjusting and controlling the flame intensity. Consequently, a propane torch was used as an additional, uneven heat source. At this stage, the process of moisture removal from the powdered FLiNaK had yet to be employed; the initial idea being that using a test tube as a vessel should suffice in making smooth pucks that readily detached from the walls of its container. However, this was not the case. Figure 4.6 shows photos of this first sample during its synthesis process.
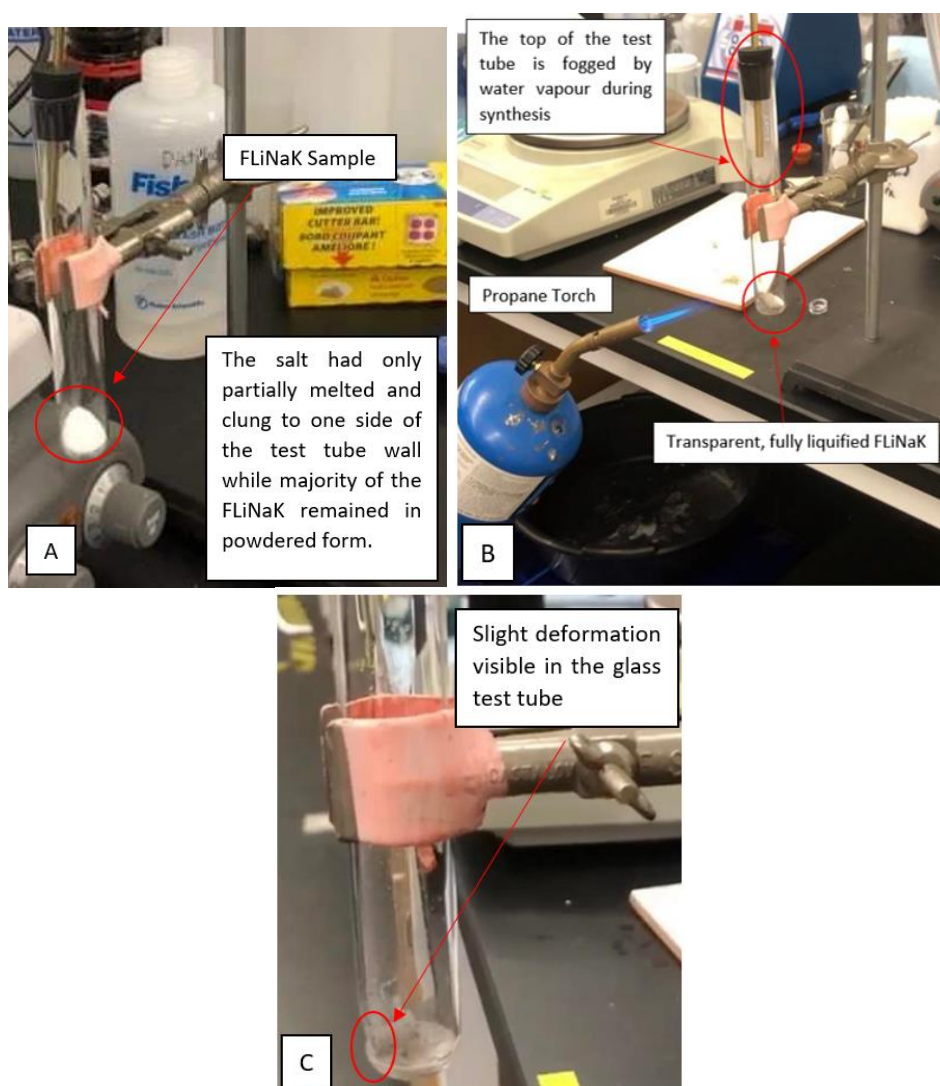
Figure 4.6 (a): Partially melted FLiNaK (b): The propane torch fully melted the FLiNaK, water vapour was observed to cloud the upper lengths of the test tube (c): Glass deformation caused by prolonged heating.

Powdered FLiNaK clung onto the walls of the test tube during the initial melting process in irregular patches, having been partially melted then quickly resolidifying. The added heat from the propane torch completely liquefied and the molten FLiNaK pooled at the bottom of the test tube, where a slight deformation in the glass can be observed. This deformation was the result of prolonged, concentrated heating of a particular area of the test tube. Since propane torches could reach temperatures between 1250 -2000 °C, the glass test tube, which had a melting temperature of 1700 °C, began to deform after about three to four minutes of being in contact with the torch. Once removed from heat, the molten salt remained transparent for a few seconds before solidifying, first along the edges, which had turned opaque, then gradually towards the centre and becoming a white puck taking the shape of the base of the test tube. The sample was rough and had irregular ridges along its edges that adhered to the inner glass walls. There was an obvious presence of water vapour in the melting chamber as well as immediate signs of salt migration in the form of sporadic salt crystals that have spread away from the main salt mass while the sample was left to cool to room temperature. The sample could not be removed or transported for storage elsewhere as it was stuck firmly to its vessel as shown in Figure 4.7.

Figure 4.7: The FLiNaK sample had stuck to the bottom and walls of the test tube and could not be removed.

Consequently, the sample was stored in the test tube sealed with a rubber stopper. Figure 4.8 is a photo of the sample taken after one week of storage; salt migration could be observed and caused the walls of the test tube to become clouded. The migrated crystals had become larger in size, forming patches that appear damp and translucent.
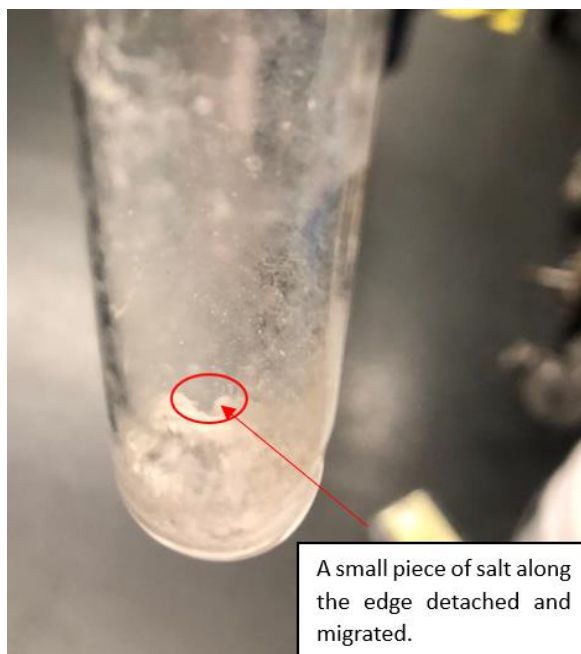
Figure 4.8: Photo of FLiNaK sample taken a week after synthesis displaying aggravated signs of salt migration; the test tube became cloudy from larger salt patches and granules.

These initial findings prompted a series of modifications to the experimental procedures. These changes emphasized the removal of any water moisture that the pre-mixed, powdered FLiNaK may have absorbed during its storage.

To further investigate the relationship between the hygroscopicity and salt migration of FLiNaK, the four Cycle- A samples were synthesized with varying procedures. Then, a final set of five FLiNaK samples, Cycle-B, were produced. Each sample simulated a potential environment that the molten salt may be subjected to at the time of decommissioning. Cycle-B samples were also used to quantify the phenomenon and patterns noted. For all samples, the timeline of the observed results was described in two ways. The first was stating the number of days since the preparation of the sample to describe elapsed time. The second was to include the specific dates on which the samples were prepared and whenever physical changes were noticed and photographs were taken; this would provide a sense of the season

in which observations were made. As stated in Section 2.9, the amount of atmospheric moisture in the laboratory space fluctuated throughout the year; summers tend to be humid while winters are dry. Knowing the time of year provided some context regarding the amount of moisture in the air, which could be related to the extent of salt migration documented. The results of these salt characterization experiments are presented in the following sections.

4.3.2 Synthesis and Storage Parameters

This section describes the different synthesis and storage parameters and how they affect the extent of salt migration in individual FLiNaK samples produced in Cycle-A. The samples from this cycle were consecutively synthesized so that they shared the same observation timeline. All samples produced were prepared using only the Bunsen burner as a heat source. Physical changes in FLiNaK salt appearance can span the course of several months, thus it is crucial that samples share a uniform baseline.

Cycle-A

The purpose of the four samples produced in Cycle-A was to verify the effects of moisture/contaminant removal on the quality and the properties of the resulting FLiNaK salt. Synthesized on August 6th, 2021, this set of experiments manipulated the processes and parameters during the synthesis and storage of a sample. These changes were outlined in test matrices in Section 3.8. Although the adjustments were relatively minor, they were also meant to test the efficacy of incorporating the vacuum pump and two-staged heating method for preparing FLiNaK. The experimental data of the four samples are summarized in Table 4.1 below. The time recorded is accurate to +/- 1 second while the temperature, measured using the infrared camera and laser thermometer, is accurate to 0.5 °C.

Table 4.1 Cycle-A Experimental Data for FLiNaK Salt Synthesis.

Sample Number	Mass (g)	Time to Melting Onset (min)	Time to Fully Melt (min)	Melting Temperature (°C)
A-1	1.25	6:39	8:45	389
A-2	1.50	3:43	6:17	426
A-3	2.31	4:12	6:48	410
A-4	2.50	4:07	6:31	398

All four samples successfully detached from the bottom of the test tube in one piece despite their differences in the melting process. They were stored in their respective test tubes which were sealed using Parafilm. The melting temperature was measured using the infrared imaging and laser thermometer, which yielded readings with notable variances. Given that the melting temperature of FLiNaK is 454°C, this discrepancy in the recorded temperature is likely the result of a long laser ray path or that sample was synthesized under a partial vacuum, which reduces that melting point. Photos of samples A-1 through A-4 are featured in Figures 4.9, and 4.10.
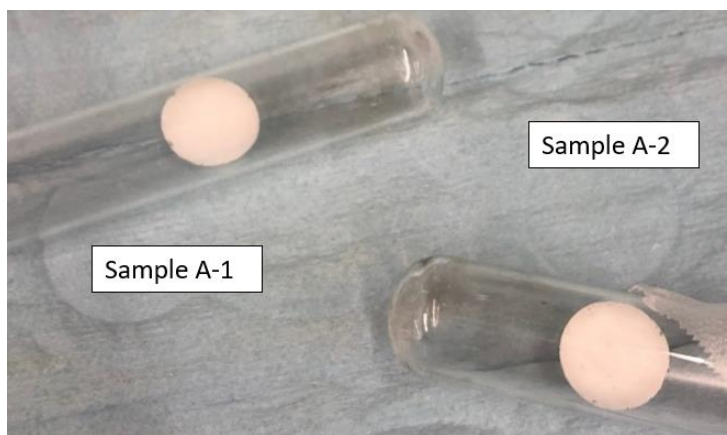
Figure 4.9: Initial Conditions of Sample A-1 and A-2 -The Slight Pink Hue of the Salt Pucks in this Photo is the Result of Low Lighting during Photography.
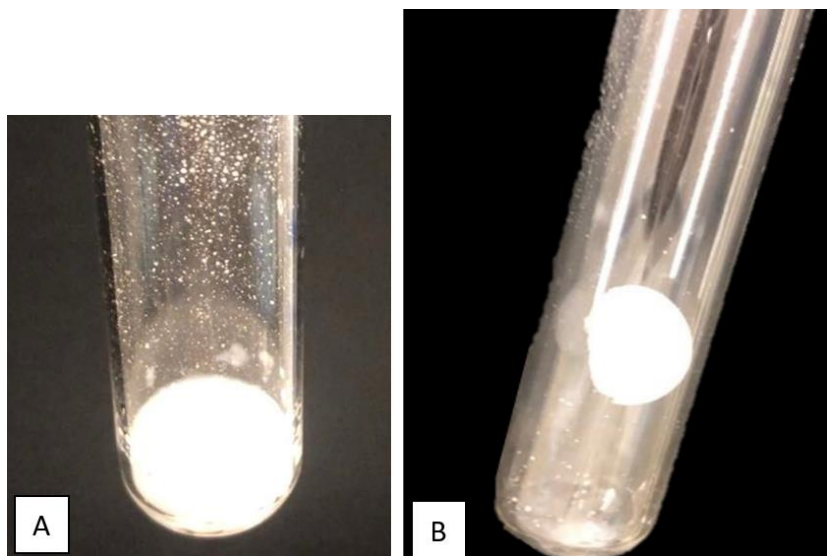
Figure 4.10 (a): Initial Conditions of Sample A-3 (b): Initial Conditions of Sample A-4.

The appearance of the newly synthesized samples was similar to literature descriptions as depicted in Figures 2.21 and 2.22; they are opaque and pure white in its entirety when crystallized. The surface of the salt is smooth, and they take the shape of the bottom of test tubes used to melt them. Most importantly, the four samples were physically consistent. For samples A-2 through A-4, where the vacuum pump was on both during melting and cool-down, a small, mountain shaped tip formed at the centre of the salt puck as a result of suction from the pump through the inserted thin metal tube. This feature will be much more noticeable in photos included later in this section.

The samples were stored in the laboratory and were visually inspected for any physical changes, first every three days, then weekly, then finally bi-weekly. Phenomena such as salt migration and moisture retention were noted whenever observed and photographs were taken. The first of the samples to show signs of physical change was sample A-1. After 13 days (August), the sample appeared wet, and some salt particles detached from the main salt adhered to the glass walls as seen in Figure 4.11; the inner walls of the test tube were no longer spotless compared to Figure 4.9 but remained mostly transparent despite the crystal growth.
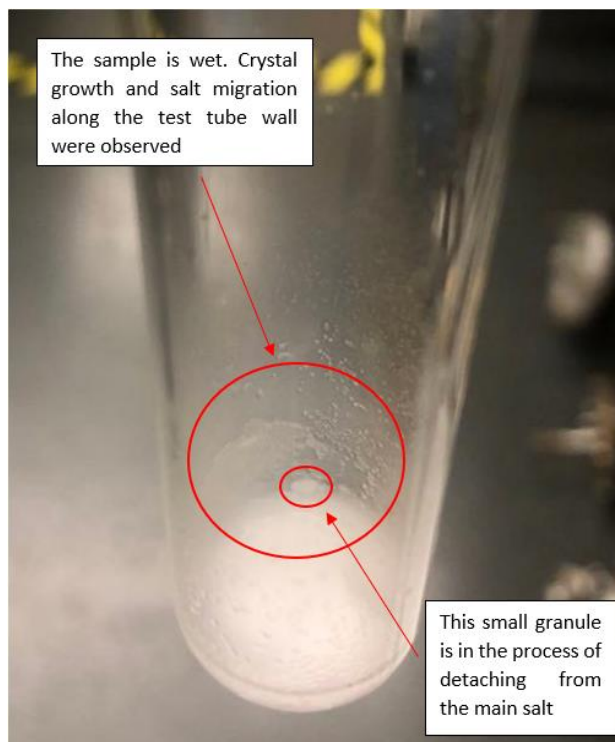
Figure 4.11: Sample A-1 Displaying Signs of Salt Migration and Moisture Absorption (Two Weeks after Synthesis).

Except for sample A-1, no significant physical changes were observed in the other three samples until September. Photos taken a month (September) after synthesis, presented in Figures 4.12 through 4.14, showed some signs of salt migration in samples A-3 and A-4 while sample A-2 appear unaffected.

Figure 4.12: No Physical Changes were Observed in Sample A-2.

Tip formed as a result of vacuum pump suction

Figure 4.13: Sample A-3 Showing Signs of Salt Migration as Salt Crystals begin Detaching and Reattaching Away from the Main Salt Mass.
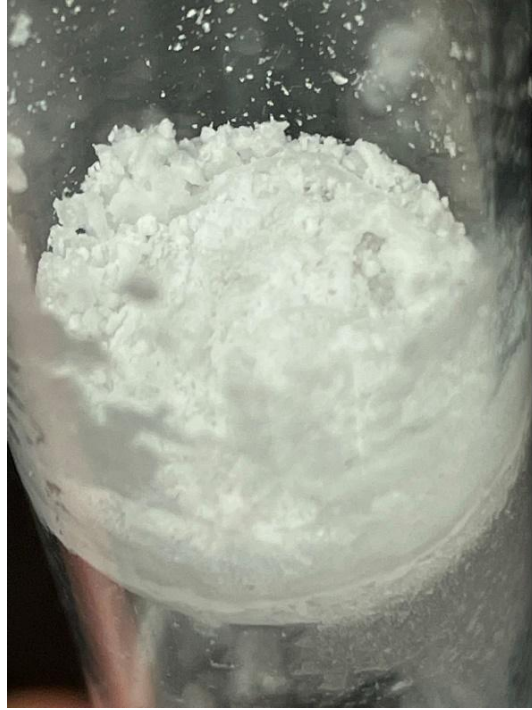
Figure 4.14: The Top Layer of Sample A-4 Fragmented and Some Disintegrated into Powder.

Another set of photos, seen in Figures 4.15 to 4.18, was taken on October 5th, 60 days after the preparation of the Cycle-A samples.
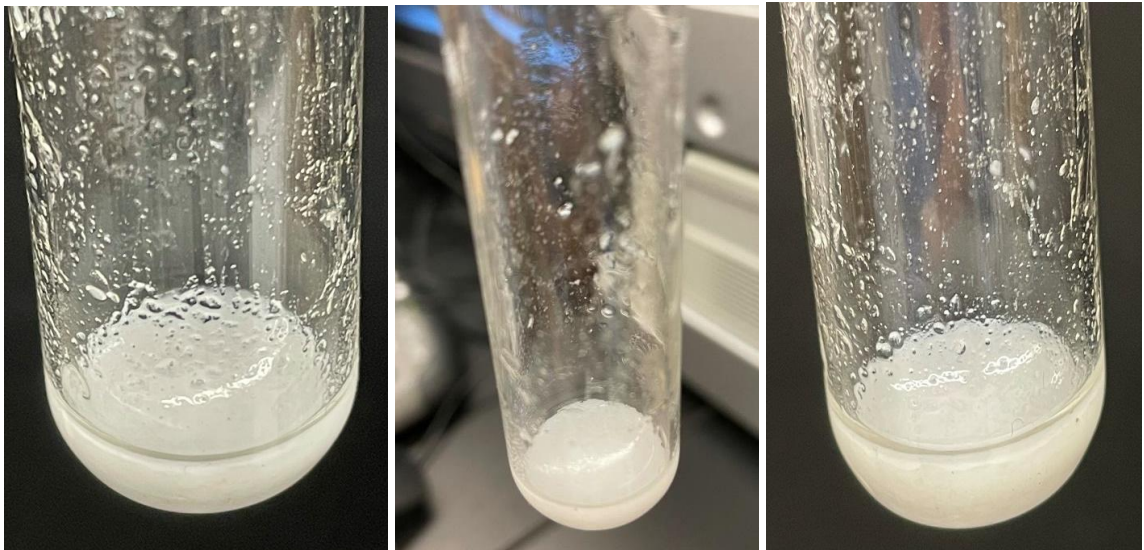
Figure 4.15: Photos of Sample A-1 from different angles - the sample had absorbed such significant amounts of water it became fully submerged in liquid.
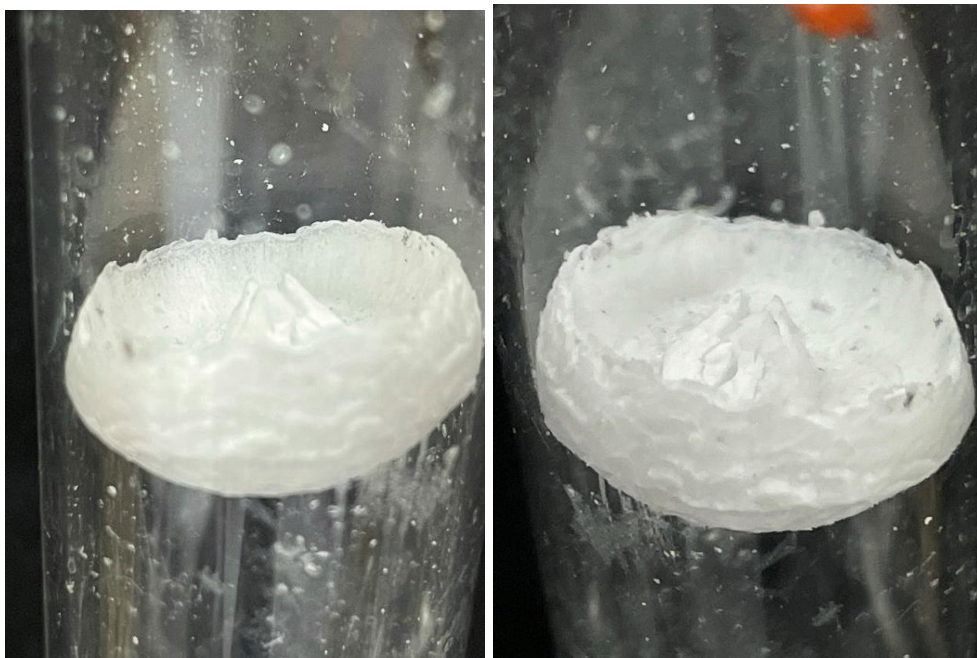
Figure 4.16: Photos of Sample A-2 from different angles – though the signs of salt migration are minimal, the surface of the salt appears cracked with flaking edges.
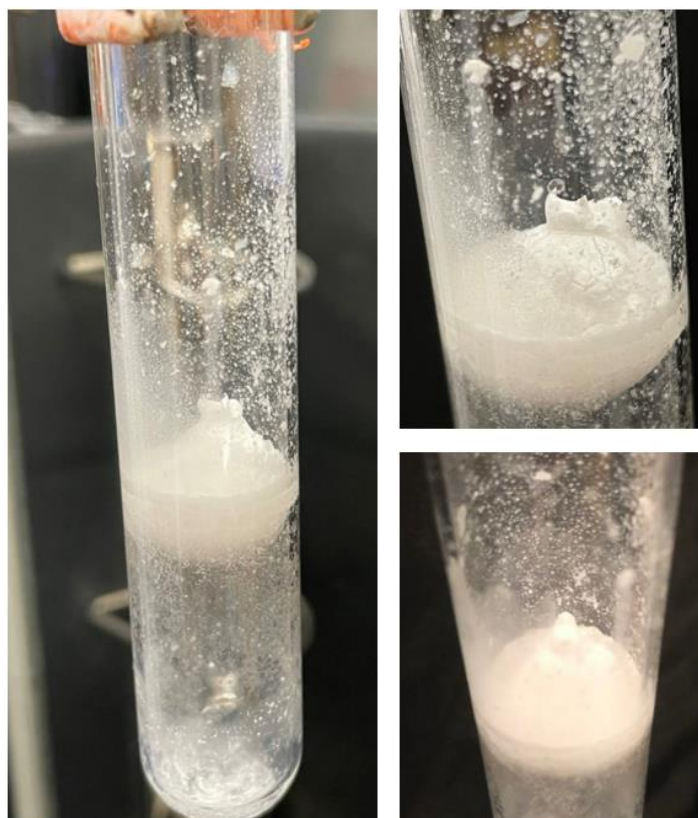
Figure 4.17: Photos of Sample A-3 from different angles – Particles and small crystals of FLiNaK migrated extensively away from the main salt.
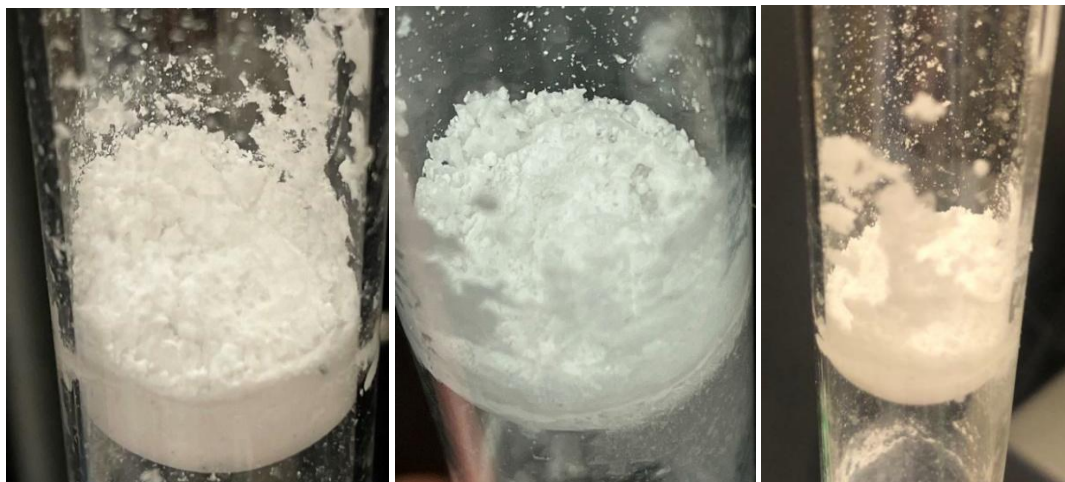
Figure 4.18: Photos of Sample A-4 from different angles – Salt migration of FLiNaK powder patches from the disintegrated top layer of the initial salt puck.

Sample A-1 was fully submerged in liquid. The inner walls of the lower half of the test tube were coated in wet granules and streaks of FLiNaK salt solution. Sample A-3 also displayed much more aggravated signs of salt migration and some crystal degradation. Sample A-2 best retained its original shape with the fewest detached particles; however, the edges of the crystal have started to flake and peel in thin layers. For sample A-4, the salt movement observed appeared to have little to do with moisture; the top layer of the salt puck has disintegrated in powder. Patches of powder latched onto the inner glass walls on the test tube, dispersing away from the salt puck at the centre.

The results presented above suggest that the moisture removal of FLiNaK powder is indeed the key to producing consistent, high-quality samples that detach easily from its synthesis vessel. The two-staged heating method was effective in evaporating the absorbed water content within the powdered FLiNaK throughout the melting process; released water vapour, as well as any contaminants, would then be pumped out of the melting chamber by the vacuuming pump through the thin metal tube inserted. Since the Bunsen burner could only heat the bottom end of the test tube where the FLiNaK was, the evaporated water vapour would then condense onto the inner walls of the top 1/3 length of the test tube where the glass remains relatively cool (70-80°C). For sample A-2 this condensate was fully removed by the vacuum pump, but for samples A-3 and A-4 the condensate persisted and was manually removed via a small microfibre cloth attached to a Q-tip. This was likely due to the two larger

masses of the two samples and thus higher amount of absorbed moisture in the FLiNaK powder. Manual condensate removal was also applied to sample A-1 which was melted without the use of the vacuum pump.

Similarly, from the four samples, it was noted that keeping the vacuum pump on during cooling as well as throughout melting can better mitigate the effects of salt migration but may result in the breakdown of the salt crystal as seen in samples A-2 and A-4. No moisture or water droplets were observed within their respective test tubes throughout their storage, which lasted more than a year. The extra two to three minutes of vacuuming during the cool-down period likely removed any remaining particles in the test tubes' atmosphere and the samples were stored in vacuo. The significance of using the vacuum pump is best demonstrated in sample A-1, which was synthesized without the use of a vacuum pump but still underwent two-stage heating and manual condensate removal. Upon solidifying, the salt appeared dry, smooth, and detached easily from the bottom of the test tube similar to the other three. However, sample A-1 showed the most extensive signs of salt migration and extreme physical changes, suggesting that the vacuum pump removed a noteworthy amount of water vapour during the melting process then previously believed and reinforced the hygroscopicity of FLiNaK, even in powder form.

Full submersion in liquid has only been previously observed in the furnace-synthesized sample prepared by the undergraduate capstone students shown in Figure 4.13. For sample A-1 to undergo such drastic changes implies that the initial appearance of the FLiNaK has little bearing on the eventual extent of salt migration; the differentiating factor being the parameters during synthesis, in this case, the use of the vacuum pump. This idea is supported by Zong et. al., a "vacuum melting platform" was used for the preparation of all samples studied in the work due to its ability to produce stable and consistent specimens [96].

Another crucial factor that has been observed to affect the extent of salt migration and water absorption is the storage of these samples. This process starts the moment FLiNaK samples are sealed with Parafilm, once the test tubes have cooled enough to be manipulated manually. This is rather intuitive: the quicker and more air-tight the seal, the lower the possibility for the sample to come into contact with air and thus the water vapour in it. This process takes anywhere between three to five seconds. Although the relative humidity in the room was not

recorded on the day of salt production, record trends show that the value should be around 50-65%.

Minimal contact with water vapour would in turn better preserve the FLiNaK crystal. Samples A-2 and A-4 were observed to have much fewer indications of salt migration and the FLiNaK remained entirely dry. On the other hand, a slight delay of roughly 10 seconds in the sealing of sample A-1, on account of having to cut a piece of Parafilm, contributed to the extensive salt migration and water absorption of the salt. After six months (February 2022), the entire test tube of sample A-1 was covered in patches, granules, and particulates of FLiNaK salt while the liquid that used to pool at the bottom has all but disappeared. Such behaviour was not observed in the other three samples that were sealed immediately. Figure 4.19 documents the physical changes of this sample.
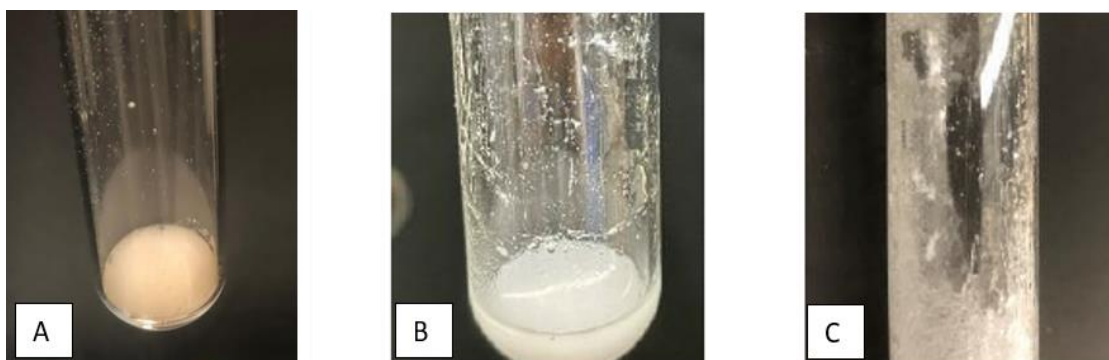
Figure 4.19 (a): Initial Conditions of Sample A-1 (August- Day1); (b): Deliquescence and Salt Migration Observed (Oct.- Day 50); (c): Extensive Levels of Salt Migration (Feb.- Day 185).

An unfortunate accident caused the test tube of sample A-1 to fracture in February. Consequently, the main FLiNaK crystal was transferred and stored in a new, vacuumed test tube. The sample was weighed prior to being stored again; the new mass of the FLiNaK recorded was 1.16 g, indicating that 0.09 g of sample A-1 has migrated away from this main crystal and adhered itself onto the now broken test tube. No visible salt chunks were observed to have broken off during the accident nor were they found during the clean-up process, but it is very likely that some amount of the salt puck was lost when the test tube fractured. In the six months since its synthesis, sample A-1 had lost 7.2% of its original mass, mainly due to salt migration. Once transferred to a newly air-tight test tube, salt migration in sample A-1 subsided (see Figure 4.20), but chunks of salt along the edges were missing.
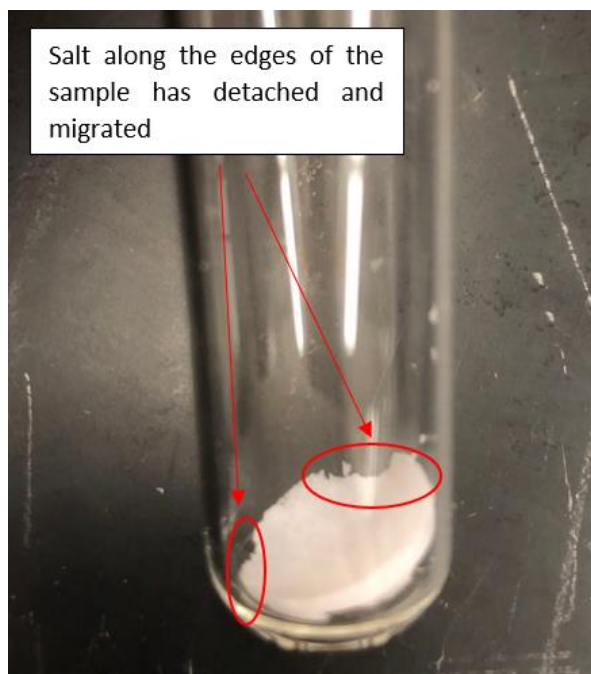
Figure 4.20: Sample A-1 Stored in a New Test Tube – Notable Chunks were Missing Along the Crystal's Edges as a Result of Salt Migration.

Similarly, the maintenance of the seal during the year of storage, also affected the behaviour of the samples. When sample A-3 began to display more-than-anticipated amounts of salt migration and the presence of moisture was noticed in September (a month after synthesis), the seal on the test tube was re-examined and a small rupture was found in the Parafilm. It was concluded that the film had been overstretched, which caused it to fatigue over time and split in some areas. Figure 4.21 is a photo of the tear in the sealing Parafilm.
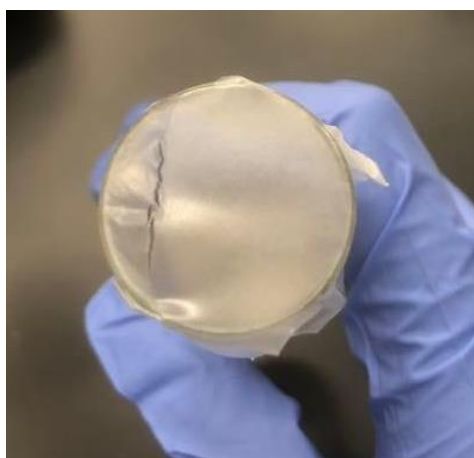
Figure 4.21: The Parafilm Seal of Sample A-3 had Ruptured.

The results of Cycle-A affirmed the hypothesis that contact with moisture was the main cause and an aggravating factor of salt migration in FLiNaK salt. However, these observations were qualitative, and until this point could not be quantified. Thus, methods for salt migration analysis were devised and utilized for samples produced in Cycle-B, which sought to emulate a series of potential MSR decommissioning scenarios. The results of these experiments will be discussed in detail in the following section.

4.3.3 Quantifying FLiNaK Salt Migration

This section presents the results of quantitative methodologies formulated to assess the physical changes observed in synthesized FLiNaK salt. This was achieved through employing two FLiNaK salt migration analysis methods - measuring tape stickers application and time-lapse video recording – on a new set of five FLiNaK samples, Cycle-B, prepared using the vacuum test tube melting system. In addition to quantifying the extent of salt migration, the five Cycle-B samples were also used to simulate potential decommissioning challenges and environments of an MSR by manipulating the amount of water in the test tubes that store these samples.

Cycle B

The purpose of the five samples produced in Cycle-B was to quantify the extent of FLiNaK salt migration given variations in storage conditions. This was to investigate how far FLiNaK can physically migrate in response to contact with different quantities of water. The samples were produced on May 19th, 2022; this set of experiments emulated specific environmental conditions that the salt may be subjected to at the time of reactor decommissioning. These scenarios included catastrophic failure, leakage in reactor vessel, commercial salt handling (refuel and transport), long term storage, and cyclic remelting.

By studying and evaluating the extent of ensuing salt migration in each sample, relevant considerations and challenges regarding D&D activities of MSRs were identified then discussed. The experimental data of the five samples of Cycle-B are summarized in Table 4.2.

Table 4.2 Cycle-B Experimental Data for FLiNaK Salt Synthesis.

Sample Number	Mass of FLiNaK (g)	Mass of Water Added (g)	Phenomenon Observed	Time Since Heating	Temperature Measured (°C)
B-1	1.497	1.03	Water vapour visibly condenses on inner test tube wall	0:08	62.1
			FLiNaK begins to melt	2:14	208.5
			FLiNaK completely melts	6:35	434.2
B-2	1.502	0.55	Water vapour visibly condenses on inner test tube wall	0:10	73.2
			FLiNaK begins to melt	1:58	242.8
			FLiNaK completely melts	5:16	389.1
B-3	1.498	0.00	Water vapour visibly condenses on inner test tube wall	0:13	83.5
			FLiNaK begins to melt	5:14	237.3
			FLiNaK completely melts	11:63	463.2
B-4	1.499	0.00	Water vapour visibly condenses on inner test tube wall		71.4
			FLiNaK begins to melt	1:45	301.7
			FLiNaK completely melts	4:19	458.6
B-5	1.501	0.00	Water vapour visibly condenses on inner test tube wall	0:59	63.5
			FLiNaK begins to melt	1:34	262.9
			FLiNaK completely melts	3:28	441.3

All five samples successfully detached from the test tube in one piece once solidified including sample B-3, which did not employ the vacuum pump during its synthesis However, once water was added to samples B-1 and B-2 (via an eyedropper), they became slightly adhered to the bottom of the test tube as a result of surface tension but can still slide along its surface. The samples were stored in their respective test tubes sealed at the top using Parafilm.

The temperature readings of the five samples during salt preparation were made using a K-type thermometer probe with its tip inserted directly into the molten salt. This method yielded results that better aligned with literature values and were more accurate than those measured using an infrared laser thermometer. For some samples, the salt crystal readily separated from the bottom of the test tube but was stuck to the thermocouple probe instead. Light tapping along the top of the thermocouple with a screwdriver would cause the synthesized salt to detach and fall back into the test tube. Photos of the synthesized samples are featured in Figure 4.22.
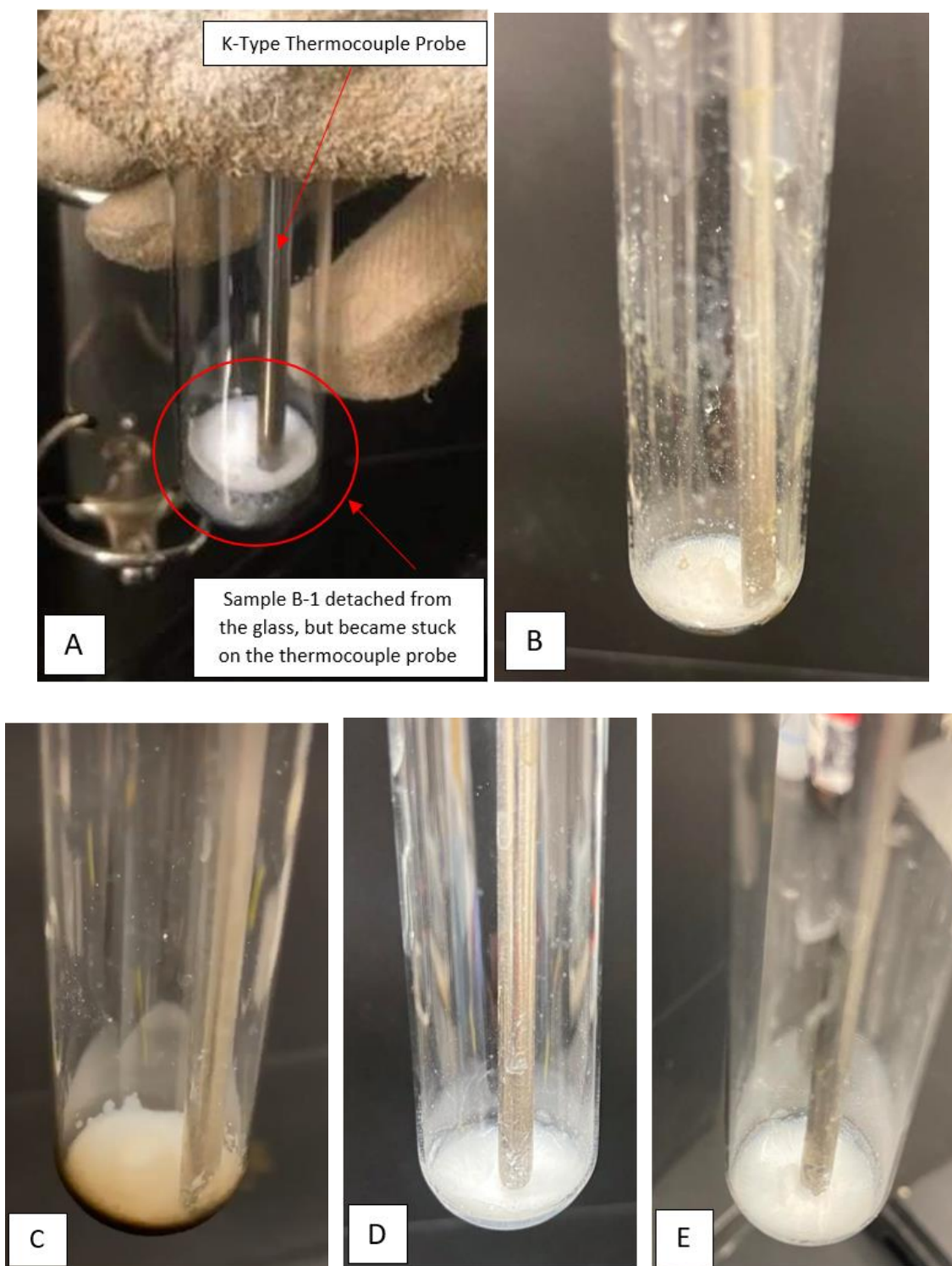
Figure 4.22: Initial Conditions of Cycle-B Samples Upon Synthesis (a): Sample B-1 (b): Sample B-2 (c): Sample B-3 (d): Sample B-4 (e): Sample B-5.

Similar to Cycle-A, the physical appearance of these five samples were consistent with literature descriptions and the previous four samples. All samples, except for B-3, had the vacuum pump on during both the melting process as well as the cool-down period. Thus, samples B-1, B-2, B-4, and B-5 all have the small, mountain shaped tips at the centre of the puck from the suction of the pump.

Larger test tubes (18 mm diameter) were used for Cycle-B to accommodate the size #3 two-holed rubber stoppers, which were required so that both the thin metal tube connected to the vacuum pump and K-type thermocouple could be inserted into the test tube. The wider base of these test tubes made uniform melting more difficult and increased melting time because the salt powder was spread out over a larger area. The positions of the Bunsen burner flame and test tubes were constantly being shifted so that the salt could completely liquefy. The smears of salt along the inner walls of sample B-2 were the result of this jostling motion being overdone. The walls of these 18 mm test tubes were thinner than that of test tubes used for Cycle-A. The effects of which were observed in Figure 4.22 (c), where the bottom exterior of the test tube became blackened due to extended contact with heat. Sample B-3 took significantly longer to melt not only as a consequence of using a larger test tube, but also because the vacuum pump was not used during synthesis, which extended the process of water evaporation.

The five samples were labelled once sealed. In addition, a strip of measuring tape sticker with units in centimetres was adhered to the exterior of each test tube with its "zero" marking aligned to the top edge of the salt crystal. The samples were then stored in the laboratory on a custom test tube rack and visually inspected for any physical changes such as moisture retention and salt migration, first weekly, then bi-weekly. The extent of salt migration over time was quantified through documenting the distance between detached specs of salt and the "zero" on the measuring tape sticker each time the samples were inspected. Photographs were taken whenever such phenomena were noted.

For the first three weeks, no signs of physical change were observed in any of the five samples. However, the samples with added water, samples B-1 and B-2, became firmly stuck to the bottom of the test tube when they previously were able to slide along the curved inner surface. The water was completely absorbed by the salt crystal; yet neither sample looked damp or wet

and displayed no signs of salt migration whatsoever. In late June, 35 days after salt synthesis, signs of salt migration were observed in sample B-3; the bottom of the test tube became clouded and salt particles began to disperse, though no farther than 1-2 cm from the edge of the crystal. Salt stains, in the form of thin, translucent film, can be seen along the length of the test tube. These stains do not contain any solid mass (specs, granules, chunks, *etc.*) of salt and were not accounted for. Figure 4.23 shows sample B-3 during this time. Samples B-4 and B-5 remained physically unchanged.
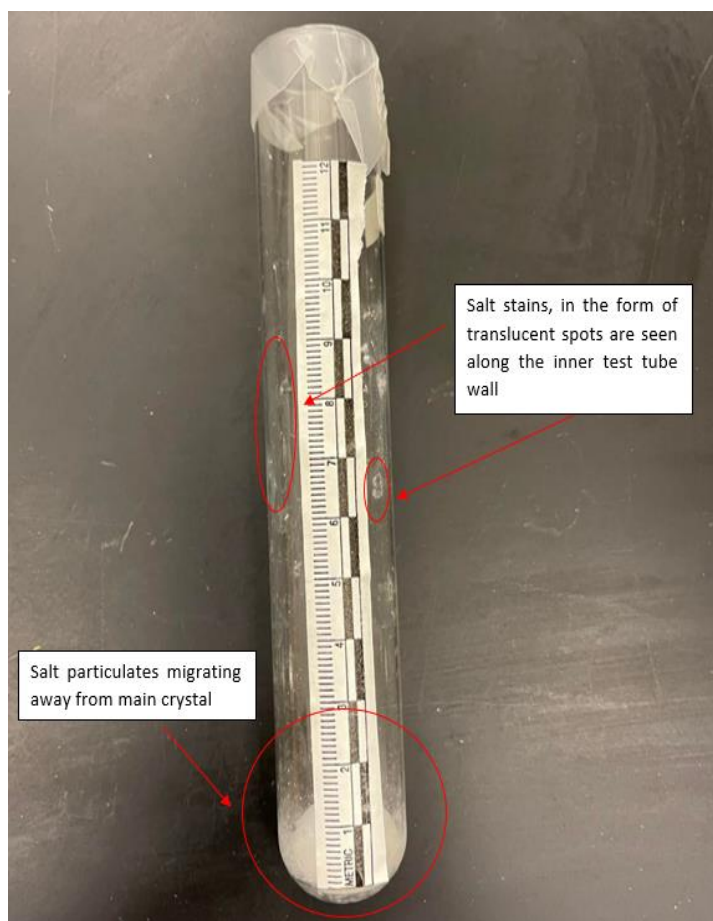
Figure 4.23: Signs of Salt Migration Observed in Sample B-3 (4 weeks after synthesis).

The samples remained stable for another four to five weeks, during which minute signs of salt migration were observed more prominently in sample B-1 and less so in B-2. Sample B-1 showed signs of deliquescence and salt looked wet. The most drastic changes were noted in sample B-3. The salt crystal had become wet; similar to sample A-1, sample B-3 appeared

fragmented and was partially dissolved in aqueous solution. This prompted a set of photos, Figures 4.24 through 4.28, to be taken of all five samples. It was late July, 68 days after salt synthesis. Sample B-4 remained entirely unchanged while sample B-5 had been remelted in new, vacuumed test tubes twice to investigate the effects of cyclic remelting on prepared FLiNaK salt.
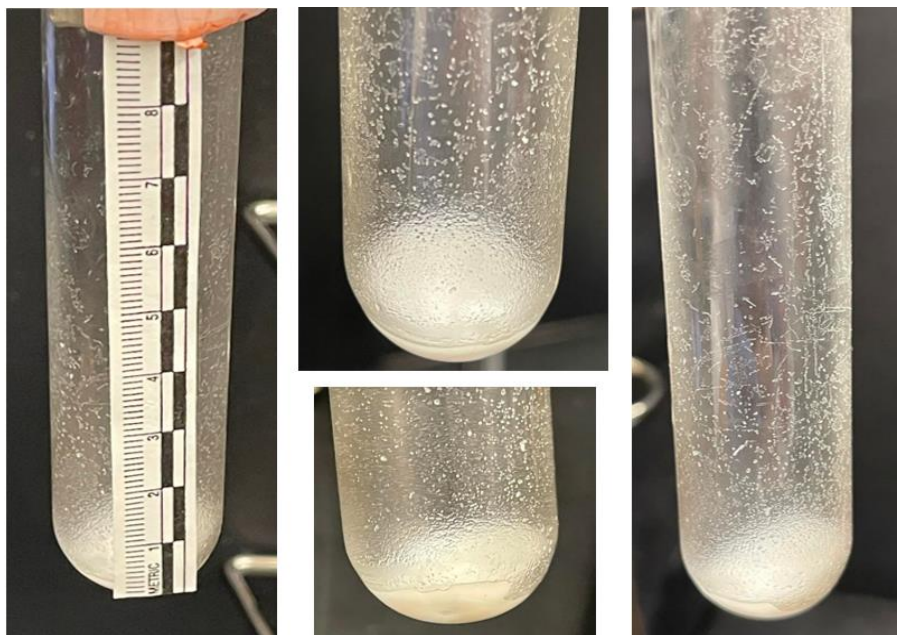
Figure 4.24: Photos of Sample B-1 from Different Angles - the measuring tape sticker was temporarily removed to better capture the presence of water and salt migration.
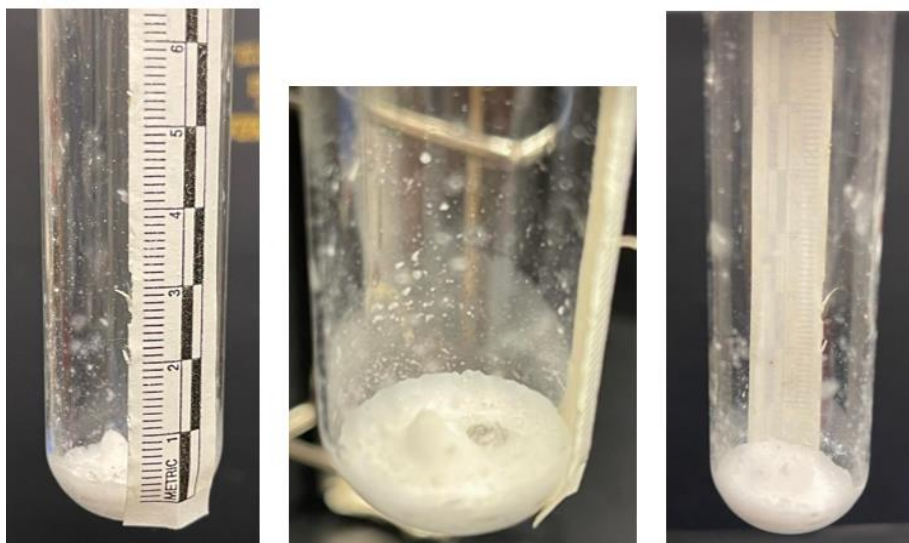
Figure 4.25: Photos of Sample B-2 from Different Angles.

> The salt appears to have decreased in sized compared to when it was first synthesized

> Advanced salt migration along the test tube wall up to 6.8 cm
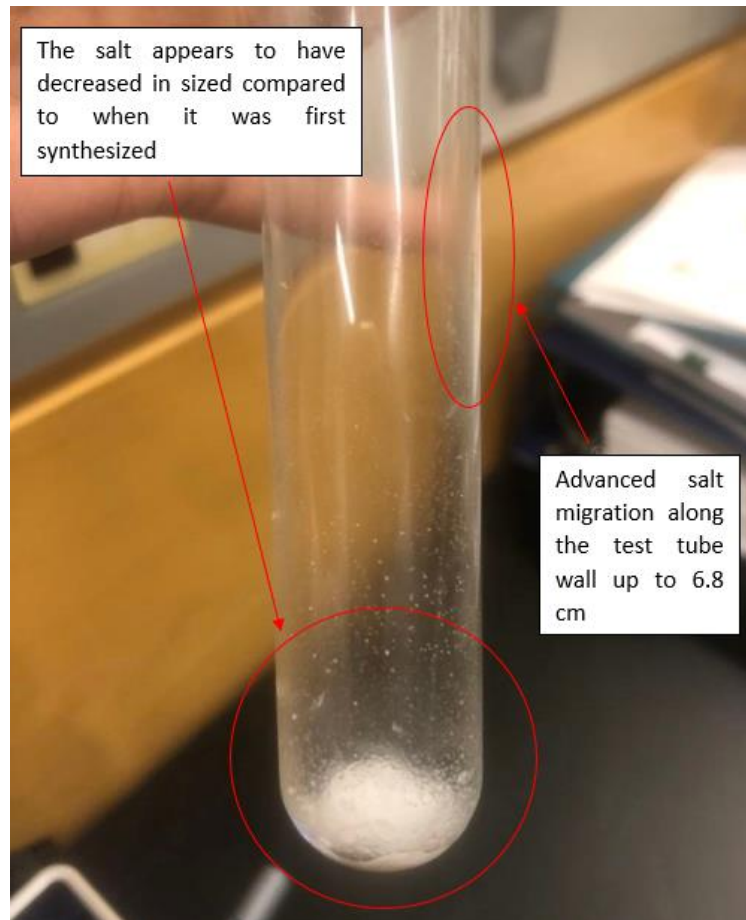
Figure 4.26: Photos of Sample B-3 from Different Angles - the measuring tape sticker was temporarily removed to better capture the presence of water and salt migration.
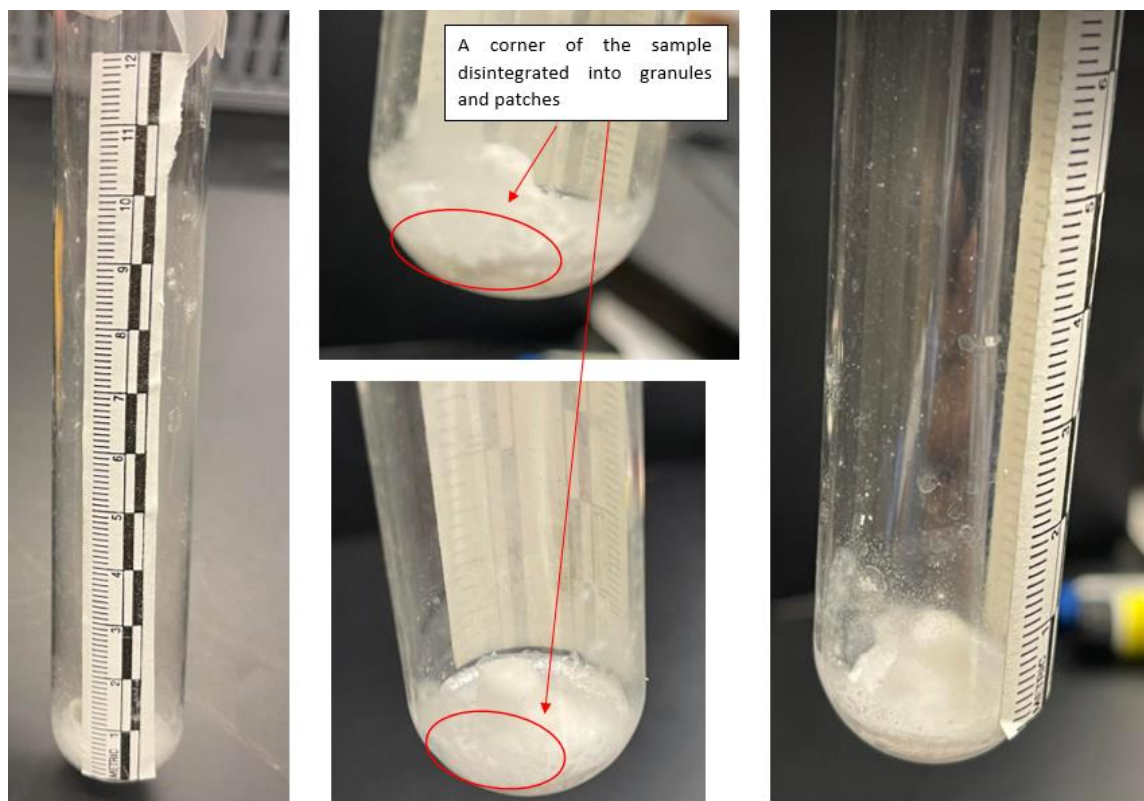
Figure 4.27: Photos of Sample B-4 from Different Angles.
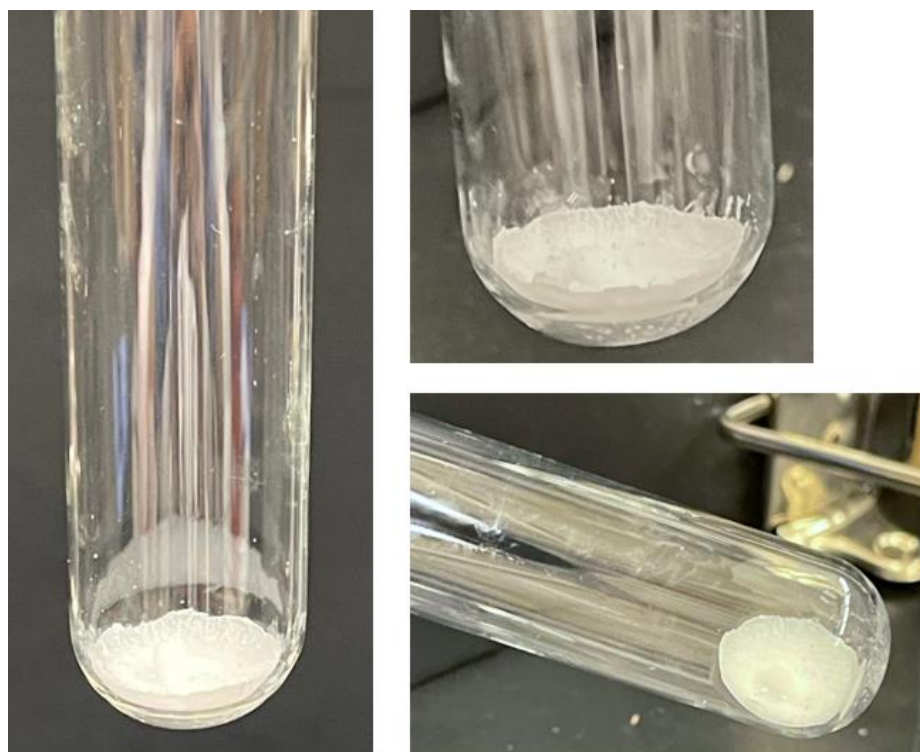
Figure 4.28: Photos of Sample B-5 from Different Angles.

Chapter 4. Results and Analysis

The results presented above from Cycle-B reaffirmed the findings of Cycle-A: contact with water vapour in the air causes synthesized FLiNaK to physically change and migrate along its vessel. This set of experiments also verified the effectiveness of the methodology discussed in Chapter 3 regarding the production of FLiNaK salt. A combination of using the vacuum pump during the melting process and cool-down, removing moisture through two-staged heating, and sealing of the sample immediately yielded consistent FLiNaK specimens that remain stable over long storage periods.

Furthermore, the experimental data recorded in Cycle-B was able to quantify the previously elusive concept of salt migration. Defining the extent of salt migration allowed for the systematic evaluation of individual samples and accurate comparisons between them to be conducted. Table 4.3 below is a summary of the extent of salt migration observed in all five samples from May to September, the complete observation table for which can be found in Appendix F. To visualize the data, Figure 4.29 and 4.30 illustrates the trendline for salt migration during this period.

Table 4.3: Summary of Physical Changes Observed and Recorded in Cycle-B FLiNaK Samples.

Observation Date	Sample Number	Phenomenon Observed	Salt Migration Extensiveness (mm)
May 19th, 2022	B-1	- Date of synthesis. - All five samples are physically uniform. - Samples B-1 and B-2 are able to slide along the bottom of the test tube	0
	B-2		
	B-3		
	B-4		
	B-5		
June 9th, 2022	B-1	- salt firmly stuck to the bottom of the test tube. - Some signs of salt migration observed in both samples.	3 - 7
	B-2		
	B-3	- Sample appears damp. - Increase in salt migration	10 - 17
	B-4	- No significant changes observed .	0 - 5
	B-5	- Sample remelted and resealed.	

June 23rd, 2022	B-1	- Salt firmly stuck to the bottom of the test tube.	4 - 9
	B-2	- Slight increase in salt migration.	
	B-3	- Sample is wet and mall amounts of is liquid observed.	15 - 23
	B-4	- No changes observed.	0 - 5
	B-5		
July 26th, 2022	B-1	- Salt migration not as extensive as anticipated	3-21
	B-2		
	B-3	- Sample is wet, and mostly submerged in the aqueous solution pooling at the bottom. - Drastic increase in FLiNaK salt migration - More patches of salt are found along the inner walls of the test tube. - Tear in Parafilm seal ruptured and split. Sample was resealed with a new piece of Parafilm but not vacuumed.	15 - 78
	B-4	- No significant changes observed.	0 - 6
	B-5	- Sample remelted and resealed.	0

Figure 4.29: Plot of Salt Migration Distance of Cycle-B Samples based on Salt Formation Observed Furthest Away from Main Crystal.
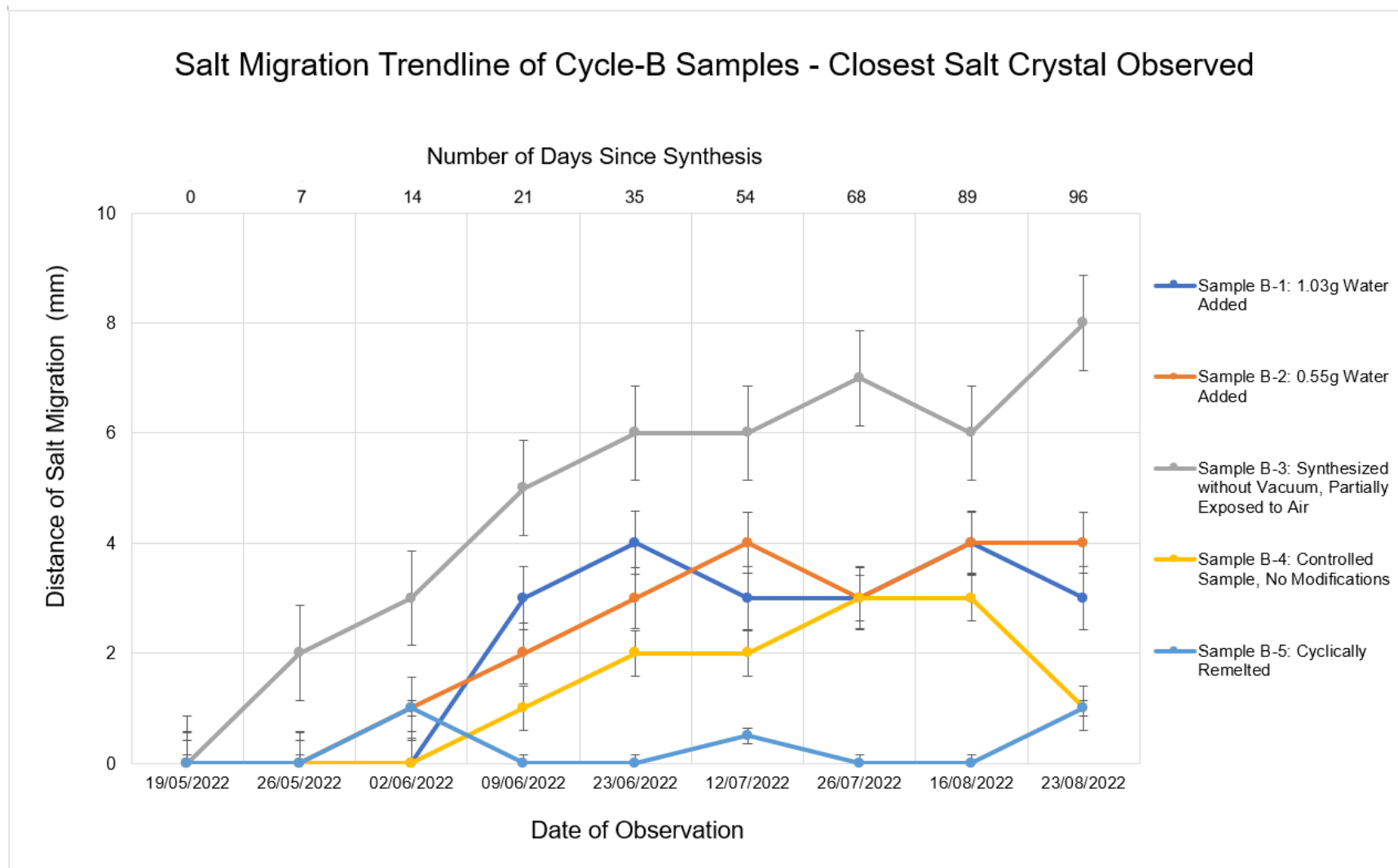
Figure 4.30: Plot of Salt Migration Distance of Cycle-B Samples based on Salt Formation Observed Closest to Main Crystal.

As the data presented suggests, the migration of FLiNaK salt in Cycle-B samples were not nearly as extensive as those seen in Cycle-A. Even sample B-3, which displayed the most aggressive signs of salt displacement, did not appear as physically different visually than samples A-1 and A-3. Once more, the efficacy of using a vacuum platform during synthesis was demonstrated. A small modification was made during the cool-down of the samples. Instead of having the vacuum pump on continuously until the sample is sealed, for Cycle-B, the vacuum was turned off upon observing the solidification of the outer edges of the molten FLiNaK. This was able to mitigate the flaking of the samples and prevent them from disintegrating back into powder.

Contrary to what was previously hypothesized, the addition of tap water to samples B-1 and B-2 did not aggravate the rate or distance of salt migration. Although physical changes were observed in both samples, they were minimal. The level of salt migration observed was significantly less extensive compared to those of sample B-3 and Cycle-A.

It was then evident that salt migration was caused and exacerbated by being in contact with not just any form of water, but specifically atmospheric moisture. Phenomenon observed in sample B-3 supports the above statement; it was the first sample to show signs of salt migration, so extensively that over the course of four months, FLiNaK particulates were observed as far as 10-11 cm away from the original salt crystal. Sample B-3 was prepared without the use of the vacuum pump; thus, the resulting FLiNaK crystal, though sealed immediately upon solidification, was in fact stored in an environment where it was in constant contact with atmospheric moisture (instead of being in vacuo like the other samples). Depending on the relative humidity of the day, the water content found in air can vary significantly, affecting the distance of salt migration in a sample. On the day the samples were prepared, the relative humidity of the laboratory was 53%.

Furthermore, starting the week of July 11th (52 days after synthesis), the distance of salt migration increased drastically and unexpectedly in sample B-3. Simultaneously, a minuscule tear was noticed in the Parafilm seal of sample B-3 which had gradually increased in size until it ruptured. The rate of salt migration in this particular sample was at its highest during this time, some particulates migrating 3-4 cm within a single week until the salt became partially submerged in liquid. The sample was subsequently resealed with a new piece of Parafilm, but

the test tube was not in vacuo. Nonetheless, this perforation in the seal caused sample B-3 to come into contact with even more atmospheric moisture due to the higher humidity during summer months. For about a month, sample B-3 was exposed to air, which had an hourly mean relative humidity of 68%.

As an aside, it is worth noting that the Parafilm was correctly and meticulously applied to each sample given the mishap in Cycle-A. Each piece of Parafilm was pre-cut to avoid delays in sealing the samples. In addition, thickness of the seal on Sample B-3 was evenly distributed and the area near the tear did not look stretched. Since samples A-3 and B-3 were the only two samples that had a rupture in the seal and both samples were melted without using the vacuum pump, it may be possible that excess hot steam released by the salt had deteriorated the Parafilm overtime.

4.3.4   Effects of Cyclic Remelting on FLiNaK Salt Behaviour

The effects of cyclically remelting select samples of synthesized FLiNaK are described both qualitatively and quantitatively in this section. The qualitative observations made of both samples are presented first, followed by the quantitative record of salt migration distance. Finally, the implications of these observations will be discussed. Sample A-3 was remelted once on October 15th, 2021, 70 days after its synthesis, while sample B-5 was remelted about every three weeks starting on June 9th, 2022 (day 21).

The samples were first removed from their storage test tube then transferred into a new one, in which they would be melted by the Bunsen burner, each time with the use of the vacuum pump. Once solidified, the samples would be sealed with Parafilm and stored in vacuo once more. Strips of measuring tape stickers were applied on the exterior of the storage test tube to record the distance of salt migration after the remelt. These removed samples will henceforth be referred to as sample A-3' and sample B-5' to avoid confusion with their previous states. Figure 4.31 is a photo of sample A-3' the day it was remelted. A thin layer of FLiNaK can be seen on one side of the test tube; this was caused by the tilt angle of the test tube during melting in an attempt to concentrate heat onto a smaller area thus shortening the melting time. The remelt experimental setup is illustrated in Figure 4.32.
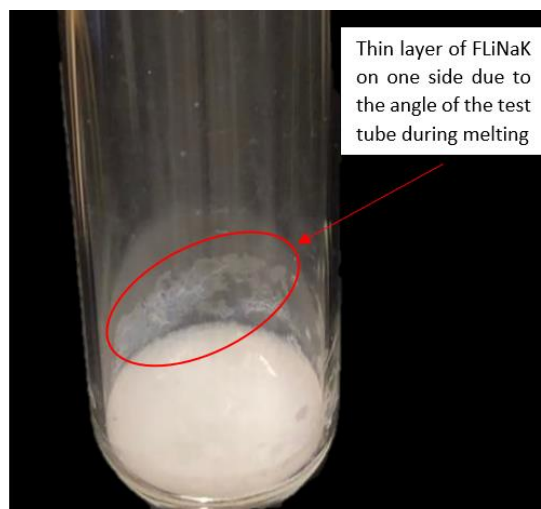
Figure 4.31: Photo of Sample A-3' After Being Remelted, Taken Upon Solidification.
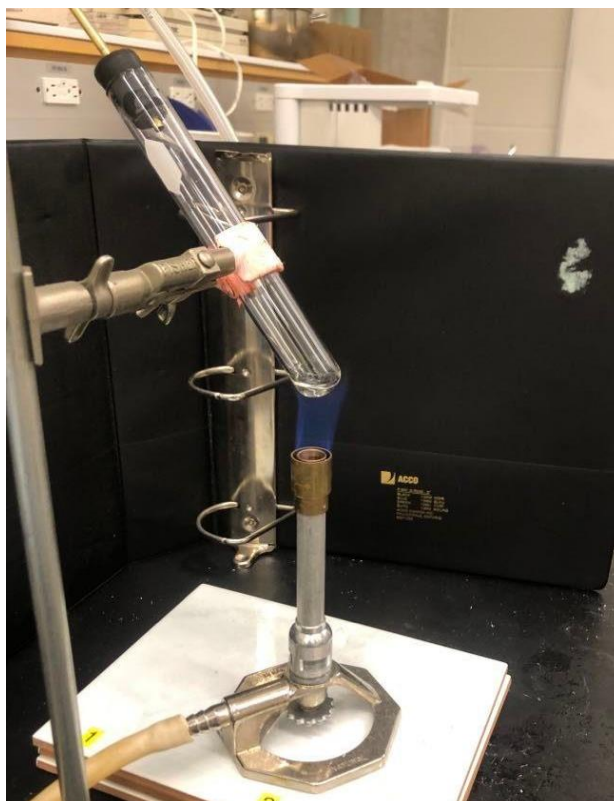
Figure 4.32: Sample A-3' was Remelted using the Vacuum FLiNaK Salt Melting System.

No physical changes were observed in sample A-3' for approximately three weeks. Photos taken about one month after the remelt showed some minute signs of salt migration. The previously thin layer of FLiNaK had become thicker, opaque, and more granular; small lumps

138

of salt can be seen forming. No signs of moisture were observed. The same trend continued throughout the winter; there were very little signs of salt migration in the test tube. However, the layer of FLiNaK on the side continued to thicken and eventually became fully opaque. Photos of sample A-3 throughout this time are presented in Figure 4.33. The last photograph of the sample, taken in February (four months after the remelting) showed a cessation of physical changes and the salt has remained stable since.
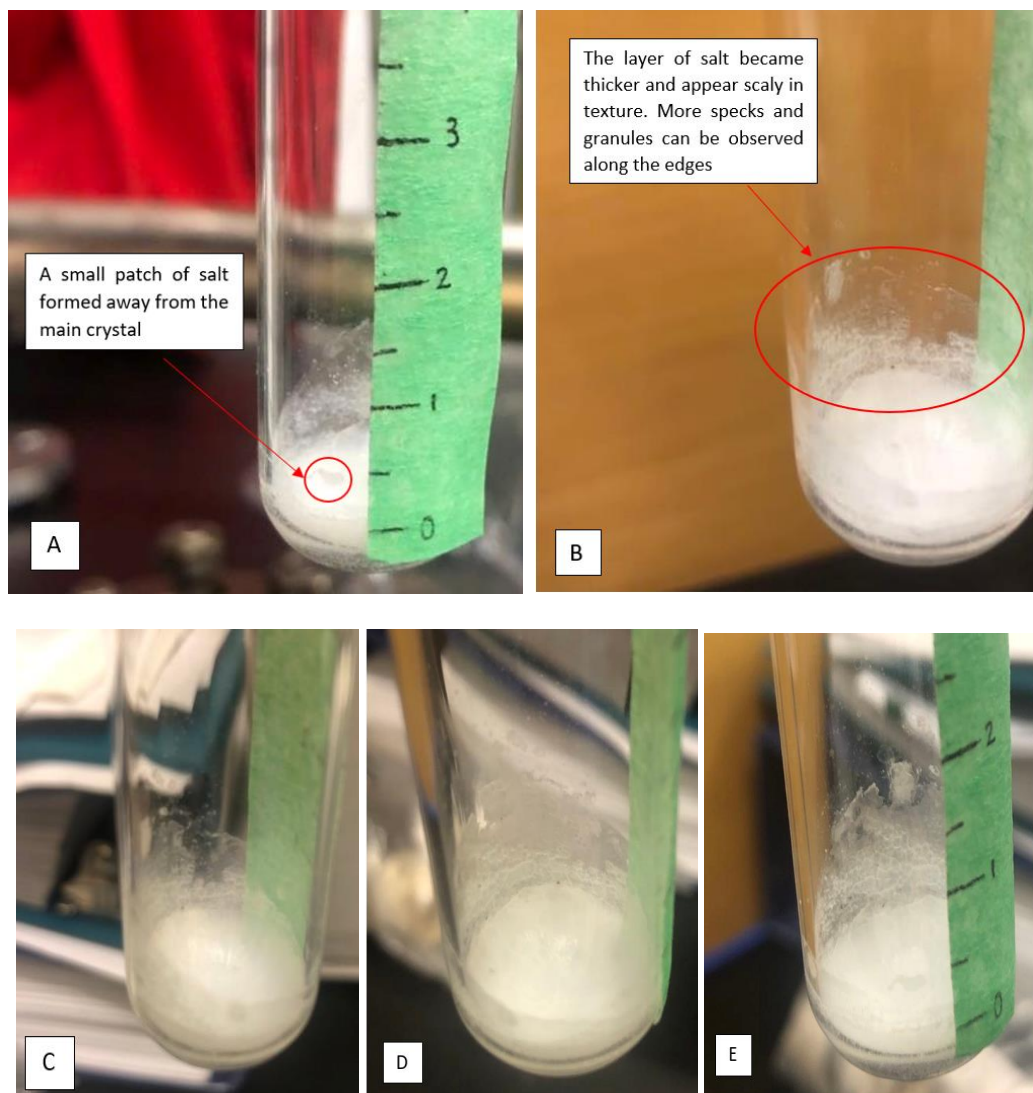
Figure 4.33: Salt Migration Observed in Sample A-3' over the Course of Four Months (a): Some Salt Migration Visible; (b): Slight Advancement; (c): No Significant Changes were Noticed; (d): Patches of Salt Moved Away from Main Layer; (e): Final Conditions.

The results suggest that by remelting FLiNaK, excess water content in the salt can be further removed through boiling. Combined with the vacuuming of air in the test tube, sample A-3' was successfully stored in an environment with minimal contact with water molecules or any contaminants. Therefore, the FLiNaK crystal did not undergo significant physical changes.

The same was observed for sample B-5', which displayed minimal signs of salt migration from its original synthesis until four months after. Throughout the two cycles of remelting, sample B-5' appeared physically the same. There were a few dots of salt observed away from the main crystal, but the distance was within the range of 2.5 mm, which was practically negligible compared to most other samples. The rate of salt migration also coincided and decreased with the cyclic remelting of the two samples as seen in Figures 4.34 and 4.35.
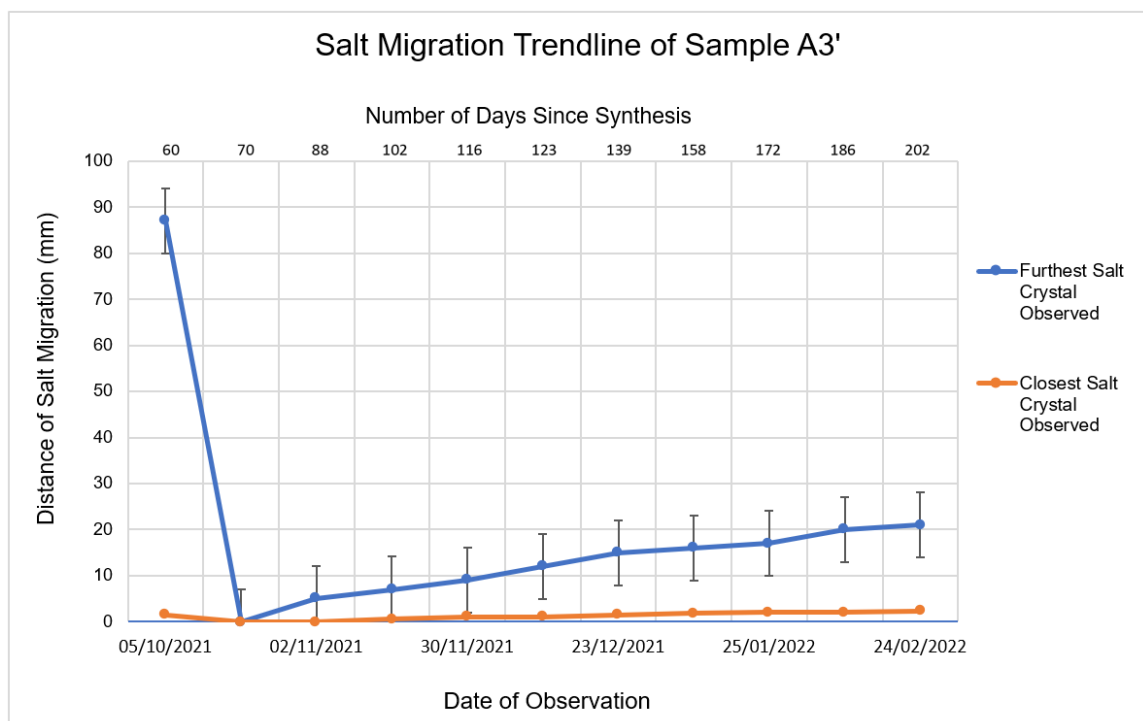
Figure 4.34: Plot of Sample A-3' Salt Migration Distance based on Salt Formation Observed Furthest Away from Main Crystal and Closest to Main Crystal.
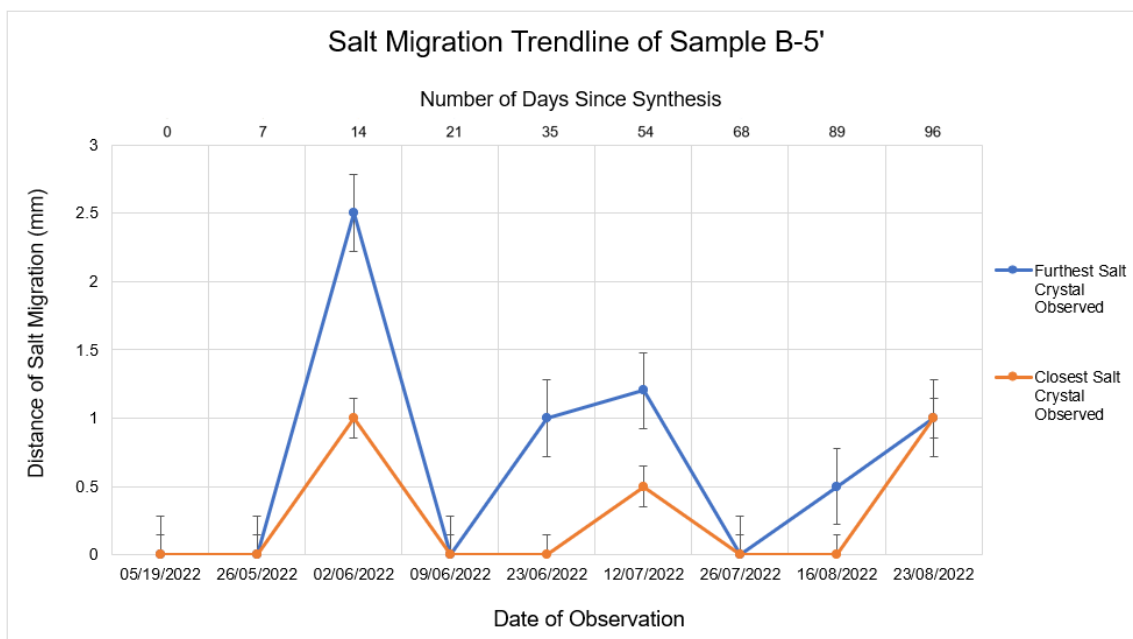
Figure 4.35: Plot of Sample B-5' Salt Migration Distance based on Salt Formation Observed Furthest Away from Main Crystal and Closest to Main Crystal.

4.3.5 Effects of Relative Humidity on FLiNaK Salt Migration

Having established that contact with water molecules in the air is the predominant cause for the observed salt migration in synthesized FLiNaK, it was then logical to investigate the relationship between the level of water vapour content in air, that is, relative humidity, and the extent of salt migration in distance. For this work, the relative humidity of the laboratory in which both Cycle-A and B samples were stored was recorded whenever the samples were inspected for salt migration. The temperature of the laboratory was recorded since it is a factor that would affect relative humidity. Pressure is not considered because it remained constant at atmospheric level throughout this work.

The recorded values, relative humidity and temperature, were individually plotted against time with the observed salt migration distance to determine whether a relationship between them exists or is plausible. Figures 4.36 and 4.37 compared the distance of FLiNaK salt migration observed in sample A-3' with the relative humidity and temperature of the laboratory, respectively, over time.
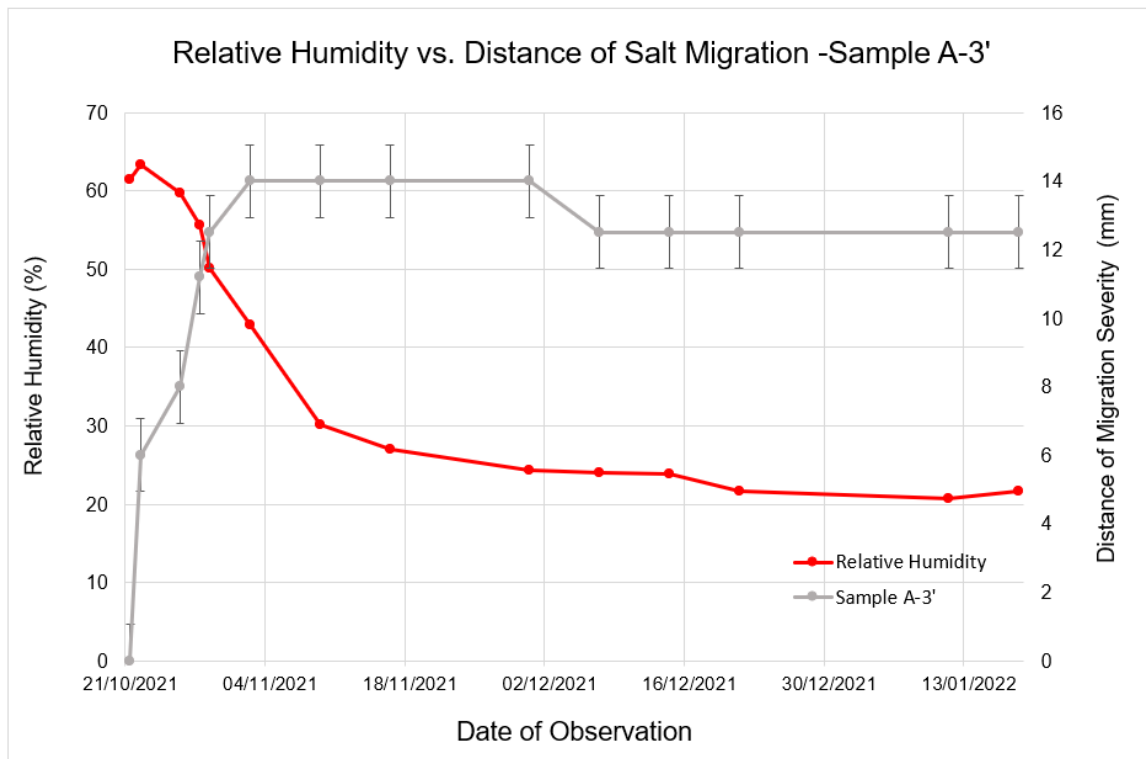
Figure 4.36: Relationship between Relative Humidity and Salt Migration: Sample A-3'.
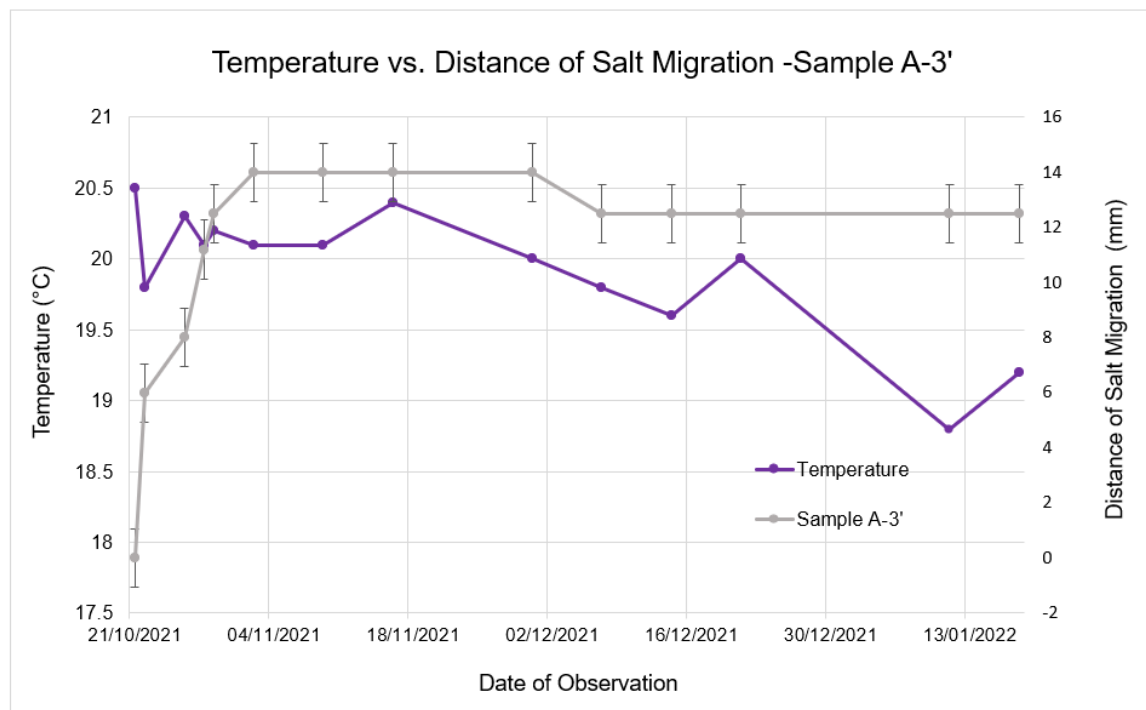
Figure 4.37: Relationship between Temperature and Salt Migration: Sample A-3'.

Preliminary results based on sample-A3, presented in the two figures above, inferred that higher levels of relative humidity are directly correlated with the acceleration of salt migration, whereas temperature had little to no effect.

To verify these results, the same study was repeated for all five Cycle-B samples to examine whether similar trends would be observed. Figures 4.38 and 4.39 show the relationships between the distance of salt migration of each Cycle-B sample and the relative humidity, and temperature of the room, respectively, over a four-month period.
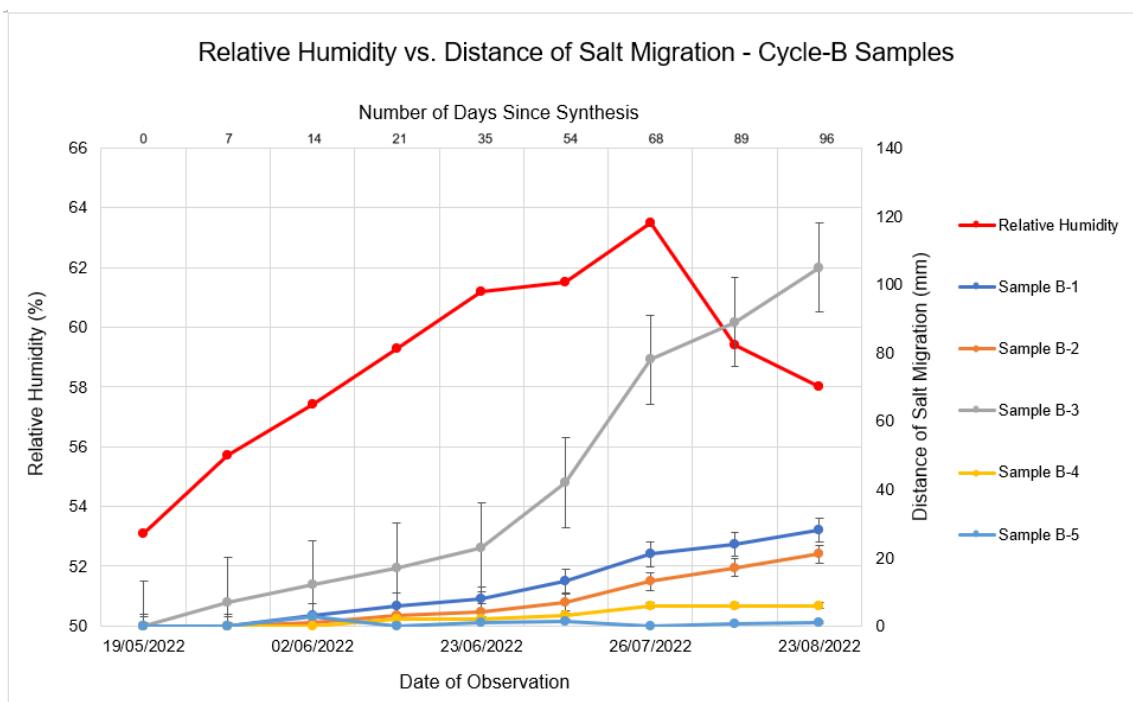
Figure 4.38: Relationship between Relative Humidity and Salt Migration: Cycle-B Samples.

The above figure reaffirmed the observation regarding the relationship between salt migration and relative humidity as observed in Sample A-3'. For all five Cycle-B FLiNaK samples, an increase in relative humidity was consistently noted to be correlated with some acceleration in the rate of salt migration. The scale of the plots was chosen specifically to accentuate this. Higher humidity levels coincided with advanced levels of salt migration being observed throughout the summer months. On the other hand, relative humidity levels near and below 20 % are associated with slow-downs and cessations in salt growth.
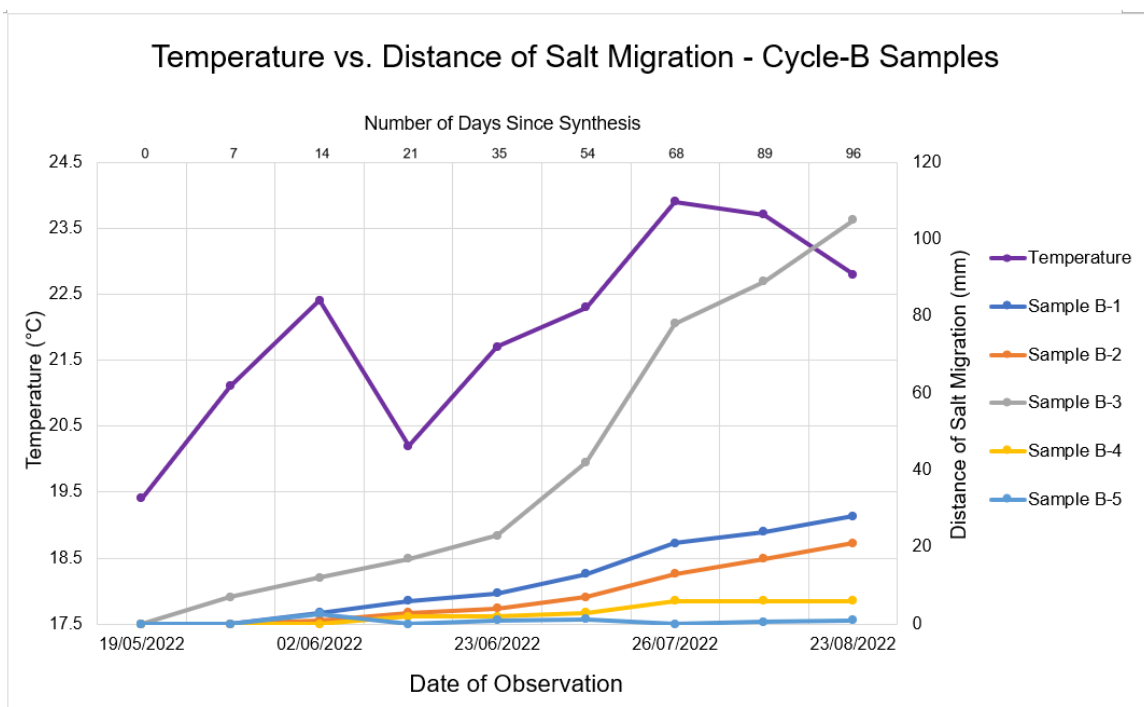
Figure 4.39: Relationship between Temperature and Salt Migration: Cycle-B Samples.

There was no distinct correlation between the temperature of the laboratory space and the extent of salt migration. However, it is important to note that the temperature did not vary significantly because the room is air-conditioned year-round, hence the limited data range. On the other hand, the laboratory did not have humidity controls (such as humidifiers or dehumidifiers), consequently, the samples may experience larger fluctuations in relative humidity throughout the year compared to temperature. Since the ambient temperature at atmospheric pressure largely determines the amount of water content air can hold, it can be said that the temperature of any space in which FLiNaK is to be used or stored is indirectly related to the severity of salt migration.

These results suggest that in order to limit and prevent the phenomenon of salt migration, temperature and humidity controls may be necessary for the service environments of FLiNaK salt, especially if there are risks of the salt coming into contact with air and thus the water molecules as well. For example, the outdoor temperature of numerous days throughout the observation period was well above 35 °C with 100% relative humidity, one may expect aggravated and extreme cases of salt migration under such environmental conditions.

4.4 Remelting and Draining FLiNaK from the MSL Tube Segment

This section describes the qualitative and quantitative observations made during the remelting and draining of residual FLiNaK salt from the Hastelloy-C MSL Tube Segment. These experiments emulated FLiNaK salt removal from a representative, metallic reactor system component at the time of reactor shutdown and decommissioning. Both qualitative and quantitative phenomena observed throughout each iteration of the experiment were described and discussed.

Then, the physical condition of the drained FLiNaK and the salt-facing portion of the Hastelloy-C segment were examined and analysed for contamination and corrosion. Finally, the results of preliminary spectroscopic analysis of contaminants found in drained FLiNaK salt were presented and discussed.

4.4.1 Attempts at Remelting and Draining FLiNaK

There were a total of six reheating attempts at removing the residual FLiNaK salt plug within the MSL Tube Segment. Table 4.4 on the next page summarizes the key processes and outcomes of all experiments performed. The complete observation table featuring detailed time and temperature data for each experiment can be found in Appendix G.

In this section, the experimental setup and results for each iteration of the salt remelting experiment are presented, along with any challenges encountered and subsequent modifications implemented to address them. Figure 4.40 is a schematic of the approximate location of the salt plug within the tube and the orientation of the component. The figure labeled the two faces of the salt plug as either Side-A or Side-B. Side-A faces towards gravity and is marked by a prominent cavity in the salt surface. The other side was then labelled Side-B. A set of photos were taken by the borescope prior to the first remelting experiment in May of 2021.

Table 4.4: Summary of Key Observations and Parameters of the MSL Tube Segment FLiNaK Salt Remelting Experiments.

Trial Number	Key Observations	Duration of Experiment (min)	Maximum Temperature Reached (°C)	Method of Temperature Measurement	Change in Pressure (inHg)
1	- Heater tape glowed red in the dark - Large temp. difference between flanges and middle tube	110	External: > 275 °C Internal: N/A	Infrared Camera	N/A
2	- Heater tape glowed red in the dark - Longer heating time, but significant temp. difference between flanges and middle tube persisted	160	External: > 275 °C ~385 °C Internal: N/A	Infrared Camera Infrared Laser Thermometer	N/A
3	- Plastic tubing melted and rupture - Experiment ended prematurely	87	External: 412°C Internal: N/A	Thermocouple Wire	N/A
4	- Despite extensive heating, internal temp. did not increase beyond 187 °C - Flanges continue to act as heat sinks	375	Internal: 187 °C External: 480 °C	Internal: Thermocouple Probe External: Thermocouple Wire	+ 2 (-30 to -28)
5	- Smoke continuously emitted from underneath the wool insulation - Experiment ended prematurely - Heater tape severely damaged	18	Internal: 112°C External: 167 °C	Internal: Thermocouple Probe External: Thermocouple Wire	0
6	- Consistent increase in temp. (~1°C per 10-15 seconds) - No smoke emitted - Heater tape glowed in the dark - FLiNaK fully melted and drained	125	Internal: 465°C External: 514°C	Internal: Thermocouple Probe External: Thermocouple Wire	+34 (-30 to +4)
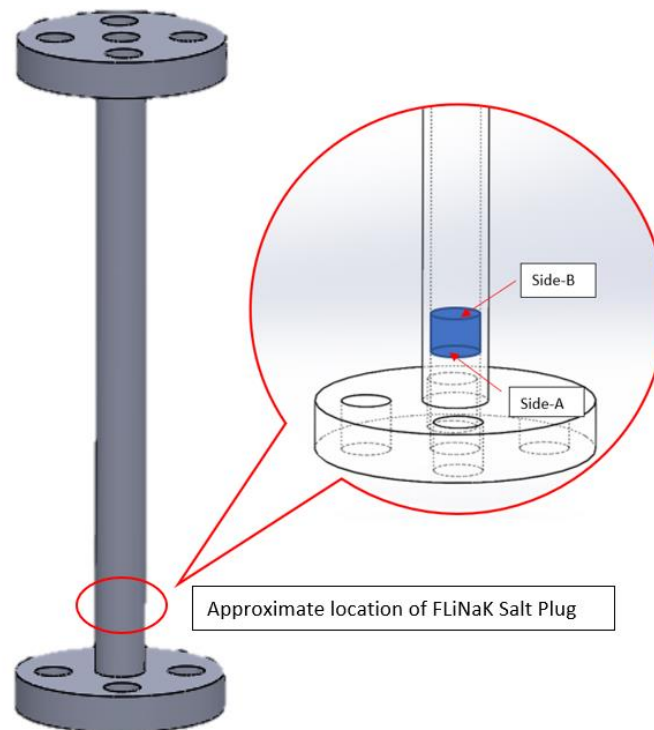
Figure 4.40: The Approximate Location of the FLiNaK Salt Plug within the MSL Tube Segment with Surfaces Side-A and Side-B Labelled.

A set of photos were taken by the borescope prior to the first remelting experiment. Shown in Figures 4.41 through 4.43 below, these images establish and serve as the baseline or "initial conditions" in terms of the internal contents and environment of the MSL Tube Segment.
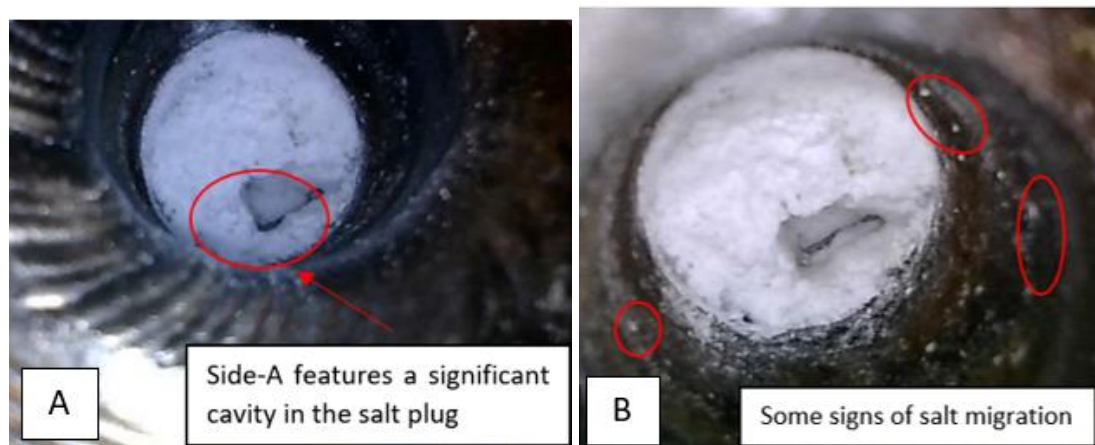
Figure 4.41 (a): Side-A of the Salt Plug Features a Large Cavity (b) Some Signs of Salt Migration were Observed Near the Salt Plug.

Figure 4.42: Side-B of the Salt Plug Features a Small Cavity Along the Hastelloy Wall.

The salt plug was coarse, dry, opaque, and white on Side-A; Side-B appeared smoother. The red circle in Figure 4.42 highlighted an area in the tube segment that looked slightly dented, but was actually the result of lighting, reflection, and the angle of the borescope camera during the photographing and video recording process.
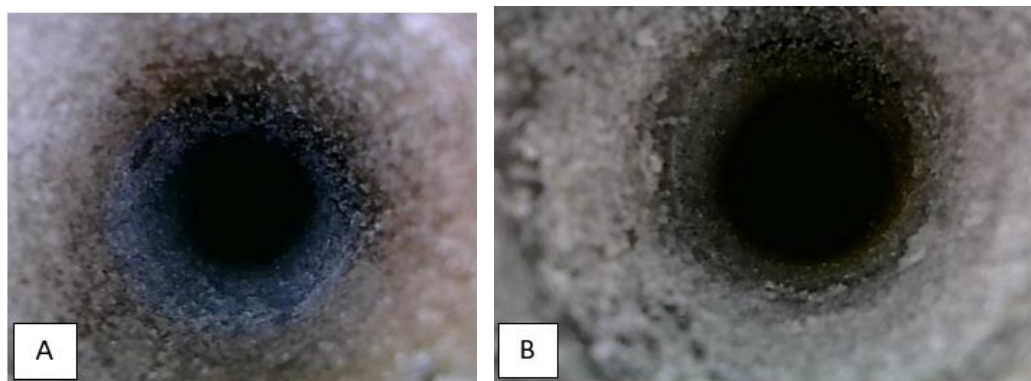
Figure 4.43 (a): Extensive Salt Migration along the Inner Walls of the MSL Tube Segment – Side-A (b): The Same Phenomenon was Observed for Side-B.

In addition to the large divot on Side-A, some granules of salt were observed to have migrated away from the main salt mass. More extensive salt migration was observed farther away from the salt plug on both sides of the blockage. Salt granules were found to densely cover the inner walls of the MSL Tube Segment; the metallic walls looked dull and rough as the result of

FLiNaK crystal growth. This segment had previously been placed in storage for more than a year and it was likely that the FLiNaK salt bridge had come into contact with atmospheric moisture. After a month, Side-A of the salt plug became smooth and slightly translucent from increased humidity as seen in Figure 4.44.

Figure 4.44: Increased Moisture in the Summer Caused the Surface of Side-A to Become Smooth and Translucent.

The very first salt remelting experiment was conducted on September 16th, 2021. The experimental setup was rudimentary; it consisted of the MSL Tube Segment, heater tapes, the electric heater, and the vacuum pump, which had been connected to the opening of the tube segment via plastic tubing and a self-devised adapter. This adaptor, presented in Figure 4.45, was a male to female brass fitting with a plastic push-fit attachment on the female end.
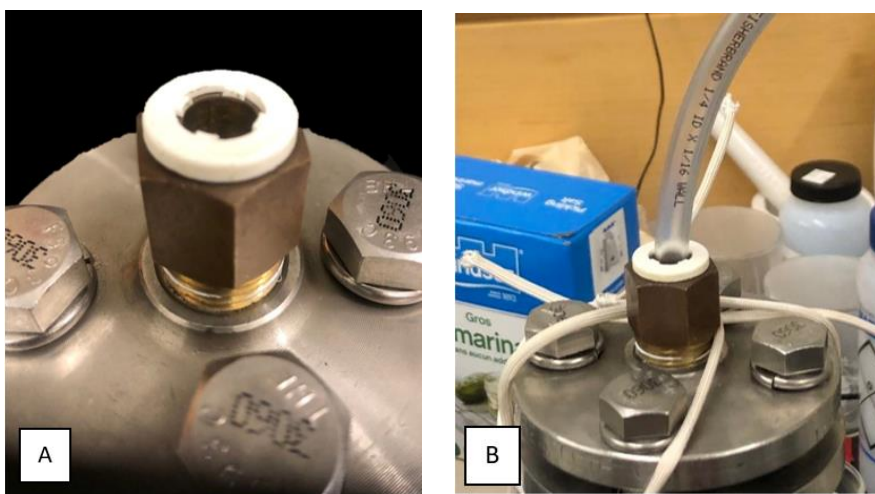
Figure 4.45 (a): Turn-fit Attachment on the Brass Adaptor (b): Plastic Tubing Connected to the MSL Tube Segment via the Adaptor.
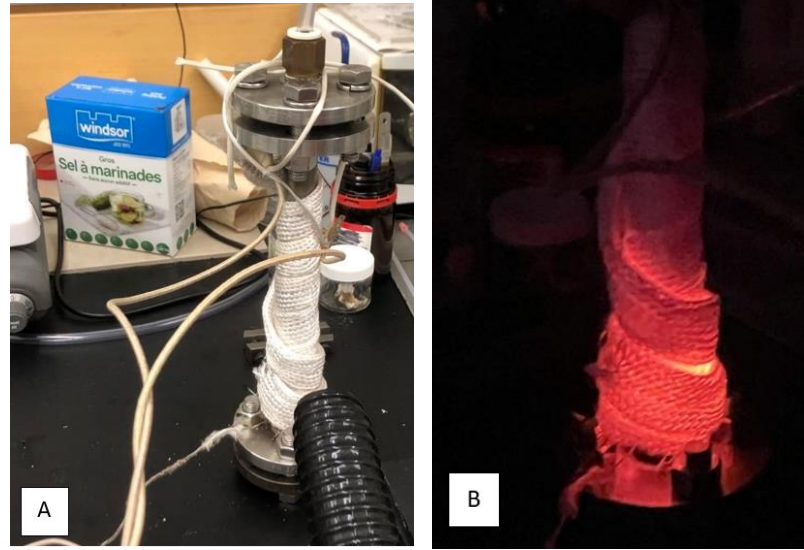
Figure 4.46 (a): The Experimental Apparatus used for the First MSL Tube Segment FLiNaK Remelting Experiment (b): The Heater Tape Had Glowed Red During the Heating Process.

A thermal infrared camera was used for external temperature readings and generation of monochrome images of the temperature distribution of the MSL Tube Segment during heating. Figure 4.47 are thermal images of the experimental setup during its first heating trial.
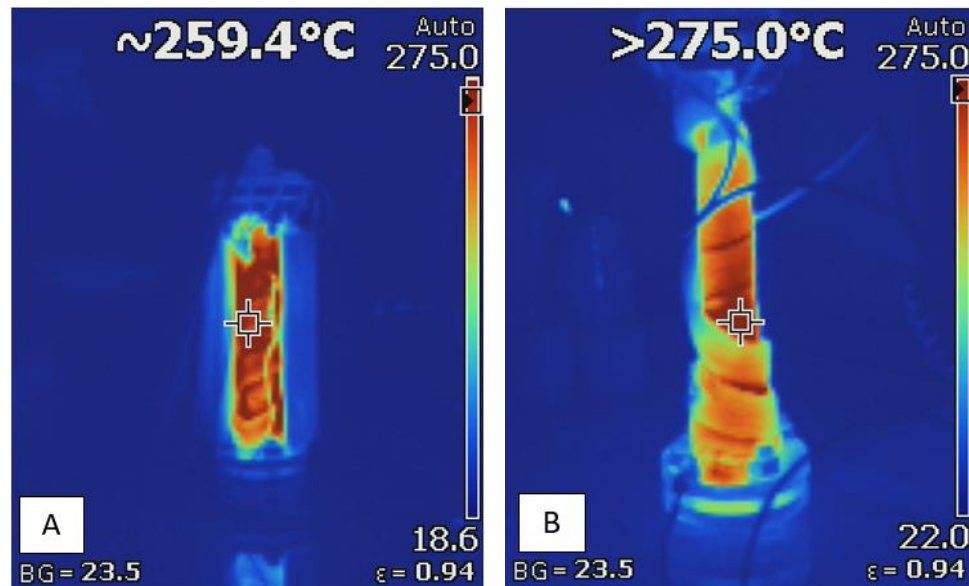
Figure 4.47(a): Temperature distribution of the MSL Tube Segment during Heating; the Two Flanges were around Background Temperature -23.5 °C (b): Reading Displayed by the Infrared Camera for Temperatures Beyond 275°C.

One limitation of the infrared camera was that it could only register temperature as high as 275 °C, given that the setting of the electric heater was at 465°C, the actual external temperature of the MSL Tube Segment could not be captured as it was greater than 275 °C.

The experiment lasted one hour and fifty minutes and was terminated when the internal wire thermocouple of the electric heater registered a temperature reading of 465°C. Despite this constraint, the resulting thermal images were effective in highlighting and identifying areas that acted as heat sinks. Heat loss occurred most predominantly in the two exposed flanges of the tube segment as seen in Figure 4.48.
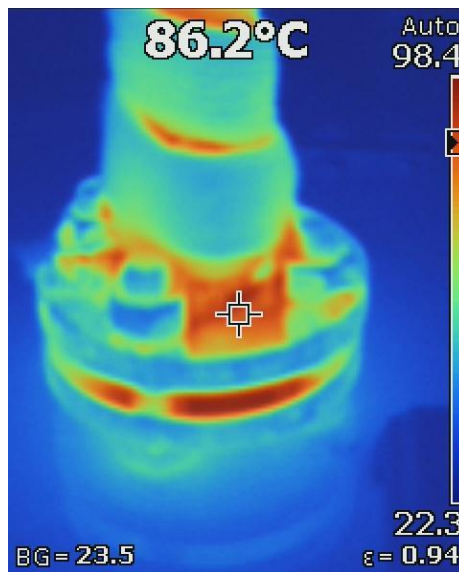
Figure 4.48: The Exposed Bottom Flange is a Heat Sink and Dissipated Heat.

There was a temperature disparity of 383°C between the middle of the MSL Tube Segment and its two flanges which lowered the overall system temperature. Consequently, the salt plug inside did not fully melt. When the system was examined the next day with a borescope, it was noted that the position of the salt plug had lowered slightly, only the edges of the salt displayed any signs of melting. Most the salt mass remained as it was

The images presented in Figures 4.49 and 4.50 are borescope photographs taken of the FLiNaK salt plug one day after the experiment. The side walls, where streaks of white can be seen, were fuzzy in the photographs, this was due to the angle limitations of the camera.

Streaks of FLiNaK was observed to have melted then resolidified along the edges of the salt plug

Figure 4.49: The Salt Plug Had Melted along the Walls of the Tube Segment.

Direction of gravity: out of the page

Contaminants, in the form of small, black specks were found through Side-B of the salt plug.
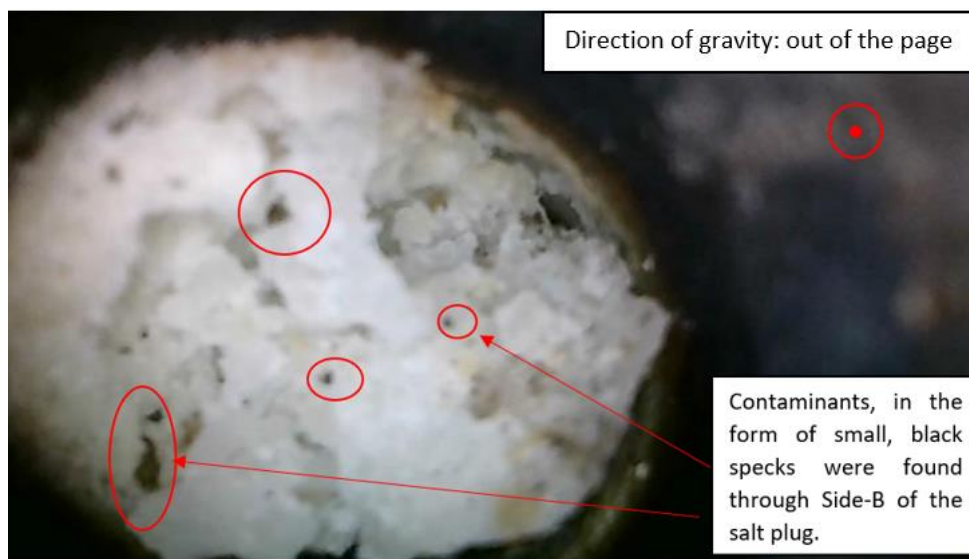
Figure 4.50: The Surface of Side-B was No Longer Smooth; Black Specks were Found in the Salt on the Surface of Side-B.

The physical appearance of the salt plug had changed significantly on both sides. Side-A looked much more similar to its initial conditions, while the previously smooth surface of Side-B became crystalline and rough, with loose chunks of FLiNaK as the top layer.

Results observed in Side-A, mainly the restoration of its colour and texture, were likely because of the evaporation of moisture within the salt plug. Though the heater tape did not supply enough heat to fully melt the salt plug, it was able to liquefy some of the FLiNaK that interfaced with the Hastelloy-C tube. The molten salt would then flow downwards toward the bottom flange due to gravity and re-solidify again rapidly from the drastic temperature drop near the flanges away from the heater tape.

Contaminants, in the form of black dots and some larger specks, were observed on both sides of the salt plug, though more predominantly on Side-B. The constitution of this contaminant was unknown and cannot be determined until the salt is fully drained as it was too difficult to separate from the salt at this point. The physical changes in Side-B may have been the result of the salt melting partially; insufficient heat prevented the FLiNaK to liquefy enough to reconfigure and form a smooth surface while uneven cooling formed the pockets of crystalline salt chunks found on the surface. The lack of a layer of small, dense salt granules along the walls surrounding Side-B suggests that the change in physical appearance observed was unlikely to be crystalline growth.

The internal K-type wire thermocouple of the electric heater had been used to measure the external surface temperature of the tube close to the location of the salt plug, but it was discovered that the exposed wire of the thermocouple was in contact with the heater tape instead. This meant that the electric heater had been registering the temperature of the heater tapes instead of the tube and thus prematurely decreased the heat output having assumed that the pre-set temperature had been reached. Since the setup did not provide sufficient heat to melt the salt plug and had significant heat sinks throughout the system, modifications were made for the second trial of draining the MSL Tube Segment.

A fibreglass insulation sleeve was added for the second trial of the experiment; it was fastened around the middle of the tube segment over the heater tapes to prevent excess heat loss. The thermocouple wire was carefully tucked against the exterior of the tube to avoid inaccurate temperature reading due to poor contact. The modified experimental setup is presented in Figure 4.51 in the following page.

The experiment took two hours and forty minutes for this second trial; the heater setting was increased incrementally by 50 °C until 500 °C. The system was held at this temperature for ten minutes before the heater was turned-off.
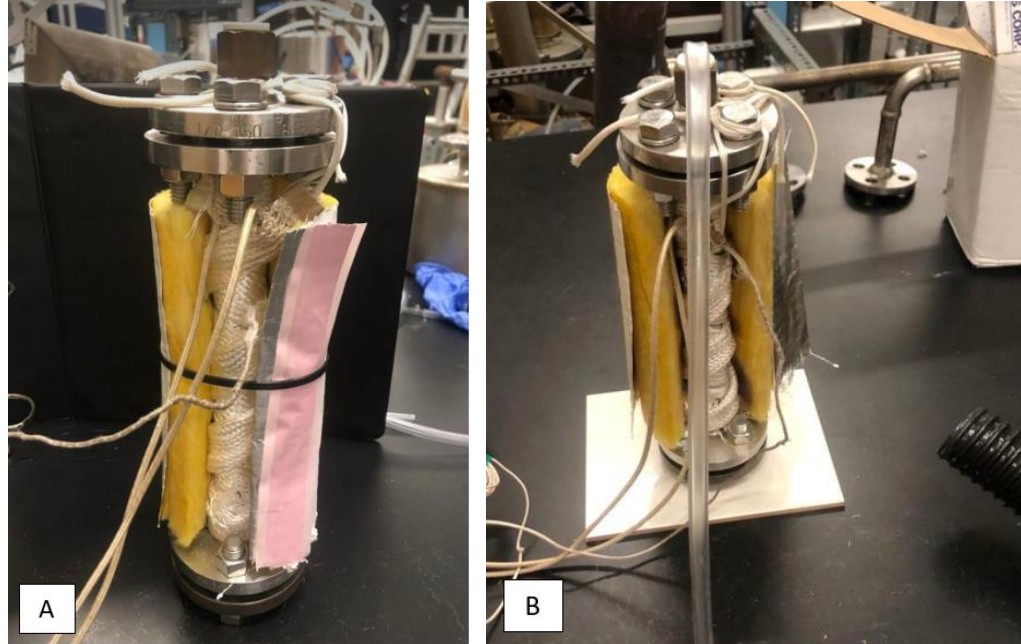
Figure 4.51 (a): A Fiberglass Insulation Sleeve was Added (b): The MSL Tube Segment during Heating; the Plastic Tubing near the Adaptor Collapsed due to Heat.

The results of this experiment were similar to the previous trial. The position of the salt plug lowered slightly and signs of partial melting along the edges were observed. The two sides of the salt plug did not appear significantly different; borescope photographs taken are presented in Figure 4.52 and 4.53.

Figure 4.52: Borescope Photo of Side-A of the Salt Plug - Second Trial.

154

Figure 4.53: Borescope Photo of Side-B of the Salt Plug - Second Trial.

Side-A became less coarse on the surface and was translucent along the outer rim; the large cavity in the middle was smaller in size as well. The crystals on Side-B, however, had merged together to form larger chunks of FLiNaK, although the colour and texture remained identical. The heating of the MSL Tube Segment was still insufficient despite longer heating time at a higher temperature. The flanges continued to dissipate far too much heat; they were entirely uncovered and too wide to fit into the insulation sleeve.

The next trial would see the use of a wider and longer heater tape that covered some portions of the top and bottom flanges, but the heating process ended prematurely when the plastic tubing that was connected to the vacuum pump on the other end ruptured from heat of the brass fitting near the turn-fit attachment, which had also melted. The temperature registered by the thermocouple at the time was 412 °C. The sudden failure of the two plastic components suggested that the system reached higher temperatures than previous trials, implying that the 1-inch-wide heater tape was more effective than the ½ -inch-wide heater tape used before.

The thermocouple, though better placed, still continued to register the temperature of the heater tape instead of the Hastelloy tube due to their inevitable proximity. There was also no gauge for the internal temperature or pressure of the MSL Tube Segment. This challenge led to the design and construction of the MCMA, which was intended for quantifying the internal environment of the MSL Tube Segment during heating. Throughout the design, procurement, and construction period of the MCMA, which lasted two months, the MSL Tube Segment

was sealed using Parafilm and monitored for signs of salt migration, the details of which will be discussed in the next section.

The construction of the MCMA was completed in early February and leak tests were conducted at each fitting interface of the assembly. For the fourth drainage attempt, the MCMA attached to the top connecting flange of the MSL Tube Segment. The K-Type thermocouple probe of the MCMA enabled accurate temperature readings within the tube segment; the thermowell hovered just millimetres above Side-A of the salt plug.

A photo of the modified experimental apparatus is featured below in Figure 4.54. For this experiment and those following, the MSL Tube Segment was turned upside down; the salt plug, previously close to the bottom flange, was now near the very top with Side-A facing upwards as seen in Figure 4.55. This was done to better observe signs of melting in the FLiNaK salt since it created a longer downwards track length.
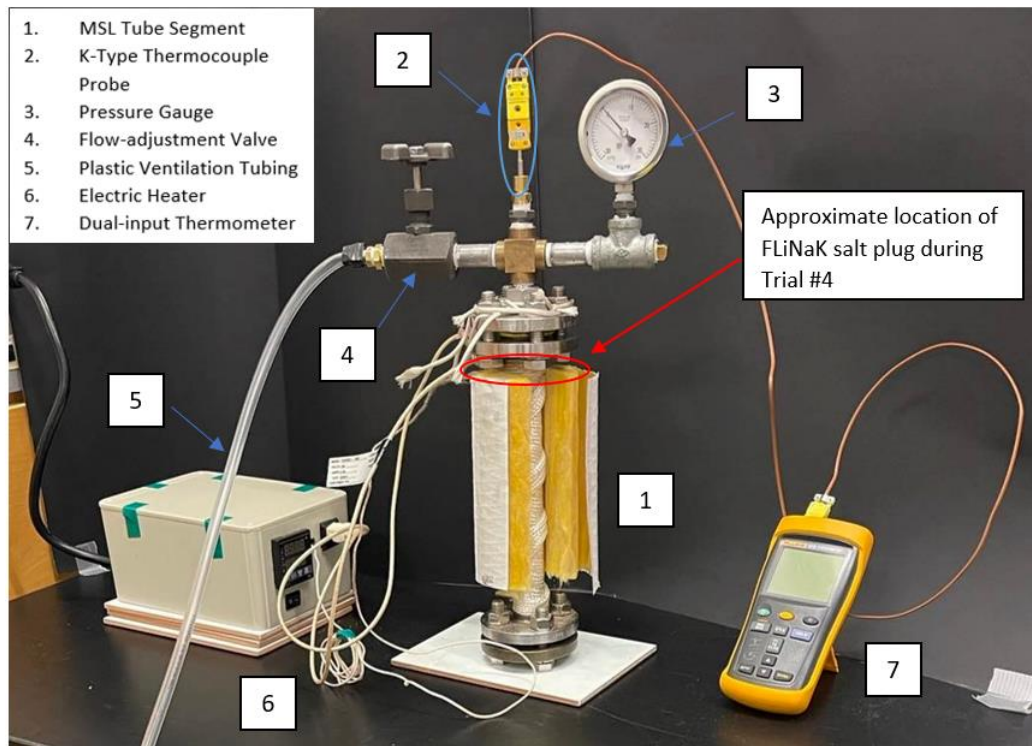
Figure 4.54: Modified Experimental Setup of Fourth MSL Tube Segment Salt Melting Experiment.
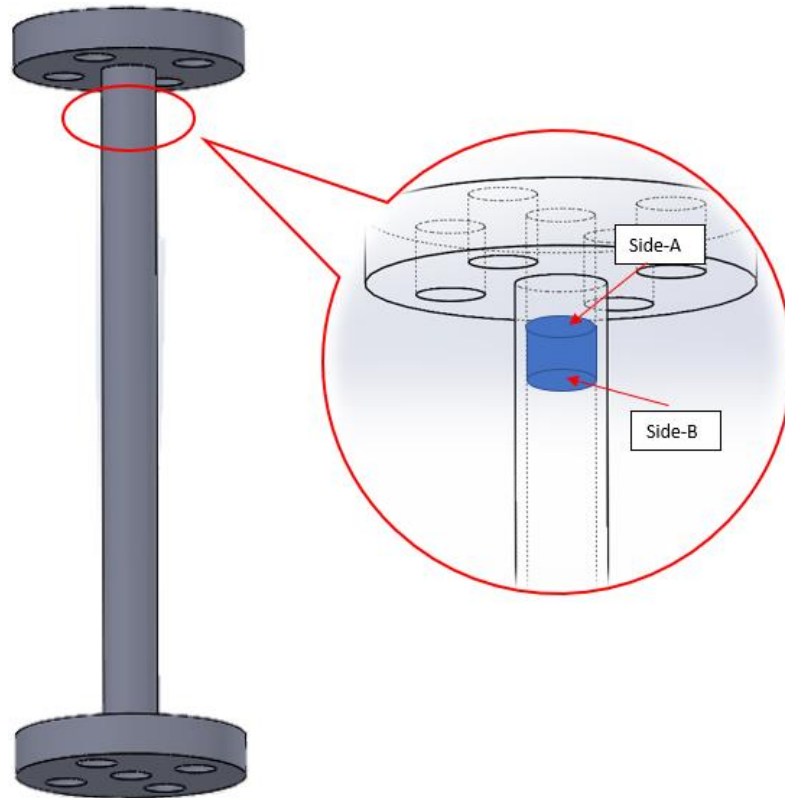
Figure 4.55: The Approximate Location of the FLiNaK Salt Plug within the Inverted MSL Tube Segment with Surfaces Side-A and Side-B Labelled.

The heating process lasted six hours; the temperature setting on the electric heater increased by increments of 100-150°C with a final temperature of 480 °C. However, despite this extensive heating time, the thermocouple reading of the internal temperature within the MSL Tube Segment plateaued at and did not increase beyond 187 °C. During this time, the pressure within the melting chamber increased by only 2 in. Hg from -30 in. Hg: this demonstrated that the MCMA was effectively sealed, any leakage was minimal.

The salt plug did melt significantly more around the edges compared to previous trials. Borescope images presented in Figures 4.56 and 4.57 describe the condition of the salt. The salt looked light grey on the surface and more black contaminants were observed. The large cavity on Side-A became two smaller cavities and a thick streak of salt seen along the edges proved that the salt plug had slid downwards during heating.
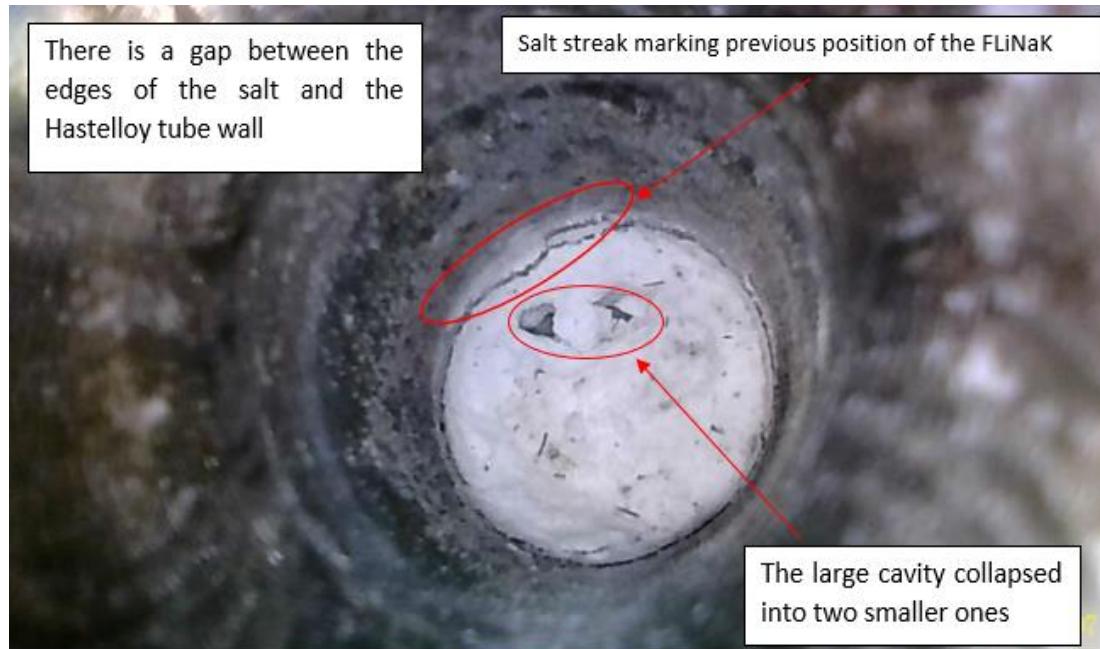
Figure 4.56: Borescope Photo of Side-A of the Salt Plug- Fourth Remelt Experiment.
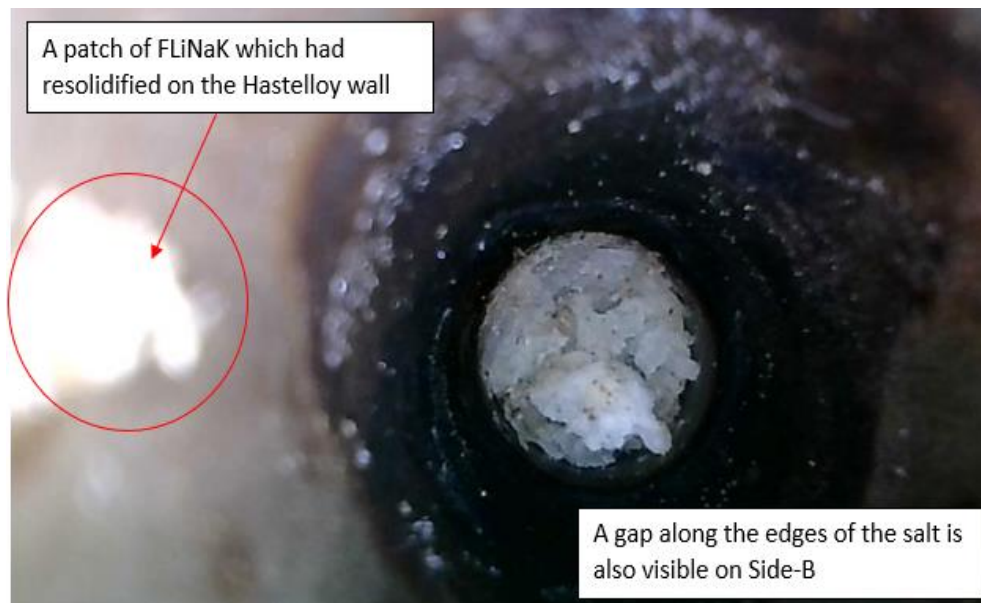
Figure 4.57: Borescope Photo of Side-A of the Salt Plug - Fourth Remelt Experiment.

For both sides, the edges of the salt had faintly detached from the inner walls of the tube. The salt in these areas had melted and pooled ever so slightly downwards, which was a promising sign that the selection of heater tape was suitable. However, there was still no method for

insulating the top and bottom flanges of the system, the most predominant heat sinks; it became apparent that unless the flanges are heated and insulated as well, it would be impossible to fully remelt and drain the FLiNaK. Thus, for the following trial, the same heater tape was used and wrapped differently along the MSL Tube Segment; any overlap was eliminated in favour of wrapping the extra length around the two flanges instead. Furthermore, rolls of fibreglass wool were used instead of the sleeve for insulation as it was capable of fully covering the two flanges as well as the middle tube section.

The fifth MSL Tube Segment FLiNaK remelting experiment took place nearly five months after the previous trial. The tube segment was sealed with Parafilm and kept in storage in the laboratory; the intention was to observe whether there was a correlation between increased humidity of the summer and the salt migration within the Hastelloy tube.

This iteration of the experiment included two major modifications to the apparatus. Firstly, a longer heater tape was used to thoroughly wrap the MSL Tube Segment, including both flanges. Then, two layers of fibreglass wool insulation, six pieces in total, were tightly fastened around the MSL Tube Segment and heater tape using stainless steel hose clamps. The heater tape was damaged during this experiment, it was then discarded and replaced.

This incident demonstrated that the exterior temperature of the MSL Tube Segment was too high while the internal temperature lagged behind. The drastic increase in heat intensity was the result of excessive insulation. Despite the mishap, it was also clear that sufficient heating of the system could be achieved. Though the salt plug had not melted, Side-A of the salt became dark grey and powdery. In addition, the two cavities have merged into a small pocket. Side-B, on the other hand, had significantly larger flakes of black contaminants found throughout the translucent crystals. Borescope photographs of the two sides of the salt plug are in Figures 4.58 and 4.59.

Figure 4.58: There was a small cavity left on Side-A and the salt appeared dark grey.

Figure 4.59: Very Large Flakes of Black Contaminant were Found Amongst the Crystals.

Having had the opportunity to identify and then address the series of challenges that arose throughout the five iterations of the remelting experiment, the sixth trial encompassed a compilation of all previous apparatus modifications as well as any procedural changes to the heating process. This is discussed in the next subsection.

4.4.1.1. Modifying the Experimental Setup to Achieve Salt Drainage

The sixth and final trial of the MSL Tube Segment Salt remelting experiment corrected the errors previously identified. A new heater tape, 1" wide and 4' in length, was used to tightly wrap around the tube segment and both bottom and top flanges without overlap. Then, one layer of fibreglass wool insulation (3 pieces) was fastened around the wrapped tube section using three stainless steel hose clamps. Figure 4.60 is a photo of this upgraded experimental setup.

The heating process only took two hours, with a higher initial temperature setting of 275 °C that subsequently increased in increments of 100 °C. The temperature climb was steeper compared to previous experiments, at about 1°C every 15 to 20 seconds. This rapid heating reached the pre-set final temperature of 465°C in just under two hours. A temperature discrepancy of roughly 100°C was consistently noted between the internal and external temperature of the MSL Tube Segment. The pressure, however, increased significantly, from -30 inHg to 4 in Hg, this suggested that the FLiNaK not only melted, but some portion may have been vaporized.
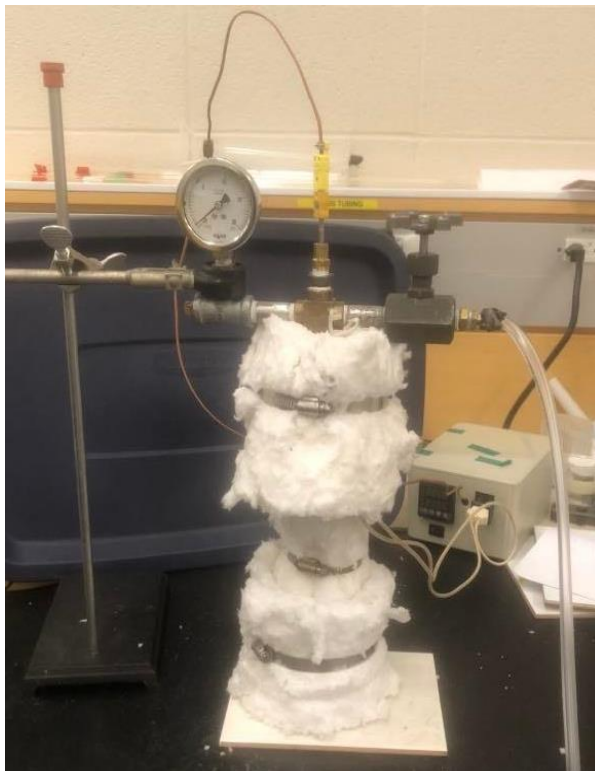
Figure 4.60: The MSL Tube Segment Remelting System with Loose Wool Insulation.

The experimental apparatus was disassembled the following day and the FLiNaK salt had fully melted and drained to the bottom. Figure 4.61 show the salt crystals, which were white (but slightly translucent) with visible black contaminants embedded within. These FLiNaK crystals were then removed and stored in a glass jar as illustrated in Figure 4.62.

Figure 4.61: Close-up Photo of the Drained Salt Chunks.
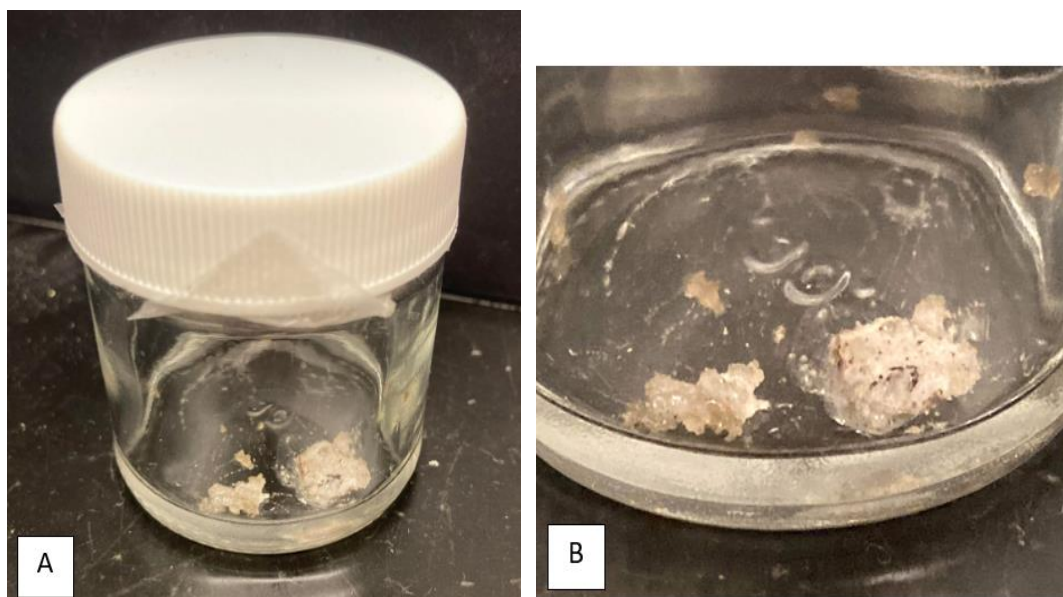
Figure 4.62 (a): Drained FLiNaK Salt, Sealed First with Parafilm and Stored in a Glass Jar (b): Close-up Photo of the Salt Chunks.

162

Finally, the borescope was used to take photographs within the tube to determine if there was any remaining FLiNaK salt and observe the salt-facing sections for signs of corrosion.

Figure 4.63 specifies the zones in which observations were made; the inspections started from the top-flange opening and ended at the bottom plug flange.
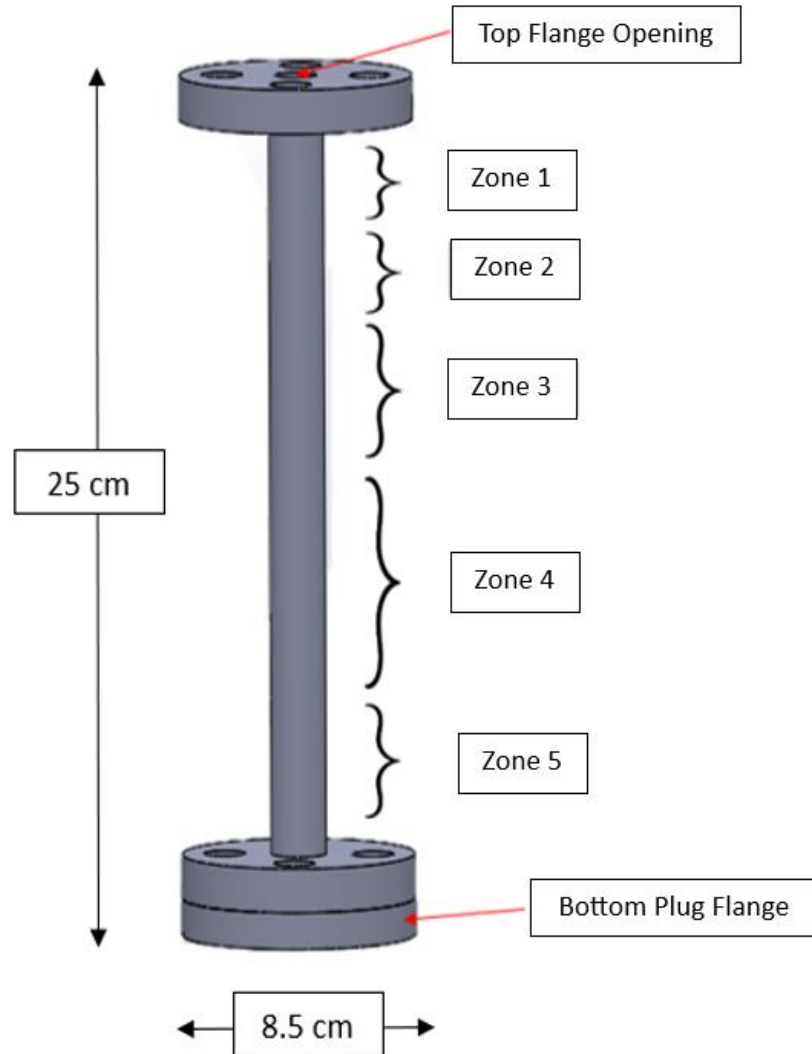
Figure 4.63: The Zones are Divided by the Contents Observed within the Tube Segment.

Figures 4.64 to 4.69 are photos taken of the findings in each zone.

The Hastelloy at the top opening of the MSL Tube Segment had become blackened and dull

Figure 4.64: The Top Flange Opening of the Drained MSL Tube Segment.

Patches of FLiNaK visible along the walls

Thin layer of residual FLiNaK
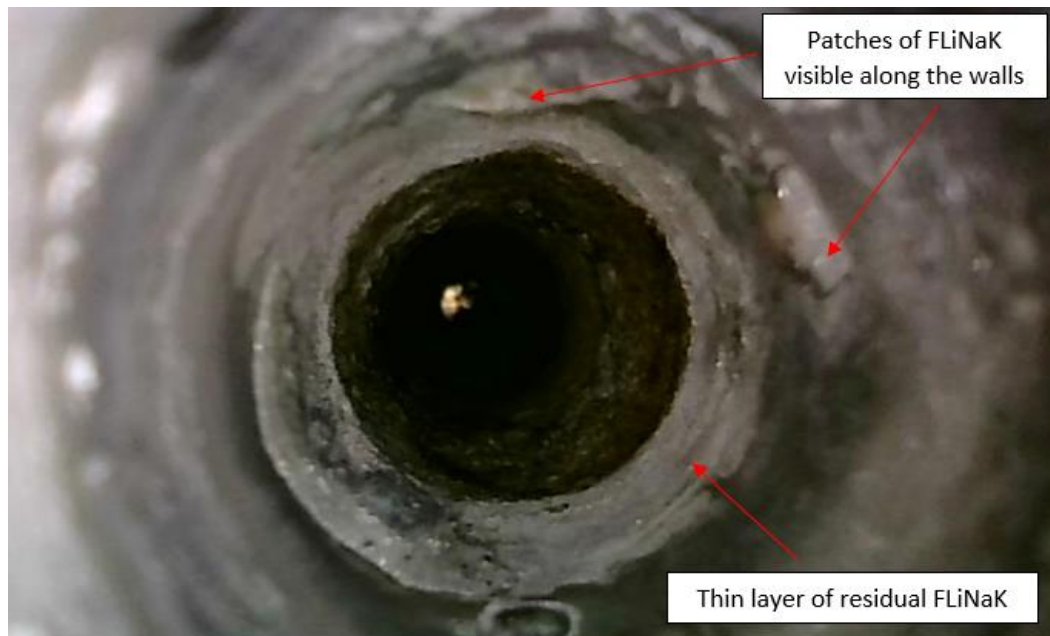
Figure 4.65: Photo of Zone 1 within the Drained MSL Tube Segment.

Figure 4.66: Photo of Zone 2 within the Drained MSL Tube Segment.
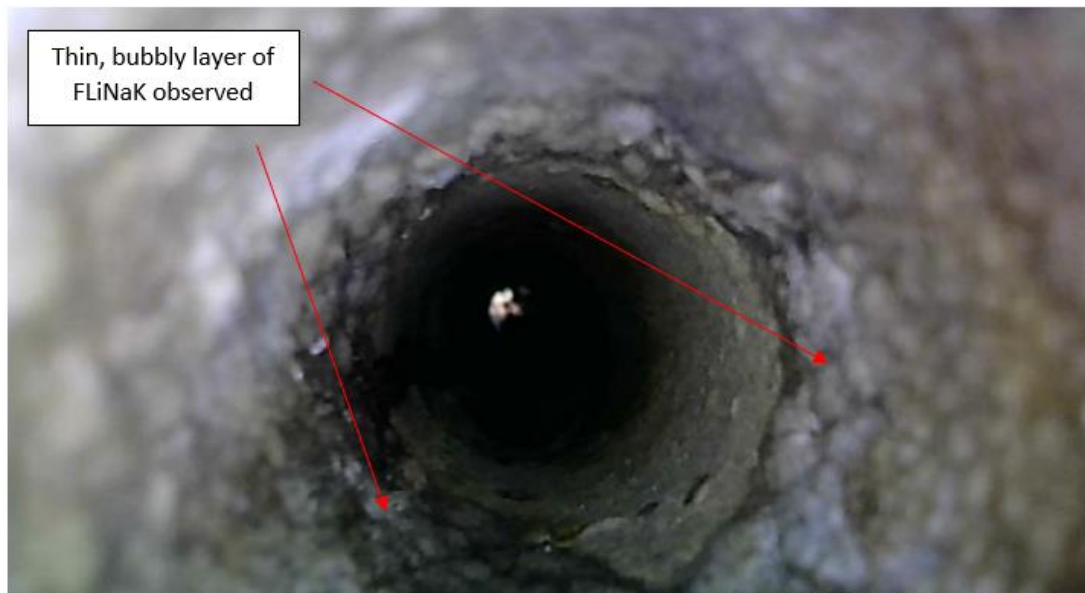
Figure 4.67: Photo of Zone 3 within the Drained MSL Tube Segment.

Figure 4.68: Photo of Zone 4 with Salt Plug Melting Trail.

Figure 4.69 (a): Large, Thick Patches of FLiNaK was Observed on One Side of the Tube Wall (b): A Thin Layer of Green Hues was Observed on the Surface of the Salt.

The images above demonstrated the presence of residual FLiNaK salt in every zone of the tube segment except for Zone 4. Thin patches and pockets of FLiNaK were noted along the Hastelloy tube wall in both Zones 1 and 2. Since the salt plug was initially positioned in Zone 1, it was likely that during the melting process, as the FLiNaK liquefied and fell downwards, some salt remained and re-solidified on the walls. The same reasoning could also apply for Zone 3; however, the residual salt in this section of the tube had appeared thin and evenly coated around the walls. This salt layer consisted of small, dense mounds that appeared bubble-like which spanned about 4 cm in length. The bubbling salt layer then abruptly ended, marking the transition into Zone 4. Zone 4 is the longest of all five zones; no presence of FLiNaK salt crystals or granules were noted. However, a dark streak, about 8-10 in length was observed on the inner walls along which salt had slid downwards. The last section, Zone 5, saw the presence of thick, even patches of salt along one side of the tube wall. This inferred the existence of a "cold spot" during heating, wherein the molten FLiNaK was able to re-solidify in larger quantities. In addition, an oxide layer, thin and green in colour, was observed on the surface of these salt patches. This could be a nickel oxide; nickel, a predominant element in Hastelloy-C276, produces a green oxide when in contact with air.

The results of the FLiNaK salt remelting experiments conducted on a representative Hastelloy component, demonstrated the challenges and difficulties in completely draining a reactor of molten salt. In the context of nuclear decommissioning, given the goal of preventing the spread of radioactivity, the removal of residual salt from an MSR would likely require numerous extensive reheating processes before long-term storage can be considered.

4.4.2 Salt Migration within the MSL Tube Segment

This section describes FLiNaK salt migration observed in the MSL Tube Segment as a result of the residual salt plug. The tube was kept in storage for months between iterations of the remelting experiments. The inner walls of the tube segment were inspected for salt migration using the borescope in between and after each experiment; photographs were taken. Qualitative descriptions and quantitative measurements (made using the 3-D printed column ruler) documented the progression of salt migration on both sides of the salt plug. The effects of numerous reheating of the MSL Tube Segment on the salt were also investigated. Table 4.5 summarizes the distance of salt migration observed on both sides of the salt plug.

Table 4.5: Observation Table for Salt Migration Distance within the MSL Tube Segment.

Observation Date	Side of Salt Plug	Phenomenon Observed	Salt Migration Distance (mm)
May 14th, 2021	Side-A	- Small, granular salt layer, covering a length of 2-4 cm observed.	25.5 – 38.0
	Side-B		
June 18th, 2021	Side-A	- New, larger salt crystals seen near the salt plug - An opaque, continuous salt arc formed near Side-A	38.0 – 50.8
	Side-B	- No changes observed.	25.5 – 38.0
September 17th, 2021	Side-A	- Tube wall was covered by streaks of melted FLiNaK that resolidified.	Not Applicable
	Side-B	- Tube wall was glossy and lustrous. - Salt melted and resolidified on the salt plug.	0
October 14th, 2021	Side-A	- Salt deposited near and on top of the salt streaks.	~ 0
	Side-B	- The tube walls became cloudy; Side-B appeared blackened and dull.	~ 6.4
November 3rd, 2021	Side-A	- An even layer of salt observed. - 3-D printed column ruler prototype used to measure salt migration distance.	12.7-25.5
	Side-B		6.4-12.7
February 11th, 2022 (Post-Experiment)	Side-A	- Streaks of FLiNaK noted on both sides of the salt, which appeared rough and uneven.	0
	Side-B		
July 7th, 2022	Side-A	- Side-A was damp; parts of the surface was translucent and grey. - Salt migration observed.	0-6.4
	Side-B	- Thin layer of salt melted and flowed downwards.	0
July 14th, 2022 (Pre-Experiment)	Side-A	- Side-A became dark grey and damp. - A few larger specks of salt were observed further away from the surface of Side-A.	12.7-19.1
	Side-B	- No significant changes were observed, some very minute signs of salt migration.	0-12.7

Borescope photographs documenting the progression of FLiNaK salt migration Sides-A and B of the salt plug are presented in chronological order in Figures 4.70 and 4.71.
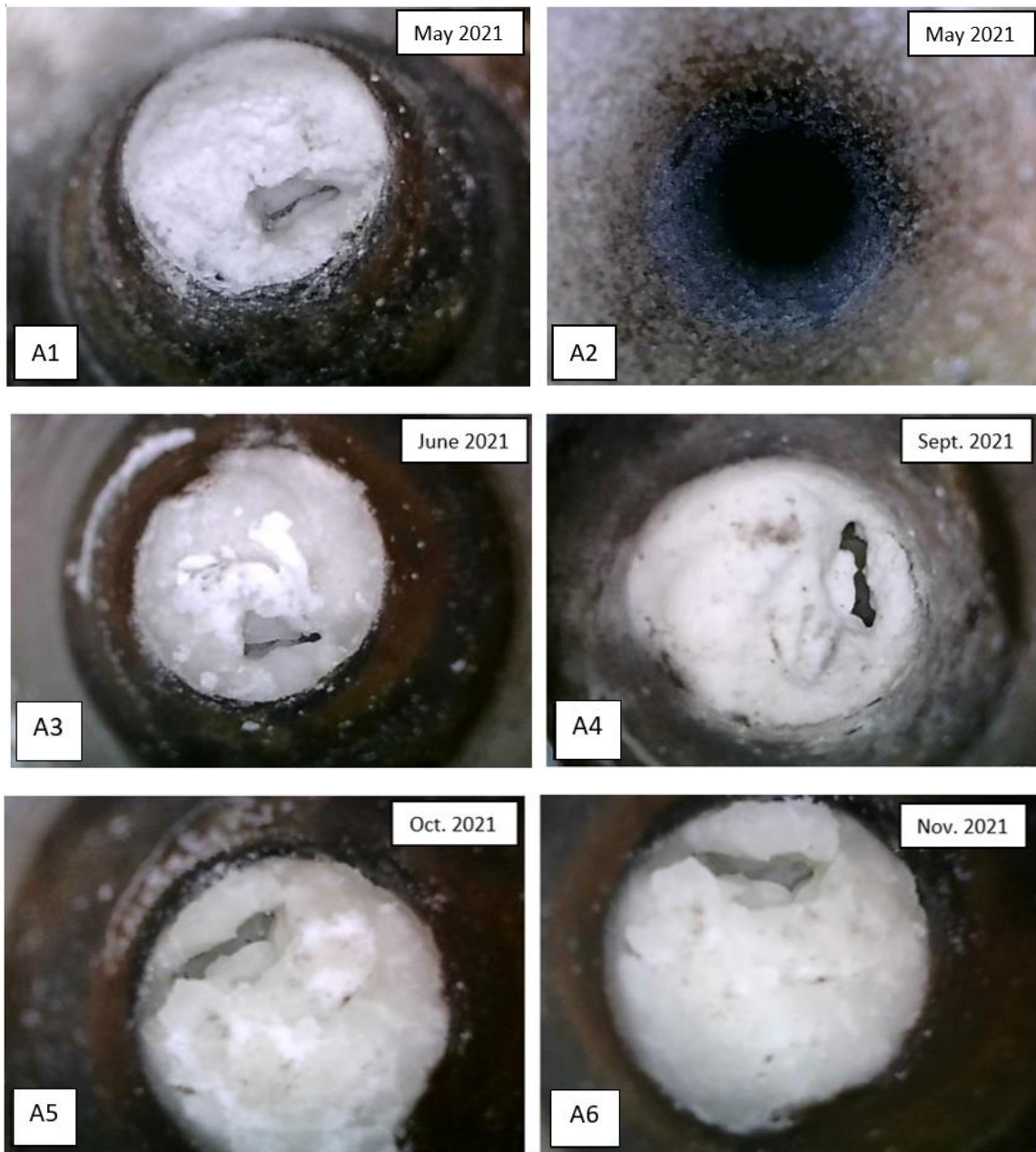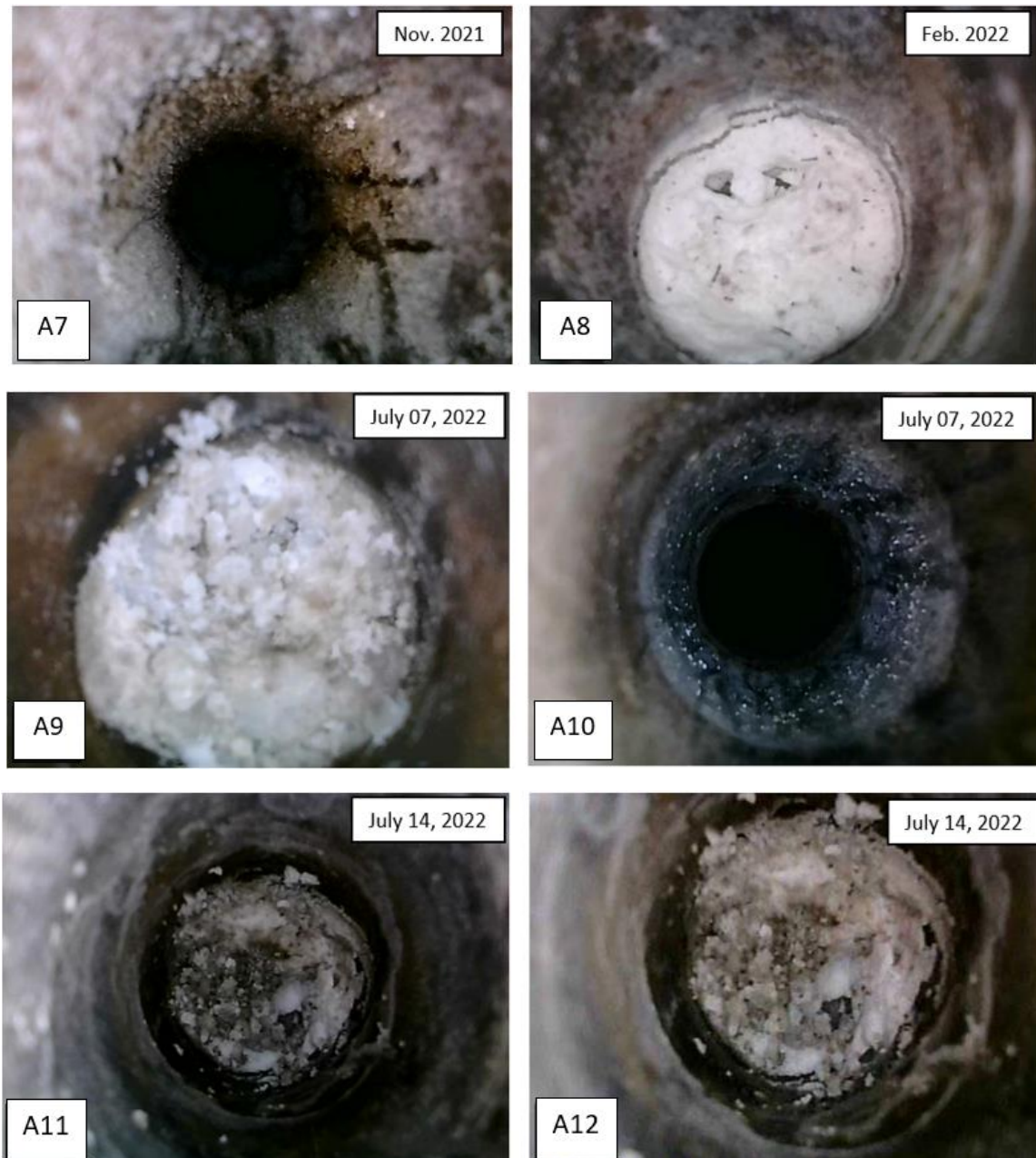
Figure 4.70: Progression in Salt Migration Severity on Side-A of the Salt Plug from May 2021 to July 2022.
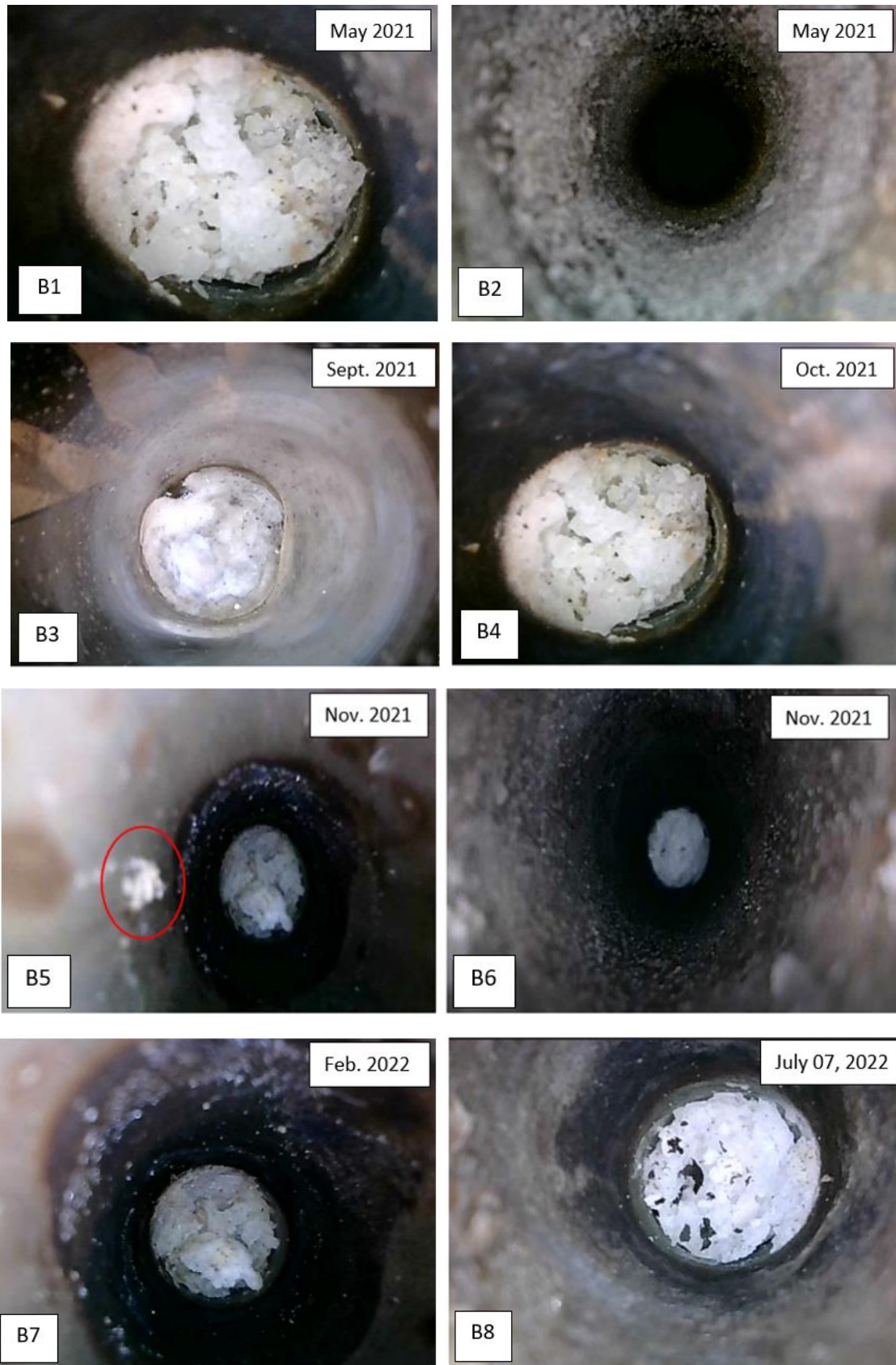
Figure 4.71: Progression in Salt Migration Severity on Side-B of the Salt Plug from May 2021 to July 2022.

For both sides of the salt plug, physical changes and salt migration mostly occurred between iterations of remelting experiments. The reasoning is intuitive, the salt in the MSL Tube Segment had contact with air. The tube segment was not under vacuum like the test tube samples; it was sealed on both ends with Parafilm that were often removed for observations using the borescope and was in constant contact with air. Hence, when left in storage and undisturbed, the FLiNaK would absorb the water molecules in air and start to migrate near the surfaces of the salt plug.

Similarly, after each reheating of the MSL Tube Segment, the thin layer of migrated salt would disappear, having been melted and recombined with the main salt mass. This was most evident in Side-B, where the lustrous surface of the inner walls of the Hastelloy tube was restored, after the experiments. However, observations made following trial three and five showed that both the salt plug and migrated salts crystals had barely melted. This was caused by the premature termination of the heating process. The distance of salt migration within the tube segment did not exceed 63.5 millimeters at any given time; this is due to the melting of the smaller salt particles along the walls during each experiment. These FLiNaK particulates tend to deposit further from the surface of the salt plug, yet they are the smallest in size and hence easiest to liquefy.

On the other hand, observations made immediately after a remelting experiment also yielded confusing results; the salt streaks that resulted from FLiNaK partially melting looked nearly identical to migrated salt patches. To address this, salt streaks observed furthest away from the

surface of the salt plug would then be marked as the new "zero" for salt migration distance measurements. The careful documentation of the time and date of observations mitigated such confusions. These results suggest that during decommissioning, besides waste FLiNaK storage tanks, all salt-facing components with traces of residual molten salt inside must be airtight to avoid the spread and dispersion of radioactivity through salt migration.

4.4.3 Microscope Analysis of Contaminants in Drained FLiNaK

This section presents and discusses the qualitative results of observing the black contaminants extracted from drained FLiNaK salt using a microscope. Spots of small, black contaminants were noted to be embedded within the FLiNaK salt plug since the second iteration of the salt remelting experiments; visible throughout all subsequent observations, these contaminants became larger in size over time. Photographs taken of Side-B of the salt plug in early July saw the drastic increase in size of the black specks, which had grown from small dots to larger flakes that were a few millimeters wide.

These flakes had remained intact upon the successful remelting of the FLiNaK salt plug. The contaminants were removed from the FLiNaK salt crystals using tweezers then placed onto a microscope slide with a square cover glass so that they could be examined under the microscope. These flakes were first observed and photographed under 10 X magnification, then 40 X magnification was used to capture details and textures.

The colour and textures of the contaminants suggest they are metallic in composition; the examined flakes are opaque, dark brown with a copper undertone, and lustrous in some areas under the microscope. The surfaces of these specks were also coarse and flaky, with thin films that were nearly transparent in some areas where metallic sheen was most visible. Figure 4.72 are photographs of the three largest black flakes that were extracted undamaged as seen under 10 X magnification while Figures 4.73 through 4.75 are images of them under 40 X magnification.
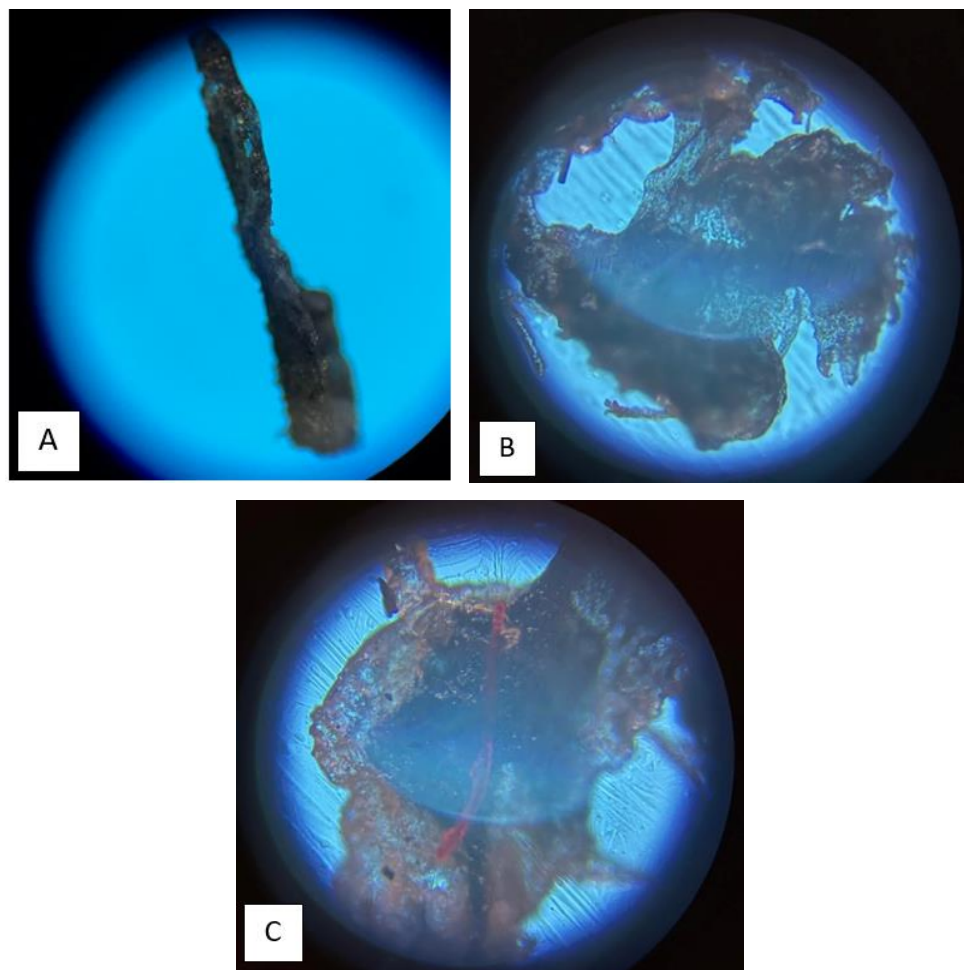
Figure 4.72: Photo of Metallic Contaminant Found in Drained FLiNaK Salt under 10X Magnification (a):Thin, Twisted Strip (b): Circular Flake (c): Irregular Flake.

Figure 4.73: Photo of Twisted Strip under 40X Magnification- the Midsection was Dull.
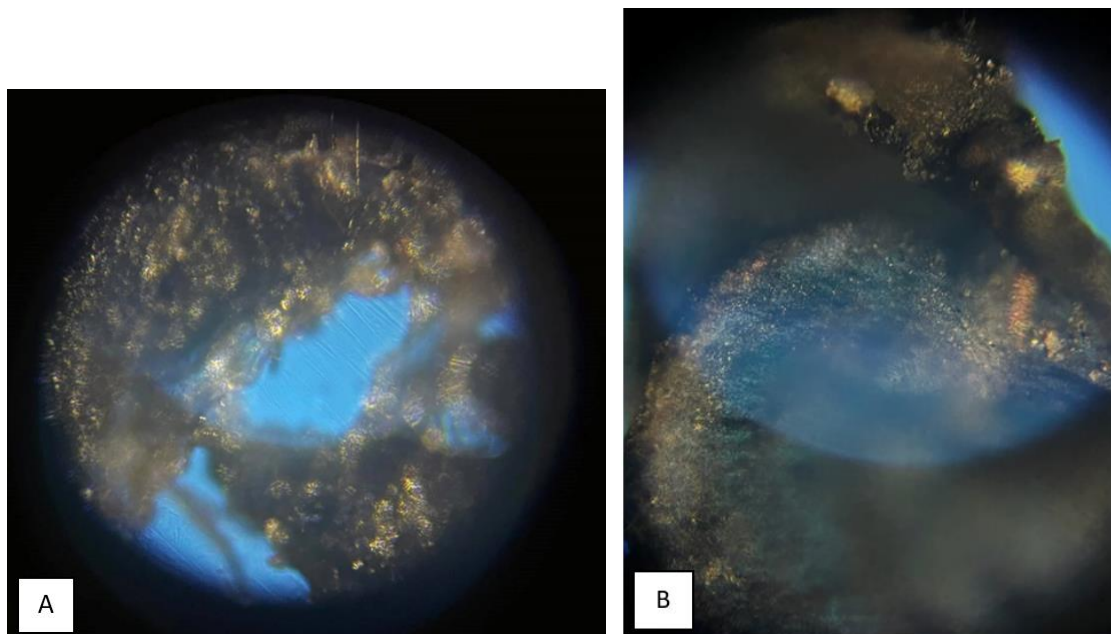
Figure 4.74: Photo of Contaminant under 40X Magnification (a): Shimmery Filaments were seen on the Large Circular Contaminant (b): The Colour and Texture of the Contaminant is that of Rusted, Flaky Metal.
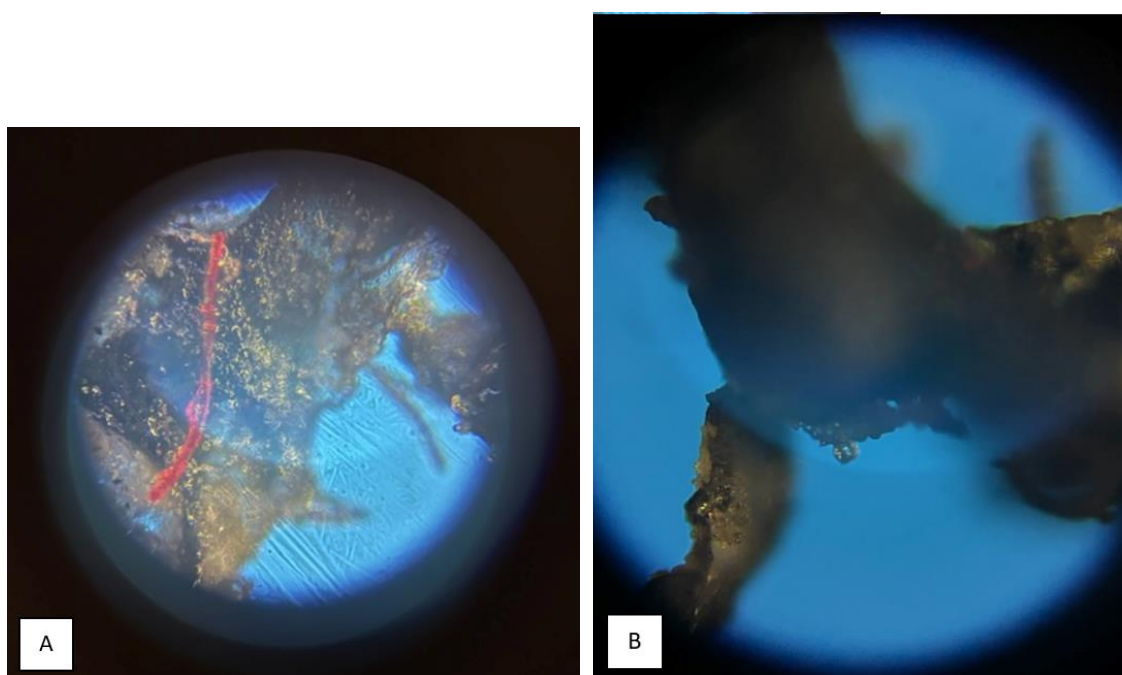
Figure 4.75: Photo of Contaminant under 40X Magnification (a): Shimmery Filaments were seen on the Irregular-Shaped Contaminant Along with a Bright Red Line (b): The Corners were Dull, Darker in Colour and Seemed to be Peeling.

Under 40X magnification, shimmery, metallic filaments were observed; they were more gold than black with distinctive ridges in their surface texture. They appeared to be small, thin pieces of an oxide layer that likely originated from the inner walls of the Hastelloy-C tube segment. In addition to the larger contaminants, some small dots of contaminants embedded in salt crystals were also examined under the microscope for a size comparison and an opportunity to see the crystal structure of FLiNaK. Figures 4.76 and 4.77 are photographs of these smaller contaminants and the FLiNaK crystals under 40X magnification.
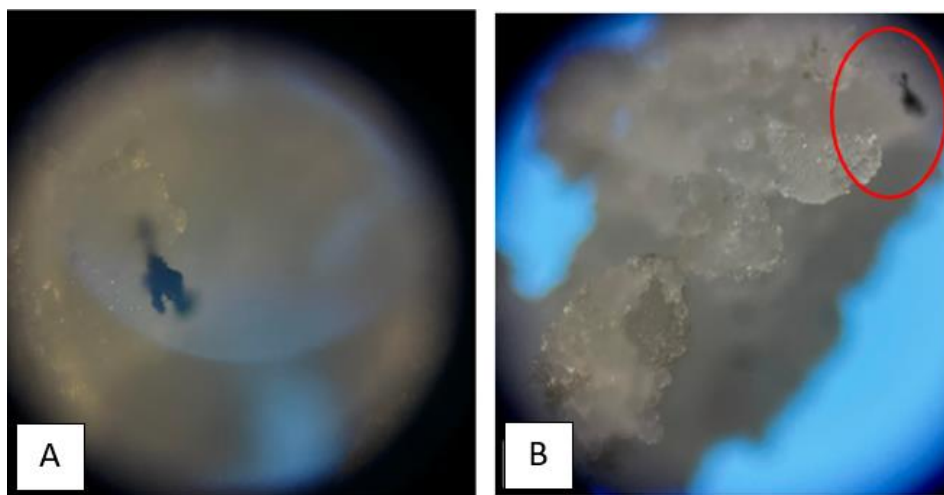
Figure 4.76 (a): Smaller Pieces of Contaminants in FLiNaK (b): Crystal Structure of Drained FLiNak with Contaminant Embedded in the Corner.
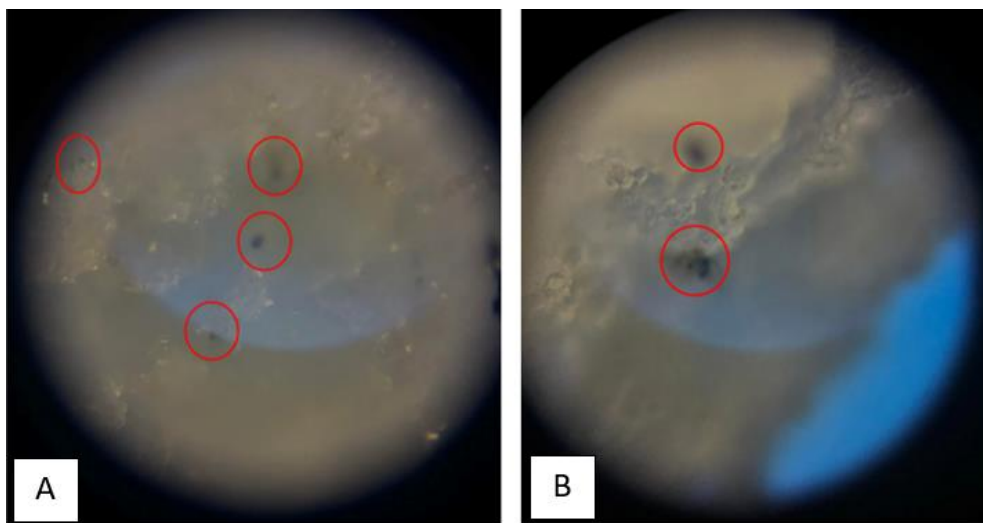
Figure 4.77 (a): Tiny Dots of Metallic Contaminants were Found Throughout the Salt (b): Most Smaller Contaminants are Deeply Embedded.

The results of this microscope analysis confirmed that the contaminants were a metallic substance, though its specific constitution still remained unknown. It was hypothesized that these flakes originated from the inner walls of the Hastelloy tube, but their exact source was also unclear. Consequently, spectroscopic analysis was conducted to identify the elemental composition of these contaminants; the results and details of which are presented in the next section. It is clear that these contaminants, found in drained salt, could introduce potential challenges to for the operation as well as its eventual purification and reprocessing of FLiNaK during D&D activities given how consistently they were found within the salts.

4.4.4 Identification of Contaminants through Spectroscopic Analysis

Spectroscopic analysis was used in an attempt to determine the elemental composition of the black contaminants extracted from the drained FLiNaK salt. The specific process of this spectroscopic method is demonstrated and presented in *Investigation of Radionuclide Contaminants Released by Plasma Torches in Nuclear Dismantlement* [130].

Figures 4.78 to 4.80 feature spectroscopic snapshots as a result of the experiment. Each figure shows the spectra from ignition to those from approximately 200 seconds afterwards. Since it is expected for the sample to be consumed, any emission lines associated with the contaminants should appear at ignition, before and as it is consumed. It is also assumed that the sample should be fully consumed sometime before 200 seconds due to its extremely small size. Therefore, peaks associated with the sample should appear closer to ignition and not near the 200 second mark; in addition, these peaks should not be associated with that of argon. In Figure 4.100, a peak at approximately 221.5 nm was observed which was not apparent at the 267 second mark. However, due to the narrow range of the wavelength scale (too "zoomed-in"), it is implied that such detailed peaks are negligible and may not be directly associated with the sample. Similarly, at approximately 248 and 358 nm, the same rationale applies; this is shown in Figures 4.79 and 4.80 On the other hand, the emission line at approximately 252 nm seen in Figure 4.79 is not considered because it had persisted beyond the 267 second mark and consequently cannot be associated with the sample as it would have been consumed by then. Table 4.6 below summarizes the specific candidate emission lines associated with the peaks observed.
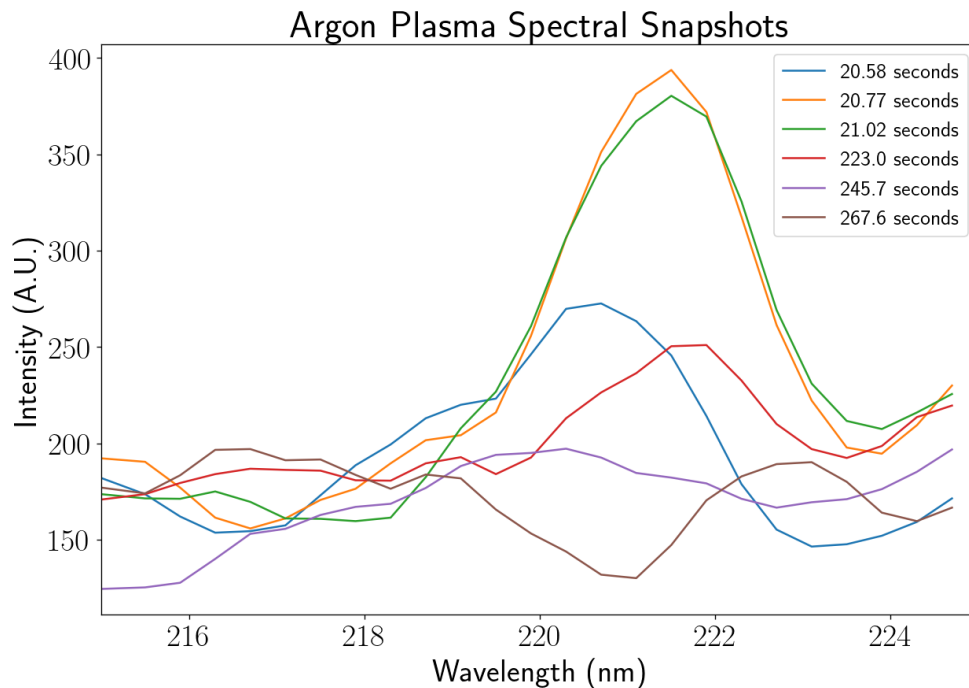
Figure 4.78: Argon Plasma with FLiNaK Salt Contaminants in the 215 nm to 225 nm wavelength range – A Peak that Can be Associated with the Sample was Observed near 221.5 nm.
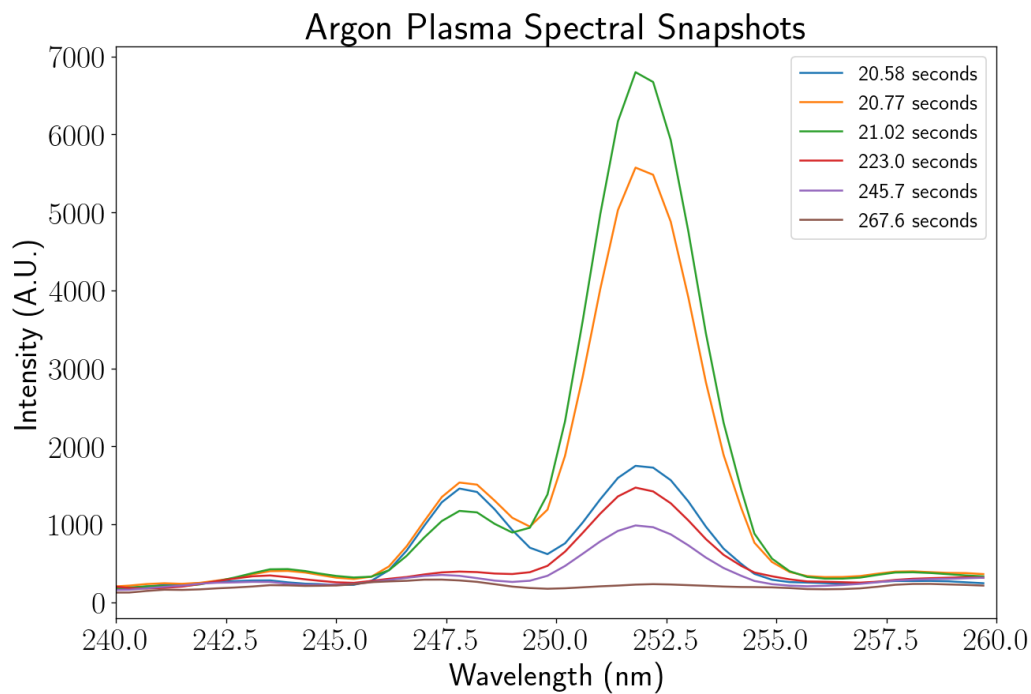
Figure 4.79: Argon Plasma with FLiNaK Salt Contaminants in the 240 nm to 260 nm wavelength range – A Peak that Can be Associated with the Sample was Observed near 248 nm.
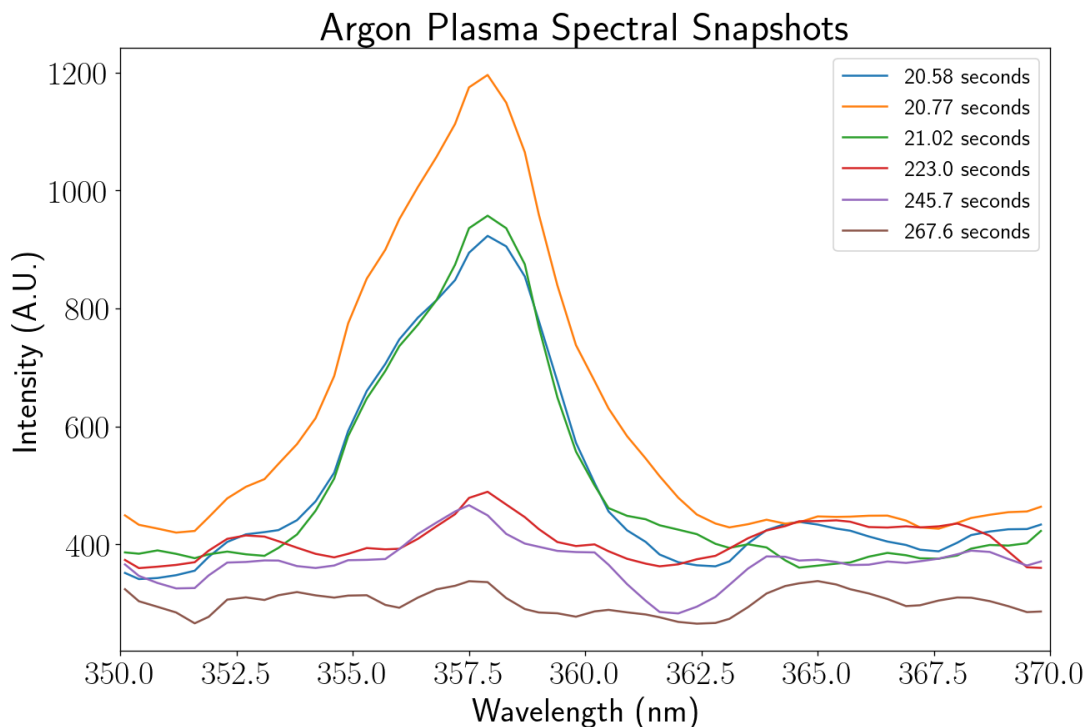
Figure 4.80: Argon Plasma with FLiNaK Salt Contaminants in the 350 nm to 370 nm wavelength range – A Peak that Can be Associated with the Sample was Observed near 358 nm.

Table 4.6: Peaks Observed in Argon Plasma Spectrum and Their Associated Candidate Emission Lines [131].

Peaks Observed (nm)	Candidate Species	Associated Emission Line (nm)
~ 221.5	Ni$^+$	221.6482
	Si	221.6669
~ 248	Fe	248.32708
~ 358	Cr	357.8682
	Fe	358.11931

The candidate species identified above coincided with some key elements that comprise Hastelloy-C276 such as Nickel, Iron, and Chromium. The complete table of the chemical composition of Hastelloy-C276 can be found in Table 3.5 of Chapter 3. It is worthy to note that the Silicon emission line identified here is the result of the glass wool that enrobed the contaminant sample during the experiment. As mentioned previously, due to their extreme small size, the samples would be consumed almost immediately after ignition and thus it was not possible to identify the full range of their elemental composition through spectroscopic

analysis. However, preliminary results yielded from the samples in this work implied that these black contaminants were indeed flakes of corroded or oxidized Hastelloy-C from the inner walls of the MSL Tube Segment. It is also worthy to note the presence of Silicon in the peaks observed near 221.5 nm; the element originated from the fused quartz tube and fused quartz wool, both containing Silicon, that was used in the experiment.

Chapter 5

Discussion

This section interprets the results of the experiments conducted in this work which aimed to highlight and outline the technical implications and considerations regarding the decommissioning of a molten salt reactor through using FLiNaK as a modelling salt.

5.1   Interpretation of Test Tube FLiNaK Synthesis Experimental Results

The synthesis of powdered FLiNaK within glass test tubes using a Bunsen burner allowed for the production of consistent salt samples which were then used for investigating the phenomenon of salt migration. This process, as detailed in Chapter 3 and 4, required the FLiNaK to be thoroughly liquefied in addition to containing minimal moisture and impurities.

The removal of moisture from the salt throughout its melting process was effective in producing consistent FLiNaK samples. The resulting salt pucks have a uniform white colour with no visible porosity; the samples can easily detach from their vessels to be transported or stored.

The appearance of samples produced in this work is consistent with those produced by other laboratories as described in the open literature sources [8][66][79].   The phenomenon and extent of salt migration was observed to be directly correlated to the moisture content in the air, with which FLiNaK came into contact with when not carefully handled. The extent of hygroscopicity of FLiNaK was also explored; the time frame in which salt can migrate throughout its entire vessel is observed and recorded. The findings suggest that when FLiNaK is not stored under vacuum conditions, salt migration will occur and can cover the surfaces of its storage vessel within weeks.

 While there is still uncertainty in the behaviour of FLiNaK in bulk volumes for reactor applications, it is beyond doubt that the spread of radioactivity through salt migration should

be prevented at all costs to protect both workers and the environment. Thus, a series of considerations and options, made in the context of nuclear decommissioning, will be presented in the following sections based on results from the FLiNaK synthesis and salt migration evaluation experiments.

5.1.1 Salt Migration and Deliquescence

The phenomenon of FLiNaK salt migration as observed in the samples produced in this work likely occurred in stages in the storage test tube. The specific mechanism of this behaviour is postulated and discussed in Section 2.9.

Likewise, deliquescence was also observed in numerous samples in this work but is most prominent in samples A-1 and B-3. The final condition of sample B-3, photographed four months after its synthesis, is presented in a collage below in Figure 5.1. The main salt puck had disintegrated while its fragments were suspended and floating in a pool of the aqueous solution formed.
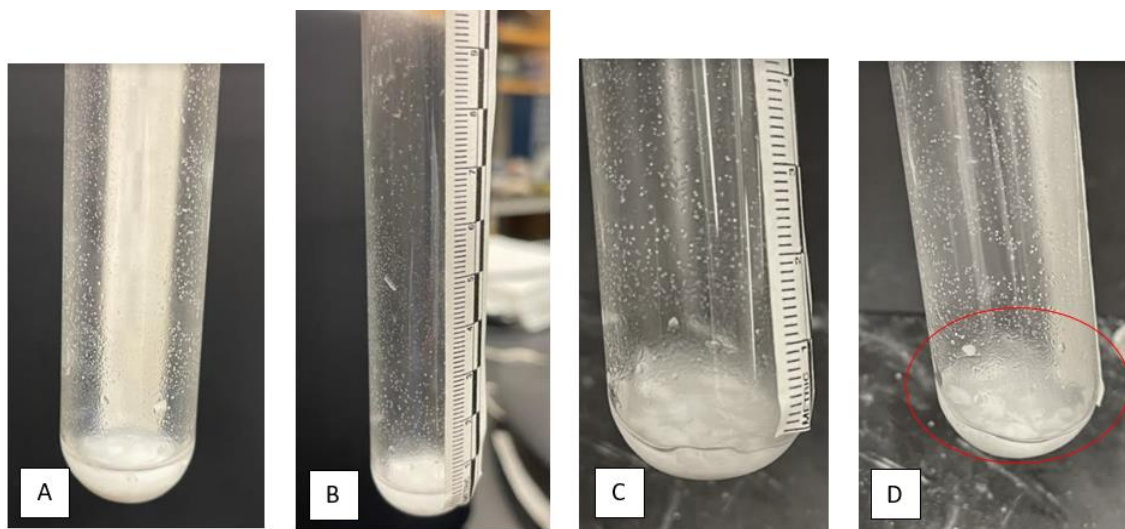
Figure 5.1 (a): Sample B-3 Completely Submerged in Liquid (b): FLiNaK Salt Migrated Along the Entire Length of the Test Tube (c): Main FLiNaK Crystal Dissolved into Small Chunks (d): Pieces of FLiNaK Salt Suspended in Aqueous Solution.

The results thus far demonstrate that the physical changes in synthesized FLiNaK are the consequence of the interactions between the salt and water molecules in the atmosphere. Once absorbed, the moisture should be able to be removed again by remelting the salt, which occurs

at a temperature of 454 °C, significantly higher than that of the boiling point of water. Thus, the cyclic remelting FLiNaK is another crucial aspect of MSR decommissioning investigated in this work, the results of which were discussed in Section 4.3.4.

5.1.2   Maintenance and Surveillance of FLiNaK

The physical changes observed in the FLiNaK samples of this work, be it the test tube synthesized pucks or the salt plug lodged in the MSL Tube Segment, suggest that there would be a need for maintenance and surveillance strategies regarding the drained fuel and flush salt of an MSR. This is especially crucial if there are no immediate decommissioning activities planned for the reactor upon shutdown and the salts are to be put into storage for extended periods of time. This concept is also supported by and already in practice at the ORNL, where tanks of drained waste salts have been stored since 1969.

Samples of both Cycles A and B of this work showed that the extent of salt migration depended heavily on the moisture content of its storage environment and can easily be aggravated by any contact with the atmosphere, should the storage vessels ever be opened for inspection or maintenance. The phenomenon of FLiNaK salt migration also happens relatively quickly when compared to the usual time scale of nuclear decommissioning; the salt can migrate throughout the entirety of its storage container in a matter of a few months as seen in the experiments in this work. Since the molten salt used in an MSR would contain radioactive species, any salt migration within the reactor system may spread radioactivity. Thus, monitoring systems should be in place and routinely maintained to detect any spread of radioactivity as result of salt migration.

Workers entering any operating environment of an MSR containing FLiNaK should be equipped with appropriate the PPE, *i.e.*, fully enclosed nuclear radiation protective clothing along with individual air supply lines. In addition, Ventilation systems are also necessary in all rooms where FLiNaK is handled as a safety measure since fluorine is known to escape from the fuel salt and may need to be off-gassed periodically. Finally, given the direct relationship between moisture and the extent of salt migration, temperature and humidity controls, which will be discussed in more detail in the next section, would also be critical in ensuring the safe storage of waste, radioactive FLiNaK.

5.1.3   Limiting FLiNaK Contact with Air and Humidity Control

The FLiNaK samples synthesized in Cycle B confirmed that the extensiveness of salt migration can be minimized by limiting its contact with air during production and storage. This was done using the vacuum pump, which removed the air and any contaminants or moisture that was previously absorbed by the powdered FLiNaK. The concentration of water vapor present in the air of a given space can be represented by the measured relative humidity.

It is evident that humidity and temperature controls are necessary for the surrounding air and reactor system within any environment in which FLiNaK is handled. From a decommissioning perspective, these control measures are crucial in preventing residual salt migration within the drained reactor system as it awaits or undergoes dismantling, decontamination, or disposal. The process of nuclear decommissioning can span over the course of decades while requiring extensive amounts of manual labour. Each time a salt-facing component containing any amount of FLiNaK is exposed to air, there is an increased risk of the salt within to migrate and taking along with it, radioactivity. Improperly managed, this spread of salt and radioactivity can subject workers to unexpected doses as the salt migrates further away from its source over time. Thus, the ambient temperature of the environment should be strictly controlled and kept cooled, with relative humidity level kept as closes to 0 % as possible to ensure worker safety.

5.1.4   Routine Salt Remelting

Experiments involving the cyclic remelting of FLiNaK samples A-3' and B-5' demonstrated the effectiveness of routinely remelting and reheating the salt in preserving the properties of FLiNaK over extended periods of time while limiting the effects of salt migration. This method can be used to maintain FLiNaK salt stability under long-term storage during reactor decommissioning and dismantling. The concept is not novel, mentioned in Chapter 2, the waste fuel and flush salt of the MSRE was annually reheated to about 150°C until 1989, though it was done to stabilize the physiochemical properties of FLiBe- fluorine was being freed from the salt due to radiolysis at low temperatures. The experimental results of this work suggest the same method can be applied to FLiNaK, especially if it contained radioactive fuel. Remelting molten salt periodically may become a necessary procedure for the long-term

maintenance and storage of fuel salts as well as serve as a solution to both salt migration (if at any point the salt came into contact with air) and the release of fluorine from radioactivity.

5.1.5 Considerations for Accident Scenarios

As discussed in Chapter 2, many molten salt reactor technology vendors claim that their designs are "walk away safe". However, results yielded in Sections 4.3.3 through 4.3.5 highlight the need for considerations to be made regarding the decommissioning of an MSR under accident scenarios. Samples B-1 and B-2 (Figures 4.24 and 4.25) from Cycle-B of the synthesis experiments had contradicted an earlier hypothesis and demonstrated that the addition of tap water did not aggravate the rate or extent of salt migration. Hence, direct contact with liquid water in the event of natural disasters may not necessarily lead to spread of radioactivity via salt migration but is still dangerous because FLiNaK is soluble in water and can be transported through this medium. In addition, the hygroscopic nature of FLiNaK would require immediate reactor shut-down and remediation in the case of molten salt leakage to control the dispersion of radiation. Contingency plans such as reinforced containment or salt capture systems should be in place to minimize the migration of salt once it is exposed to air. It is clear that under such circumstances, there would be added complexity to the technical challenges and radiological risks associated with the clean-up of molten salt systems.

5.2 Interpretation of MSL Tube Segment FLiNaK Salt Drainage Experimental Results

This section serves to interpret the main takeaways from the experiments involving the drainage of a FLiNaK salt plug stuck within a section of the Hastelloy-C276 Molten Salt Loop and the analysis of both the metallic components and the drained salt crystals.

5.2.1 Challenges in Salt Removal and Drainage

The FLiNaK salt plug remelting experiments illustrated some of the challenges that may arise in draining molten salts from the reactor in preparation for decommissioning. Firstly, it would be difficult to achieve complete drainage by reheating the reactor system only once; residual salt is likely to be present within some smaller salt-facing components even after several

drainage procedures. Borescope inspections of the MSL Tube Segment after draining the salt plug saw the presence of several salt deposits that remained along the walls (Figure 4.65 to 4.69). Out of the 4.32 g of FLiNaK salt initially lodged within the MSL Tube Segment, which was determined through weighing an empty tube and the tube with salt prior to any heating experiments, about 1.1 g of residue remained, which is just over 25% of the total mass of salt.

In the case of the MSL Tube Segment Remelting experiment, only about 70 % of the original salt bridge was drained while the rest of the FLiNaK remained within the tube. Another possibility would be to first drain the fuel salt and then flush the reactor system with flush salts only once. After which the components can be filled with water because the deliquescence of FLiNaK would allow the salt to dissolve within the water; this solution can then be separated through boiling for the collection of residual FLiNaK

Despite the dilution in radioactivity, internal salt deposits can start to migrate given any contact with atmospheric moisture, spreading the contamination. Consequently, salt-facing components may need to be flushed several times before the dismantling and recycling of metal structures can be considered. Alternative decommissioning methods such as in-situ disposal and long-term underground storage (deep borehole disposal) have been proposed by vendors such as Terrestrial Energy and MoltEx [5][6], which bypass the issues surrounding salt drainage by discarding the entire reactor core or tubes with salt solidified within, respectively. However, molten salt that remain within pipes over long periods of time can also intensify corrosion. There is significant uncertainty in the plausibility of these options based on the limited publicly-available information; they may be further explored should the vendors release more details throughout the CNSC licensing process of their designs.

5.2.2 Contamination of FLiNaK

The presence of metallic contaminants, oxides formed on the inner walls of the MSL Tube Segment were found embedded throughout the drained FLiNaK salt crystals based on observations made under the microscope. The candidate emission lines yielded from spectroscopy analysis are associated with some of the main elements that comprise Hastelloy-C276. The observed degradation of the Hastelloy-C deviated from literature and vendor descriptions; as discussed in Chapter 3, the alloy has been experimentally determined to be

extremely corrosion resistant when used in molten FLiNaK applications. However, most of these sources imply the use of newly synthesized molten FLiNaK for each experiment performed instead of repeatedly remelting the same sample of salt as done in the salt drainage experiments of this work. Consequently, it is very likely that the reheating trials of the MSL Tube Segment had elevated the corrosion rates by the FLiNaK periodically. Exposure to the air and atmospheric moisture during the numerous assembly and disassembly processes may have also contributed to changes in chemical structures of the salt. Corrosion tests conducted by Ouyang et. al. [132] noted that higher moisture content and residual moisture in the FLiNaK would lead to aggravated intergranular corrosion and pitting in Nickel-based alloys, namely Hastelloy-N and Hastelloy-B3 and it is not hard to imagine that the same would also apply to Hastelloy-C276.

As emphasized by literature sources [80][96] and discussed in length in Chapter 2, the physiochemical and thermal properties of FLiNaK depend heavily on its purity and precise chemical composition. Undoubtedly, the discovery of contaminants demonstrated the chemistry of the FLiNaK salt plug has deviated from its original condition given the experiments conducted before and during this work. These changes in salt environment accelerated the corrosion of the Hastelloy-C276 walls, resulting in the black flaky contaminants, which when incorporated into the molten salt, further disrupts the chemistry of the FLiNaK, thus creating a cycle of deterioration for both materials with each reheat.

The requirements regarding maintaining molten salt purity in order to ensure its properties suggest the need for frequent refuelling of fresh salts so that reactor operation is not otherwise compromised. Vendors such as Terrestrial Energy propose that the core of their reactor, the IMSR-400, be entirely replaced every seven years while the used core is returned to it originating facilities while other vendors have not presented their respective decommissioning plans to regulating authorities at this time [5][6]. Though specific end-of-life strategies are not yet determined, it is clear that uncertainties regarding the contamination levels of molten fuel and flush salt would further complicate the decommissioning process. Similarly, depending on the level of corrosion and radioactive contamination (resulting from contact with fuel salts), metallic reactor structures may require alternative decontamination methods or be discarded entirely. The discovery and analysis of metallic contaminants found within the FLiNaK salt

plug in this work imply that the end-state of a molten salt reactor can be unpredictable should salt chemistry not be properly maintained.

5.2.3 Salt Chemistry Restoration and Defueling

The experiments involving the analysis of the drained FLiNaK produced evidence that suggest the degradation of FLiNaK salt throughout the iterations of reheating. Thus, salt chemistry restoration and fuel (Uranium) recovery may be necessary in preventing salt migration and its complications. The drained fuel salts will likely sit in storage for the duration of the decommissioning of the MSR and this method has been proven effective in keeping the fuel and flush FLiBe salt of the MSRE in safe and stable condition. The FLiNaK will need to be melted and chemically treated using the Hydrofluorination process mentioned in Chapter 2. This process involves sparging the molten salt with a mixture of hydrogen fluoride, hydrogen, and helium to restore the chemical balance within the salt by ensuring uranium is in the form of UF_4. Finally, the uranium in the salt can be condensed into cold traps and removed using chemical traps.

5.2.4 Molten Salt Reactor Structure Decontamination and End-of-Life Options

One of the most essential of the unanswered questions regarding the decommissioning of an MSR, besides the end-state of the salts, is how to approach the extensive metallic reactor structure upon reactor shut-down. The results presented in Chapter 4 illustrate the feasibility for decontaminating the Hastelloy-C276 components so that they may eventually be recycled or repurposed. Although signs of corrosion were observed through the presence of contaminants within the drained FLiNaK (Figures 4.72 to 4.77), the severity was far from a level at which a component should be discarded. However, it is also worthy to note that such mild results are due to the very small amount of FLiNaK within a small test section over the course of two years, the effects of corrosion in a full-sized MSR during it entire decommissioning horizon will likely be much worse.

A critical part of nuclear decommissioning, the deployment of decontamination techniques has been proven effective in reducing workplace hazards, limiting the potential release of

radioactive materials, and facilitating waste management. Usually, the decision to decontaminate is based on total dose removed and cost; however, there are very few historical data or literature sources that discuss which of the numerous presently available decontamination techniques may best suit an MSR. Methods such as chemical washes, which were used to clean the Hastelloy-N components of the MSRE, may be a good starting point for rector structure reprocessing. In addition, the decontamination of salt-facing components can remove residual salt deposits and eliminate the hazards associated with the migration of radioactive salt. Finally, a 1997 study investigating alternative end-of-life options for the MSRE fluoride salts also noted that the Hastelloy-N remained in good condition over 30 years with minimal signs of corrosion [133], implying that it is possible to salvage the metallic components of MSRs.

5.3   Comparison of Results

Both molten FLiNaK experiments provided some insight into the challenges and considerations that will arise during the decommissioning of an MSR. Through observing and characterizing the phenomenon of salt migration and identifying various factors that can aggravate or minimize such physical changes. The test tube synthesized samples demonstrate a clear and direct relationship between access to air, and thus the water content within it, and the extent of salt migration as seen in experimental cycles A and B. The MSL Tube Segment salt remelting experiments exemplified the difficulties in completely draining molten FLiNaK from a representative Hastelloy-C component as well as illustrated that even small amounts of residual salt can quickly migrate and spread throughout the reactor system.

5.3.1   FLiNaK Behaviour in Common

The relationship between atmospheric moisture and the extent of FLiNaK salt migration as a consequence of the salt's hygroscopic nature were observed for both sets of experimental set-ups. Table 5.1 summarizes the common physical changes and migration behaviour of synthesized FLiNaK between the test tube samples and the salt plug in the MSL Tube Segment. Salt migration in Cycle-A and B samples are much more easily described and documented; this is due to the transparency of the glass test tubes. On the other hand, observations of the extent

of salt migration within the tube segment is limited to the photographs taken by the borescope, which may contain blind spots. Even with built-in LED lights, there are likely areas in the tube segment where the texture or presence of salt is not well-characterized. Similarly, the results from the ultrasonic study performed in this work also led to inconclusive results. Thus, in practice, this uncertainty may suggest the need for more advanced detection technologies or methods in order to identify any hidden, previously undetected radioactive salt residue deposits within the reactor structure of an MSR throughout its decommissioning. Extensive safety considerations should be made for activities where workers might be expected to handle salt-facing components.

Table 5.1: Common Salt Phenomenon Observed for both Test Tube Synthesis and MSL Tube Segment Drainage Experiments.

Sample	Experiment	Maximum Salt Migration Severity (mm)	Deliquescence	Contact with Air	Contact with Liquid Water
A-1	Test Tube Synthesis of FLiNaK	Observed (Not Quantified)	Observed (Fully submerged)	Some	No contact
A-2			None	Minimal	
A-3				Temporarily Exposed	
A-4				Minimal	
B-1		28	Observed (Partially submerged)	None	1.03g added
B-2		21	None	None	0.55g added
B-3		105	Observed (Fully submerged)	Temporarily Exposed	No Contact
B-4		6	None	None	
B-5		3.5		None	
FLiNaK Salt Plug	MSL Tube Segment Drainage Experiments	50.8	None, though damp salt surfaces were observed	Frequent	No contact

5.3.2 Differences in Appearance of FLiNaK in their Respective Vessels

It was discussed in Chapter 4 that the physical appearance of the FLiNaK samples stored in test tubes had differed from that of the salt plug within the MSL Tube Segment (Figures 4.9 vs. 4.64). The contamination of the salt plug caused the FLiNaK to have appeared either grey or green while the samples from Cycles A and B remained a pristine white. Since FLiNaK would be expected to operate within the metallic components of a molten salt reactor, the results from the drainage experiments would be much more representative in terms of what

FLiNaK may look like during or at the end of reactor operations. Hence, the discoloration of salt could be used as a sign of precaution in identifying contaminated FLiNaK in need of further processing.

5.4 Decommissioning Options

Due to limited public information, the analysis and evaluation of MSR decommissioning options largely falls back on the examination of literature sources regarding the only historical precedent, the MSRE (despite it being a test reactor). Chapter 2 elaborated in detail about the decades-long, on-going assessment process in selecting a method for final salt disposition and reactor facility decommissioning. During this time, alternative solutions including permanent disposal of the salt in drain tanks, disposal of key contaminants in federal repositories, reuse of salt, and interim storage were proposed, all of which were rejected. They either pose a threat to the environment (the MSRE drain tanks lie below the water table) or require the availability of repositories or processing facilities that have yet to be designed or constructed. Beyond the spread of radiation through salt migration, these issues presented above, both technical and regulatory, are present challenges that future MSRs will continue to face. It is then abundantly clear that there is still extensive work to be done in terms of exploring the decommissioning options for molten salt nuclear technologies.

Although the scope and pathways of decommissioning for future Gen. IV MSRs remain uncertain, the experimental results of this work can be used to highlight some of the technical challenges that can be associated with the end-of-life operations of molten salt reactor technologies. Given the current regulatory framework, any proposed decommissioning strategy would likely still fall under the three main options for nuclear decommissioning as defined by the IAEA, namely, DECON, SAFSTOR, and ENTOMB, which have been applied to commercial nuclear reactors. The following subsections will seek to demonstrate how the results from the experiments of this work may be applied to each of the three decommissioning options in addition to any associated implications.

5.4.1 Immediate Decommissioning (DECON)

The most ideal option, the immediate decommissioning of a molten salt reactor, would allow for the release of the nuclear facility from regulatory control within a shorter time frame compared to those of the other two options. The MSR's decommissioning can commence within months of the reactor shut-down; the fuel and flush salts drained into designated tanks while decontamination and dismantling activities take place.

This option would minimize the time in which radioactive salts remain stagnant in storage containers where they are expected to be regularly maintained, during which the risks of salt migration could increase should the salts come into contact with air and moisture through human errors. Similarly, the sooner the reactor structure is decontaminated and dismantled, the less severe the salt migration within these components will likely be. Any remaining contaminated equipment can be further treated or removed as radioactive waste depending on their category. By immediately decommissioning an MSR, the time for the salts to absorb moisture and migrate is reduced, and thus should mitigate the effects of radioactivity dispersion.

Despite the seemingly attractive benefits of addressing salt migration and eliminating any future liability, there is still an overwhelming amount of technical challenges regarding the removal, transport, and final disposal of waste salts. This is mainly because no such facility currently exists for the long-term or permanent disposal of molten salts. Likewise, the option to reuse the salts is also presently improbable due to the lack of reprocessing capabilities or investment.

5.4.2 Deferred Decommissioning (SAFSTOR)

The current decommissioning status of the MSRE, the option of deferred decommissioning allows the owner of a nuclear facility to postpone its release from regulatory control for extended number of years. This is done by maintaining the facility in safe storage condition through performing various surveillance and maintenance activities, then followed by the building's eventual decontamination and dismantlement.

Aside from the uranium migration and its deposit onto the charcoal bed, the postponed decommissioning of the MSRE has been effective; the facility has been in stable condition for

the last 30 years. The most probable option for the decommissioning of an MSR, the considerations presented in previous sections of this chapter also largely focused on the caveats of FLiNaK salt migration under safe storage conditions. It must be reiterated that extended storage time and maintenance procedures can increase the probability of the waste salt, should FLiNaK be used, coming in contact with atmospheric moisture and aggravating salt migration.

As the facility and equipment age, components become more likely to fail. This can in turn lead to radiological leakage or the spread of molten salt. Such hazardous conditions also make for challenging work environments; workers tasked with remediation would require extensive PPE, specialized tools, even portable maintenance shields while potentially being exposed to higher doses of radiation. Finally, the delays in technological capabilities and any subsequent decisions on final salt waste disposal will be very costly as surveillance and maintenance activities continue. Changes in regulatory policy can also easily fluctuate the costs associated with keeping a facility under safe storage. Regardless, without an ultimate disposition solution available for the waste fuel and flush salts, it is most likely that a retired MSR would remain under safe storage.

5.4.3 Entombment and In-Situ Disposal (ENTOMB)

An option explored in a much lesser extent, the entombment option would involve encasing the contaminated portions of an MSR facility in materials such as concrete or grout to isolate the source of radioactivity from the surrounding environment. The main objective of this decommissioning option aligns with the findings of the work, which is to keep water and moisture out of the containment. In this scenario, the main source of exposure is likely due to a contamination leakage from the otherwise sealed structure. Likewise, in-situ disposal is essentially on-site entombment, though the area is usually minimized. For both cases, land use controls are required to prevent trespassing or sabotage. Entombment may be the best viable option at the end of the safe storage period should options for final salt waste disposal never materialize. However, this is highly unlikely from a regulatory standpoint since decommissioning plans are required by the CNSC during a design's licensing process. Vendors such as Terrestrial Energy and MoltEx have both been promoting the possibility of deploying fleets of their molten salt reactors in the form of SMRs [5][6], which, if realized, would also

decrease the chances for in-situ disposal as it would require significant amounts of restricted land and become unsustainable.

5.5 Fulfillment of Thesis Goals

All of the objectives of this thesis, as outlined in the introduction chapter, can be said to have been fulfilled.

1. Produced controlled and experimental samples of FLiNaK salt that ensured control of the inputs to the experiments.

2. Assessed and evaluated FLiNaK Salt behaviour under different environmental conditions and their implications for decommissioning.

3. Emulated the drainage of salt from a representative Hastelloy-C276 component by re-melting and removing the FLiNaK salt inside the MSL tube segment.

Objective 1 was completed using the test tube FLiNaK synthesis system. Consistent, stable samples of FLiNaK were produced in two batches. The removal of moisture from powdered FLiNaK through the use of a vacuum pump throughout melting and cool down yielded samples that closely reflected literature descriptions. Qualities such as colour, texture, and salt behaviour were explored as a consequence of input synthesis parameters and storage conditions. The phenomenon of salt migration was determined to be a consequence of the FLiNaK's hygroscopic nature as it readily absorbs water vapour whenever it had contact with air. This phenomenon was further quantified through accomplishing Objective 2, which was addressed through both the test tube synthesis experiments and the MSL Tube Segment salt drainage experiments. Samples from Cycle-B of the test tube synthesis experiments investigated the relationship between salt migration with different forms of water whilst simulating potential decommissioning environments. Similarly, the salt drainage experiments examined the effects of multiple reheating on FLiNaK salt behaviour and migration. The results of which implied potential complications for the end-of-life operations of MSRs as discussed earlier in this chapter.

Objective 3 was successfully completed using the MSL Tube Segment Salt Remelting System. Throughout the six iterations of the experiment, the main challenge had been providing

sufficient heating to the tube segment to completely melt the FLiNaK. Even after drainage, it was noted that some patches of residue still remained within the component. This highlighted the difficulties in thorough molten salt, and by extension, radioactive contamination removal and drainage from a salt-facing system once the reactor has shut down. A preliminary spectroscopy analysis suggested minor corrosion in the Hastelloy-C vessel upon discovery of metallic contaminants in the drained FLiNaK.

Chapter 6

Concluding Remarks

This work has completed a study of FLiNaK salt synthesis, storage behaviour, remelting, and drainage experiments using self-devised exploratory methods with the purpose of applications towards nuclear decommissioning. Hence, as a result of this work, the following concluding remarks are made:

➢ The FLiNaK salt pucks synthesized using the vacuum salt melting system appeared physically consistent with one another and the description of FLiNaK in open literature sources (see Figures 2.21 and 2.22). The use of a vacuum aids in removing any moisture within the powdered FLiNaK.

➢ When the synthesized FLiNaK salt comes into contact with atmospheric moisture, salt migration, as a result of the salt's hygroscopy and deliquescence is observed. The extent of salt migration is related to the relative humidity of the room in which the FLiNaK is stored and how impermeable (airtight and waterproof) its containers are.

➢ Unlike the FLiNaK used in experiments in this work, the decommissioning of an MSR would involve radioactive molten fuel salt. In such cases, salt migration could lead to the uncontrolled spread of radioactivity throughout the reactor system. The same could apply to extended periods of maintenance and salt re-filling where the FLiNaK is allowed to solidify and may come into contact with air.

➢ The MSL Tube Segment was used as a representative component to illustrate the process of FLiNaK salt draining at the end of the operating life of an MSR. From the FLiNaK remelting experiments in this work demonstrated that it would be difficult to completely drain the salt by reheating the reactor system only once;

residual salt is likely to be present. Flush salts and other decontamination processes can be applied to the reactor structure prior to dismantling, disposal, or recycling.

➢ Reactor components and all receptacles containing FLiNaK should be sealed airtight and in vacuo. Improper sealing would lead to moisture ingress from the surrounding air and the resulting salt migration can introduce additional challenges to the decontamination and dismantlement process.

➢ FLiNaK is capable of corroding Hastelloy-C276 on the order of particulate size under a relatively short time at high temperatures; general corrosion did not occur.

➢ Although the level of corrosion observed in the Hastelloy-C tube segment in this work is minimal, the same may not be true for commercial MSR systems that circulate multiple tonnes of molten salt over the course of seven or more years continuously. Thus, considerations must also be made with regards to the degradation of the reactor structure at the time of decommissioning.

Chapter 7

Future Work

This work has provided a basis for considering some of the issues associated with decommissioning a molten salt reactor. The findings indicate that there are several areas where further investigations are warranted, both for short term and long-term consideration. The following suggestions for future work are proposed based upon the findings of this study:

➢   The bulk behaviour of FLiNaK can be analyzed to see if the same phenomena occur. It is possible that the phenomena are related to surface area and the surface area to volume ratio was very high in this work. Higher quantities of salt (25g +) can be synthesized and put into storage to observe for salt migration while correlating the extensiveness to parameters presented in this work

➢   Contaminants, or small quantities of UF_4 can be purposely introduced into the molten FLiNaK to determine whether they could be transported through salt migration and its subsequent effects on the decommissioning of an MSR.

➢   Complete the construction of the laboratory's molten salt loop (to which the MSL Tube Segment belongs). Fill the MSL with FLiNaK and circulate the molten salt within the loop for various time spans, then examine the drained system for signs of corrosion in the salt-facing components as well as residual internal salt deposits each time. This may provide a more representative decommissioning scenario.

➢   Purify FLiNaK synthesized using hydrofluorination. The laboratory of this work did not have the facilities to perform the hydrofluorination process and thus high purity samples could not be obtained. While it is expected that even high purity salts would deteriorate in the reactor over time, it would be useful to benchmark the findings against the purity of the original sample.

➢   Explore and attempt to apply decontamination techniques that may be suitable for MSRs using FLiNaK, where salt migration can be a concern.

Appendix A

Experimental Procedures

This section provides a list of all experimental procedures developed throughout this work for future users along with an encapsulated description of their purpose.

A.1 List of Experimental Procedures

Table A.1: List of Internal Experimental Procedures and their Purpose/Associated Experiment

Document Title	Purpose of Document
NDL-MSL-LPROC-001: One Hour Plan for Furnace Performance Testing	To ensure the proper functioning of the furnace
NDL-MSL-LPROC-002: UTEX 340 Pulser-Receiver and Oscilloscope Setup Instructions	Documented procedure for Pulser-Receiver setup and triggering
NDL-MSL-LPROC-003: 20 Minute Performance Testing Procedures for Heater Tapes and Electric Heater	To ensure proper functioning of heater tapes
NDL-MSL-LPROC-004: Manufacturing/ Synthesis Procedures for FLiNaK Salts	Procedure for FLiNaK synthesis within test tubes
NDL-MSL-LPROC-005: Test Tube FLiNaK Salt Remelting and Simulated Decommissioning Environment Conditions Experiment Procedures	Outline, justification, and setup for decommissioning simulation environment
NDL-MSL-LPROC-006: MSL Tube Segment Remelting Experiment	Procedure for remelting FLiNaK within the MCMA
NDL-MSL-LPROC-007: Design of an Adaptor to Quantify Internal Physical Conditions of MSL Tube Segment During Melting	MCMA design documentation
NDL-MSL-LPROC-008: Collection and Storage of FLiNaK Drained from the MSL Tube Segment	Procedure for the preservation and storage of FLiNaK drained from the MSL Tube Segment

NDL-MSL-LPROC-009: Observation Methods and Recoding Procedures of FLiNaK Salt Migration	Devise methods for quantifying the observed FLiNaK salt migration
NDL-MSL-LPROC-010: Time-lapse Camera Setup Procedures	To ensure proper functioning and setup of camera
NDL-MSL-LPROC-011: Quick Microscope Setup and Adjustment Guide	To ensure proper usage of microscope
NDL-RCT-PRO-011: Determination of Contaminant Emission Lines when introduced into Argon Plasma	Methodology for salt contaminant emission line analysis

A.2 Description of Experimental Procedures

Brief descriptions of the key experimental procedures are featured in the following subsections.

A.2.1 Furnace Performance Testing Procedures

The furnace performance testing procedures provide instructions for determining the accuracy and consistency of heating objects using VULCAN D -1750 furnace. Emphasis was placed on safety and the proper use of PPE due to the required handling of materials at high temperatures. The procedures include guidelines for using the control knob and display screen to change performance parameters of the furnace to obtain the desired temperature using the desired heat rate.

The One Hour Plan

A "one-hour plan" was developed as a heating trial run with the intention of using the furnace for future FLiNaK synthesis. The purpose of the plan is to heat randomly selected objects to some desired temperature, and through familiarizing with the operations of the furnace, can achieve this within an hour. The plan included a table with two columns: the first being some amount of time allotted, while the other describes associated tasks that must be performed within that time. The "one-hour plan" was also practice for using various equipment for temperature measurement.

A.2.2 Vacuumed Test Tube FLiNaK Salt Synthesis Procedures

A more detailed procedure for FLiNaK salt synthesis in test tubes as well as instructions for experimental setup is described in this section. The procedure outlines the construction of a vacuumed melting chamber where FLiNaK salt is melted, synthesized, then stored. In addition, it also illustrates the process of moisture removal, flame intensity adjustment, and staged vacuuming to reproduce the same results as the FLiNaK salt synthesized in this work.
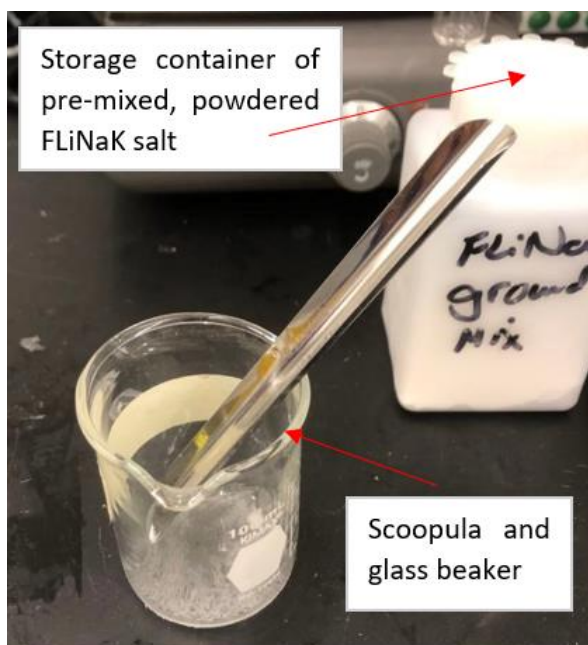
Figure A.1: A scoopula was used to transfer the powdered FLiNaK from its container; when not in use, the scoopula was temporarily stored in a beaker to prevent the spread of salt
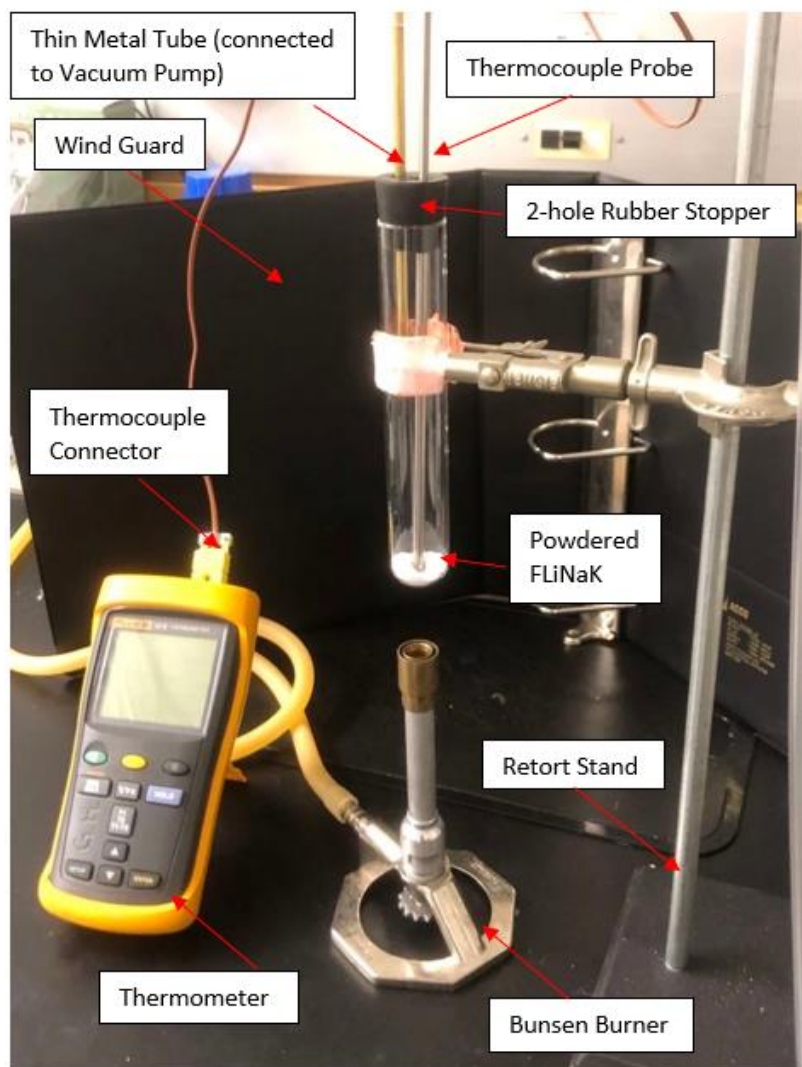
Figure A.2: Setup for FLiNaK synthesis; a wind guard was added to protect the Bunsen Burner flame from the strong air drafts in the room (HVAC ventilation)

For all experiments that involve the handling of FLiNaK salt, whether it be in the form of loose powder or synthesized pucks, a NIOSH approved Type N100 half-face respirator was worn to prevent the inhalation of hazardous fluorine gas released by the FLiNaK salt, especially during heating. The respirator and its cartridges, model H3387, are manufactured by 3M. This model filters both organic vapor and acid gases. An image of the respirator is featured in Figure 3.35. In addition, clear safety goggles were worn to protect the eyes from encountering any chemicals. Other required PPE include a laboratory coat, nitrile gloves, and heat resistant gloves.

Figure A.3: N100 Respirator used for experiments involving any handling of FLiNaK

FLiNaK Salt Synthesis in Test Tubes with Vacuum Melting System

FLiNaK salt synthesis with the vacuum melting system involves heating powdered FLiNaK until it reaches the eutectic point, where the salt is fully liquified and transparent. The sample is then removed from heat and allowed to cool into a solid mass. The salt samples go through the synthesis process within a vacuumed test tube, which slightly lowers their melting temperature, and are sealed immediately after cooling. The incorporation of the vacuum allowed the FLiNaK samples synthesized in this work to be relatively pure. Procedures were revised to emphasize the removal of moisture and careful isolation from contaminants, factors which have been observed to be correlated with the changes in physical appearance of salt over time.

FLiNaK Salt Melting in Test Tubes

This procedure was an exploratory first attempt at melting FLiNaK salt in a test tube using a Bunsen Burner. The experiment involved just the three items; only one sample was synthesized in this manner. Though heat intensity was adjusted throughout, problems such as long heating time, fluorine corrosion at the bottom of the test tube, and salt adhesion to the

vessel were observed. The process was then revised and gradually evolved to address them over the next iterations of the experiment.

Construction of Test Tube Vacuum Chamber

An extension and revision of the previous procedure, this document details the design and construction process of the test tube vacuum chamber- through the addition of a vacuum pump that removed air and moisture from within the test tube via an inserted thin metal tube and plastic tubing.

Moisture Removal of FLiNaK through Two-Stage Heating

Another extension and the final revision to the previous document, this procedure outlined the methods used to remove the maximum amount of moisture from the FLiNaK powder during its synthesis process. This procedure was devised upon observing the effects of moisture on salt migration and the adhesion of salt to their vessels. Three samples of FLiNaK were synthesized using a both the vacuum pump and two-stage heating.

Remelting Synthesized FLiNaK

This procedure investigated the repeated remelting of synthesized FLiNaK and its effect on the physical conditions, stability, and migration behaviour of the sample.

Simulated D&D Environments

The procedure is extended from the Remelting of Synthesized FLiNaK, the purpose being to further investigate and characterize the previously observed migration behavior of FLiNaK Salt in a quantitative manner. Results from past experiments had suggested a correlation between the extent of salt migration and the water/moisture content in the samples' environment.

This document outlines the simulation of a set of different potential environments that FLiNaK salt may be subjected to at the time of reactor decommissioning and end-of-life

operations. Table A.2 below describe each simulated scenario, the approach, and their rationale.

Table A.2: Simulated Decommissioning Environments of FLiNaK Salt

Sample Number	Environment Simulated	Salt Sample Processing	Justification
1	Catastrophic Failure	Vacuumed Moisture Removal Water Added (~ 50 % salt mass)	This simulates scenarios where the salt is exposed to massive amounts of moisture or has direct contact with water either as the result of rupture or severe leak.
2	Improper Sealing or Leak in Vessel	Vacuumed Moisture Removal Water Added (~10-20% salt mass)	This scenario investigates whether migration patterns of FLiNaK can be aggravated (maybe even optimized) or that it is entirely unpredictable.
3	"As is"	Moisture Removal No Vacuuming	This investigates the behaviour of commercially purchased ingots of FLiNaK.
4	Long-Term Storage	Vacuumed Moisture Removal	The purpose is to examine salt migration for long-term storage and whether vacuum sealing would suffice in preventing migration.
5	Long Term Storage with Routine Remelt and Vacuum (off-gas)	Vacuumed Moisture Removal	This scenario investigates the effects of repeatedly remelting of synthesized FLiNaK following the example of the MSRE

Salt Migration Observation and Recording

This procedure outlines the materials and analysis methods used for the observation and recording of FLiNaK salt migration within test tube samples as well as the salt plug and residue in the MSL Tube Segment.

A.2.3 MSL Tube Segment Remelting Procedures

A series of six experiments were performed with the goal of fully remelting and draining the salt plug and crystalline residue within the Hastelloy-C MSL Tube Segment. This also included the use of ultrasonic methods to detect salt presence within the tube. This section discusses the procedures that were developed, revised, and expanded upon to achieve this goal. Revisions sought to address any challenges that arose in previous iterations as well as increased experience and familiarity with the materials and equipment used.

Ultrasonic Pulser-Receiver and Oscilloscope Settings

This procedure provided instructions for configuring the settings of both the ultrasonic pulser-receiver and oscilloscope so that a signal can be triggered and viewed on the display screen. A method for verifying the signal is also included.

Heater Tape and Electric Heater Testing

A subsection of the MSL Tube Segment Remelting Procedures, this document was used to test the performance and proper functioning of the heater tapes and electric heater. This procedure also investigated the various heating modes and settings of the electric heater.

Construction and Assembly of MCMA

This document consisted of two main sections. The first section described the design process and the rationale behind the construction of the MCMA. The design requirements, engineering drawings and models, as well as procurement records are documented. The second section illustrates the assembly procedures of the MCMA.

Draining of Residue FLiNaK from MSL Tube Segment

This procedure described in detail, through its numerous revisions, the proper assembly and setup the MSL Tube Segment Remelting System and the processes implemented to remelt and drain residual FLiNaK from the MSL Tube Segment.

Collection and Storage of Drained FLiNaK

This procedure outlined the collection, transfer, and storage of the drained FLiNaK salt that deposited onto the bottom blind flange of the MSL Tube Segment once the system has cooled down from its vacuumed heating. The salt crystals were stored in airtight glass containers.

Appendix B

The Bunsen Burner

A Bunsen burner was used as the heat source in melting powdered FLiNaK in test tubes. This heating method was selected for FLiNaK synthesis because it provided a controlled, concentrated, source of heat that was suitable for melting salt samples in test tubes rapidly and consistently.

The Bunsen burner uses natural gas that is connected to a gas nozzle on the laboratory bench with rubber tubing and lighted using a spark lighter. The localized heating from the Bunsen burner allows rapid changes in temperature within the FLiNaK, the salt also cools quickly making it safer to transport or store. The flame of the Bunsen burner was controlled through adjusting the air hole at the base of the of the barrel. Since the temperature of the flame can be identified by its color, the desired heat intensity in the three melting stages was visually determined through flame color and supported by temperature readings of the flame and salt sample within the test tube. Instruments used for temperature measurements are discussed in a later section.

B.1 Bunsen Burner Heat Intensity Controls

During the moisture removal stage of the FLiNaK synthesis process, the air hole is slightly open to achieve an orange, reddish flame as seen in Figure B.1 (b); this allows any water moisture trapped in the FLiNaK powder to evaporate. Then, the air hole is opened half-way for about two minutes before it is opened entirely, where hotter, more intense blue flames illustrated in Figure B.1 (c) and (d) initiate the melting process. This way, the sample melts completely with minimal moisture trapped within.

Appendix B. The Bunsen Burner

Air hole positions and their associated flame colour and heat intensity is outlined as follows:

Table B.1: Bunsen Burner Flame Control and Colour
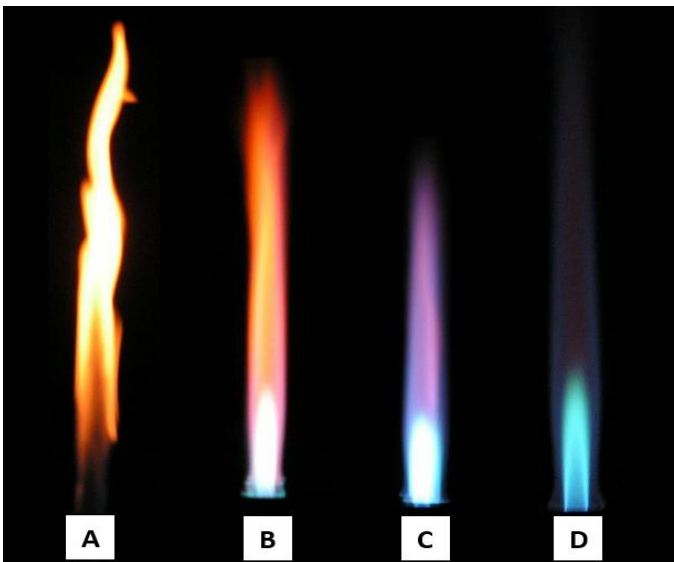
Air Hole Position	Flame Colour	Visual Reference
Closed	Yellow	
Slightly Open	Orange Red	
Half Open	Purple Blue	Figure B.1: Air hole position and corresponding flame colour
Fully Open	Blue	(a): air hole is fully closed – yellow safety flame (b): air hole slightly open – orange-red flame (c): air hole half-open – blue-purple flame (d): air hole fully open – roaring blue flame

Appendix C

Molten Salt Loop Design Requirements

C.1 List of Design Requirements

This is an excerpt from the Undergraduate Capstone report NDL-MSL_RPT-006

1. **The piping material must retain its mechanical strength and resist corrosion from molten salt.**
    -   The material is required to be a material which retains its mechanical strength above the hot leg operating temperature of 750ºC and is highly resistant to corrosion with sufficient margin.
2. **Non-welded pipe connections must use sealing gaskets.**
    -   Sealed gaskets will accommodate swelling and leaks.
3. **Piping configuration must minimize horizontal lengths, and flow disruptions.**
    -   Natural circulation is based on a vertical density displacement. Extended horizontal sections increase flow resistance. Gaskets and pipe intrusions must be limited to prevent disrupting natural circulation.
4. **The loop must have a means of filling and draining the molten salt.**
    -   Before operation the loop must be able to be filled with molten salt. After completing the experiment, the molten salt must be able to be drained.
5. **The piping schedule must have an internal diameter less the 1.5 cm.**
    -   This diameter supports the overall heating time and power requirements as well as scale of experimentation.
6. **There must be a means of disassembling the loop, for maintenance and inspection.**
    -   In the event of solidification, or egress of impurities the loop must be able to be cleaned, without permanently damaging the loop.

7. **The vessels and piping must be securely attached to the frame, using an insulating material.**

   - The loop must be structurally supported, but also not conduct significant amounts of heat to the frame.

8. **Any equipment that must be operated manually must be accessible and safe to touch.**

   - Due to the extreme temperatures within the loop equipment such as valves that require manual operation could cause safety concerns. Equipment requiring operation must be both safely accessible and at a safe temperature to touch.

9. **The loop must reduce likelihood of solidification.**

   - The molten salt (FLIBE) will begin to solidify below 500ºC. The loop must be designed so that sufficient heating can ensure that the salt will not solidify within the loop.

Appendix D

Properties of Hastelloy N

Hastelloy-N was the structural alloy invented specifically for the MSRE and is compatible with the fluoride salts FLiBe and FLiNaK. The properties of Hastelloy-N are presented below as a reference. Tables D.1, D.2, D.3 and D.4 list the chemical composition, mechanical and thermal properties, as well as the aqueous corrosion data of Hastelloy-N as featured in the Haynes International Product Specification and Data Brochure.

D.1 Nominal Composition

Table D.1: Chemical Composition of Hastelloy-N

Element	Weight %
Nickel	71
Cobalt	0.02
Chromium	7
Molybdenum	16
Iron	4
Tungsten	0.5
Manganese	0.8
Vanadium	0.5
Silicone	1
Carbon	0.06
Copper	0.35
Aluminum + Titanium	0.5

D.2 Mechanical Properties

Table D.2 : Mechanical Properties of Hastelloy-N

Property	Value
Density	8.86 g/cm^3
Poisson's Ratio	0.32
Toughness (Charpy V-notch 10 mm Plate)	138 J
Young's Modulus	219 GPa
Shear Modulus	77 Gpa
Yield Strength	308-323 MPa
Ultimate Tensile Strength	789-796 MPa
Elongation at Failure	50.7 %
Hardness	96 HRB (Rockwell B)

D.3 Thermal Properties

Table D.3: Thermal Properties of Hastelloy-N

Property	Value
Thermal Conductivity	13.1 W/(m°C)
Coefficient of Thermal Expansion	12.3 μm/(m°C)
Specific Heat	531 J/kg °C
Melting Range	1040-1372 °C

D.4 Corrosion Data in Aqueous Solutions

Table D.4: Corrosion Data of Hastelloy-N in Various Aqueous Media

Media	Concentration (%)	Temperature (°C)	Corrosion Rate (mpy)
Hydrochloric Acid	2	RT	1
	2	66	18
	2	Boiling	73
	5	RT	1
	5	66	20
	15	RT	3
	25	RT	2
	37	RT	<1
Sulfuric Acid	5	RT	1
	5	66	11
	5	Boiling	11
	25	RT	1
	25	66	10
	50	RT	<1
	80	RT	<1
	96	RT	<1
Phosphoric Acid	10	RT	<1
	10	66	1
	10	Boiling	6
	30	RT	1
	30	66	1
	50	RT	<1
	85	RT	<1
Hydrofluoric Acid	5	RT	2
	5	79	20
	25	RT	3
	45	RT	5
	48	79	31
Acetic Acid	10	RT	1
	10	66	3
	10	Boiling	1
	50	RT	1
	50	66	3
	50	Boiling	2
	99	RT	<1
	99	66	<1
	99	Boiling	<1

*RT=Room Temperature

The Melting Chamber Monitoring Attachment

Figure E.1 below is the preliminary engineering drawing of the MCMA assembly, completed using SolidWorks. Some subcomponents were eventually substituted with fittings already available in the laboratory to avoid redundant purchases.

ITEM NO.	PART NUMBER	DESCRIPTION	QTY.
1	SS-8-VCR-CS	316 Stainless Steel VCR Face Seal Fitting, 1/2 in. Union Cross	1
2	SS-4-E	Stainless Steel Pipe Fitting, Elbow, 1/4 in. Female NPT	1
3	SS-8-RA-4	Stainless Steel Pipe Fitting, Reducing Adapter, 1/2 in. Female NPT x 1/4 in. Male NPT	1
4	SS-8-HRCG-6	Hex Reducing Coupling	1
5	9796T204	Single Scale Pressure Gauge with Plastic Case and Certificate	1
6	SS-8-CP	Modified Stainless Steel Pipe Fitting, Pipe Cap, 1/2 in. Female NPT	1
7	Thermocouple	NDL Thermocouple	1
8	9414T3	Set Screw Shaft Collar	1

MATERIAL: See BOM		NAME	DATE	TITLE:
	DRAWN	Y. Lin	Dec. 12, 2021	MSL Tube Fittings Assembly
Comments: Top level assembly drawing	CHECKED			
DO NOT SCALE DRAWING				PART. NO. MSL_TB_FT_01

Figure E.1: Preliminary Engineering Drawing of the MCMA Assembly.

Appendix F

Observation Table of Cycle-B Test Tube-Synthesized FLiNaK Samples

Table F.1: Physical Changes Observed and Recorded in Cycle-B FLiNaK Samples

Observation Date	Sample Number	Phenomenon Observed	Extent of Salt Migration (mm)
May 19th, 2022	B-1	- Date of synthesis, measuring tape sticker applied to all samples - All five samples are physically uniform: smooth, opaque white, and take the curved shape of the bottom of the test tube - Samples B-1 and B-2 are able to slide along the bottom of the test tube	0
	B-2		
	B-3		
	B-4		
	B-5		
May 26th, 2022	B-1	- Sample sticks to the bottom of the test tube, likely the result of surface tension	0
	B-2	- Water added seems to be absorbed by the sample, yet it does not appear damp or wet	0
	B-3	- Sample appears slightly damp - A few particulates of FLiNaK have adhered onto the inner walls of the test tube away from the main salt crystal	3 - 7

Appendix F. Observation Table of Cycle-B Test Tube-Synthesized FLiNaK Samples

	B-4	- No changes observed	0
	B-5		
June 2nd, 2022	B-1	- FLiNaK salt firmly stuck to the bottom of test tube	0 - 3
	B-2	- A few specks of salt observed to have migrated away from main crystal	
	B-3	- Sample appears slightly damp - Particulates and granules of FLiNaK have adhered onto the inner walls of the test tube away from the main salt crystal	5 - 12
	B-4	- No changes observed	0
	B-5		
June 9th, 2022	B-1	- FLiNaK salt firmly stuck to the bottom of test tube	3 - 7
	B-2	- Some signs of salt migration observed in both samples	
	B-3	- Sample appears damp - Increase in salt migration as FLiNaK granules along the inner teat tube walls become more abundant	10 - 17
	B-4	- No significant changes observed, one small granule detached from main sample	0 - 5
	B-5	- Sample remelted and resealed	
June 23rd, 2022	B-1	- FLiNaK salt firmly stuck to the bottom of test tube - Slight increase in signs of salt migration: more particulates are observed away from main crystal, but not much further	4 - 8
	B-2		
	B-3	- Sample appears wet - Steady increase in FLiNaK salt migration	15 - 23

		- Small amounts of liquid observed at the base of the test tube where the main salt crystal is located	
	B-4	- No changes observed	0 - 5
	B-5		
July 12th, 2022	B-1	- FLiNaK salt firmly stuck to the bottom of test tube	3 - 14
	B-2	- Slight increase in signs of salt migration	
	B-3	- Sample appears wet, and is partially submerged in liquid (water) - Drastic increase in FLiNaK salt migration - Patches of salt are found along the inner walls of the test tube - Minuscule tear in Parafilm seal observed	18 - 42
	B-4	- No significant changes observed, one small granule detached from main sample	0 - 5
	B-5		
July 26th, 2022	B-1	- FLiNaK salt firmly stuck to the bottom of test tube - Continued increase in signs of salt migration, though not severe like anticipated: more particulates are observed away from main crystal	3-21
	B-2		
	B-3	- Sample is wet, and mostly submerged in the aqueous solution pooling at the bottom - Drastic increase in FLiNaK salt migration - More patches of salt are found along the inner walls of the test tube	15 - 78

		- Tear in Parafilm seal ruptured and split - Sample is resealed with new piece of Parafilm but not vacuumed	
	B-4	- No significant changes observed, one small granule detached from main sample	0 - 6
	B-5	- Sample remelted and resealed	0
August 16th, 2022	B-1	- FLiNaK salt firmly stuck to the bottom of test tube - Continued increase in signs of salt migration, more so in sample B-1, still not severe like anticipated: more particulates are observed away from main crystal	3-24
	B-2		
	B-3	- Sample is wet, and mostly submerged in the aqueous solution pooling at the bottom - No significant increase in FLiNaK salt migration observed - Patches of salt remain	14 - 89
	B-4	- No significant changes observed, one small granule detached from main sample	0 - 6
	B-5		
August 23rd, 2022	B-1	- FLiNaK salt firmly stuck to the bottom of test tube - Continued increase in signs of salt migration for both samples, more particulates were observed in sample B-1	3-28
	B-2		
	B-3	- Sample is wet, and mostly submerged in the aqueous solution pooling at the bottom	17 - 105

Appendix F. Observation Table of Cycle-B Test Tube-Synthesized FLiNaK Samples

		- No significant increase in FLiNaK salt migration observed - Patches of salt remain but did not increase	
	B-4	- No significant changes observed, one small granule detached from main sample	0 - 6
	B-5		

Appendix G

Experimental Data from MSL Tube Segment Drainage Trials

G.1 Trial Number One: Sept. 16ᵗʰ, 2021

Table G.1: Temperature and Time Data of First MSL Tube Segment Salt Drainage Experiment

Time (min)	Electric Heater Setting (°C)	Temperature Reading – Ext. Thermocouple (°C)	Temperature Reading – Infrared Camera (°C)	Comments
0	50	22	18.1	The heating began almost immediately; however, the initial ramp-up is slow
10	50	43	33.6	
20	150	107	87.5	
45	200	159	143.6	
60	250	220	198.4	Rapid temperature increase, almost 2 °C every 15 seconds
75	300	289	236.3	
90	350	321	268	The heater tapes began to glow red; this is especially obvious when the room is dark
100	450	424	> 275	
110	475	455	> 275	

G.2 Trial Number Two: Nov. 5th, 2021

Table G.2: Temperature and Time Data of Second MSL Tube Segment Salt Drainage Experiment

Time (min)	Electric Heater Setting (°C)	Temperature Reading – Ext. Thermocouple (°C)	Temperature Reading – Infrared Camera (°C)	Comments
0	50	21	20.8	The heating began almost immediately; however, the initial ramp-up is slow
10	50	38	36.4	
20	75	61	58.5	Held the temp. for extra 10 min due to slow increase in heat
30	75	72	71.8	
40	100	83	79.3	Vapour was observed condensing in the plastic tubing
50	150	108	103.6	
60	200	171	164.8	
70	250	202	186.3	The temp. increase was especially slow, held for extra 10 min each.
80	250	238	236.2	
90	300	259	248.1	
100	300	286	267.2	Vacuum pump continuously removing condensed moisture
110	350	335	274.3	Temp. gap between the two instruments continue to increase (~170 °C)
120	400	374	286.7	
130	450	396	318.4	
140	450	446	336.5	
150	500	486	367.2	
160	550	548	385.9	End of Experiment, equipment turned off

G.3 Trial Number Three: Dec. 3rd, 2021

Table G.3: Temperature and Time Data of Third MSL Tube Segment Salt Drainage Experiment

Time (min)	Electric Heater Setting (°C)	Temperature Reading – Ext. Thermocouple (°C)	Comments
0	50	21	Steady heating, no burnt smell from the insultation
10	150	125	Drastic temp. Increase to shorten experiment time. Vacuum pump turned on.
20	200	192	Vapour was observed condensing in the plastic tubing
30	250	235	
40	300	282	
50	350	309	
60	350	327	Reflecting insulator fell-off, will need to be fastened next time
70	400	369	
80	450	422	
87	450	412	Plastic tube on adaptor ruptured, experiment ended

G.4 Trial Number Four: Feb. 11ᵗʰ, 2022

Table G.4: Temperature and Time Data of Fourth MSL Tube Segment Salt Drainage Experiment

Time (hour)	Electric Heater Setting (°C)	Temperature Reading – Ext. Thermocouple (°C)	Temperature Reading – K-Type Internal Thermocouple (°C)	Pressure within Test Section (in. Hg)	Comments
0:00	50	21	20.9	-30	The vacuum held very well throughout the experiment.

However, over time, the temperature discrepancy between the internal K-Type thermocouple and the external wire thermocouple increased.

By the end of the experiment this temperature difference was 293 °C, which very significant. |
0:20	150	150	42.6		
0:40		235	54.2		
1:00	250	250	76.8	-29.5	
1:20			88.9		
1:40	350	344	93.9		
2:00		350	99.2		
2:20			120.6	-29	
2:40	450	416	127.6		
3:00		445	149.8		
3:20			162.7		
3:40			166.9	-28.5	
4:00		450	168.2		
4:20			171.2		
4:40			174.3		
5:00	480	475	172.9	-28	
5:20			181.0		
5:40		480	185.3		
6:00			187.0		

Appendix F. Observation Table of Cycle-B Test Tube-Synthesized FLiNaK Samples

G.5 Trial Number Five: Jul. 6ᵗʰ, 2022

Table G.5: Temperature and Time Data of Fifth MSL Tube Segment Salt Drainage Experiment

Time (min)	Electric Heater Setting (°C)	Temperature Reading – Ext. Thermocouple (°C)	Temperature Reading – K-Type Internal Thermocouple (°C)	Pressure within Test Section (in. Hg)	Comments
0	50	22.6	22.5		Burnt smell detected
5	100	98	56.8		Significant amount of smoke was continuously emitted from underneath the wool insulation

Consequently, the experiment ended prematurely and the heater tape severely damaged |
10	150	126	93.6	-30	
15	200	159	104.3		
18		167	112.0		

G.6 Trial Number Six: Jul. 14th, 2022

Table G.6: Temperature and Time Data of Sixth MSL Tube Segment Salt Drainage Experiment

Time (min)	Electric Heater Setting (°C)	Temperature Reading – Ext. Thermocouple (°C)	Temperature Reading – K-Type Internal Thermocouple (°C)	Pressure within Test Section (in. Hg)	Comments
0	50	23	20.8	-30	Consistent temp. reading between two methods
10	150	152	127.0		
20	250	251	214.6	-29.5	No smoke or burnt smell detected
40	350	367	289.4		
60	400	413	378.5	-29	Temperature increase is about 1°C every 10 to 15 seconds
80	450	453	415.1	-28.5	Fibreglass insulation made the external temp. higher than that of the heater setting.
100		464	438.2	-28	
120	470	480	459.7	-27.5	Internal temp. has reached above melting temp. of FLiNaK; thus, the experiment was ended.
125		514	465.0	-27	

References

[1]   IAEA Nuclear Energy Series: Technical Report, "Technology Roadmap to Small Modular Reactor Deployment", International Atomic Energy Agency, Vienna, Austria, 2021.

[2]   S. Delpech, C. Cabet, C. Slim, and G. Picard, "Molten fluorides for nuclear applications", *Materials Today*, vol. 13, no. 12, pp. 34-41, 2010.

[3]   D. LeBlanc, "Molten salt reactors: A new beginning for an old idea", *Nuclear Engineering and Design*, vol. 240, no. 6, pp. 1644-1656, 2010.

[4]   B. Elsheikh, "Safety assessment of molten salt reactors in comparison with light water reactors", *Journal of Radiation Research and Applied Sciences*, vol. 6, no. 2, pp. 63-70, 2013.

[5]   I. Scott, T. Abram, and O. Negri, "Stable Salt Reactor Design Concept" in *2015 Int. Thorium Energy Conference: Gateway to Thorium Energy Conf. Proc. (ThEC15)*, October 12-15, 2015, pp. 1-6.

[6]   D. LeBlanc and C. Rodenburg, "Integral Molten Salt Reactor," in *Molten Salt Reactors and Thorium Energy*, 1st ed., Sawston, UK: Woodhead Publishing, 2017, pp. 541–556, ISBN: 978-0-08-101126-3

[7]   M.W. Rosenthal, P.N. Haubenreich, H.E. McCoy, and L.E. McNeese "Recent Progress in Molten-Salt Reactor Development", *Atomic Energy Review*, vol. 9, no. 3, pp. 601-650, 1971.

[8]   R.B. Briggs, "Molten Salt Reactor Program Semi-annual Progress Report for Period Ending July 31st, 1964", Oak Ridge National Laboratory, Tennessee, 1964.

[9]   Canadian Nuclear Safety Commission, REGDOC 2.5.2 Section 7.24 –Design of Reactor Facilities. 280 Slater St., Ottawa, Ontario, Canada: Canadian Nuclear Safety Commission, 2022.

[10]   J. Serp et al., "The Molten Salt Reactor (MSR) in Generation IV: Overview and Perspectives", *Progress in Nuclear Energy*, vol. 77, pp. 308–319, 2014.

[11]   C. W. Forsberg, "The Advanced High-Temperature Reactor (AHTR) for Producing Hydrogen to Manufacture Liquid Fuels," in *2004 Americas Nuclear Energy Symposium*, October 6, 2004, pp. 1-13.

[12]   D. Jiang et al., "Fluoride-salt-cooled high-temperature Reactors: Review of Historical Milestones, Research Status, Challenges, and Outlook," *Renewable and Sustainable Energy Reviews*, vol. 161, p. 112345, 2022.

[13]   C. H. Yamaguchi, G. L. Stefani, and T. A. Santos, "A General Overview of Generation IV Molten Salt Reactor (MSR) and the Use of Thorium as Fuel" in *2017 International Nuclear Atlantic Conference (INAC)*, Oct. 22-27, 2017, pp. 1-10.

[14]   B. Zohuri, *Molten Salt Reactors and Integrated Molten Salt Reactors: Integrated Power Conversion,* 1st ed., London, UK: Academic Press, 2021. ISBN: 9780323906388

[15]   S. Ladkany, W. Culbreth, and N. Loyd, "Molten Salts and Applications I: Molten Salt History, Types, Thermodynamic and Physical Properties, and Cost," *Journal of Energy and Power Engineering*, vol. 12, no. 11, pp. 1–10, 2018.

[16]   International Atomic Energy Agency, 2018, "Molten Salt Reactors - Advanced Reactor Information System (ARIS)," IAEA, https://aris.iaea.org/sites/overview.html

[17]   "Molten Salt Reactors," in *Advances in small modular reactor technology developments: A Supplement to the IAEA Advanced Reactors Information System (ARIS)*, Vienna, AT: IAEA, 2020, pp. 241–282.

[18]   Z. Dai, Y. Zou, and K.Chen, "Thorium Molten Salt Reactors (TMSR) Development in China" in *2016 Technical Meeting on the Status of Molten Salt Reactor Technologies,* Oct.31- Nov. 3, 2016.

[19]   R. R. Romatoski and L. W. Hu, "Fluoride Salt Coolant Properties for Nuclear Reactor Applications: A Review," *Annals of Nuclear Energy*, vol. 109, pp. 635–647, 2017.

[20]   U. Gat and J. R. Engel, "Non-proliferation Attributes of Molten Salt Reactors," *Nuclear Engineering and Design*, vol. 201, no. 2-3, pp. 327–334, 2000.

[21]   C. W. Forsberg, "Molten-Salt-Reactor Technology Gaps," in *2006 International Congress on the Advances in Nuclear Power Plants (ICAPP)*, June 4–8, 2006, pp. 1-8.

[22]   E. S. Bettis et al., "The Aircraft Reactor Experiment—Design and Construction," *Nuclear Science and Engineering*, vol. 2, no. 6, pp. 804–825, 1957.

[23]   W.B. Cottrell (Ed.) et al., "Reactor program of the Aircraft Nuclear Propulsion Project", Oak Ridge National Laboratories, Tennessee, 1952.

[24]   E. S. Bettis et al., "The Aircraft Reactor Experiment—Operation," *Nuclear Science and Engineering*, vol. 2, no. 6, pp. 841–853, 1957.

[25]   W. K. Ergen et al., "The Aircraft Reactor Experiment—Physics," *Nuclear Science and Engineering*, vol. 2, no. 6, pp. 826–840, 1957.

[26]   W.D. Manly et al., "Aircraft Reactor Experiment—Metallurgical Aspects", Oak Ridge National Laboratories, Tennessee, 1958.

[27]   H.W. Savage et al., "Components of the fused-salt and sodium circuits of the Aircraft Reactor Experiment", Oak Ridge National Laboratories, Tennessee, 1958.

[28]   W.B. Cottrell et al., "Operation of the Aircraft Reactor Experiment", Oak Ridge National Laboratories, Tennessee, 1955.

[29]   W.B. Cottrell (Ed.) et al., "Aircraft Reactor Experiment Hazards Summary Report", Oak Ridge National Laboratories, Tennessee, 1952.

[30]   W.B. Cottrell et al., "Disassembly and postoperative examination of the Aircraft Reactor Experiment", Oak Ridge National Laboratories, Tennessee, 1958.

[31]   H. G. MacPherson, "The Molten Salt Reactor Adventure," *Nuclear Science and Engineering*, vol. 90, no. 4, pp. 374–380, 1985.

[32]   R.E. Thoma, "Chemical Feasibility of Fueling Molten Salt Reactors with PuF_3", Oak Ridge National Laboratories, Tennessee, 1968.

[33]   J. R. Engel and P. N. Haubenreich, "Temperatures in the MSRE Core During Steady-State Power Operation", Oak Ridge National Laboratories, Tennessee, 1962.

[34]   Oak Ridge National Laboratories, *Molten Salt Reactor Experiment*. U.S. Atomic Energy Commission, Oak Ridge, TN, 1965.

[35]   T. Morgan and E. Abelquist, "Decommissioning Challenges at the Molten Salt Reactor Experiment Site" in *2021 Virtual Molten Salt Reactor (MSR) Workshop*, Oct. 12, 2021.

[36]   J. R. Engel and P. N. Haubenreich "Experience with the Molten-salt Reactor Experiment," *Nuclear Technology*, vol. 8, no. 2, pp. 118–136, Feb. 1970.

[37]   J.H. DeVan, "Effect of Alloying Additions on Corrosion Behavior of Nickel-Molybdenum Alloys in Fused Fluoride Mixtures" Master's Thesis, Department of Metallurgical Engineering, University of Tennessee, 1960.

[38]   M. Fratoni et.al., "Molten Salt Reactor Experiment Benchmark Evaluation," Oak Ridge National Laboratories, Tennessee, 2020.

[39]   H. G. MacPherson, "Molten-Salt Reactor Project Quarterly Report – For Period Ending January 31, 1959", Oak Ridge National Laboratories, Tennessee, 1959.

[40]   M.W. Rosenthal, P.N. Haubenreich, and R.B. Briggs, "The Development Status of Molten Salt Breeder Reactors", Oak Ridge National Laboratories, Tennessee, 1972.

[41]   R. B. Briggs, "Tritium in Molten-Salt Reactors," *Reactor Technology*, vol. 14, no. 335, 1972.

References

[42]   P. N. Haubenreich, "Tritium in the MSRE: Calculated Production Rates and Observed Amounts", Oak Ridge National Laboratories, Tennessee, 1970.

[43]   J.R. Keiser, "Status of Tellurium-Hastelloy N Studies in Molten Fluoride Salts", Oak Ridge National Laboratories, Tennessee, 1977.

[44]   M. Liu et al., "Investigation on corrosion behavior of Ni-based alloys in molten fluoride salt using synchrotron radiation techniques", *Journal of Nuclear Materials*, vol. 440, no. 1-3, pp. 124-128, 2013.

[45]   K.J. Notz, "Decommissioning of the Molten Salt Reactor Experiment: A Technical Evaluation", Oak Ridge National Laboratories, Tennessee, 1988.

[46]   F.J. Peretz, "Disposition of the Fluoride Fuel and Flush Salts from the Molten Salt Reactor Experiment at Oak Ridge National Laboratory", Oak Ridge National Laboratories, Tennessee, 1996.

[47]   K.J. Notz, "Extended Storage-in-Place of MSRE Fuel Salt and Flush Salt", Oak Ridge National Laboratories, Tennessee, 1985.

[48]   G.D. Del Cul et. al., "Overview of the Recovery and Processing of U233 from the Oak Ridge Molten Salt Reactor Experiment", in *Global 2001 Conference*, Sep. 9-13, 2001, pp. 1-10.

[49]   R.J. Kedl, "The Migration of a Class of Fission Products (Noble Metals) In the Molten Salt Reactor Experiment", Oak Ridge National Laboratories, Tennessee, 1972.

[50]   F.J. Peretz et. al., "Removal of Uranium and Salt from the Molten Salt Reactor Experiment", Oak Ridge National Laboratories, Tennessee, 1998.

[51]   T. Morgan and A. Johnson, "Molten Salt Reactor Experiment (Lay-Up)" in *2019 Annual Waste Management Conference (WM2019)*, Mar. 3-7, 2019, pp.1-7.

[52]   M. W. Rosenthal, P. R. Kasten, and R. B. Briggs, "Molten-salt Reactors—History, Status, and Potential," *Nuclear Applications and Technology*, vol. 8, no. 2, pp. 107–117, 1970.

[53]   D.H. Kim, and Nuclear Data Validation Group, KAERI Table of Nuclides (ver. 2.5.2), [Online]. Korea Atomic Energy Research Institute, Daejeon, SK. 2012.

[54]   D. Holcomb, G. Flanagan, and M. Poore, "MSR Fuel Salt Qualification Guidance Development," *in 2021 ORNL-GAIN MSR Workshop*, Oct. 13, 2021.

[55]   Y. Zhu and A. I. Hawari, "Thermal Neutron Scattering Cross-Section of Liquid FLiBe," *Progress in Nuclear Energy*, vol. 101, pp. 468–475, 2017.

[56]   D. Holcomb, G. Flanagan, and M. Poore, "MSR Fuel Salt Qualification Technology", Oak Ridge National Laboratories, Tennessee, 2020.

[57]   S. Cantor et. al., "The Physical Properties of Molten Salt Reactor-Fuel-Coolant-Flush Salts", Oak Ridge National Laboratories, Tennessee, 1968.

[58]   D. Holcomb, "Module 2: Overview of MSR Technology and Concepts" in *Presentation on MSR Technology for the US Nuclear Regulatory Commission*, Nov.7-8, 2017.

[59]   K. Baral et. al., "Temperature-Dependent Properties of Molten Li_2BeF_4 Salt Using *Ab Initio* Molecular Dynamics," *American Chemistry Society Omega*, vol. 6, no. 30, pp. 19822–19835, 2021.

[60]   D.F. Williams, L. M. Toth, and K. T. Clarno "Assessment of Candidate Molten Salt Coolants for the Advanced High-Temperature Reactor (AHTR)," Oak Ridge National Laboratories, Tennessee, 2006.

[61]   L. M. Toth, J. B. Bates, and G. E. Boyd, "Raman Spectra of $Be_2F_7^{3-}$ and Higher Polymers of Beryllium Fluorides in the Crystalline and Molten State," *The Journal of Physical Chemistry*, vol. 77, no. 2, pp. 216–221, 1973.

[62]   L. M. Toth et. al., "Molten Fluoride Fuel Salt Chemistry" in *1995 Space Nuclear Power Conference*, January 9-11, 1995, pp. 1-6.

[63]   P. Young et. al., "Simultaneous voltametric generation of uranium(III) and spectrophotometric observation of the uranium(III)-uranium(IV) system in molten lithium fluoride-beryllium fluoride-zirconium fluoride," *The Journal of Physical Chemistry*, Vol. 71, no. 3, pp.: 782–783, 1967.

[64]   P. Young and J.C. White, "Absorption Spectra of Molten Fluoride Salts. Solutions of Several Metal Ions in Molten Lithium Fluoride-Sodium Fluoride-Potassium Fluoride," *Analytical Chemistry*, Vol. 32, no.7, pp.799-802, 1960.

[65]   C. Forsberg, "Safety and Licensing Aspects of the Molten Salt Reactor" in *2004 American Nuclear Society Annual Meeting,* June 13–17, 2004.

[66]   C. Bahri et. al., "Characteristic of molten fluoride salt system LiF-BeF2 (Flibe) and LiF-NaF-KF (Flinak) as coolant and fuel carrier in molten salt reactor (MSR)" in *2017 American Institute of Physics Conf. Proc. (AIP17)*, January 6, 2017, pp. 1-9.

[67]   M.S. Sohal et. al, "Engineering Database of Liquid Salt Thermophysical and Thermochemical Properties", Idaho National Laboratory, Idaho, 2013.

[68]   D. Holcomb, "Module 3: Module 3: Overview of Fuel and Coolant Salt Chemistry and Thermal Hydraulics" in *Presentation on MSR Technology for the US Nuclear Regulatory Commission*, Nov.7-8, 2017.

[69]   J. A. Lane, H. G. MacPherson, and F. Maslan, "Chapter 12: Chemical Aspects of Molten-Fluoride-Salt Reactor Fuels," in *Fluid Fuel Reactors*, Reading, MA: Addison-Wesley Publishing Company, 1958, pp. 569–592.

[70]   G. J. Janz and R.P.T. Tomkins, "Physical Properties Data Compilations Relevant to Energy Storage. IV. Molten Salts: Data on Additional Single and Multi-Component Salt Systems", National Standard Reference Data System, New Jersey, 1981.

[71]   D. J. Rogers, T. Yoko, and G. J. Janz, "Fusion Properties and Heat Capacities of the Eutectic LiF-NaF-KF Melt," *Journal of Chemical and Engineering Data*, vol. 27, no. 3, pp. 366–367, Jul. 1982.

[72]   R. Serrano-López, J. Fradera, and S. Cuesta-López, "Molten salts database for Energy Applications," *Chemical Engineering and Processing: Process Intensification*, vol. 73, pp. 87–102, 2013.

[73]   G. J. Janz, *Thermodynamic and Transport Properties for Molten Salts: Correlation Equations for Critically Evaluated Density, Surface Tension, Electrical Conductance, and Viscosity Data*, 1st ed., vol. 17. New York: Published by the American Chemical Society and the American Institute of Physics for the National Bureau of Standards, 1988.

[74]   M. Salanne, et. al., "Heat-transport Properties of Molten Fluorides: Determination from First-principles," *Journal of Fluorine Chemistry*, vol. 130, no. 1, pp. 38–44, 2009.

[75]   S. I. Cohen and T.N. Jones, "A Summary of Density Measurements on Molten Fluoride Mixtures and a Correlation for Predicting Densities of Fluoride Mixtures", Oak Ridge National Laboratories, Tennessee, 1954.

[76]   D. E. Holcomb and S. M. Cetiner, "An Overview of Liquid-Fluoride-Salt Heat Transport Systems", Oak Ridge National Laboratories, Tennessee, 2010.

[77]   N. D. Bull Ezell, R. Gallaghar, C. Agca, and J. McMurray, "Thermal Property Characterization of Molten Salt Reactor–Relevant Salts", Oak Ridge National Laboratories, Tennessee, 2021.

[78]   G.D. Robbins, "Electrical Conductivity of Molten Fluorides: A Review", Oak Ridge National Laboratories, Tennessee, 1968.

[79]   Thomas Steenberg, Peter Szabo, and Aslak Stubsgaard, "FLiNaK Salt" in *Copenhagen Atomics Salt Data Sheet and Specifications Seminar*, Sep. 13th, 2020, pp.2-7.

[80]   B. A. Frandsen et. al., "The Structure of Molten FLiNaK," *Journal of Nuclear Materials*, vol. 537, p. 152219, 2020.

[81]   Canadian Nuclear Safety Commission, REGDOC 2.11.2 – Waste Management: Decommissioning. 280 Slater St., Ottawa, Ontario, Canada: Canadian Nuclear Safety Commission, 2022.

[82]   IAEA Waste Safety Section & Waste Technology Section, "Selection of decommissioning strategies: Issues and factors", International Atomic Energy Agency, Vienna, Austria, 2005.

[83]   D.W. Reisenweaver, "Decommissioning Strategies for Facilities using Radioactive Material", International Atomic Energy Agency, Vienna, Austria, 2007

[84]   D. C. Invernizzi, G. Locatelli, and N. J. Brookes, "An exploration of the relationship between nuclear decommissioning projects characteristics and cost performance," *Progress in Nuclear Energy*, vol. 110, pp. 129–141, 2019.

[85]   S. I. Kim, H. Y. Lee, and J. S. Song, "A study on characteristics and internal exposure evaluation of radioactive aerosols during pipe cutting in decommissioning of Nuclear Power Plant," *Nuclear Engineering and Technology*, vol. 50, no. 7, pp. 1088–1098, 2018.

[86]   B. C. Mingst, "An Analysis of Decommissioning Costs and Funding," in *Decontamination and Decommissioning of Nuclear Facilities*, 1st ed, Boston, MA: Springer Publishing, 1980, pp. 739–750, ISBN: 978-1-4684-3710-2

[87]   J. L. Nelson and J. R. Divine, "Decontamination processes for restorative operations and as a precursor to decommissioning: A literature review," Pacific Northwest Laboratory, Washington, 1981.

[88]   NEA Task Group on Decontamination, "Decontamination Techniques Used in Decommissioning Activities", Nuclear Energy Agency, Paris, FR, 1998.

[89]   P. L. De (ed.),"Decontamination and Decommissioning of Nuclear Facilities", International Atomic Energy Agency, Vienna, Austria, 1989.

[90]   J. O. Adibeli, Y.-kuo Liu, A. Ayodeji, and N. J. Awodi, "Path planning in nuclear facility decommissioning: Research status, challenges, and opportunities," *Nuclear Engineering and Technology*, vol. 53, no. 11, pp. 3505–3516, 2021.

[91]   G. Harvel, "Dismantling Technologies," in *Principles of Nuclear Facility Decommissioning*, January 7, 2022.

[92]   Khurmi, R. Carlisle, and G. Harvel, "Development of a Selection Tool for Choosing Decontamination Technology for Canadian Applications", in ICONE-28 Power, Anaheim, California, 2020, pp. 1-10.

[93]   M.S. Sohal et. al, "Engineering Database of Liquid Salt Thermophysical and Thermochemical Properties", Idaho National Laboratory, Idaho, 2013.

[94]   L. J. Mauer, "Deliquescence of crystalline materials: Mechanism and implications for foods," *Current Opinion in Food Science*, vol. 46, p. 100865, 2022.

[95]   Kondo, M., et al., "Corrosion Characteristics of Reduced Activation Ferritic Steel, JLF-1 (8.92Cr-2W) in Molten Salts Flibe and Flinak," *Fusion Engineering and Design*, vol. 84, pp. 1081-1085, 2009a.

[96]   G. Zong, Z. Zhang, J. Sun and J. Xiao, "Preparation of Molten FLiNaK Salt", *Nuclear Techniques*, vol. 37, pp. 5-10, 2014.

References

[97] D. Zhang, L. Liu, M. Liu, R. Xu, C. Gong, J.Zhang, C. Wang, S. Qiu, and G. Su, "Review of conceptual design and fundamental research of molten salt reactors in China", International Journal on Energy Research, 42:1834-1848, 2018.

[98] S. Lee et al., "Comparative Studies of the Structural and Transport Properties of Molten Salt FLiNaK Using the Machine-Learned Neural Network and Reparametrized Classical Forcefields", *The Journal of Physical Chemistry B*, vol. 125, no. 37, pp. 10562-10570, 2021.

[99] L. Sögütoglu et al., "Understanding the Hydration Process of Salts: The Impact of a Nucleation Barrier", *Crystal Growth & Design*, vol. 19, no. 4, pp. 2279-2288, 2019.

[100] S. Iliopoulos et. al., "Detection and evaluation of cracks in the concrete buffer of the Belgian nuclear waste container using combined NDT techniques," *Construction and Building Materials*, vol. 78, pp. 369–378, 2015.

[101] M. Jamil et al., "Internal Cracks and Non-Metallic Inclusions as Root Causes of Casting Failure in Sugar Mill Roller Shafts", *Materials*, vol. 12, no. 15, p. 2474, 2019

[102] Guanyu Tube "Ultrasonic Velocity Acoustical Properties of Various Materials", *Tubingchina.com*, 2022. [Online]. 2020.

[103] G. Kozlovsky and G. Sivashinsky, "On Open and Closed Tips of Bunsen Burner Flames", *Theoretical and Computational Fluid Dynamics*, vol. 6-6, no. 2-3, pp.181-192 1994.

[104] *Technical Data - 64 MAX, 62 MAX+ and 62 MAX Infrared Thermometer*, Fluke 62 Max, IR Thermometer Specification Sheet, Fluke Corporation, 2012.

[105] A. Szajewska, "Development of the Thermal Imaging Camera (TIC) Technology", *Procedia Engineering*, vol. 172, pp. 1067-1072, 2017.

[106] *Ti90, Ti95 Ti100, Ti105, Ti110, Ti125 TiR105, TiR110, TiR125 Performance Series Thermal Imagers*, Fluke Ti105, Infrared Camera Users Manual, Fluke Corporation, 2012.

[107] L. Chen, R. Liu and X. Shi, *Thermoelectric Materials and Devices*, 1st ed. Amsterdam: Elsevier, 2020, pp. 2-3, 70-72, ISBN: 9780128184141

[108] *Manual on the use of Thermocouples in Temperature Measurement*, 4th ed., ASTM, West Conshohocken, PA, USA, 1993, pp. 43-56, ISBN: 978-0-8031-1466-1.

[109] *Super OMEGACLADTM XL Thermocouple Probes Data Sheet*, KQXL-316U-6, OmegaClad Thermocouple Specification Sheet, OMEGA Engineering Inc., 2013.

[110] M. Anish, B. Kanimozhi, S. Ramachandran and J. Vanjinathan, "Thermal Analysis of Square Pipes in a Reactor Vault", *International Journal of Ambient Energy*, vol. 39, no. 2, pp. 159-164, 2017.

[111] *Fluke 50 Series II Thermometers Datasheet*, 52-2 CAL, Dual Input Digital Thermometer Specification Sheet, Fluke Corporation, 2013.

[112] *UT320/UT340 Operations Manual and Software Developer's Guide*, UT340, Manual for Pulser-Receiver, UTEX Scientific Instruments Inc., 2017.

[113] A. Agarwal and J. Lang, *Foundations of Analog and Digital Electronic Circuits*, 1st ed. Massachusetts: Morgan Kaufmann, 2005, pp. 43-44, ISBN: 978-1558607354.

[114] *Principle Features, Nominal Composition, Corrosion Performance, Codes, and Specifications of HASTELLOY® C-276 Alloy*, Hastelloy-C276 Alloy Brochure, Haynes International Inc., No Date specified for brochure.

[115] K. Bal, J. Dutta Majumdar and A. Roy Choudhury, "Study on uni-axial tensile strength properties of Ytterbium fiber laser welded Hastelloy C-276 sheet", *Optics & Laser Technology*, vol. 108, pp. 392-403, 2018.

[116] J. DeVan, "Effect of alloying additions on corrosion behavior of nickel-molybdenum alloys in fused fluoride mixtures", University of Tennessee, Knoxville, 1969.

[117] J.W. Koger, "Evaluation of Hastelloy N alloys after nine years exposure to both a molten fluoride salt and air at temperatures from 700 to 560 °C", Oak Ridge National Laboratories, Tennessee, 1972.

[118] H.E. McCoy, "Evaluation of the Molten Salt Reactor Experiment Hastelloy-N Surveillance Specimens: Second Group", Oak Ridge National Laboratories, Tennessee, 1969.

[119] *High Performance Nickel Based Corrosion Resistant Alloy, HPAlloy C-276*, Product Description, Properties and General Data Sheet, High Performance Alloys, Inc., 2011.

[120] *Super Alloy HASTELLOY(r) C276 (UNS N10276)*, Hastelloy C276, Product Description Brochure, AZO Materials, 2013.

[121] S. Margarete, C. Immanuel, and G. Hubert, "Highly corrosion resistant nickel-chromium-molybdenum alloy with improved resistance o intergranular corrosion", US3203792A, 1965.

[122] *Alloy C276 (UNS N10276) W. Nr. 2.4819*, Hastelloy C276, Product Specification Sheet: Alloy C276, Sandmeyer Steel Company, 2014.

[123]   M. Manikandan et al. "Microstructure and mechanical properties of alloy C-276 weldments fabricated by continuous and pulsed current gas tungsten arc welding techniques", *Journal of Manufacturing Processes*, Vol. 16, Issue 4, pp. 563-572, 2014.

[124]   Z. Qiu et al., "Microstructure and mechanical properties of wire arc additively manufactured Hastelloy C276 alloy", *Materials & Design*, vol. 195, p. 109007, 2020.

[125]   *Flexible Heaters: Ultra-High Temperature Heating Tapes*, SST051-040, Fibreglass Heater Tape Specification Sheet, OMEGA Engineering Inc., 2009.

[126]   North American Insulation Manufacturers Association, "Facts About Fiber Glass Loose-Fill Insulation", NAIMA, Virginia, 2016.

[127]   *Corrosion-Resistant Gauge - Compound, 2-1/2" Dial, ¼ NPT Male, Bottom Connection*, 38595K12, Product Specification Sheet, McMaster-Carr Supply Co., 2022.

[128]   *High-Pressure Precision Flow-Adjustment Valve – Steel Body, 3/8 NPT Female, 0.87 Flow Coefficient,* 4644K48, Product Specification Sheet, McMaster-Carr Supply Co., 2022.

[129]   *3M 5203 NIOSH Approved Half-Face Respirator*, H3387, 5000s Respirator Specification Sheet, 3M Co., No date specified.

[130]   N. Somer and G. Harvel, " Investigation of Radionuclide Contaminants Released by Plasma Torches in Nuclear Dismantlement ", in ISNTP-12, Hokaido, Japan, 2022, pp.1-7.

[131]   A. Kramida, Yu. Ralchenko, J. Reader, and NIST ASD Team, NIST Atomic Spectra Database (ver. 5.7.1), [Online]. National Institute of Standards and Technology, Gaithersburg, MD. 2019.

[132]   F. Ouyang, C. Chang, B. You, T. Yeh and J. Kai, "Effect of moisture on corrosion of Ni-based alloys in molten alkali fluoride FLiNaK salt environments", *Journal of Nuclear Materials*, vol. 437, no. 1-3, pp. 201-207, 2013.

[133]   Molten Salt Panel of the Committee on Remediation of Buried and Tank Wastes, *Evaluation of the U.S. Department of Energy's alternatives for the removal and disposition of molten salt reactor experiment fluoride salts*. Washington, D.C.: National Academy Press, 1997.